CRANFIELD UNIVERSITY

SCHOOL OF MECHANICAL ENGINEERING
DEPARTMENT OF PROPULSION POWER AND AUTOMOTIVE

PhD Thesis

ACADEMIC YEARS 1991-94

S. WELCH

COMPUTATIONAL MODELLING OF DIESEL ENGINE SMOKE EMISSION

Supervisor: Prof. J.B. MOSS

August 1995

This thesis is submitted for the degree of Doctor of Philosophy

ABSTRACT

This thesis is addressed to the problem of predicting the emission of exhaust smoke from the diesel engine. A simulation program based on a zonal phenomenological combustion model has been developed, permitting analysis of soot modelling techniques. For the first time, a comparative study of the common soot model expressions has been undertaken. Model sensitivities and behaviour have been critically assessed in order to determine the key model parameters and to establish a more solid predictive capability. Validation of both the combustion and soot predictions was made by means of comparison with the extensive experimental data-set of Kamimoto.

The combustion model results showed a very good match between predicted and experimental heat release curves. The only notable weakness derived from the method chosen to represent the effect of air swirl on the jet. Otherwise, the combustion predictions were deemed to be sufficiently accurate to serve as an effective platform for soot model development and analysis.

The predictions of exhaust smoke for different operating conditions revealed the importance of accurately describing the overall air-to-fuel ratio in the spray. The effect of load variation was poorly represented due to neglect of the transfer of combustion products between the model zones.

Soot rate predictions were generally quantitatively poor, thus requiring expression calibration. The comparative study of soot expressions identified a ranking of sensitivities of the formation expressions. Though oxidation is conceptually simpler, more distinct qualitative differences were observed in the behaviour of the expressions. The predictions of exhaust soot were found to be highly sensitive to the 'matching' of the formation and oxidation expressions over the period of the combustion process, and with poorly matched expressions, a very high sensitivity to the soot model constants was shown. The best results were obtained by use of simple quasi-chemical rate expressions.

ACKNOWLEDGEMENTS

My sincere and grateful thanks are due to my supervisor, Professor J.B. Moss. Throughout, the advice and guidance he gave was invaluable, and he was patient, understanding and encouraging through the difficult times.

On the programming front, I owe a large debt of gratitude to Jonathan Haynes, of Cranfield Computer Centre. On many occasions, his input gave the necessary break-through when progress was halted by incomprehensible bugs in the FORTRAN coding, the Uniras software and even the FORTRAN compiler.

Barbara Wilson was long-suffering in helping with other practical matters.

I would like to thank my family for their continuous support and encouragement and without whom the project would never have been done. Finally there are many others, too many to list here, who have contributed in diverse ways. I am particularly grateful for the huge support of many friends in Cranfield Christian Union; their kindness and love will be richly rewarded.

The funding for the project was by means of an SERC grant.

"Great is the LORD and most worthy of praise;
His greatness no-one can fathom"
Psalm 145 v 3

CONTENTS

FIGURES

TABLES

NOTATION

a - soot-model constant for radical nuclei conversion to soot particulates [s^{-1}]
avg - cylinder average (Table 3.1)
A - pre-exponential constant in soot formation/oxidation equations
- pre-exponential constant in combustion rate expression [-]
- soot-model constant for the rate of spontaneous formation of radical nuclei [s^{-1}]

A_c - cross-sectional area of cylinder [m]
A_{cloud} - surface area of soot cloud [m^2]
A_{orf} - orifice area in Knight SMD expression (equ. 4.25) [m^2]
$A_{(t)eff}$ - area term in Knight SMD expression (equ. 4.25) [m^2]
AFR - air-to-fuel ratio [-]
b - soot-model constant for eliminated incipient nuclei [$m^3\,s^{-1}$]
B - soot model constant
- mass transfer number [-]
- cylinder bore [m]

B_Y - mass transfer number (equ. 4.61) [-]
c - concentration [$kg\,m^{-3}$]
c_p - specific heat capacity at constant pressure [$J\,kg^{-1}\,K^{-1}$]
$comp$ - compositional
C - carbon [kg]
- soot model constant
- turbulence model constant (equ. 4.73)

C_D - turbulence model constant [-]
C_f - velocity coefficient at given radial position in axisymmetric jet [-]
C_{pre} - constant in Kono's combustion rate expression (equ. 4.85) [-]
CA - crank angle [degrees]
d - soot particle size [m]
d_o - nozzle diameter [m]
d_o' - equivalent nozzle diameter [m]
D - droplet size [m]
- soot model constant
- nozzle diameter [m]

D_b - bowl diameter [m]
D_{32} - Sauter Mean Diameter (SMD) [m]
E - soot model constant
E_a - activation energy for spontaneous formation of radical nuclei [$J\,mol^{-1}$]

E_A - activation energy in combustion rate expression (equ. 4.83) [J mol^{-1}]
E_f - activation energy for soot formation [J mol^{-1}], or [kcal/mol] where stated
E_o - activation energy for soot oxidation [J mol^{-1}], or [kcal/mol] where stated
f - shape factor [-]
- soot-model constant for radical nuclei chain branching [s^{-1}]
f_v - soot volume fraction [-]
f_v^∞ - 'final' soot volume fraction (equ. 3.13) [-]
F - stoichiometric mass of fuel per unit mass of oxygen [-]
g - soot-model constant for radical nuclei termination [s^{-1}]
- acceleration due to gravity [m s^{-2}]
g_o - soot-model constant for the conversion of radical nuclei to soot particulates [m^3 s^{-1}]
G_{ed} - turbulence parameter in Murakami's expression (equ. 4.70)
h - instantaneous clearance height [m]
- heat-transfer coefficient [J K^{-1} s^{-1}]
HR - heat release (Table 3.1) [J deg^{-1}]
inj - injection rate profile or injection total and full description of timing (Table 3.1)
k - turbulent kinetic energy per unit mass [m^2 s^{-2}]
k_A - soot model constant for oxidation at reactive A-sites in Nagle oxidation expression (equ. 3.35)
k_B - soot model constant for oxidation at unreactive B-sites in Nagle oxidation expression (equ. 3.35)
k_{SG} - soot model constant for surface growth
k_T - soot model constant for thermal rearrangement in Nagle oxidation expression (equ. 3.35)
k_Z - soot model constant in Nagle oxidation expression (equ. 3.35)
k_1 - pre-exponential factor in Magnussen soot oxidation equation (equ. 3.32)
k_2 - pre-exponential factor in Magnussen soot oxidation equation (equ. 3.32)
K - coagulation constant (in Smoluchowski equation, equ. 3.27)
K_a - overall absorption coefficient [-]
K_1 - parameter in Magnussen soot oxidation expression (equ. 3.32) for rate of adsorption and rate of reaction (equ. 3.32)
K_2 - parameter in Magnussen soot oxidation expression (equ. 3.32) for rate of desorption (equ. 3.32)
K_7 - constant in Benson's evaporation rate expression (equ. 4.65)
K - rate of change of kinetic energy in the system [J s^{-1}]
Kn - Knudsen number (= mean free path/particle radius)
l - radial position of package [-]

l_l - macroscale of turbulence [m]
L - break-up length [m]
- latent heat [J kg^{-1}]
- nozzle length [m]
L_b - break-up length (Fig. 4.1) [m]
L_{cloud} - size of spray soot cloud [m]
Le - Lewis number (= $\lambda/\rho D_{12} c_p$) [-]
L_c - length of smooth spray column (Fig. 4.1) [m]
L_d - effective origin of deformation cone (Fig. 4.1) [m]
L_{noz} - nozzle length [m]
L_s - effective origin of spray cone (Fig. 4.1) [m]
m - mass [kg]
- mass of mixture [kg]
- mass transfer into fine structure [s^{-1}]
- mass of fuel droplet [kg]
- mean over whole of combustion period (Table 3.1)
m_{min} - smaller of the fuel mass and the air mass divided by the stoichiometric air-fuel ratio [kg]
m_{reac} - instantaneous mass of reactants [kg]
$\dot{m}$ - non-dimensionalised exchange rate of mass with fine structures [s^{-1}]
- mass transfer rate [kg s^{-1}]
map - spatially-resolved measurements (Table 3.1)
n - total number of cross-jet zones [-]
- radical nuclei concentration [particles m^{-3}]
N - engine speed [rpm]
- particle number density [particles m^{-3}]
- soot particle number density [particles m^{-3}]
- number of moles of gas [mol]
N_s - swirl speed [rpm]
O - oxygen [kg]
Nu - Nusselt number (= hD/λ) [-]
p - pressure [Pa]
par - parametric variation given (Table 3.1)
P - general parameter
Pr - Prandtl number (= $\mu c_p/\lambda$) [-]
q - constant in surface tension expression (equ. D.1)
- heat flux [J m^{-2}]
Q - heat [J]
- injection quantity [m^3/stroke]
r - radius [m]

r_{def} - tangential deflection from jet centreline [m]
r_s - swirl ratio [-]
R - gas constant [J kg^{-1} K^{-1}]
Re - Reynolds number (= $\rho UL/\mu$) [-]
Ri - Richardson number (= $g\Phi/u_{inj}^2$) [-]
R_{xfer} - rate of transfer through heated fine structure [s^{-1}]
S - radial penetration distance of jet tip, or a zone mass centre [m]
Sc - Schmidt number (= $\mu/\rho D_{12}$) [-]
S_{lam} - laminar flame speed [m s^{-1}]
S_p - instantaneous mean piston speed [m s^{-1}]
S_s - radial penetration distance of jet tip, or a zone mass centre, under swirl deflection [m]
soot - soot concentration or two-colour method KL factor (Table 3.1)
t - time [s]
t' - equivalent time [s]
- time during oxidation phase, measured relative to t_*, when soot formation has been completed (equ. A.5) [s]
t_* - time at which soot formation is completed [s]
T - temperature [K]
- flame temperature measured by 2-colour method or an appropriate model temperature (Table 3.1)
T_{br} - ratio of boiling temperature to critical temperature [-]
T_r - ratio of fuel droplet temperature to critical temperature [-]
u - general velocity [m s^{-1}]
- specific internal energy [J kg^{-1}]
u_{throat} - velocity through throat of a prechamber-type engine [m s^{-1}]
u' - turbulent velocity or turbulence intensity [m s^{-1}]
U - zone velocity [m s^{-1}]
U_o - injection velocity [m s^{-1}]
v_{sq} - instantaneous squish velocity [m s^{-1}]
V - volume [m^3]
V_b - bowl volume [m^3]
V_f - volume of fuel injected (per stroke) [m^3]
We - Weber number (= $\rho u_\infty^2 r_{drop}/\sigma$) [-]
X - mass fraction [-]
- fraction of particle surface covered by active sites [-]
- axis in direction of injection
X_{mix} - parameter defining the extent of mixing with 'spray average' mixture
$X_{reac\rightarrow pro}$ - parameter defining fraction of mixture passed from reactants to products region [-]

Y - mass fraction [-]
- axis perpendicular to injection direction and perpendicular to cylinder axis

z - distance from crown top to cylinder head [m]

Z - axis collinear with cylinder axis

α - empirical constant in turbulent entrainment equation (equ. 4.1) [-]

α_e - entrainment coefficient [-]

β - general evaporation expression constant (evaporation constant or burning constant) [$m^2 s^{-1}$]

β - empirical constant in turbulent entrainment equation (equ. 4.1) [-]

γ - mass fraction in fine structure level of turbulence [-]

δ - small change

δ_T - thickness of thermal boundary layer [m]

Δ - change

ΔH - heat of combustion [$J kg^{-1}$]

Δp - differential pressure between fuel and ambient gas [Pa]

ε - dissipation rate of turbulent kinetic energy [$m^2 s^{-3}$]
- emissivity [-]

ζ - constant for turbulence in Benson's evaporation rate equation (equ. 4.65)

η_{eff} - volumetric efficiency [-]

η_t - constant of proportionality in turbulence equation (equ. 4.76) [-]

θ - crank angle change [degrees]
- angular coordinate
- spray angle

θ_s - angle of spray cone

θ_d - angle of deformation cone

λ - thermal conductivity [$J m^{-1} s^{-1} K^{-1}$]
- Taylor microscale [m]

μ - coefficient of viscosity [$kg m^{-1} s^{-1}$]

ν - kinematic viscosity [$m^2 s^{-1}$]

ρ - density [$kg m^{-3}$]

σ - surface tension [$N m^{-1}$]
- Stefan-Boltzmann constant [$W m^{-2} K^{-4}$]

τ - period of time, timescale [s]
- relaxation time (equs. 4.64, 4.95) [s]

ϕ - equivalence ratio [-]

Φ - burner diameter [m]

χ - ratio of total burnt fuel to total fuel in fine structures or in a zone [-]

ω - angular velocity [$rad s^{-1}$]

Superscripts

- - start of calculation timestep
+ - end of calculation timestep
* - high mass transfer
l - general exponent
m - general exponent
n - general exponent

Subscripts

a - air
ab - burnt air
Ar - Argon
atm - atmosphere
b - burning
brk - breakup
B - boiling condition
c - critical
chem - chemical
cl - centreline
cloud - soot cloud in spray
comb - combustion
comp - complete spray
crit - sooting limit
cs - cylinder surface
cyl - cylinder
C_2H_2 - acetylene
d - droplet
diff - diffusion burning
drop - droplet
D - drag
ent - entrainment
eva - evaporated fuel
ex - exhaust
f - fuel
- formation
- mixture fraction, or unburnt mixture fraction

fb - burnt fuel

fl - flame front
flame - flame propagation
for - formation
g - gas
id - ignition delay
ign - ignition
incomp - incomplete spray
inj - injection
inj, m - relating to the centre of gravity of a zone (mean injection timing)
ip - injection period
ivc - inlet valve closing
j - jet
I - integral
K - Kolmogorov
l - radial position of package
last - relating to the last calculation timestep
lim - limit
liq - liquid
local - referring to conditions at a particular point in the chamber
m - mixing
mean - mean
mix - mixing
n - number of carbon atoms per molecule
nor - normal
ntp - normal temperature and pressure
nuc - radical nuclei
o - initial
- spontaneous formation
- zero-convection conditions
OH - hydroxyl
O_2 - oxygen
ox - oxidation
pm - premixed
pro - products of combustion
q - quiescent
rad - radiation
reac - reactants
ref - reference temperature and pressure
s - swirl

sg - surface growth
soot - soot
spray - within the fuel spray
sto - stoichiometric
su - surface
tan - tangential
tot - total
wall - wall
xover - cross-over from underweighting to overweighting (equ. F.4)
zone - zone

θ - radial
1 - start of calculation timestep conditions
2 - end of calculation timestep conditions
$\overline{}$ - cylinder average
∞ - bulk conditions

GLOSSARY

API	-	measure of fuel quality on American Petroleum Institute gravity scale
CO	-	carbon monoxide
CFD	-	computational fluid dynamic
CRC	-	Coordinating Research Council
DI	-	direct-injection diesel engine
EDC	-	eddy dissipation concept
EGR	-	exhaust gas recirculation
EPA	-	environmental protection agency
HC	-	hydrocarbon
IARC	-	International Agency for Research on Cancer
IDI	-	indirect-injection diesel engine
multi-D	-	multidimensional models
n/a	-	not applicable
N_2	-	nitrogen molecule
NO_x	-	oxides of nitrogen (nitrogen dioxide, NO_2; nitrous oxide, NO)
O_2	-	oxygen molecule
OH	-	hydroxyl radical
PAH	-	polyaromatic hydrocarbon
PCAH	-	polycyclic aromatic hydrocarbon
PM10	-	particulate matter having aerodynamic diameter less than 10μm, i.e. that passes through a size-selective inlet with a 50% efficiency cut-off at this point
quasi-D	-	quasi-dimensional models, i.e those having and element of dimensionality by use of zones
RCM	-	rapid compression machine
SMD	-	Sauter Mean Diameter (diameter of droplet having same surface-to-volume ratio as that of the total spray)
SOF	-	soluble organic fraction
turbostratic	-	composed of planes oriented at random
TWC	-	three-way catalyst
zero-D	-	zero-dimensional models

CHAPTER 1 - INTRODUCTION

Over the past two decades, diesel engines have captured an increasing proportion of the market for automotive powerplants. This has come about for a variety of reasons, including a narrowing of the performance gap with petrol engines, the general rise in oil prices, changing public opinion and increasing concern over environmental issues. However, despite many clear advantages, the diesel engine also has a number of drawbacks, the most serious of which is the emission of smoke. The main concern over this pollutant is connected with its potentially serious effects on human health. As a consequence, in an environment of rapidly-changing technology and legislation, the situation facing the future use of diesel engines is uncertain.

The increased popularity of the diesel is largely a reflection of its intrinsic advantages over petrol engines in terms of efficiency, maintenance, and the levels of some important emissions. Higher efficiency gives lower fuel consumption and hence a smaller output of carbon dioxide, which is the major contributor to global warming. Also, typical levels of carbon monoxide (CO) and hydrocarbon (HC) emission from a diesel engine are much lower than those of standard petrol-engined cars.

In Europe, this situation is changing following the advent of the three-way catalyst (TWC) on new petrol-engined vehicles. The use of catalysts has been necessitated by the 1992 emissions legislation (91/441/EEC)[111] which required a very severe reduction of CO, oxides of nitrogen (NO_x) and HC emissions. Catalyst-equipped vehicles emit CO and HC at levels comparable to those of a diesel whilst the diesel's advantage in terms of NO_x is reversed. Because diesel engines operate at lean fuel-to-air ratios, they cannot use TWCs, though oxidation catalysts are increasingly employed to reduce CO and HC levels. Thus, in standard mode, diesels are now at a slight disadvantage in terms of gaseous emissions. Also, in comparison to diesel, petrol-engine particulate emissions are negligible[111]. Thus, due to the improved emissions performance of TWC vehicles, the diesel engine has now become the main focus of environmental concern.

The problems mitigating against more widespread use and acceptance of diesels are not confined simply to emissions. They are in fact complex and interrelated. Diesels are generally expensive, noisy and they have a low power-to-weight ratio.

Emissions of both smoke and NO_x are a major problem. Unfortunately, the higher temperatures and longer residence times associated with low smoke give high NO_x levels and vice versa, resulting in the well-known trade-off. Unpleasant smell is associated with hydrocarbon compounds adsorbed on the soot particles in the smoke. The high smoke levels at increased loads constrain diesels to operate at overall fuel-to-air ratios 20-30% lean of stoichiometry, and this contributes to their poor power-to-weight ratio. For smaller engines, indirect-injection (IDI) is used to permit higher running speeds with lower emissions and noise, but this reduces efficiency. Besides purely technical issues, the diesel has traditionally suffered from having a poor public image.

Smoke is a broad term used to describe visible emissions from a diesel engine. A more precise expression is 'particulate' which is defined as all solid and liquid material which can be collected on a filter paper from diluted exhaust at temperatures below 52°C, excluding moisture[253,372]. Particulate composition varies considerably according to engine type and operating condition. Generally smaller proportions of solid carbon (soot) and greater proportions of soluble organic fraction (SOF) are produced by DI diesels[111] and under light loads[258] (Fig. 1.1).

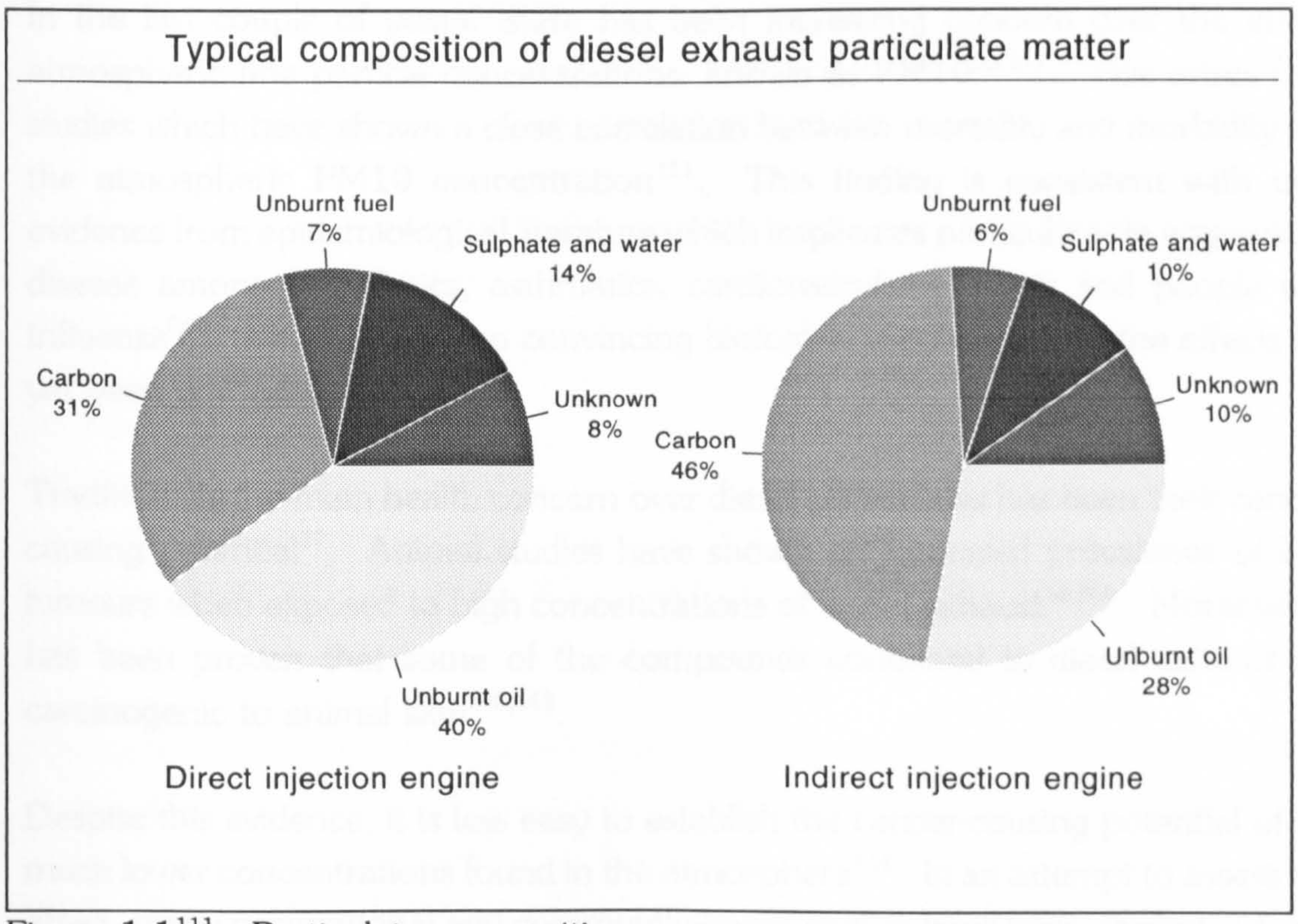

Figure 1.1[111] - Particulate composition

The contribution of diesel smoke to atmospheric suspended particulate matter has been estimated using organo-metal tracer studies. A 1984 study in Vienna, where diesels made up 8% of the vehicle population, found that diesel particulates constituted 12-33% of the total aerosol mass[111]. In terms of black smoke, which is non-reflective dark particulate matter, diesels were responsible for 39% of UK national emissions in 1991, but contributed substantially more in urban areas, e.g. 87% in London[111].

The human health implications of exposure to diesel exhaust smoke are potentially very serious. The particles contained in the exhaust are very small, about 0.2 microns in diameter, and they therefore penetrate deeply into the human lung. Adsorbed to their solid carbonaceous core are a multitude of fuel-derived hydrocarbons and inorganic compounds, including poly-aromatic hydrocarbons (PAH). It has been noted that "most of the toxic trace metals, organics or acidic materials emitted from automobiles or fossil fuel combustion are highly concentrated in the fine particle fraction"[360]. Though it is hard to establish the effects with certainty, there is now a considerable body of evidence which links emissions to respiratory diseases and cancer cases.

In the last couple of years, there has been increasing concern over the effects atmospheric fine particle concentrations, known as PM10[32,117]. This arises from studies which have shown a close correlation between mortality and morbidity and the atmospheric PM10 concentration[111]. This finding is consistent with clear evidence from epidemiological literature which implicates particulates in aggravating disease among bronchitics, asthmatics, cardiovascular patients and people with influenza[360]. Nevertheless, no convincing biological mechanism for the effects has yet been advanced[111].

Traditionally the main health concern over diesel particulates has been their cancer-causing potential[17]. Animal studies have shown an increased prevalence of lung tumours when exposed to high concentrations of diesel exhaust[18,360]. Moreover, it has been proven that some of the compounds contained in diesel exhaust are carcinogenic to animal skin[298,343].

Despite this evidence, it is less easy to establish the cancer-causing potential of the much lower concentrations found in the atmosphere[111]. In an attempt to assess this effect, many occupational and community-based studies have been carried out, and

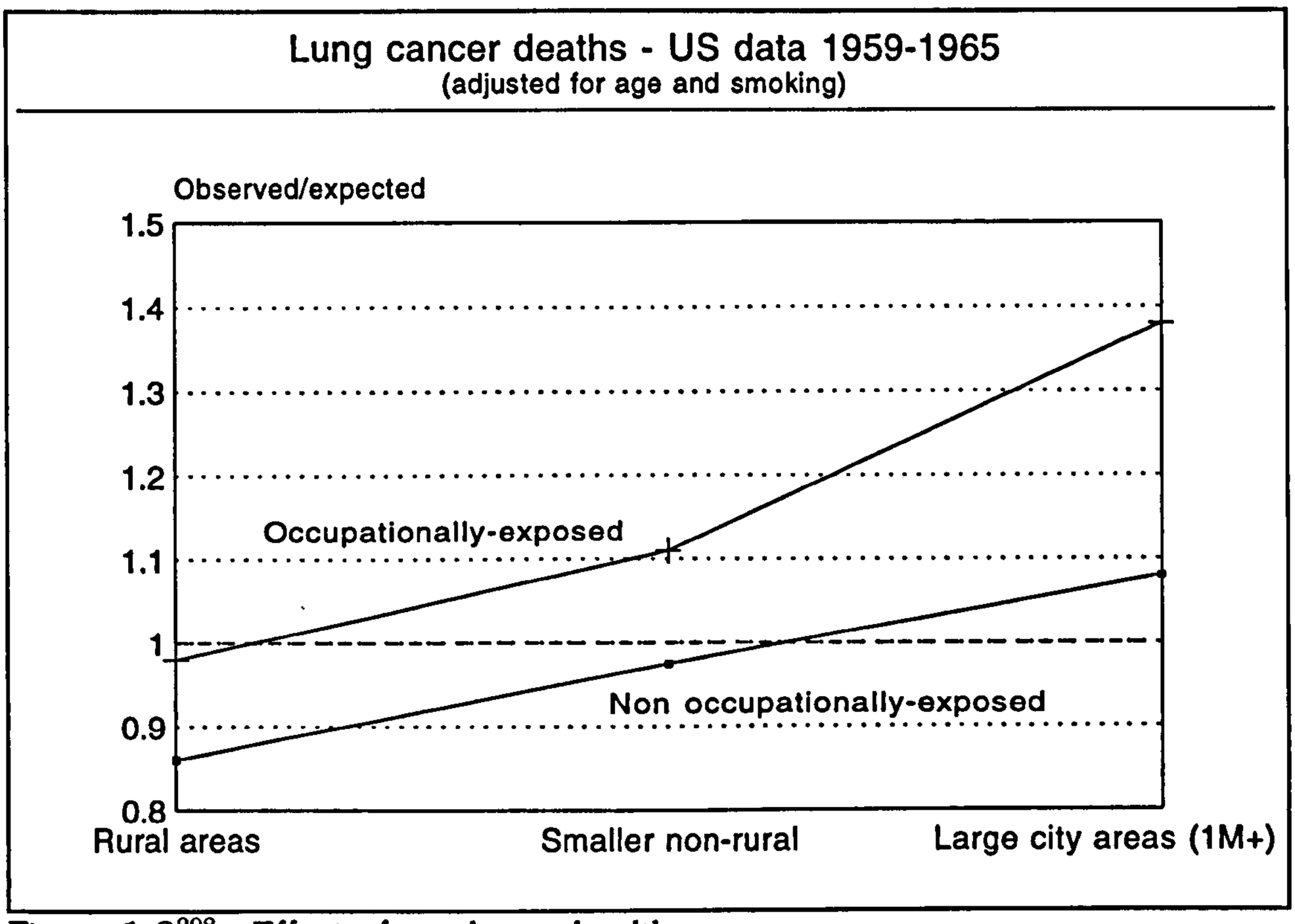

Figure 1.2[298] - Effect of smoke on health

though some have shown no enhanced risk (Terblanche, 1991[343]), others do give a positive result, including one major US study (Fig. 1.2)[298]. Together with animal studies, this has led the IARC to classify diesel exhaust as 'probably carcinogenic'[111].

Besides adverse health effects, diesel exhaust soils building fabric and has various adverse climatic effects. In fact, smoke is the major source of grime in cities[18,111], supporting a stone-cleaning industry valued at about £100M in the UK[111]. The general climatic effects of diesel smoke are complex and poorly understood, but the overall effect on global warming is probably positive[111]. Local effects are more obvious, and in the urban environment, diesel exhaust is a major source of visibility reduction and can exacerbate foggy weather conditions. Finally, the smell and smoke from traffic is found objectionable by the public, even if exposure levels are safe.

Smoke and NO_x emission are interrelated and the environmental impact of the latter is also of serious concern. NO_2 is toxic and World Health Organisation Air Quality Guidelines have been exceeded in fog-related incidents in British cities in recent years. NO_x also contributes to acid rain, photochemical ozone and global warming.

There has been a call for a 50% reduction in levels, and since a typical diesel produces twice as much as a TWC petrol engine, there is pressure to keep diesel NO_x emissions as low as possible[111].

Thus, there can be no doubt that the environmental impact of diesels is serious. A detailed UK study which looked at the effect on urban air quality concluded that "increased market penetration of diesel cars at the expense of TWC petrol cars will on balance have a deleterious effect on urban air quality"[111]. The current view of some American workers is that the potential health problems created by particulate matter far exceed those posed by gaseous pollutants[111].

The general response to the problems of particulates has been to set regulated limits. In recent years, legislation governing emissions from new and in-service vehicles has been put in place in many parts of the world. In Europe a new mass-based standard, 91/441/EEC, took effect on type approval for cars from July 1992, replacing the old visibility-based limits[111]. This sets a level of 0.18 g km^{-1} over the standard test cycle (88/76/EEC). The most recent proposal (COM (92) 572 Final SYN 448) specifies a reduced level of 0.08 g km^{-1} from January 1995. A parallel reduction in diesel sulphur content from 0.3 % to 0.05 % will assist in meeting this standard. In America, a mass-based limit of 0.124 g km^{-1} (over the EPA cycle) was introduced in 1987. This was reduced to 0.05 g km^{-1} in 1994 and low-sulphur fuel was introduced in 1993[138].

In order to meet these new legislated standards demanding the simultaneous reduction of NO_x and soot levels, a whole range of technologies has been developed. The main thrust has been towards improving the combustion process to achieve a better balance of efficiency, emissions and noise. Electronic injection is now used to give precise control of the injection profile and timing; higher injection pressures result in better fuel atomisation, whilst careful chamber and manifold design gives improved airflow and mixing; exhaust gas recirculation (EGR)[265] and turbocharging are also increasingly applied, reducing temperatures and increasing full-load aeration, respectively. Intensive work on exhaust gas after-treatment techniques is being undertaken. The use of particulate traps to filter out soot is showing good potential but is not yet commercially viable for mass production[72,134,141]. On the other hand, oxidation catalysts have been successfully applied on production cars for a number of years[177], and are likely to become standard on cars meeting 1996 limits. However, though they virtually eliminate

odour, they do not substantially reduce the mass of particulate emitted.

Generally, advances have been made by using a combination of the above strategies together with meticulous development work. Increasingly this is assisted by computer modelling techniques. A model is a flexible tool which allows the engineer to apply basic knowledge of engine sooting processes at the design stage. It draws together information derived from a range of other sources, including fundamental empirical studies in simplified combustion systems and real engines. Overall, the above technologies have brought about a considerable improvement in the all-round performance of diesels, but there nevertheless remains intense pressure for a simultaneous reduction in soot and NO_x levels.

There is no simple solution to the reduction of smoke, but the key to any significant advance will be an improved knowledge of the processes governing its emission. Despite much previous work, the fundamental aspects of these processes in diesel engines are still poorly understood. In reviewing combustion modelling of heterogeneous charge engines, Primus[280], 1987, identified "a more fundamental handling of carbon and hydrocarbon formation mechanisms for assessing carbon particulate emission" as one of the two critical issues at the time. There has been no major progress since that date, while there is an increased urgency about emissions reduction.

The lack of an in-depth understanding of diesel smoke emission is partly a reflection of the complexity of the problem and is also due to the difficulty of studying the process in the engine environment. Though there is a mass of data, both from diesels and other experimental arrangements, it is not a simple task to extract information which can be used in a predictive sense. With in-cylinder measurements, it is difficult to separate out the formation and oxidation processes, since they overlap in time and space, and fluid elements are continually mixing. Relationships derived from basic experimental studies are generally only appropriate to the idealised environment of the particular combustion system. Great care must be taken if this knowledge is to be usefully applied to the diesel.

Clearly an improved understanding of the basics of sooting processes and the development of more robust computational models go hand-in-hand. The focus of the current work is model development. Though insight into the emission process is available from other approaches, the use of simulation techniques offers the most

realistic method of addressing the enormous complexity of the diesel combustion process. Once established, a model which includes emissions prediction is a powerful tool with a variety of uses. For instance, since a soot emission model is usually based on a spatially-resolved combustion model, it allows investigation of the relationship of soot formation and oxidation to the mixture conditions. It is relatively straight-forward to use such a model to provide data on engine performance and, if needed, other emissions, and this information is an important background to the analysis of sooting behaviour. Also, by use of parametric studies it is possible to reveal the relationship between the sooting process and engine design parameters and to identify critical design features. Such knowledge contributes to the ability to produce designs which are 'right-first-time' and cuts down on the necessity of expensive development work. Finally, with reference to the current work, the key advantage of an engine simulation is that it can be used as a platform for the development of improved emissions models for diesel engines. Overall, there is a potential for gaining a deeper understanding of diesel soot emissions and for the productive application of this knowledge in engine design.

An important characteristic of emission processes is their non-linearity which means that they tend to be very sensitive to the variation in conditions across the combustion chamber. Therefore any useful model must contain some representation of the different states existing in the mixture, whether it be a spatial description, using zones, or a characterisation of the combustion regimes according to mixture composition, as in stochastic models. In addition, it is important that the computational demands are relatively low, so that the full potential of any soot models can be exploited. The above requirements are best met by phenomenological models of the quasi-dimensional (multizone) or stochastic variety. Many such models have been developed, with the majority being of the zonal type.

Soot calculations have been incorporated into ten phenomenological models. Eight of these are of the multizone type - those originating with Kau[164,165,371], Hiroyasu[124,126,127,262,197], Dent[57,198,237], Kono[184], Kouremenos[190], Payri[271], Zhou[389] and Bazari[19,327]. The others of the stochastic type include the indirect-injection engine model of Mansouri[188,227,228] which was subsequently applied to direct-injection engines by Brown[37], and the hybrid multizone model of Xiao[378] used for indirect-injection engines. Altogether, soot formation has been described using eight different expressions, whilst five have been used for oxidation. The formation mechanisms range from a simple chemical equilibrium assumption to empirical

correlations derived from both basic experimental studies and diesel engine measurements. The oxidation correlations were established using simple combustion experiments and in one case by the eddy break-up theory of turbulent combustion. Thus, no consensus has been reached on the choice of soot model correlations or method of application, though most of the later models (Kono[184], Kouremenos[190], Wade[356], Lapuerta[349], Zhou[389], Nishida[262], Bazari[19,327]) have used the simple Arrhenius equations for formation and oxidation which were proposed by Hiroyasu[126].

The main attraction of the latter model is its simplicity and ease of implementation. However, the expressions for formation and oxidation require calibration by matching the model output to measured levels of exhaust smoke concentration. Since the computed exhaust levels result from the difference between two large quantities - the total amount formed and the total amount oxidised - this approach lacks a fundamental basis. Some of the other models are more elaborate and relatively good results have been published. However, no attempts have been made to examine sensitivity to the performance of the combustion model or to extend the study to different combustion regimes and engines. Thus, little indication is given of the reasons for the apparent success of such models and their all-round strength remains questionable.

In order to adequately address the above problems, it was decided to develop a phenomenological model of the multizone type for diesel combustion simulation. An important goal is to establish with more certainty the validity of the various expressions proposed for soot prediction in the diesel. The first level of the evaluation is to examine performance of the individual models in terms of calculated rates and sensitivities. Since several of these correlations were established under conditions far removed from those encountered in diesel engines, there are many questions to be answered concerning their general applicability in the diesel engine. Further useful information is revealed by constructing the model so as to allow a comparative analysis. The relative strengths of the models may be established and those which are best-suited to use in diesels identified.

In the gas turbine field, a number of comparative studies have been undertaken which have examined several of these correlations (Ahmad, 1982[3]; Mullins, 1987[243]; Coelho, 1993[47]). However, gas turbines operate at much lower pressures than those found in diesel engines, and the analyses have been made from the point

of view of CFD prediction. In the field of diesel engine modelling, no previous work has attempted any comparative analysis. Therefore, the comparative study of several soot correlations and underlying thermodynamic structures is a novel aspect of the current work. Most of the expressions previously applied in diesel engine simulations have been examined, together with others from the general combustion literature. The overall aim of establishing a more solid predictive capability is achieved by a critical examination of the different modelling approaches.

Validation of both soot and combustion models is achieved by comparison with existing published measurements. In particular, the extensive dataset published by Kamimoto et al. at Tokyo Institute of Technology[11,158,159,160,230] has been used to establish satisfactory performance of the combustion model over a range of operating conditions.

The thesis is divided into six chapters. Following the introduction, chapter 2 describes the techniques applied to the modelling of combustion in diesel engines. Sooting-process fundamentals and modelling are reviewed in chapter 3. Chapter 4 outlines the combustion model developed in the current work, reviewing in turn each of the engine phenomena for which major sub-models have been built; basic details of the implementation are given. Chapter 5 presents the model results and findings. Chapter 6 reports the conclusions.

The following conventions are used. References are listed alphabetically at the back of the thesis. They are also numbered consecutively and referred to in the text using a superscript[xxx]. Where the author's name is given in the text, in most cases only the first author of a paper is given. In review sections, the first mention of the work of a particular group of workers is indicated by highlighting the name of the first or main author using a **bold** font.

CHAPTER 2 - COMBUSTION MODELLING

This chapter describes combustion-modelling techniques applied to the diesel bearing in mind the requirements of emissions models. In section 2.1 some key features of the diesel combustion process are described to provide a background for the modelling analysis. Section 2.2 discusses general modelling techniques with a particular emphasis on phenomenological models of the multizone or stochastic variety. Existing models are briefly reviewed.

2.1 DIESEL COMBUSTION PROCESS

The diesel-engine combustion process is described in various textbooks[13,116] and in review papers by Kamimoto[161] and Henein[115]. The essential features are as follows. Near to the end of the compression stroke, liquid fuel is injected directly into the chamber. The cylinder contains a mixture of fresh air charge and a small proportion of combustion residuals from the previous cycle. The injection pressure is between 30 and 150 MPa, whilst the chamber pressure reaches 4-12 MPa by TDC in the absence of combustion[161]. The fuel forms a high-velocity jet and is rapidly atomised to individual droplets. Spray structure is complex, but there is always a fuel-rich core region[381]. Evaporation takes place rapidly in the high-temperature environment (1000-1200 K at TDC)[161] and some of the fuel is mixed intimately with the air mainly by turbulence. During a short ignition delay period (several degrees of crank angle, or about 1ms), precursive chemical reactions begin to occur. Then, because the temperature and pressure are above the fuel ignition point, spontaneous ignition occurs at various points in the spray. Typically at the start of combustion, 70-95% of the fuel will have evaporated, whereas only 10-35% is mixed to within the flammability limits[196]. Thus, the combustion process is controlled mainly by mixing rather than evaporation[161].

Following ignition, the portion of the fuel which has been mixed to within the flammability limits during the ignition delay period is rapidly consumed. The predominant combustion mechanism is premixed burning and the pressure rises sharply. Subsequent combustion is dominated by diffusion burning, and for a while, the spray continues to burn in a quasi-steady manner, as liquid fuel is injected into the burning region. Combustion chemistry is complex, with the reactant species first being thermally decomposed to give pyrolysed hydrocarbons[147,100]. A

significant proportion of the fuel is converted to soot, though most is subsequently oxidised. The diffusion 'flame' burns with the bright yellow colour characteristic of burning soot.

The rate of diffusion combustion is controlled by the mixing rate of the reactants, which is generally about three orders of magnitude slower than the chemical rate[277]. The air, fuel vapour and combustion products tend to be confined in separate eddies of the turbulence structure. Combustion can only occur once intimate mixing has taken place at the finest turbulence level, known as the Kolmogorov scale. Thus, the local combustion rate is strongly influenced by turbulence parameters. On a global level, the heat-release rate closely follows the rate of air entrainment into the spray[159]. This in turn is related to the spray behaviour and the in-cylinder air motions on both micro and macro-scopic levels. The inter-relationship is complex, because both fuel injection and combustion give an increase in the turbulence levels, but tend to reduce the bulk air motions[147]. Also, wall impingement accelerates combustion[161]. Fig 2.1 summarises some of these processes.

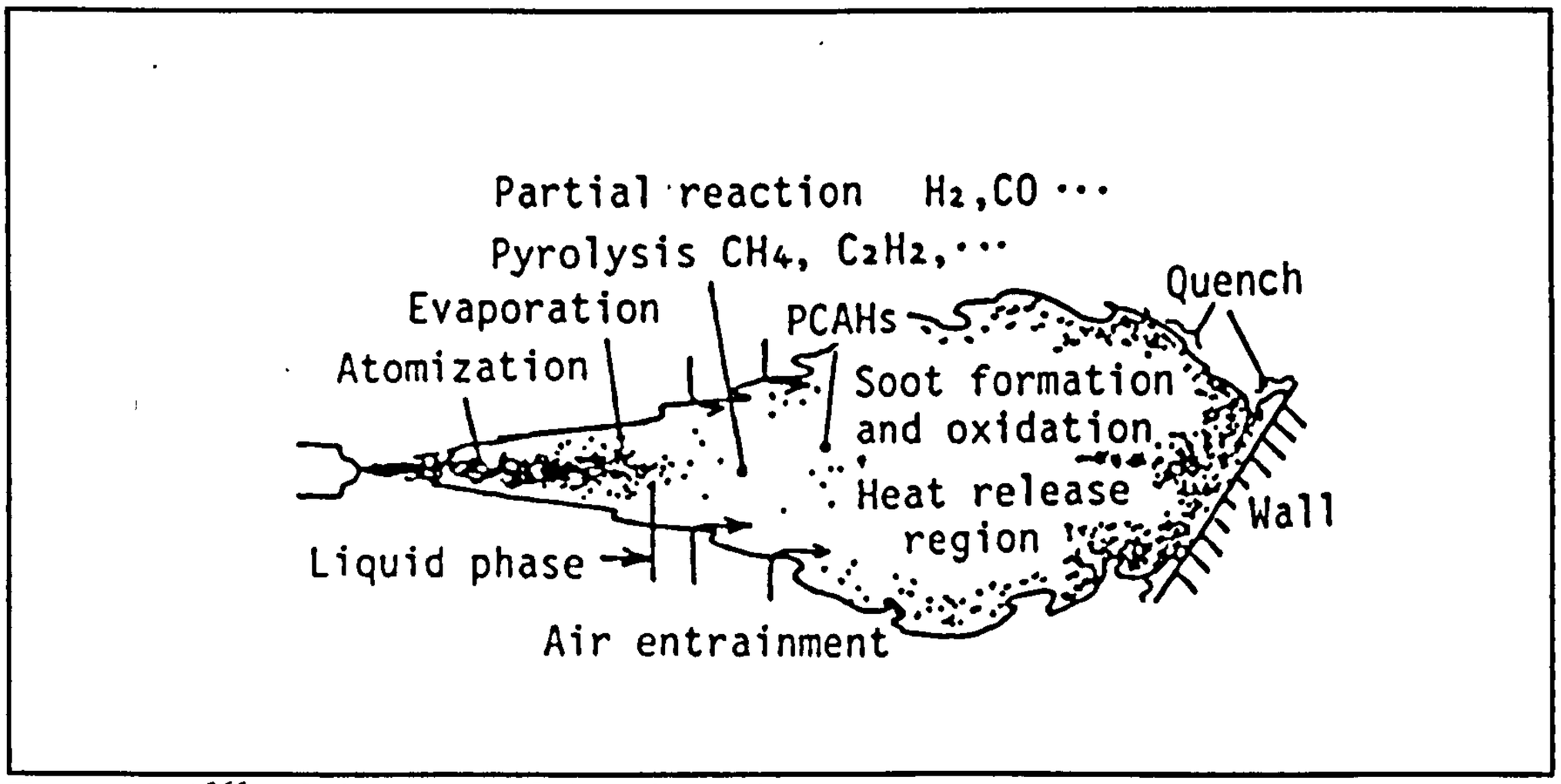

Figure 2.1[161] - Schematic of diesel combustion process

Eventually, virtually all the fuel has been atomised, vaporised, mixed and burnt. Because diesel engines are operated at equivalence ratios which are overall lean, excess air remains, and this continues to mix with the burnt products during the expansion. The chamber contents become increasingly homogeneous. Finally, because pressures are generally higher than in a spark-ignition engine, the exhaust

temperatures also tend to be higher, often above 1000 K[116].

In summary, diesel-engine combustion is fundamentally controlled by mixing processes. Kamimoto considers that the representation of the uneven structure resulting from turbulent mixing is the most significant task in mathematical modelling[161]. A number of features distinguish the combustion in a diesel engine from that of a steady turbulent diffusion flame, including the following:

(1) *Combustion is unsteady having three distinct phases: ignition delay, premixed-burning and diffusion-burning.*

(2) *Combustion takes place in a confined space and wall impingement effects are important.*

(3) *Combustion takes place in an atmosphere of varying composition.*

Some of the main characteristics of the process are summarised in Table 2.1 using modelling terminology.

Condition of combustion	Classification
Time-dependency	Unsteady
Spatial-dependency	3D
Spatial restrictions	Confined
Initial reactant condition	Non-premixed
Flow condition	Turbulent
Phase of reactants	2-phase
Rate of reaction	Finite rate

Table 2.1 - Classification of diesel-engine combustion processes

2.2 COMBUSTION MODELLING METHODOLOGY

The techniques chosen for modelling the combustion process have a big impact on emissions prediction. This is because the combustion model supplies the detailed information relating to mixture composition and thermodynamic state which are essential inputs to the soot model mechanisms. Thus, any generally useful model of emissions will always be underpinned by an accurate representation of the combustion process.

The processes leading to the emission of smoke from a diesel engine are extremely complex. The soot formation and oxidation processes are closely coupled and the former, in particular, is intimately related to the chemistry of the combustion process. Thus, care must be taken that the combustion and soot models are held together in a consistent framework. The combustion regime is also highly turbulent and reactants are often highly localised in turbulent eddies. Moreover, the sooting processes themselves are highly non-linear, so they are very sensitive to variation in conditions, on micro and macroscopic scales. Hence a further requirement of the combustion model is that it provides some representation of the different states existing in the mixture. Finally, if the simulation program is to be used for development work involving parametric studies, it is essential that the strategy adopted is relatively undemanding in computational terms.

2.2.1 Modelling techniques

Many computational models have been developed for diesel-engine simulation, though not all are well-suited to emissions work. The two main classes are phenomenological models and multi-dimensional or computational fluid dynamic (CFD) models. The former consist of a set of independent sub-models describing the important combustion phenomena structured around a thermodynamic analysis. They can be further classified into zero-dimensional models, which compute only chamber averages, and quasi-dimensional and stochastic models which provide some sort of description of the variation in compositions and temperatures within the spray. CFD models solve the governing conservation equations within a computational grid, such that the ensemble-averaged state of the mixture is fully defined at every point in space.

Phenomenological models can be further classified according to the method of representing variations of composition and temperature within the spray. At one level, mixture regions may be characterised purely by composition, which typically means partitioning the mixture into reactants and combustion-products zones. This approach is used in most zero-dimensional models; also, some models which use spatial zones to describe the spray incorporate chamber-averaged zones partitioned by composition[193,271]. Alternatively, the different regions of the mixture may be characterised using some representation of the spatial variation of properties. In most cases this is done using sets of axial and radial zones; these are known as multizone models. In other cases, zones are not used but the distribution of properties within the spray is modelled[170,56]. Each of these model types is referred to as quasi-dimensional, since the spatial information given is not exact three-dimensional information.

Stochastic models use a large number of fluid particles to simulate the range of conditions existing in the chamber. Mixing between particles is modelled statistically[49], using Monte-Carlo techniques; thus a much better description of the range of compositions existing in the spray is achieved. In the simplest case, the position of the particles in the chamber is neglected and a single mixing zone is used. In order to represent some of the macroscopic variation in conditions, a further zonal division has been employed in some cases. For the IDI diesel engine, separate zones have been used for the pre-chamber and the main chamber[228]. In one DI diesel engine model, quasi-dimensionality has been achieved by partitioning into a variable number of zones according to the total air-to-fuel ratio[37]. This represents an intermediate position between zero-dimensional stochastic models and multizone models. Finally, in one case a stochastic model has been superimposed on a zonal description, combining the advantages of both techniques[378].

Of the above model types, the zero-dimensional models are the least useful, since they do not have the required spatial resolution and heat-release calculations usually lack a fundamental basis. The strength of the CFD model is that detailed spatially-resolved predictions are given. Thus, this type of model has a role in the design of the combustion chamber to give advantageous gas flows. However, such models are poorly suited to the prediction of exhaust smoke, and little success has been reported in this area. Additionally, computational limitations do not allow exploitation of the full potential of the soot models.

The above requirements of a realistic emissions model are best met by phenomenological models of the quasi-dimensional (multizone) or stochastic variety. There are several advantages in using this type of model. Because the component submodels are generally independent, any level of detail can be built in within the bounds of experimental knowledge. Together with the fact that some model parameters may be tuned to give a good match to experiment, this ensures that the combustion process may be represented with sufficient accuracy for the purposes of emissions modelling. This contrasts with the CFD approach, where there is limited scope for tuning model constants.

In phenomenological models, there is no restriction on the complexity of the mixture description which can be fed into the emissions model. Thus, the emissions model can take full advantage of the composition and temperature information obtained from the combustion model, for example, in using reactant and combustion product temperatures and a representative range of mixture compositions. Though a CFD model supplies similar information in greater detail, it cannot be used in practice. If a presumed pdf approach is adopted, mixture fraction and soot parameters must be assumed to be uncorrelated, since these relationships are inaccessible. Alternatively, by using Monte-Carlo methods these problems may be overcome, but such models are very demanding computationally. Thus, though a CFD model provides much greater spatial detail, in practice soot-model inputs are confined to local averages.

In the class of interest, quasi-dimensional or stochastic models, much work has already been done (see Table 2.2 in next section). From independent origins, at least eighteen such models have been developed for the simulation of diesel-engine or stratified-charge engine combustion. The majority are of the multizone type and have been applied to direct-injection diesel engines; only three are stochastically-based, including one of only three models which have been specifically applied to an indirect-injection diesel. In some cases the literature reports only a single model, while for others, many versions have been developed from the original, even by independent groups, over periods of more than a decade. Naturally, where there are many versions, different engine specifications have been encompassed.

Phenomenological models are briefly described in the next section and the individual models in the literature are reviewed.

2.2.2 Phenomenological models

2.2.2.1 Introduction

A phenomenological model is a simplified representation of the combustion process, using independent submodels to describe the main physical phenomena. The submodels will often be based on simple correlations which attempt to describe empirical observations, though it is sometimes possible to use more fundamental relationships. Submodels are structured around a thermodynamic analysis which typically employs polynomial functions for the prediction of thermodynamic properties. The thoroughness of a given model is reflected in the scope of the processes it addresses, and in the sophistication of the submodels.

Phenomenological models are distinguished by the techniques used to represent the fluid mechanical processes, particularly the spray behaviour. Quasi-dimensional multizone models cannot provide the exact spatial information familiar to users of detailed or multi-dimensional models. Instead, an approximate approach is employed uses zones representing packets of mixture. The zonal motion is followed by tracking the path of the centre of mass and interaction between zones is not treated explicitly. Thus the model attempts to characterise the spray regimes, while avoiding the huge computational requirements of full and accurate representation of the flow processes. The computational demands of stochastic models are generally intermediate.

A typical range of modelled phenomena is as follows:

Engine dynamics
Gas exchange
Injection
Spray motion and fuel-air mixing
Air motion
Evaporation
Ignition delay
Premixed combustion
Diffusion combustion
Heat transfer - convection and radiation
Emissions

2.2.2.2 Review

The following review outlines the development of phenomenological modelling in diesel engines. It is impossible to give full details of these models; rather, the analysis overviews the work highlighting the contributions from each source. Table 2.2 provides summary information. In view of the importance of the spray model, reference should also be made to Table 4.1 in section 4.1 which provides basic information about the techniques used.

In 1971, **Khan** became the first to apply a quasi-dimensional model to the simulation of diesel-engine combustion[170]. The heat-release rate was obtained from the rate of micro-mixing of the fuel and the air. This represented a major advance over all previous models which used empirically-calibrated correlations. In original form, the variation of composition and temperature within the mixture was described using simple radial and axial profiles. Also, a single mixture region was used for emissions models, so the approach can only be crudely described as quasi-dimensional. However, in later work **Greeves** developed the model by incorporation of a multizone description[99].

Hodgetts[132] implemented a multizone model based on a simple and fairly restrictive spray model. Neglect of the complexity of mixing between reactants and combustion products was postulated as the reason for failure of the model under high-load conditions.

In 1976, **Kau**[164] reported results from a major five-year study for the US EPA and CRC, targeted towards diesel-engine emissions reduction. This comprehensive work included study and review of all previous models[371], the design, construction and operation of a single-cylinder research engine for acquisition of basic data, in-cylinder measurements and the construction of a new multizone phenomenological combustion model. The detailed spray model was based upon the work of Abramovich[2]. The description of fuel-air macro-mixing was identified as a key element of the combustion model. The modelling of diffusion flames using spherical droplet flames was found to be unsatisfactory but excellent predictions of pressure histories were reported.

Main author	Year	Engine	Model type	Authors
Khan	1971	DI	Quasi-D	Khan[170]
	1979	DI	Multizone	Greeves[99]
Wilson	1974	DI	Multizone	Wilson[371]
Hodgetts	1974	DI	Multizone	Hodgetts[132]
Shahed	1975	DI	Multizone	Shahed[309,45]
Hiroyasu	1976	DI	Multizone	Hiroyasu[126], Kuo[197], Shiozaki[314,315]
	1989	DI	Multizone, multi-D diffusion	Nishida[262]
	1982	IDI	Multizone	Hiroyasu[124]
Meguerdichian	1978	DI	Multizone	Meguerdichian[234]
Hiraki	1980	Stratified charge	Multizone	Hiraki[118]
Ikegami	1980	DI	Stochastic	Ikegami[144]
	1992	DI	Stochastic, 3 compositional zones	Kakegawa[157]
Dent	1981	DI	Quasi-D	Dent[56,198,57]
	1986	DI	Multizone	Mehta[104,105]
Mansouri	1982	IDI	Stochastic, 2 spatial zones	Mansouri[227,228]
	1986	DI	Stochastic, multiple compositional zones, multi-D flow	Brown[37]
Watson	1984	DI	Multizone, 1-D spray	Watson[365]
Kono	1985	DI	Multizone	Kono[184]
Kouremenos	1987	DI	Multizone	Kouremenos[190]
	1989	IDI	Multizone	Kouremenos[192,193]
Lipkea	1987	DI	Multizone	Lipkea[213]
Lapuerta	1988	DI	Multizone	Lapuerta[202]
	1991	DI	Multizone, multi-D diffusion	Lapuerta[203]
Zhou	1989	DI	Multizone	Zhou[389]
Xiao	1991	DI	Stochastic, multizone	Xiao[378]
Bazari	1992	DI	Multizone	Bazari[20,327]

Table 2.2 - Phenomenological models applied to diesel-engine combustion

The multizone model of **Shahed**[309] was the first to use a spray model taking transient effects into account. This derived from an experimental study of jet mixing[45]. The spray model also accounted for distortion of the cross-jet profile. Nevertheless, simple fuel-air distributions are imposed upon the jet as in the Hodgetts model[132]. Later work demonstrated the error in this assumption[196].

Hiroyasu first published details of a multizone combustion model in 1976[121]. This was later extended to take into account air-swirl effects[126], and further developed by the imposition of a multidimensional model for calculation of diffusion processes and chemistry involving 11 species[262]. The model was also adapted for application to IDI diesel engines[124]. The spray model is based upon Hiroyasu's own experimental study[122] and was the first to use air-entrainment calculations rather than imposed fuel-air distributions. The entrainment rate is derived from momentum conservation. Independently, **Kuo**[197] and **Shiozaki**[314,315] have applied the model to other engines.

Meguerdichian[234] attempted to reduce dependence on empirical correlations. The spray model used is one of the most sophisticated to have been applied in the diesel engine, accounting for the effects of swirl, wall impingement and notably, transient behaviour. Ignition delay was calculated purely on the basis of calculated chemical reaction rates. The success of this approach was demonstrated.

Hiraki[118] applied a multizone model to calculation of combustion in a stratified charge engine. Jet motion is obtained by the solution of detailed conservation equations, and air entrainment was calculated independently, as in the Hiroyasu model. However, this model was the first to define the entrainment rate using the turbulent-entrainment assumptions of Hoult[137]. Another novel feature is the calculation of burning rates using flame-propagation parameters derived from studies in spark-ignition engines.

In 1980 **Ikegami**[144] became the first to apply a stochastically-based model to the modelling of diesel-engine combustion. Despite use of only 500 Monte-Carlo particles, predictions of peak pressure and NO_x are good. Later the model was generalised by relating the collision frequency to modelled turbulence parameters[145]. **Kakegawa**[157] noted a weakness in this representation due to its macroscopically-homogeneous treatment of the combustion field. To remedy this, the different

regimes were represented using surrounding air, spray formation and combustion products zones. Also premixed and diffusion burning were described separately and the number of Monte-Carlo particles was increased to 10000. The generality of this model was demonstrated, though NO_x predictions remained only fair.

Dent[56] describes a combustion model in which the cross-jet distributions of temperature and composition are fully defined. This is similar to the approach of Khan, in not using zones, but generally much more detailed. Uniquely, the variation in droplet size across the jet is modelled. The amount of air in the jet is obtained directly from the correlation of Ricou[293], though Hoult's turbulent-entrainment rate is used under some circumstances (as in Hiraki's model[118]). The model was extended for use with a swirl-chamber DI engine, taking into account the effects of air swirl on the jet motion and mixing rate[57,198]. **Gupta** independently developed this model by incorporation of a zonal description[105,237].

Mansouri[227,228,188,216] applied a stochastic model to simulation of IDI engine combustion. Use of this type of model is highly advantageous for this configuration since it is straightforward to follow the processes occurring in the prechamber and the main chamber independently. As in Ikegami's later work (above), the turbulent mixing intensity is expressed in terms of modelled turbulence parameters. Heat transfer between individual mixture elements and the chamber wall is computed. Excellent agreement with measured performance parameters was shown.

A very interesting development of this model was undertaken by **Brown**[37]. A two-step approach was followed, in which the flow and combustion were first calculated using a multi-dimensional model and then post-processed in the stochastic model. The popular KIVA code was used for the first step. The output of this solution was then used to define zones within the flow according to the overall air-to-fuel ratio of the elements. The stochastic model was used to recalculate turbulent mixing and chemistry within these zones. A convergence of results was demonstrated for more than 6000 stochastic particles and more than 10 compositional zones.

The zonal model of **Watson**[365] uses a simple 1-D spray model, though wall impingement is accounted for. The burn rate is obtained by use of a first-order relaxation equation, which was originally proposed for SI engine use by Blizard[24] and was subsequently developed by Zeleznik[383]. The relaxation parameter is linked

to the chemical reaction rate. The model was applied to the simulation of a diesel engine fuelled by sunflower oil.

The model of **Kono**[184] is based upon a unique spray model. This combines elements of the spray models of Hiraki and Hiroyasu. Multiple cross-jet and axial zones are used, but the zone motion is obtained from solution of Hiraki's conservation equations. Air entrainment is calculated according to the turbulent-entrainment equation, again following Hiraki. Another novel feature of the model is expression of the rate of diffusion burning in terms of entrainment of mixture into combustion-products regions and the chemical timescale.

Kouremenos has published over thirty papers describing development of a zonal combustion model. This is apparently the first model to include a more detailed description of combustion chemistry[193]. Eleven species are computed and dissociation effects are accounted for. A related model has been applied to the simulation of IDI engine combustion[192]. This IDI model is two-dimensional in composition space, that is, zones containing reacting mixture and pure air are described separately. A detailed treatment of the spray behaviour is given, including the effects of impingement and wall motion.

Lipkea reviewed previous phenomenological models and emphasised the need to identify the phenomena of predominant importance and concentrate on their accurate representation[213]. It was concluded that atomisation and vaporisation are of relatively low importance, and in the multizone model developed, liquid phase processes were neglected. Entrainment and burning rates were identified as the most significant processes. The zone-division pattern adopted takes into account the internal recirculation within the fuel jet due to its unsteady nature. Also, combustion rates are described using a global one-step kinetics model with no artificially-imposed flammability limits.

The development of a zonal model originally implemented by **Lapuerta** has been described in a number of publications[349,202,203]. Multidimensional computation of species concentrations and enthalpy has been added to the basic phenomenological model[271]. A more recent paper gives details of an advanced treatment of impingement and wall jet behaviour[59].

The multizone model of **Zhou**[389,42] has been applied to the simulation of different types of spray and the study of heat-transfer processes. The spray models are based on that of Shahed[45] but incorporate findings from related experimental works on traditional multi-hole sprays, conical sprays with large top angles (>140°) and film-impingement sprays[42]. For the first time, radiation from the soot and combustion gases is accounted for. The soot emissivity is determined using a Rayleigh-limit expression. Combustion chemistry involves 12 species, and water and carbon dioxide are included in the radiation model. Also, this was apparently the first model for which interzone heat transfers are computed.

The model of **Xiao**[378] is unique in providing a stochastic treatment of combustion within the framework of a multizone thermodynamic model. Also, further to Mansouri's approach, heat transfer is allowed between mixture elements, and the assumption of a uniform heat-transfer coefficient is relaxed.

Bazari has developed a multizone model[20] which is similar to the early model of Hiroyasu[126]. Though none are novel, a number of more advanced features are included, such as detailed description of combustion chemistry using 11 species and radiative heat transfer from the soot. This model is part of a suite of modelling tools used to study the behaviour of the complete engine system.

2.2.2.3 The current model

It is instructive to consider how the model developed in this study relates to these previous works. A multizone model has been chosen for the simulation of combustion in DI diesel engine. Table 2.2 shows that this type of model has been extensively used in past work, and the current study makes use of the knowledge gained. In common with the recent model of Bazari[20], the current combustion simulation builds upon the approach taken in Hiroyasu's 1983 model[126]. The latter model gives a relatively simple treatment to the spray, but does attempt to account for the effects of swirl, combustion and wall impingement. Also in common with Bazari, radiative heat transfer from the soot is accounted for, though interzone transfers are neglected.

In section 2.1, the importance of representing the mixing processes and uneven turbulence structure was identified. In the above review it was noted that neglect of the details of mixing between reactants and products was a major weakness in the Hodgetts model, and Lipkea also emphasised the importance of accurately representing the mixing and burning processes. Therefore, in the current work particular attention has been paid to achieving an adequate representation of the mixture composition and burning. This centres around use of the Magnussen eddy dissipation concept for turbulent combustion, which permits computation of slow emissions chemistry and fast combustion processes within a consistent model framework (see section 4.4).

In addition, the current model uses a two-dimensional compositional description within each spray zone, with the rate of transfer between the regions being computed using the Magnussen model. Amongst the zonal models described above, only Kouremenos[193] and Lapuerta[271] have included a similar partitioning, but in these cases, it seems that chamber-averaged compositions have been used in each compositional zone. A number of zero-dimensional models have used this technique, but mixture has generally been partitioned simply between reactants and products. In the current model, the combustion-products region may contain air or unburnt fuel if combustion is lean or rich respectively. The consequence of allowing unburnt fuel to mix with hot combustion products may be very significant from an emissions point of view.

CHAPTER 3 - SOOT MODELLING

The focus of this chapter is the modelling of sooting processes in the diesel-engine environment. The analysis is built upon an understanding of the fundamentals of the soot formation and oxidation processes using information derived from soot studies in a wide range of combustion systems. Modelling techniques are discussed and previous work is reviewed.

The chapter is divided into five sections. In section 3.1, the details of the soot formation and oxidation processes are considered in general terms. A description of phenomena peculiar to the diesel environment and summary of existing in-cylinder measurements is given in section 3.2. Soot modelling methodology is described in section 3.3 whilst expressions used in soot modelling are reviewed in section 3.4. Section 3.5 looks at models which have previously been applied to the diesel.

3.1 SOOTING PROCESS FUNDAMENTALS

The basic features of the sooting processes are described in this section. A great amount of research work has been addressed to this subject and literature pertaining to the different aspects of these processes is abundant[357,139]. Haynes[113] published a review in 1981, and other reviews are given in various textbooks (e.g. Hucknall[139]). A number of books report the proceedings and discussion at international symposia on the subject, including those edited by Siegla[318], Lahaye[200], Jander[148] and Bockhorn[26]. Reviews of sooting processes in diesel engines are given by Murayama[245], Smith[328], Kittelson[175], Heywood[116] and Amann[7].

Many studies described in the literature are highly specific and there are many disputed and unresolved areas. Therefore, for the purpose of this thesis, only the main features of the process are described, with a particular emphasis on those aspects which are of interest from a modelling point of view. The analysis is divided into sections according to the well-known mechanistic steps of the emission process.

3.1.1 Nucleation

Nucleation or particle inception describes the process by which solid-phase particulates are initiated. These soot particle precursors are formed primarily from the oxidation and pyrolysis products of the fuel molecules by vapour-phase polymerisation and condensation reactions. The chemistry is complicated, with different mechanisms predominating according to conditions, but the major species involved are known to include unsaturated hydrocarbons, especially acetylenes, and aromatics, including polyaromatic hydrocarbons (PAH)[357,328,245]. These intermediate compounds are relatively stable thermodynamically and kinetically, and they are fairly abundant in the high temperature environment of a flame[357].

Tentatively, the chemistry of build-up can be described as follows. First aromatic compounds of 2 or 3 rings are formed. Condensation and polymerisation reactions, together with dehydrogenation, rapidly produce larger PAH-based molecules which coagulate to form the first spherical nuclei[279]. These are about 1 to 4 nm in diameter and contain about 2000 - 10000 atomic mass units[279]. They are distinguished from large PAH molecules in having a more compact 3-D shape[50].

Nucleation rate is very sensitive to the pre-particle chemistry and hence to the temperature[23]. For example, in the case of formation from aromatic compounds, Graham demonstrated the existence of different reaction mechanisms at different temperatures[95]. Also, it has been found that the effect of varying the oxygen concentration is very significant[245]. In a diffusion flame, nucleation is confined to the fuel-rich side of the heat-release zone where concentrations of oxidising species are very low[328]. Hydroxyl radicals will be the main oxidising species, and despite their low concentration, they may still play an important role in the pyrolysis reactions leading to nucleation[328,89]. On the fuel-lean side, oxygen concentration is about 10^6 times higher and nucleation is negligible[257,328].

It is expected that nucleation rates will increase with temperature because of the strong link to chemical reaction rates. This is observed in pyrolytic systems[279], but in premixed flames, the opposite trend has been demonstrated[328]. This is thought to be due to the fact that the concentration of oxidising species is relatively high so that there is an increased rate of oxidation as the temperature rises.

There has been much debate over the role of ions in the nucleation process. PAH ions are easier to observe than molecules and radicals and it has been shown that their concentration decreases rapidly as soot appears[217,367]. Calcote[268,38] and others argue that the ionic mechanism is the dominant formation path, but this is not generally accepted[113,78]. The ionic pathway is more often taken to be an image of free radical and molecule nucleation, or even as a product of the process[113]. Some estimates of the fraction of young soot particles which are charged range from 1 to 40%[217,38,328].

Once the number of solid-phase particles has risen to a certain level, nucleation drops off rapidly because sufficient surface area has become available for gaseous molecule deposition[116]. The total mass loading of the nuclei formed is negligible compared to the mass of soot arising from the nuclei. This is illustrated in Fig. 3.1.

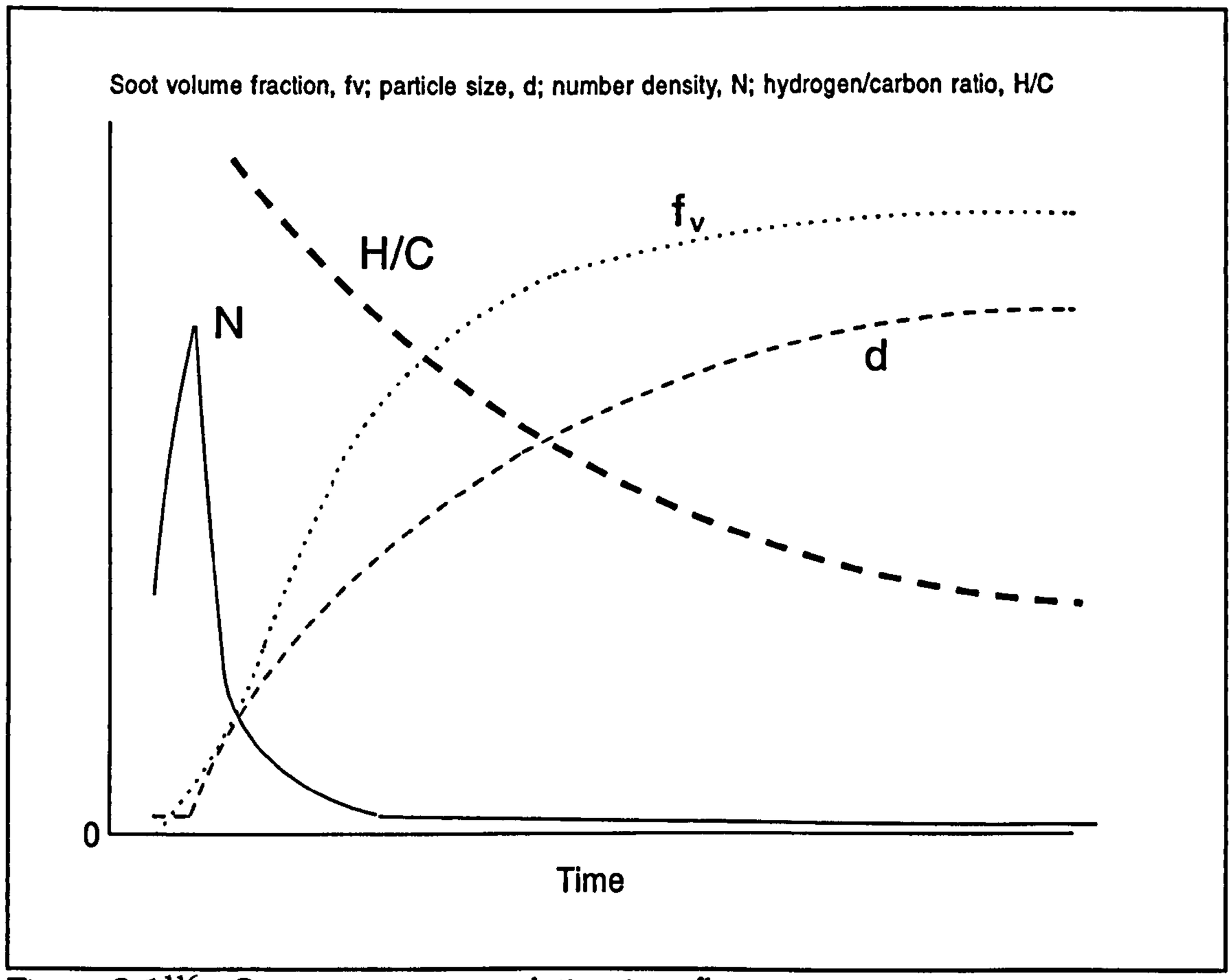

Figure 3.1[116] - Soot parameter evolution in a flame

3.1.2 Coagulation

Coagulation is the process where individual spherules join up and form new particles which are basically spherical. This requires a fairly low viscosity and most of the particles involved are young and relatively small (less than 20-30 nm)[116,279]. Besides morphological change, rapid surface growth may contribute to the restoration of a spherical shape.

Diesel soot particles are generally fairly large compared with the mean free path of gas atoms, so that the coagulation process can usually be represented by a simple free-molecule model. However, at higher pressures and temperatures, the Knudsen number (mean free path/particle radius) drops below unity and coagulation occurs in the continuum regime[325].

Coagulation is a simple physical process, so model calculations are straightforward. These show that after enough time, the particle number should become independent of the initial value[199,279]. This has been confirmed empirically and the timescale is about 1ms at medium temperatures of 1800 K[113,95]. Moreover, the final number density has often been observed to be very similar under widely different conditions[357]. For example, a study of benzene pyrolysis demonstrated that the final number density of particles tends towards a constant value for initial volume fractions ranging from 0.25 to 10% fuel[279]. This is physically reasonable because of the rapid fall-off in collision rate as the particle number decreases. Measurements from diesel engines have also shown a tendency towards a constant number density, though in this case, invariance with operating conditions has not been clearly established[116]. The effect can be seen in Fig. 3.1[116]. The final number density is about three orders of magnitude below the peak. A further useful result is that the size distribution tends to a log-normal function and varies little with operating conditions[357]. Altogether, these findings lead to the conclusion that coagulation is a property of the soot itself, independent of the parent molecules or the mode of generation[199,279].

3.1.3 Aggregation

Once spherules have solidified and surface growth rates have diminished, collisions no longer produce new spherical particles. Rather, 'aggregates' are produced in which it is still possible to identify the component spherules. The change in character of the spherules results from the thermal tempering[26] and dehydrogenation which occurs as the particles age. These processes lead to the progressive solidification and the higher viscosity precludes coagulation[113,279]. Aggregates usually have a chain-like structure, probably due to the common occurrence of positive charging of the particle chains[116]. In a transition phase, when surface growth reactions are still significant, the particle structure may resemble a cluster[116].

Gay and Smith have argued that dehydrogenation is too slow to be the cause of the termination of coalescent processes[325]. Rather, they propose that atom-atom forces are responsible for the coalescence of small particles and that these are inoperative for those larger than 10 nm.

The particles produced during aggregation have a much higher surface-to-volume ratio than the spherules, which affects oxidation rate. However, it is unlikely that aggregates are formed in significant quantities during the diesel-engine combustion process[328,36]; most of those measured in exhaust gases or in-cylinder sampling studies would have been formed outside the engine.

3.1.4 Surface growth

Surface growth is the gaseous deposition of hydrocarbon intermediates on the surface of existing particles. It is generally well-separated from nucleation in diffusion systems[279], and provides the bulk of the final soot mass fraction. The precise chemistry involved is not well-known, though acetylenes play a major role[116]. Also, the character of the particle surface is thought to be important[26]. It has been suggested that 10-30% of the CH bonds in PAHs become active radical sites in young soot particles, though this proportion will reduce with thermal tempering[26]. Internal surface area has also been shown to be important, and 'mass growth' may be a better description of the process[26].

3.1.5 Particle structure

The particles formed by the above processes exhibit a remarkable uniformity over a wide range of combustion systems. Many studies have shown that the final size of the component spherules is strongly grouped in the range 10 to 40 nm[357,199,116]*; this corresponds to over 1 million atoms. The size of aggregates is more variable, and depends on residence time and other conditions. However, chain-like particles often grow to a length of over 500 nm[116].

The fully-formed soot particles also show a common internal structure. This can be described as intermediate between amorphous carbon and crystallite[245,82]. A generally turbostratic structure[199] contains crystallites composed of layers of platelets[328]. Towards the surface, a fairly uniform layering is found, but crystallites are also arranged around internal centres[199]. The latter are representative of the component particles which merged during coagulation. In aggregates, the individual spherules are usually contained within an external coating[279]. Generally the material is not porous, though the density is usually less than that of graphite due to a higher interplanar spacing in the crystallites[357]. The hydrogen mass fraction is typically 10%[357,116].

3.1.6 Oxidation

Oxidation may operate in parallel with all of the above formation processes and it too is enhanced by temperature. Soot particles are very small and it is not necessary to consider the effect of diffusion of the oxidising species to the particle surface[7]. Rather, the process is kinetically-controlled. Under fuel-rich conditions, the concentration of hydroxyl ions is usually greater than that of oxygen molecules, and they are the principal oxidising species. Neoh demonstrated a better correlation with this species than with oxygen molecule concentration for equivalence ratios ranging from 0.85 to 1.15 [257]. Oxygen molecules may play a role in oxidation under leaner conditions and at lower temperatures. Many studies have been made of carbon oxidation in the solid phase, but the quantitative

---

* However, recent results from a diesel obtained by Pischinger, using an electrical aerosol analyzer, go against this trend - it was found that 95% of particles were smaller than 10 nm at the end of the combustion process[275].

relationship of this data to the oxidation of soot in combustion systems remains unclear[113]. This issue is addressed further in the modelling section (3.4).

Low-temperature studies have revealed preferential oxidation of the inside of the particles, due to the internal structure being less uniform[199]. It is not yet known whether this is the case under flame conditions. An indication that it might be is given by the fact that only a small percentage of collisions with oxidants are successful (10-30% for OH, much less for O_2), so that these species would be expected to penetrate deep within a molecule[257]. Also, an order of magnitude increase in number density has been observed at the tip of diffusion flames, clearly showing that some sort of fragmentation process results from oxidation[257].

3.1.7 General sensitivities and dependencies

Having looked at the details of the soot emission mechanism, it is useful to consider the parameters to which the process is most sensitive. Some of these are represented by the expressions reviewed in section 3.4 but others are more general observations which have not been used in a predictive sense.

Glassman[306,89] and others[16,103] consider that soot formation in an atmospheric diffusion flame is influenced predominantly by diffusion flame temperature and fuel structure, whilst the concentrations of fuel and oxidiser are of secondary importance. In the diesel it is also important to consider the effects of pressure and turbulence. The effects of each of these parameters are briefly reviewed below.

Cowley[51] thoroughly investigated the influence of fuel composition on sooting propensity in the diesel. Sulphur in the fuel directly affects the particulate mass and the effect is easily calculated, but other chemical effects are minor. Studies in other combustion systems have demonstrated an independence from fuel type at pressures of above 10 atm[79]. Metal additives have been found to have a significant effect, but they are expensive. Their study is beyond the scope of this thesis. Therefore, the effect of fuel chemistry is not considered further.

Soot formation has been correlated to fuel and oxidiser concentrations by many authors (see section 3.4). Generally, the formation rate increases with fuel concentration and decreases with oxidiser concentration as would be expected.

However, the variety of combustion systems and model mechanisms is such that no universal relationships can be identified.

A couple of engine studies have attempted to correlate soot emission in terms of flame temperatures[4,142]. In 1981, Ahmad[4,276] examined the overall effect of flame temperature on soot emission. O_2 or N_2 were added to the intake air in order to influence chemical kinetics without affecting the fuel-air mixing. A good correlation was obtained between the exhaust soot and the calculated adiabatic flame temperature. The correlation was independent of engine load and speed, though different overall activation energies were found using high and low swirl engines. The latter effect was explained in terms of a change in the competition between formation and oxidation processes. In 1993, Iida also obtained good correlations with calculated flame temperature and further demonstrated independence with injection timing[142]. In addition to the diesel studies, others have correlated sooting rates in terms of temperature in turbulent diffusion flames, with mixed success[114,260].

The interpretation of these results is debatable. Both of the engine studies showed a drastic reduction in soot yield with increased temperature. This contrasts with the results obtained using a classical diffusion flame[89]. Ahmad considers that because of the intense recirculation found in an IDI diesel, the emission process is dominated by oxidation and that the latter is more temperature sensitive[4]. However, the overall activation energy of 97 kcal/mol is much higher than that expected for oxidation of carbon. This is said to be due to the effect of parallel formation processes. Iida found an even higher overall activation energy of 146 kcal/mol, and likewise concluded that oxidation is more strongly affected by temperature than formation[142].

The analysis presented in Appendix A shows that if soot formation and oxidation are viewed as occurring substantially sequentially, rather than in parallel, it is not necessary to conclude that oxidation is more temperature sensitive. The oxidation rate is proportional to the mass of soot in existence, so that the decay is exponential with an exponent proportional to the rate. The rise in soot mass during formation, though, is linearly dependent on the formation rate. Thus, even if the activation energies for formation and oxidation are equal, the yield will be expected to fall substantially with temperature.

Despite the difficulty of interpretation, the fact remains that yield is well-correlated by flame temperature. This raises the possibility of describing the formation and oxidation processes in terms of a simple pair of Arrhenius chemical rate equations. However, it would be surprising if this approach was completely successful, in view of the fact that the formation process consists of several different mechanistic steps. In particular, the nucleation process may have a very different temperature dependency, and during the premixed phase, the nucleation rate may actually drop off with temperature. Glassman suggested that soot number density is of predominant importance, governing the mass emitted[26*]. It would seem that the above temperature correlations contradict this finding, suggesting rather the overall dominance of surface growth.

Attempts to correlate rates and yields in terms of overall pressure have been less successful. Recent results obtained from premixed combustion systems show that at pressures under 10 atm, yield is well-correlated by the square of overall pressure[30], whilst between 10 and 100 atm, a linear dependency results[28]. Earlier, MacFarlane[220] reported an overall pressure exponent of 2-3 for turbulent premixed flames. In diffusion flames, also, several studies have shown that formation is promoted by increased pressure[113]. In the range up to 22 atm, the dependency on pressure is given by an exponent of between about 0.7 and 2 [238,304,77,79,242]. However, for a burning droplet, Kadota obtained a linear correlation for the yield at pressures below 10 atm, and independence at higher pressures[155]. Thus, it is apparent that no simple dependency will be found under diesel engine conditions.

A further empirical finding is the importance of turbulence and intermittency on sooting processes. Magnussen was an early proponent of these concepts. In 1971 he demonstrated that by applying laminar rate equations with the local time-mean values of species concentrations and temperature, soot oxidation in a turbulent flame is seriously overestimated[221]. Results presented in 1975[222] showed a highly intermittent appearance of soot, suggesting that it is contained in eddies. Becker disputed this finding[21], but Magnussen subsequently demonstrated the success of a model based on this concept (discussed in more detail later in this chapter)[226]. Dent lent support to Magnussen's interpretation by successfully correlating exhaust smoke in terms of the mixing rate[55].

---

* General discussion, pp. 193-196.

3.1.8 Conclusions

Overall, some broad similarities in behaviour have been observed in various combustion systems and at different operating conditions. This is helpful from a modelling point of view.

Nucleation occurs very rapidly, producing a large number of very small particles, but contributing little to the soot mass loading. The rate is strongly dependent on chemistry and temperature, but the final number density may not be, since the process rapidly terminates once solid surface area is formed. In diffusion systems, the rate increases with temperature.

Coagulation also takes place rapidly, giving a reduction in particle number density of about three orders of magnitude. The resulting spherules exhibit a remarkable uniformity, being about 10 to 40 nm in diameter whatever the combustion environment. The size distribution is also uniform and the final number density tends to a constant value in simple combustion systems. The latter effect may not be so pronounced in a diesel due to the inhomogeneity across the chamber and the parallel oxidation processes.

Nucleation ceases as surface growth takes over. Initially the latter process occurs in parallel with coagulation, and altogether it contributes the bulk of the soot mass. The timescale is much longer than that of particle inception. Finally oxidation becomes the dominant process. The timescale is also long, of the order of a few milliseconds, and the rate is strongly affected by the turbulent structure of the mixture.

Good correlations are obtained with calculated flame temperatures. However, it is difficult to interpret these results because of the competition and overlap between formation and oxidation processes. Also, the conclusion that trends can be predicted using very simple equations is not in accord with other results or the overall understanding of the processes. Smoke has also been successfully correlated in terms of the timescale of turbulence.

Generally, little success has been reported in establishing dependencies on other global features such as pressure and species concentrations. This is to be expected in view of the overall complexity of the process.

3.2 SOOT IN DIESEL ENGINES

This section looks at sooting processes in the context of diesel-engine combustion. The analysis will provide guidelines as to the expectations and requirements of a practical model of emission. Knowledge of the relationship between soot emission and the combustion process derives mainly from in-cylinder studies. Despite the difficulty of making such measurements, quite a number of these studies have been undertaken and a significant amount has been learnt about sooting in the diesel environment. The parameters measured in some of these studies are set out in Table 3.1. The main features of the process are described in section 3.2.1 whilst the related issue of model validation is addressed in section 3.2.2.

3.2.1 Process description

Most of the smoke emitted from a diesel stems from incomplete combustion of the fuel, with an additional component originating from the lubricating oil. The former process gives rise to solid-phase carbonaceous soot, whilst the lubricating oil is the source of some of the heavier hydrocarbons which are absorbed to the solid particles[84]. Oil components may constitute up to 80% of the 'soluble organic fraction' (SOF), though the actual proportion depends on operating conditions[116].

Kittelson has reviewed the timing of the appearance of soot, concluding that it varies between the start of combustion and just after the start of the diffusion phase[175]. Other investigators have found peak concentrations in the early part of the diffusion-burning stage, between 5 and 10 degrees after ignition[357,275]. Kittelson's measurements revealed that the initial rate of formation is substantially independent of load and speed[175]. In a DI engine, the highest concentrations are found in the fuel-rich core region. With a quiescent chamber, values corresponding to 50% of the local fuel carbon have been measured[116]. Peak values for bowl-in-piston chambers with air swirl average lower at around 10%[275,11], due mainly to better mixing. The very intense mixing in an IDI diesel will also tend to give lower maximum concentrations, but this is balanced by the higher fuel concentration found in the prechamber[116]. In DI engines, peak concentrations vary little with load and speed, whilst a four-fold increase with doubling of equivalence ratio has been observed in an IDI diesel. This stronger dependency is probably due to the higher average equivalence ratio in the combustion zone.

Combustion photography shows that rapid formation of soot continues as fuel is injected into the burning region[116]. In parallel, soot is quickly oxidised as air is mixed into the spray; mixing within the spray leads to a more uniform soot distribution. In a DI diesel engine, Greeves measured a nearly even distribution only 21° after injection start[98] and Kamimoto's data confirms this[11]. Other evidence suggests a steep fall-off in soot concentration away from the centreline[116]. Also, it has been observed that the soot concentration rises in spray near the bowl or chamber wall due to poor mixing[116]. This soot decays more slowly than that formed earlier in the core of the spray[116].

Finally, oxidation takes over. Kittelson reviewed measured values of peak/exhaust concentration and found a variation of between 1.2 and 70. However, the upper values derive from localised sampling data and a typical value is nearer 10. The lowest value applies to the high-load condition in a DI diesel engine. A similar drastic reduction in oxidation was observed in a prechamber engine where oxidation ceased for oxygen concentration of less than 5%[81].

Another critical issue affecting emission is the timescale of the burn-out[113,168]. Hiroyasu showed that if the exhaust valve opens while significant oxidation is ongoing, exhaust smoke levels are very high[123]. At the temperatures existing late in the diffusion-phase, oxidation can continue until very low concentrations remain. However, once the port opens, the rapid drop in temperature brings the process to an end. By making an analogy with the burn-out of a turbulent diffusion flame, the controlling features can be readily identified. The mixing rate and overall air-to-fuel ratio are key, but the most fundamental constraint is that of time, which is dependent on engine speed.

Overall, it is apparent that most of the soot forms in mixture which is generally hot and fuel-rich. Moreover, the soot is often contained in fuel-rich eddies which are surrounded by relatively soot-free air. Thus, pyrolysis of rich mixture is an important source of soot. In fact, elimination of soot is practically impossible, due to the nature of diffusion burning and because of the constraints imposed by other parameters, including the injection process, operating speed, efficiency and NO_x emission.

Author[Ref.]	DI	IDI	p	HR	T_{vCA}	$soot_{vCA}$	ϕ_{vCA}	$soot_{ex}$	inj
Nakakita[254]		*	*	*	*	*	*	*,*	
Zellat[386,387]		*	*,*	*	*	*	*		*
Mansouri[227,228]		*	*,*	*	*	*	*		*
Xiao[378]	*		*,*	*		*		*	
Bazari[20,327]	*		*	*	*	*	*	*	*
Hiroyasu[126]	*		*,*	*	*	*		*,*	*
Nishida[262]	*		*,*	*,*	*	*	*	*,*	*
Kuo[197]	*		*,*	*,*	avg,**avg**	**avg**		*_*	*
Kono184	*			*,*				*,*	
Payri[271]	*			*		*			
Dent[57]	*		*,*	*		*		*	*
Kyriakides[198]	*		*,*	*		*		*,*	*
Mehta[237(11)]	*				*	*,*	*,*	*,*	
Wade[356]	*				*	*	*	*	
Kakegawa[157]	*		*,*	*,*	**map**			*	*
Kittelson[176]		*	*			*			
Kort[188]		*	*	*					
Fujiwara[81]		*	*	*	*	par	*	*	*
Du[60]		*	*	*		*, avg		*	*
Lepperhoff[208]		*		*		*	*	par	*
Senda[308]		*	*	*	*	*	*	*	*
Sato[303]		*	*	*				par	*
Okajima[267]	bomb		*	*				*	*
Iida[142]	RCM		*		*			par	*
Ohkoshi[266]	*		*	*				*	
Odaka[265]	*		*	*				*	
Murayama[246]	*		*	*				*	
Uchida[354]	*		*	*				par	*
Tsukuhara[351]	*		*	*				par	

Author[Ref.]	DI	IDI	p	HR	T_{vCA}	$soot_{vCA}$	ϕ_{vCA}	$soot_{ex}$	inj
Hiroyasu[123]	*		*	*				par	*
Kawazoe[166]	*		*	*				par	*
Suzuki[336]	*		m	*				par	*
Zhang[388]	*		m	*	*			par	
Konno[183]	*		m	*	avg			par	*
Kobayashi[181]	*			*	*,avg	*			
Chmela[46]	*		*	*	*	*			*
Kittelson[175]	*		*	*	*	par		par	*
Ning[259]	*		*		*	*		par	*
Wölfle[375]	*		*			par	par		*
Quoc[281]	*				*	*		par	
Fukuda[83]	*					par	par		
Yates[380]	*				avg,map	map			
Norris-Jones[264]	*					avg			*
Kadota[156]	*				*	*	*		
Takeuchi[340]	*			*	*,map	map	map		
Mohammad[239]	*		*		*	*			
Greeves[98]	*		*			*, avg			*
Kontani[186]	*		*			N			*
Kittelson[174]	*		*			avg,par		par	*
Saito[300]	*		*	*		par		par	
Hiroyasu[130]	*		*	*		avg,par		par	*
Kamimoto[159]	*		*	*	*,avg	*	*		*
Matsui[230]	*		*	*	*	*		*	*
Kamimoto[160]	*		m		*	*	*	*	
Aoyagi[11]	*		*	*	map	map	map	*	*

Table 3.1 - Parameters measured or calculated in in-cylinder studies

(inj - injection rate profile or injection total and full description of timing, HR - heat release rate diagram or burn rate diagram, T - flame temperature measured by 2-colour method or an appropriate model temperature, soot - soot concentration or two-colour method KL factor, avg - cylinder average, map - spatially-resolved measurements, par - parametric variation given, m - mean over whole of combustion period, **bold** - calculated value, shading - chosen experimental data-set)

3.2.2 Model Validation

It is appropriate at this point to consider model validation. An extensive data-set of soot measurements is required, together with the values of as many associated combustion-process parameters as possible. For instance, combustion-model validation requires a measured heat-release rate and preferably temperatures and pressure too. In-cylinder soot data is essential and will be much more useful if spatially-resolved and backed up by fuel concentration and temperature measurements. A further constraint is added because the current modelling efforts have been concentrated on the DI diesel.

Table 3.1 shows that only one group of workers have presented in-cylinder soot data together with temperature measurements and a heat-release diagram for a DI diesel* - viz T.Kamimoto, S.Matsuoka, Y. Matsui, Y.Aoyagi and Y.Miyairi at Tokyo Institute of Technology[158,159,11,160,230] (see bottom of the second page). Fortunately, the data-set given by this group is very detailed, covering a wide range of parametric variations (though only one running speed). Thus, it was the obvious choice for validation of the models developed in the current work. It is subsequently referred to by the name of the chief author, Kamimoto.

---

* Note: Takeuchi presented temperatures for one crank angle position only[340].

3.3 SOOT MODELLING METHODOLOGY

This section reviews general approaches to the modelling of soot emission from diesel engines. The methodology is not well-established - no previous study has specifically addressed this issue and there is no substantial review material in the literature. However, as before, the analysis can draw on the knowledge base from a wide range of combustion systems, since much of this can be usefully applied in the context of diesel work.

Two main factors impact on the form of a soot model - the modelling environment and the information source which provides a relationship between sooting processes and various physical parameters. The following analysis considers each of these subjects in turn, before describing the strategies adopted. The overall aim is to highlight the important issues and to provide a background for assessing use and performance of various models; no specific cases are dealt with.

3.3.1 Effect of modelling environment

The acceptable form of any soot model will be governed in part by the underlying thermodynamic framework. In this respect, it is very important to consider the integration and consistency of the different modelling techniques used.

The previous chapter illustrated the range of thermodynamic descriptions available. The degree of detail is variable - average thermodynamic properties may be described at several levels: using simple chamber averages, on a zonal basis, or according to multidimensional grid cells. Various sub-structures are then built on top of this - the reacting mixture may be divided into non-burning and burning regions, or a full stochastic description of thermodynamic states may be computed.

To obtain an accurate description of the sooting phenomena, it is important to follow the thermodynamic history of representative soot particles and mixture elements[168]. For instance, it is particularly important to know how long a given element spends in the high-temperature region where the fuel concentration is also high. In order to do this, the ideal model would fully describe the relationship between the soot and species concentrations and temperature. In theory, it would be possible to construct such a model based on the diffusion-flame concept, since

the reaction rate can be estimated and the temperature and species gradients approaching the flame can be computed. However, this type of model is not available. Stochastic techniques have been developed, though, which attempt to supply this information.

Two main types of stochastic model are used - those which use a presumed pdf and those employing a modelled pdf equation which is generally solved using Monte-Carlo techniques. The first type is severely limited in application to soot modelling, since the relationship between the soot concentration and the other parameters is inaccessible. Mixture fraction and soot parameters are assumed to be uncorrelated and the direct effect of turbulent fluctuations must be ignored. This is a major simplification since it is known that high soot concentration will in fact be strongly correlated with high temperature and high fuel concentration. The second type of pdf model completely solves the closure problem associated with non-linear reaction rates[278]. However, it is more computer-intensive and this factor is usually limiting.

The applicability of a given soot model will generally depend on the level of detail represented by the combustion model. For example, a semi-global soot model fitted to measured mean concentration data is likely to be inappropriate for use with a model which gives the full range of thermodynamic states in the mixture. Similarly, soot formation expressions deriving from a narrow range of empirical conditions, for example from partially pre-mixed burning in a jet-stirred reactor, may be a poor match for combustion models which employ an averaged description of the mixture composition.

Finally, it is noted that the utility of any models developed will be greatly enhanced if they are simple. For instance, a soot model involving several species concentrations is simply impractical for use in the CFD environment.

3.3.2 Application of sooting-process information

Knowledge of sooting phenomena is available from various sources and in different forms. Consideration is now given to the methods of applying this knowledge in useful models.

The most important information source is the set of empirically-determined correlations for various aspects of the sooting process. There are a large number of such expressions, covering both the individual mechanistic steps and the overall formation process. They are reviewed in more detail in section 3.4. Most derive from experiments performed in simplified combustion systems, such as premixed flames and laminar diffusion flames, though a number apply to more complex systems, including turbulent diffusion flames and even diesel engines. Generally the expressions may be described as semi-empirical - that is, the basic form of the correlation was postulated according to the general understanding of the process and the constant values were fitted by matching empirical data. This procedure is particularly important in the more complex combustion systems, where expression derivation must be done in close conjunction with modelling work.

Some of the empirical observations described in section 3.1 are not given in the form of a correlation, but are nevertheless of interest for modelling. Examples include:

(1) The uniformity in the initial soot-particle size and size distribution
(2) The uniformity in the initial particle number density
(3) The good correlation of growth rate with flame temperature
(4) The good correlation of yield with turbulent mixing rate

Building on the picture of most soot formation occurring on the fuel-rich side of the diffusion flame, the following could be added:

(5) The temperature at which soot is formed is close to the flame temperature
(6) The fuel concentration at which soot is formed is close to stoichiometry

However, an apparent inconsistency can be observed between points (3) and (4): if it is possible to correlate smoke in terms of a flame temperature, it does not

follow that it will be well-correlated with a turbulent mixing timescale, and vice versa. In fact, the correlations in each case were not perfect, and the indication is that both processes are important in the diesel. This suggests that some sort of hybrid model may be required which can take both of these processes into account.

Another source of model information is provided by theoretical concepts which can be applied to various aspects of the process. Examples include kinetic theory which has been used to predict collision rates and hence formation[255], coagulation[116] and oxidation[257]. Likewise, the Magnussen eddy dissipation concept (EDC) is based upon a conceptual model of the turbulence structure in a fluid.

Generally, the most powerful models achieve an accurate representation of a complex process by identifying parameters which are fundamental. They are usually simple and efficient. A good example is the Magnussen EDC which provides a consistent framework for describing fast and slow chemistry. The accuracy and validity of such models depends very much on the selection of the correct rate-controlling parameters. For instance, attempts to fit a kinetic correlation for soot oxidation rate in a turbulent diffusion flame show much scatter due to the effects of turbulence[261]. On the other hand, correlation in terms of turbulent mixing timescale shows a good correlation[55].

Finally, the importance of matching use of correlations and information to the conditions of its origin was referred to in section 3.3.1. Further to the issue of model detail, care must also be taken when applying correlations derived in a much different environment to that found in the diesel engine. The following features of the diesel combustion environment should be noted in particular:

(1) Uses diesel fuel
(2) High pressure and temperature (1-150 atm, 300-3000 K)
(3) Hence, high partial pressure of oxygen, up to 10 atm
(4) High levels of turbulence

3.3.3 The current work

Spatial resolution and flexibility are essential in representing highly non-linear emissions processes and in this work, phenomenological models of the quasi-dimensional type have been shown to be the most appropriate. A thermodynamic structure encompassing heated fine structure and surrounding fluid regions has been employed in an attempt to provide an approximation to the thermodynamic history of mixture elements. The alternative pdf method was viewed as desirable but not essential to the work, and was not implemented due to the restriction of time. Thus, the thermodynamic structure used in the current work may be described as semi-global, i.e. it does not model the full range of local conditions existing in the mixture, but rather describes some representative average states. This must be borne in mind in the soot-expression analysis. In fact, the approach adopted permits analysis of sooting rates over a wide range of thermodynamic conditions, since many different mixture states are represented in the zones and sub-zones. Whilst it may not predict soot yields as accurately as a pdf model, rate information should be adequate at the stage of model development.

3.4 SOOT MODELLING REVIEW

There is an abundance of literature on sooting processes in combustion. Review papers by Hiroyasu[128] and Mullins[243] list correlations, and Mullins[243], Coelho[47] and others have done comparative studies. This section is concerned only with those works which have provided or examined analytical expressions to describe some aspect of the process (though some recent work also involves data libraries[25]). Some of these are listed in Table 3.2*.

The basic form of these expressions has usually been postulated according to a theoretical model or general experimental trend; the values of the model constants are set by matching to empirical data. Due to this technique, there is considerable overlap between the evaluation of expressions in experimental work and development in a modelling context. Table 3.2 includes a few models which are heavily weighted towards the latter and others which have been used in many different situations, sometimes with slightly different constant values and slightly modified form. However, a comprehensive treatment is beyond the scope of this thesis and the table is not exhaustive; rather, significant contributions are identified and some are discussed in the following analysis.

The review has been broken down into subsections considering soot formation processes and oxidation. It has been observed that correlations are often limited to a very narrow range of thermodynamic conditions. Also, different fuels and combustion systems were employed in their derivation. Therefore, this information is included in summary tables (Tables 3.3-3.7). The name of the main author is given in **bold** at first mention of a particular model.

Within each section, expressions of similar form are considered together and some key model parameters are given in the summary tables. Also, to facilitate comparison, each equation has been re-expressed in terms of a common set of variables, e.g., concentrations have been converted to masses.

---

* Most entries are for the earliest published paper but later reviews are also included where appropriate.

Soot expression sources

Researcher	Year	Data source	Formation	Coagulation	Oxidation
1. Parker, Hottel[270]	1936	Solid carbon			✓
2. Schalla[304]	1955	Laminar diffusion flame	✓		
3. Lee, Thring, Beer[207]	1962	Laminar diffusion flame			✓
4. Nagle, Strickland, Constable[249]	1962	Solid carbon			✓
5. MacFarlane, Holderness, Whitcher[220]	1964	Laminar + turbulent premixed			
6. Green[97]	1964	Aerosols		✓	
7. Narasimhan[255]	1965	Plug-flow reactor	✓		
8. Tesner, Tsibulevsky[344]	1967	Laminar diffusion flame			✓
9. Field, Gill, Morgan, Hawksley[75]	1967	Solid carbon			✓
10. Shibayama, Koizumi, Aoki[311]	1968	Spray flame			✓
11. Fenimore, Jones[71]	1969	Laminar diffusion flame			✓
12. Magnussen[221]	1971	Turbulent diffusion flame			✓
13. Tesner, Snegiriova, Knorre[345]	1971	Laminar diffusion flame	✓		
14. Khan, Greeves, Probert[170,173]	1971	Diesel engine	✓		

Researcher	Year	Data source	Formation	Coagulation	Oxidation
15. Khan, Wang, Langridge[171]	1971	Diesel engine (motoring)		✓	Lee[236]
16. Hein[114]	1972	Turbulent diffusion flame	✓		
17. Feugier[73,74]	1972	Laminar diffusion flame			✓
18. McArragher, Tan[232]	1972	Various	✓		Nagle[307]
19. Park, Appleton[269]	1973	Shock-tube			Nagle[307], etc
20. Wersborg, Howard, Williams[367]	1973	Premixed flame		✓	
21. Jensen[150]	1974	Rocket motor	✓		
22. Graham, Homer, Rosenfeld[95]	1975	Shock-tube		✓	
23. Surovikin[335]	1976	Thermal decomposition	✓		
24. Kau, Tyson, Heap[164]	1976	Diesel engine	✓		✓
25. Ulrich, Milnes, Subramanian[355]	1976	Laminar diffusion flame		✓	
26. Laurendeau[204]	1978	Solid carbon			✓
27. Magnussen, Hjerter[223]	1976	Turbulent diffusion flame	Tesner[233]		✓
28. Edelman, Turan, Harsha, Wong, Blazowski[61]	1979	Jet-stirred reactor	✓		
29. Friswell[79]	1979	Gas-turbine combustor	✓		✓
30 Nishida, Mukohara[260]	1979	Turbulent diffusion flame	✓		✓

Researcher	Year	Data source	Formation	Coagulation	Oxidation
31. Dent[55]	1980	Diesel			✓
32. Najjar, Goodger[251,252]	1981	Gas-turbine combustor	✓		Nagle[307]
33. Farmer, Edelman, Wong[69]	1981	Reacting furnace, diesel engine	✓		Nagle[307]
34. Wang, Matula, Farmer[363]	1981	Shock-tube	✓		
35. Harmadi[110]	1982	-	✓		✓
36. Ahmad, Plee, Myers[4]	1982	IDI diesel engine	✓		✓
37. Mansouri, Heywood, Ekchian[227]	1982	IDI diesel engine	equilibrium		Nagle[307]
38. Hiroyasu, Kadota, Arai[125]	1982	Turbulent diffusion flame	✓		✓
39. Naegeli, Dodge, Moses[248]	1983	Gas-turbine combustor	✓		
40. Du, Kittelson[60]	1983	Diesel engine		✓	
41. Rao, Barodon[287]	1984	Laminar diffusion flame	✓		
42. Flower[77]	1986	Laminar diffusion flame	✓		
43. Abbas, Lockwood[1]	1985	Turbulent diffusion flame	Khan[293]		Magnussen[81]
44. Simmons, Williams[320]	1988	Shock-tube	✓		
45. Hargreave, Pourkshanian, Williams[109]	1986	Solid carbon	✓		
46. Mullins, Simmons, Williams[243]	1987	Shock-tube	✓		Many

Researcher	Year	Data source	Formation	Coagulation	Oxidation
47. Moss, Stewart, Syed[242]	1988	Laminar, turbulent diffusion flame	✓		Nagle[307]
48. Huth, Leuckel[140]	1990	Turbulent plug-flow reactor	✓		
49. Sato, Tree, Hodges, Foster[302]	1990	Jet-stirred combustor	✓		
50. Nakakita, Nagaoka, Fujikawa, Ohsawa, Yamaguchi[254]	1990	Diesel engine	Tesner[233], Farmer[229]		Nagle[307], Magnussen[76]
51. Kennedy, Kollman, Chen[167]	1990	Turbulent diffusion flame	✓		
52. Xiao, Borgnakke[378]	1991	Diesel engine	Khan[293]	✓	Nagle[307], Fenimore[206]
53. Leung[209]	1991	Laminar diffusion flame	✓	✓	✓
54. Iida[142]	1993	Diesel engine	✓		✓
55. Coelho, Farias, Pereira, Carvalho[47]	1993	Turbulent diffusion flame	Khan[293], Moss[91]		Nagle[307], Lee[236], Magnussen[76]
56. Bockhorn[25]	1994	Premixed flame	✓		

Table 3.2 - Summary information on soot expression sources

3.4.1 Soot formation

Most soot-formation expressions include the Arrhenius term which is conventionally used to describe the effect of temperature on chemical kinetics. This assumes that the main soot-formation processes of nucleation and surface growth are chemically controlled. The majority of analytical expressions have lumped these processes together using an apparent first-order reaction correlation[320]. These are described in sections 3.4.1.1 and 3.4.1.2. In these classes, the rate expression of Narasimhan[255] is an exception in including terms for soot mass and number density.

Much recent work has used a different type of soot-formation expression which correlates surface growth rate using experimental data from simple combustion systems. Empirical data has also been used to describe a 'final' soot volume fraction in some of these models[25]. These models are briefly described in section 3.4.1.3.

Finally, a small number of models have included a more detailed mechanism describing the processes of nucleation, coagulation and surface growth separately. These are reviewed in section 3.4.1.4.

Of the models which lump formation into a single mechanism, the largest class are simple expressions which do not separately account for the effect of oxygen. These are described first in section 3.4.1.1.

3.4.1.1 Single-step expressions

The simplest form is that given by **Rao**[287], **Nishida**[260] and **Hein**[114]:

$$\frac{dm_{soot}}{dt} = A\,\phi\,e^{-\frac{E_f}{RT}} \qquad (3.1)$$

Rao's work examined soot production in a laminar H_2O-HC diffusion flame, and concentrated on the temperature-dependence effect. In contrast, Nishida and Hein made measurements in a turbulent diffusion flame. In Nishida's study, the data points are a poor fit to equ. 3.1, which must be due to the effect of turbulent fluctuations. Also, for the data points corresponding to temperatures above 900 K, the slope of the plot giving the activation energy is much steeper; for this region 40 kcal/mol is a better estimate than the value of 12.5 kcal/mol given in the paper. This is in much better agreement with the data from other sources, none of which give an activation energy of less than about 25 kcal/mol. Hein also obtained a low value of 21.5 kcal/mol.

Narasimhan[255] used an expression developed from the bimolecular collision equation of kinetic theory to fit soot measurement data from a turbulent diffusion flame in a plug-flow reactor. The expression applies after the rapid initial precipitation of nuclei.

$$\frac{dm_{soot}}{dt} = A\,\phi\,m_{soot}^{\frac{2}{3}}\,N_{soot}^{\frac{1}{3}}\,T^{\frac{1}{2}}\,e^{-\frac{E_f}{RT}} \qquad (3.2)$$

The above studies were all done at atmospheric pressure, so reveal no information on pressure dependencies. **Khan**[170], however, has used a computer simulation to fit a soot-formation equation using exhaust measurements from a diesel engine. This study has been extensively used so it is examined in more detail.

The combustion model was developed from the fuel-spray model of Grigg[101]. This predicts the rate of heat release mainly by calculating the rate of air entrainment and the rate of micromixing of fuel and air. The instantaneous equivalence ratio in the soot-formation region is defined according to these two parameters, and the

temperature is taken as the mean temperature of the jet. Soot formation is followed through the combustion process, though in the original work soot oxidation is neglected. In a later work[173], coagulation is included and oxidation is followed using Lee's expression[207]. A further modification was the introduction of concentration and temperature gradients for the soot-formation region. Therefore, as far as emissions are concerned, the model can be described as quasi-dimensional.

Khan[170] fit the following Arrhenius-type equation using exhaust data from three medium-sized diesel engines:

$$\frac{dm_{soot}}{dt} = A\,\phi^3\,p_{eva}\,e^{-\frac{E_f}{RT}} \qquad (3.3)$$

An Arrhenius expression was chosen since it was considered that soot formation rates are controlled mainly by the rate of nucleation, which in turn is governed by the chemical kinetics of the formation of the gaseous precursors. The activation energy of 40 kcal/mol was taken from previous work on the effect of inlet air temperature on exhaust soot[164,169]. The equivalence-ratio term was included because other studies had shown exhaust soot to be proportional to ϕ^n; the exponent and the constant *A* were set according to the experimental data.

Wilson[371] and **Kau**[164] used a related expression in their zonal combustion model:

$$\frac{dm_{soot}}{dt} = A\,\frac{\bar{T}}{T}\phi^3\,p\,e^{-\frac{E_f}{RT}} \qquad (3.4)$$

However, rather than partial pressure of evaporated fuel, the total pressure has been used, and the equivalence ratio is that of the products rather than the reactants. Wilson[371] states that for propane and methane, typical values of the equivalence-ratio exponent and activation energy are 1 and 32-58 kcal/mol respectively, though no source is given.

More recently, Abbas[1] has tested Khan's expression in prediction of soot levels in a turbulent diffusion flame. The original form of the expression was used, though the constant *A* was extended to include the Richardson number. In conjunction with the oxidation models of Lee[207] and Magnussen[223,224], tolerably good results

were obtained across a broad range of operating conditions.

Xiao[378] applied the Khan model to prediction of soot in a diesel using a stochastic combustion model. Good results were obtained using the value of *A* obtained by Khan for the case where oxidation is considered[173].

Coehlo[47] has examined the performance of the Khan model in CFD prediction of turbulent diffusion flames. A sensitivity study determined that the best value of the constant *A* was that evaluated in an earlier work by Abbas. This is similar to the oxidation-case value[173], but significantly smaller than that determined in Abbas's later work[1]. Though predictions were found to be generally good considering the simplicity of the model, the results suggested that the equivalence-ratio exponent is too high. No alternative value was given.

Naegli[248] examined the effect of fuel composition and flame temperature on soot formation in a highly turbulent, small-scale research combustor using kerosine-type fuels. The pressure varied from 7 to 13 atm. For each fuel type, a correlation of the following form was obtained:

$$\frac{dm_{soot}}{dt} = A\,\phi^{3.425}\,p\,e^{-\frac{E_f}{RT}} \qquad (3.5)$$

The equivalence-ratio exponent is in good accord with that given by Khan[170], taking into account Khan's additional term for the partial pressure of the fuel. The measured activation energy is 57.8 kcal/mol. However, it is assumed that oxidation competes for soot in the highly turbulent flame, so that this value represents the difference between the formation and oxidation activation energies. Using Lee's value for the latter gives an estimate of 97 kcal/mol for the formation process. Naegeli considers that this value compares favourably with the results of Tesner[345,346] and Glassman[90], but Tesner's values apply to the nucleation process, and this is usually a small part of the overall production of soot in a flame[25]. Glassman[90] was unable to identify the process of very high activation energy indicated by his results, though he observed that the overall activation energies determined from pure pyrolysis studies were much lower. Nishida's measurements in a turbulent diffusion flame gave an activation energy of 12.5 kcal/mol[262] (though see above discussion), and all other measurements in turbulent flows give a lower value (see Table 3.3 below). Thus, the current value appears to be rather high, and

perhaps it is inappropriate to determine the activation energy for formation by adding the oxidation value to the measured value. Hence the original measured value is given in the summary table (Table 3.3).

In an early work, **Hiroyasu**[121] postulated a soot formation equation embodying some general observations from measurements in diffusion flames[304,345], premixed flames[220], the gas turbine combustor[210] and the diesel engine[172]:

$$\frac{dm_{soot}}{dt} = (A\frac{dm_f}{dt} + B\,m_{f,liq})\,p\,e^{-\frac{E_f}{T}} \qquad (3.6)$$

A and B are constants to be determined by matching to experimental soot levels. The first term is proportional to the calculated fuel burn rate and the second, to the mass of liquid fuel existing in the model zone. It is now known that virtually all soot is formed in vapour-phase pyrolysis. Thus, this expression is poorly grounded.

In 1982, **Hiroyasu**[125,184] proposed a modified expression taking into account updated soot formation measurements[155,12]:

$$\frac{dm_{soot}}{dt} = A\,m_{evap}\,p^{\frac{1}{2}}\,e^{-\frac{E_f}{RT}} \qquad (3.7)$$

The activation energy value is set to 12.5 kcal/mol following Nishida[262] (see above). The usual form of the expression makes use of experimental results due to Kadota[155] and Arai[12]. For the pressure range 0.1 to 1 MPa, the former study demonstrated a linear relationship between the mass of soot formed from a single hydrocarbon drop and pressure; above 1 MPa, the mass was essentially independent of pressure. The different behaviour may result from the transition to turbulence at higher pressures. The Arai[12] study measured fuel and soot concentrations in a kerosine spray flame, but did not fit a correlation to the data. Hence, the value of the constant *A* is selected so as to give a match to the experimental exhaust levels when the model is run in a combustion simulation.

In a contemporary study at Hiroshima, **Harmadi**[110] obtained an alternative expression for soot formation:

$$\frac{dm_{soot}}{dt} = A\,\phi^{1.25}\,T^{-1}\,e^{-\frac{E_f}{RT}} \qquad (3.8)$$

This expression derived from experimental work in an open diffusion flame and the Khan value for activation energy has been used. It was implemented in an IDI simulation model by Hiroyasu[124], though rather unsuccessfully. In all other versions of Hiroyasu's simulation program, from 1982 onwards, equ. 3.7 given above has been preferred.

Conclusions

Single-term expressions for soot formation typically include an Arrhenius term, and some measure of the fuel concentration. Those derived from measurements over a range of pressures also include a pressure term.

Table 3.3 (over) shows that activation energy estimates vary widely, the lowest being 12.5 kcal/mol[262] and the highest 120 kcal/mol[89]. The lower value is uncertain as the original data shows much scatter, and 40 kcal/mol seems a more realistic value. Fuel concentration dependence also varies widely: for initial burning, several authors give an exponent of unity[287,262,126,93], whilst its initial value is 4 for the Khan expression[170] (including the fuel partial pressure). Different combustion systems were used in the derivations, and it is not possible to find a trend. Variation with pressure is not well-established due to the difficulty in isolating the formation rate in measurements from practical combustion devices, and the problems of extrapolating measurements from basic configurations to real systems.

Despite the uncertainties, both the Khan[170] and the Hiroyasu[125] expressions (equs. 3.3 & 3.7) have given satisfactory performance in combustion simulations[1,126,184].

Researcher	Year	Combustion system	Fuel	E_f (kcal/kmol)	ϕ^n	p^m	T range (K)	P range (atm)
Rao[287]	1984	Laminar diffusion	H_2O-HC	28675	1	n/a	1900-2000	1
Nishida[262]	1979	Turbulent diffusion	propane	12500 (much scatter) (40000 for T>900K)	1	n/a	770-1220	1
Hein[114]	1972	Turbulent diffusion	propane	21500	1	n/a	700-1500	1
Narasimhan[255]	1965	Plug-flow reactor	methane	57000	1	n/a	1300-1700	1
Khan[170,173]	1971	Diesel engine	diesel	39740	3	1	-	40-100
Wilson[371]	1974	-	CH_4,C_3H_4	32000-58000	n/a	n/a	-	-
Kau[164]	1976	Diesel engine[293]	diesel	40000[293]	3	1	-	-
Abbas[1]	1985	Turbulent diffusion[293]	acetylene	40000[277]	3	1	-	1
Naegeli[248]	1983	Gas-turbine combustor	kerosine	58000	3.425	n/a	2100-2320	7-13
Glassman[90]	1981	Laminar diffusion	various	80000-120000	n/a	n/a	2150-2550 (flame)	1
Hiroyasu[121]	1976	Various	various	10000	n/a	1	-	-
Hiroyasu[125]	1982	Single droplet combustion[394], spray flame[370]	paraffins[394], kerosine[370]	12500[245]	1	0.5	-, 1000-1300	1-10[394]
Harmadi[110]	1982	Open diffusion flame	-	40000[293]	1.25	n/a	-	-

Table 3.3 - Single-step soot formation expressions

3.4.1.2 Expressions accounting for oxidation

Many of the expressions in the first class (3.4.1.1) involve an equivalence-ratio term. The significance varies from one expression to another, since ϕ may be taken as the average equivalence ratio in the burning region[170], a local value, or may even be defined in terms of combustion products concentrations[371]. However, in each case, the effect of oxygen is accounted for, and the soot formation rate is always reduced by an increase in its concentration.

A number of studies have expressed dependence on oxygen concentration directly. These are reviewed below.

A group of researchers including **Edelman**[61], **Wang**[363] and **Farmer**[69] have made extensive investigations into soot formation mechanisms and associated combustion models. This work recognises that all previous models have been limited by a lack of coupling between soot emission and chemical kinetic approaches, and addresses this by calculating the combustion chemistry in considerable detail (up to 31 species)[69]. New formation correlations were obtained using model calculations in conjunction with experimental work in a jet-stirred combustor[61] and shock-tube[363].

In the jet-stirred combustor experiments, combustion is essentially premixed and adiabatic; temperatures are in the range 1650 to 1850 K and the pressure is atmospheric. The shock-tube data of Wang covers a broader range of conditions (1400 to 2500 K and 2.5 to 10 atm), so the effect of pressure could be included in the correlation.

Edelman used a quasi-global model to describe the combustion chemistry, accounting for pure pyrolysis, oxidative pyrolysis, partial oxidation and elementary steps to completion, as well as NO_x formation. Aldehydes are considered as intermediates and a total of 42 reactions are included. Oxidation was incorporated using the Lee correlation[207] or that of Nagle[249,69], though it is fairly insignificant in a jet-stirred combustor, reducing soot emission by 25% at most. Coagulation was neglected. A variety of fuels and fuel combinations were used, though a single soot model was proposed based on data from the toluene case and an averaged hydrocarbon concentration. The following formation correlation includes tentative values of the variable model parameters:

$$\frac{dm_{soot}}{dt} = A\, m_f^{1.75}\, m_{O_2}^{-0.5}\, T^{-2}\, e^{-\frac{E_f}{RT}} \qquad (3.9)$$

Edelman demonstrated excellent results in predicting the jet-stirred combustor soot emission using this model. In contrast, the Khan[170] and Tesner[345] models were found to perform poorly and this was attributed partly to the method used to obtain the rate constants in these studies.

Wang[363] fit the following equations to shock-tube data:

For T < 1800 K:

$$\frac{dm_{soot}}{dt} = A\, m_f^{2.06}\, m_{O_2}^{-0.36}\, m_{Ar}^{0.35}\, e^{-\frac{E_f}{RT}} \qquad (3.10)$$

For T > 1800 K:

$$\frac{dm_{soot}}{dt} = A\, m_f^{2.06}\, m_{O_2}^{-0.36}\, m_{Ar}^{0.35}\, e^{-\frac{E_{fA}}{RT}+\frac{E_{fB}}{R}\left(\frac{1}{T}-\frac{1}{1800}\right)} \qquad (3.11)$$

The argon concentration exponent in these expressions causes the soot formation rate to rise with increased pressure, though the exponent value of 0.35 is relatively small. Yield comparisons were made with the predictions of the Khan[170] and Edelman[61] models and reasonable agreement was shown. However, the Edelman model[61] shows a stronger dependence upon the hydrocarbon concentration than on the temperature, which is not shown in the current study. This is attributed to the narrow temperature range of the Edelman[61] experiment and uncertainties in the temperature measurements. Thus, this model is considered to be an improvement on the Edelman correlation.

Farmer's review paper[69] provides more detail relating to the above studies. Final values of the constants used in equ. 3.9 are given, but these vary little from Edelman's original estimates. The importance of building the soot model on top of accurate predictions of fuel chemistry is stressed. Preliminary work showed the importance of including the hydroxyl radical in the mechanisms. The satisfactory performance of the Edelman model is further demonstrated, particularly the

accurate prediction of the rich limit where the soot yield rises rapidly.

Najjar[251] made measurements of soot concentration in a model gas-turbine combustor using a range of kerosine-like fuels. Pressures varied between 3 and 10 atm. The following expression was proposed to describe soot formation in the primary zone:

$$\frac{dm_{soot}}{dt} = A\, m_f e^{-\frac{E_f}{RT}} - B\, m_{O_2} m_{soot} e^{-\frac{E_{O_2}}{RT}} \qquad (3.12)$$

A combustion calculation was run in parallel to determine the fuel concentrations, whilst gas temperatures were estimated from radiation measurements and the calculated adiabatic flame temperatures. The constants A, B and the activation energies were determined by fitting the predictions to the experimental data[250].

Though this expression is described as a formation rate, it could be better described as a net formation rate, i.e. the difference between formation and oxidation. However, this cannot be deduced simply from the form of the expression, since this is very similar to that proposed by Tesner for pure formation (see below) where the second term represents the termination of soot precursors. Rather, the fact that oxidation is otherwise neglected in the primary zone suggests that this expression represents both processes; in the second part of the paper[252], a modified form of the Nagle[249] expression is used to describe the oxidation of soot in the secondary zone. In fact, it is very hard to separate the formation and oxidation processes, and it may not be possible to divide up the expression to fit this simplistic concept.

Simmons[319] proposed a similar relationship for describing soot formation in furnaces:

$$\frac{dm_{soot}}{dt} = A\, m_f^{2.36} e^{-\frac{E_f}{RT}} - B\, m_{O_2}^{1.3} e^{-\frac{E_{O_2}}{RT}} \qquad (3.13)$$

The form of the expression is such that it can deal with pyrolytic production in a generally accepted form, whilst accounting for the destruction of soot-forming precursors in oxidative reactions. The constant values were determined using data

from shock-tube experiments with benzene, toluene and n-heptane fuels. The pressure range was 2.6 to 3.6 atm, temperatures lay between 1500 and 1950 K, and the equivalence ratio varied between 6 and 11. The data was correlated satisfactorily, though the pressure range was too small to determine a pressure dependency.

Simmons discusses the correlations of Khan[170], Abbas[1], Harmadi[110], Naegli[248] and Najjar[251] and compares predictions with the experimental data. The Khan[170] correlation broke down for mixtures richer than ϕ=8, and is not applicable for pyrolytic conditions due to the inverse relationship with unburnt air. A similar situation applies to the Harmadi model. Najjar's expression[251] yielded formation rates which were an order of magnitude too high, though the second term in the equation was omitted due to lack of a soot concentration estimate. Mullins[243] reports the same work and tabulates the calculated formation rates. At ϕ=7 and 3 atm, the values for the Khan[170], Wang[363], Najjar[250] and Simmons[319] correlations were approximately 0.2, 7, 700 and 1.5 respectively. The poor agreement is attributed to the fact that the expressions were derived for different combustion systems[243].

Conclusions

Models have been proposed which treat the chemistry of the soot-formation process in more detail while maintaining the concept that all processes can be represented by an apparent first-order reaction. The distinctive feature of these models is the separate description of the effect of oxygen. In Simmon's work, oxidative destruction of soot precursors is accounted for explicitly. Overall, very good results have been obtained for simple combustion systems and a model combustor. However, caution is necessary since the conditions in these combustion devices differ greatly from those in the diesel.

The short-comings of some of the simple models described in section 3.4.1.1 arise partly because the models have been applied beyond the range of operating conditions for which they were derived. Only one of the models in the current section attempts to include pressure effects; the dependency found is quite small, with an exponent value of 0.35.

Researcher	Year	Combustion system	Fuel	E_f (kcal/kmol)	m_{fuel}^n	$m_{O_2}^m$	T range (K)	p range (atm)
Edelman[61,69]	1979	Jet-stirred combustor	ethylene, toluene, isooctane	32000	1.75,1.71	-0.3	1650-1850	1
Wang[363]	1981	Shock-tube	toluene, benzene, acetylene	61800 T<1880K, >25000 @T=2500K	1.71, 2.06	-0.5	1400-2500	2.5-10
Najjar[251]	1981	Gas-turbine combustor	3 jet fuels	23850	1	n/a	-	3-10
Mullins[243]	1987	Shock-tube	toluene, benzene, n-heptane	26630	2.36	n/a	1300-1850	2.6-3.6
Bockhorn[25]	1993	Premixed flame	several	28700-38420	1	n/a	1400-2000	1-100
Sato[302]	1990	Jet-stirred combustor	toluene	n/a	n/a	n/a	1150-1500	1
Kennedy[167]	1990	Laminar diffusion	ethylene	n/a	n/a	n/a	<2500[98]	1

Table 3.4 - Soot formation expressions accounting for oxidation, and surface-growth expressions

3.4.1.3 Surface-growth expressions

Bockhorn[25], **Wagner**[27,28,29,30], **Sato**[302], **Kennedy**[167] and **Garo**[86] have developed a new type of model based on surface growth and data-sets of measured rates/yields. A review is given by Bockhorn[25]. Bockhorn and Wagner use a basic equation of the form:

$$\frac{df_v}{dt} = k_{SG}(f_v^{\infty} - f_v) \tag{3.14}$$

k_{SG} is interpreted as a chemical rate coefficient and can be expressed in terms of simple chemistry and surface reactivities. f_v^{∞} is the 'final' soot volume fraction attained after the rapid formation phase of soot shortly after the main reaction zone of the flame in premixed systems. Maps of data for f_v^{∞} against carbon-to-hydrogen ratio and temperature have been constructed from empirical measurements. For the former, the relationship may be expressed as:

$$f_v^{\infty} \propto \left(\frac{C}{O} - \frac{C}{O}_{crit} \right)^n \tag{3.15}$$

where C/O_{crit} is the C/O ratio at the sooting limit

$n \approx 2.5$ - 3 for ethylene, ≈ 4 for propane, ≈ 2.8 for benzene

The dependency on pressure has also been determined. For pressures between 1 and 10 atm:

$$f_v^{\infty} \propto p^2 \tag{3.16}$$

For pressures between 10 and 100 atm:

$$f_v^{\infty} \propto p \tag{3.17}$$

These results apply to premixed flames and simple fuels. The concept cannot be extended to diffusion-flame systems, because no unique relationship exists between mixture fraction and yield. Though *rates* may be mapped in terms of temperature and mixture fraction, different modelling techniques are required. In any case, the required libraries of rate data are not yet available for diesel fuel. Therefore, these techniques are not discussed further.

3.4.1.4 More detailed mechanisms

This section reviews those expressions which have attempted to model the soot formation process using a more detailed mechanism of two or more steps; these models are reviewed by Fairweather[68]. All such models account separately for the coagulation and nucleation processes. This makes it necessary to introduce a new variable, a number density of radical nuclei or soot particles. Summary data is given in Table 3.5 below.

Tesner[345] proposed a two-equation model describing the formation rate of radical nuclei and soot particles. Measurements of particle formation rates during thermal decomposition of acetylene in a laminar diffusion flame were used to determine the constant values in the following equations:

$$\frac{dn_{nuc}}{dt} = n_o + (f - g)\, n_{nuc} - g_o N_{soot}\, n_{nuc} \qquad (3.18)$$

$$\frac{dN_{soot}}{dt} = A(a - bN_{soot})\, n_{nuc} \qquad (3.19)$$

where n_{nuc} is the concentration of radical nuclei in particles per unit volume
N_{soot} is the concentration of soot in particles per unit volume

In the upper equation, n_o is the spontaneous origination rate of nuclei. Nuclei are not small soot particles, but rather 'active particles' which are some sort of soot precursor[325]. The second term represents chain branching with f being the linear branching coefficient and g the linear termination coefficient. The final term is for termination on soot particles with coefficient g_o. The second equation sets the rate of formation of soot particles which depends on the interaction between the radical nuclei and the original hydrocarbon molecules and is limited by termination on the surface of soot particles[345]. a is representative of the reciprocal of the time for formation of the smallest soot particles, about 1 nm in size, from radical nuclei[325]. The model does not predict soot particle size, so this must be assumed if the mass formed is to be evaluated.

The nucleation rate is defined by assuming a first-order reaction of the acetylene fuel:

$$n_o = \frac{A\, m_f\, e^{-\frac{E_f}{RT}}}{\rho} \tag{3.20}$$

The measured value of the activation energy, E_f is very high, namely 170 kcal/mol.

These equations are expressed in terms of concentrations and the measurements were made at atmospheric pressure. However, if they are to be applied under conditions of varying pressure, the saturation values of soot mass and nuclei number will have to rise and fall to maintain a constant number density. This seems physically unrealistic, and for use in a diesel engine **Nakakita**[254] has suggested the following modifications of the constants g_o and b:

$$g_o = g_{o,ref} \frac{T_{local}}{T_{ref}} \frac{p_{ref}}{p_{local}} \tag{3.21}$$

$$b = b_{ref} \frac{T_{local}}{T_{ref}} \frac{p_{ref}}{p_{local}} \tag{3.22}$$

There are many adjustable constants in this model and the particle growth step does not incorporate any physical understanding of the process. Surovikin[335] found that very different constant values were necessary for prediction of benzene pyrolysis, but on the other hand, Magnussen[224] obtained a good match to turbulent acetylene-air flame data using slightly adjusted values.

Surovikin developed a detailed analytical model accounting for formation and growth of radical nuclei, and growth of soot particles, though neglecting coagulation of the latter[335]. Extensive use is made of collision rates from kinetic theory. The mechanism requires two further independent variables - the size of the radical nuclei and soot particles. Model constants were fitted using experimental data from benzene decomposition. A value of 116 kcal/mol was determined for the activation energy for radical formation, which is lower than Tesner's value. The activation energy of surface growth is very low at 6-9 kcal/mol.

Jensen has developed an elaborate soot-formation model which includes five controlling processes: gas reactions producing radical fragments on which nucleation may begin, nucleation, coagulation, growth and oxidation[150]. The soot is described

in terms of a set of fifteen representative particle sizes, and the other processes are calculated using rate coefficients appropriate to each size. The model was successfully applied to prediction of exhaust soot levels in a rocket motor fuelled by isopropyl nitrate.

Moss[242] has developed the soot-formation model proposed by Gilyazetdinov[88]. This uses the following pair of equations to describe the evolution of soot-particle number density, N_{soot}, and mass, m_{soot}:

$$\frac{dN_{soot}}{dt} = A\rho T^{\frac{1}{2}} m_f e^{-\frac{E_{nuc}}{RT}} - BT^{\frac{1}{2}} N_{soot}^2 \qquad (3.23)$$

$$\frac{dm_{soot}}{dt} = C\rho T^{\frac{1}{2}} m_f e^{-\frac{E_{nuc}}{RT}} + DT^{\frac{1}{2}} m_f N_{soot} e^{-\frac{E_{sg}}{RT}} \qquad (3.24)$$

The first term in the upper equation represents nucleation whilst the second is for coagulation; the terms of the lower expression describe the contributions of coagulation and surface growth respectively. The particle size can be calculated from the values determined.

In conjunction with Nagle's oxidation model, the values of the constants A, B, C and D were set to give satisfactory agreement between predictions and data from a laminar ethylene-air diffusion flame at pressures of 1 to 3 atm. Generally, surface growth will be a function of soot particle size and the following modification was introduced to represent this:

$$CT^{\frac{1}{2}} m_f m_{soot}^{\frac{2}{3}} N_{soot}^{\frac{1}{3}} e^{-\frac{E_{sg}}{RT}}$$

Later work extended applicability to modelling of non-premixed kerosine-air flames. It was found necessary to enhance sensitivity to the fuel mass by including additional exponents, two for the nucleation term and five for surface growth[334].

Fairweather (1991)[209,67,68,211] has introduced a similar pair of equations for soot number density and mass formation rates:

$$\frac{dN_{soot}}{dt} = A\, m_{C_2H_2} e^{-\frac{E_{nuc}}{RT}} - BT^{\frac{1}{2}} m_{soot}^{\frac{1}{6}} N_{soot}^{\frac{11}{6}} \qquad (3.25)$$

$$\frac{dm_{soot}}{dt} = C\, m_{C_2H_2} N_{soot} e^{-\frac{E_{sg}}{RT}} + D\, m_{C_2H_2} m_{soot}^{\frac{1}{3}} N_{soot}^{\frac{1}{6}} - Em_{O_2} T^{\frac{1}{2}} m_f m_{soot}^{\frac{2}{3}} N_{soot}^{\frac{1}{3}} e^{-\frac{E_{nuc}}{RT}} \qquad (3.26)$$

The terms have the same significance as those of the Moss[242] model with the addition of a final term for oxidation. In this case, the fuel concentration is expressed in terms of acetylene, which is an important intermediate in the sooting process; thus, accurate prediction of its concentration is a requirement of the combustion model. Constants were chosen to match the data of Nishida for a turbulent non-premixed propane flame[261].

Conclusions

The models described in this section introduce a level of flexibility into the modelling of soot formation. The Tesner model is the simplest, but has been used most extensively. The Surovikin, Moss and Fairweather models are more sophisticated in being able to track the size of the particles as well as the mass. Jensen's model is the most elaborate, giving a soot description in terms of fifteen representative carbon particle sizes. The Moss, Fairweather and Jensen models were all successfully applied in engine modelling.

The comparative study of Coehlo[47] includes the Moss[242] and Fairweather[67] models. A fair match with the Nishida data was obtained with each, though the results were taken to indicate that the Moss[242] model is more sensitive to variation in conditions.

Researcher	Year	Combustion system	Fuel	E_f (kcal/kmol)	m_{fuel}^n	T range (K)	p range (atm)
Tesner[345]	1971	Diffusion flame	acetylene	170000 (nucleation)	1 (nucleation)	1900	1
Surovikin[335]	1976	Pyrolysis	benzene	116000,30000 (formation & growth of radical nuclei), 6000-9000 (growth)	1 (nucleation), 1 (growth)	1400-1800	1
Jensen[150]	1974	Rocket motor	isopropyl nitrate	n/a	n/a	1500	28-110
Moss[242]	1988	Diffusion flame	ethylene, kerosine	91610 (nucleation), 25040 (growth)	1 (nucleation), 1 (growth)	600-1800	1-3
Fairweather[209,67]	1991	Diffusion flame	propane	41930 (nucleation), 24040 (growth)	1 (nucleation), 1 (growth)	500-1800	1

Table 3.5 - Soot formation expressions using more detailed mechanisms

3.4.2 Coagulation

In the detailed models reviewed above, formation rates are expressed in terms of number densities, and coagulation is an essential feature. For the models of the preceding sections, however, formation rates involve mass alone so that coagulation may be ignored. Nevertheless, coagulation models may be usefully employed in conjunction with these models for the purpose of estimating the particle size to be input to the oxidation calculations. Thus the subject is considered briefly below; summary data is given in Table 3.6.

The simplest coagulation-rate expression is the Smoluchowski equation:

$$\frac{dN_{soot}}{dt} = \frac{1}{2} K N_{soot}^2 \qquad (3.27)$$

Various authors including **Green**[97], **Khan**[171], **Wersborg**[367], **Ulrich**[355] and **Du**[60] have obtained theoretical and empirical values of the coagulation constant, K, in this equation (see Table 3.6). Khan's value is noticeably higher than the others, which Khan and Du[60] consider may be due to the higher turbulence intensity in the diesel engine. Smith[325] thinks this interpretation is unlikely.

For particles which are small with respect to the mean free path of the gaseous medium, coagulation occurs in the 'free molecule' regime (see section 3.1.2). Applying bimolecular collision theory and assuming uncharged particles which coalesce on every collision, various theoretical studies have obtained a modified form of the above expression[325,113]:

$$\frac{dm_{soot}}{dt} = A\, T^{\frac{1}{2}}\, m_{soot}^{\frac{1}{6}}\, N^{\frac{11}{6}} \qquad (3.28)$$

In applying this equation to sooting processes in a shock-tube, **Graham**[95] obtained excellent agreement with the experiment, confirming the theoretical assumptions. Fairweather's model incorporates this expression[209], whilst the models of Tesner[345], Jensen[150] and Moss[242] use a form of the Smoluchowski equation.

Coagulation

Researcher	Year	Source	Coagulation constant in equ. 3.27 ($m^3 particle^{-1} s^{-1}$)	T range (K)	p range (atm)
Green[97]	1964	Aerosols	0.5×10^{-15}	-	-
Khan[171]	1971	Diesel engine (motoring)	5.93×10^{-11}	300-900	1-20
Wersborg[367]	1973	Premixed flame	1.7×10^{-13}	-	0.026
Du[60]	1983	Diesel engine blowdown bag	2.7×10^{-15}	-	20-50
Ulrich[355]	1976	Oxide synthesis flame	n/a	<1975	1
Graham[95]	1975	Diffusion flame	n/a	1600-2300	1
Tesner[345]	1971	Diffusion flame	10^{-15}	1900	1
Moss[242]	1988	Diffusion flame	$1.67 \times 10^{-15} T^{0.5} = 5 \times 10^{-14}$	600-1800	1-3
Fairweather[67]	1992	Diffusion flame	n/a	500-1800	1

Table 3.6 - Coagulation expressions

3.4.3 Soot oxidation

The body of research work devoted to the oxidation of soot is of comparable size to that done on formation. However, the oxidation mechanism is conceptually simpler, and there is a much greater degree of uniformity in the expressions used to describe the process. Soot particles are so small that the rate of oxidation will not be limited by diffusion under typical chamber conditions[243]. Thus, the vast majority of models consider oxidation to be essentially chemically-controlled, and are based on simple Arrhenius expressions. These are reviewed in section 3.4.3.1 below. In turbulent combustion, though, the physical separation of the reactants means that combustion may be dominated by mixing processes and an alternative approach based entirely upon a fluid mechanical concept has also been extensively used[226]. This is described in section 3.4.3.2.

As in the case of formation, the differences between expressions often arise because of the variation in the thermodynamic conditions and fuels used in the evaluation. It is important to take this into consideration when comparing models, and basic experimental details are presented at the end of this section in Table 3.7. Also, some of the key model parameters are tabulated to facilitate comparison.

3.4.3.1 Chemical rate

The exact nature of the chemical attack on soot particles will depend upon the surrounding gas and thermodynamic conditions. Many mechanisms are based on the assumption that the most important oxidising species is the O_2 molecule and in fact some were derived under conditions where this is certainly the case[171]. However, it is known that the hydroxyl radical is the dominant oxidising species in flames, at least under fuel-rich conditions[113], but only one study has obtained a correlation in terms of its concentration. This is described at the end of this section.

Many authors have used a soot-oxidation correlation of the following general form (*m* is often set to unity, and *n* to zero):

$$\frac{dm_{soot}}{dt} = A\, m_{soot}\, X_{O_2}\, p^m\, T^n\, e^{-\frac{E_a}{RT}} \qquad (3.29)$$

Feugier[73,74], **Shibayama**[311] and **Nishida**[260] reduced this expression to:

$$\frac{dm_{soot}}{dt} = A\, m_{soot} X_{O_2} e^{-\frac{E_o}{RT}} \qquad (3.30)$$

There is no significance in the omission of the pressure term, since the experiments were conducted at atmospheric pressure. Feugier's study examined a laminar diffusion flame at 2000 to 2300 K. Shibayama made measurements in a fuel-oil spray-flame at temperatures below 1650 K and obtained a good correlation with temperature. Nishida's results from a turbulent diffusion flame at temperatures below 1350 K are less satisfactory. The rate data obtained shows a lot of scatter, so the activation energy value derived from it should be treated with caution.

Hiroyasu[125] introduced a pressure dependency of 1.8 though the source papers given[12,155] did not directly examine the effect of pressure on oxidation. A more likely source would be the diesel engine study by these authors[123].

Lee[207] obtained the following correlation from measurements in a laminar diffusion flame covering the temperature range 1300 to 1680 K and at oxygen partial pressures of 0.05 to 0.1 atm:

$$\frac{dm_{soot}}{dt} = A\, m_{soot} X_{O_2} p\, T^{-\frac{1}{2}} e^{-\frac{E_o}{RT}} \qquad (3.31)$$

Khan[171] used measurements from a motoring diesel engine to check the values of the constants in this expression and obtained a slightly larger value of A. However, with Khan's study the pressure reached 20 atm. By comparison with data from the studies of Field[75] and Parker[270] on solid carbon oxidation, Khan deduced that the combustion rate of soot is two orders of magnitude lower. This is attributed partly to Lee's[207] neglect of coagulation, which results in a very large specific surface for the particles. Taking this into account, Khan[171] estimates a discrepancy of only one order of magnitude.

Magnussen[221] compared Lee's data with measurements made for solid carbon by Field[75], Parker[270], Tu[352], Nagle[249] and Golovina[93], and also concluded that the specific surface reaction-rate is two orders of magnitude lower. The possibility that

this is partly due to the neglect of agglomerates is mentioned in the 'Comments' section. Another possibility is that desorption of oxygen is a significant process and a new expression is proposed based on this assumption:

$$q = \frac{K_1}{1 + \frac{K_1}{K_2}} \tag{3.32}$$

where q is the surface reaction rate, and:

$$K_1 = k_1 p_{O_2}{}^2 e^{-\frac{E_{a1}}{RT}} \tag{3.33}$$

$$K_2 = k_2 e^{-\frac{E_{a2}}{RT}} \tag{3.34}$$

Here, K_1 represents the rate of adsorption and the rate of reaction, and K_2 is the rate of desorption. Using Lee's data, Magnussen determined the constants in this expression and demonstrates a closer correlation than with the original expression. Thus, it is assumed that the new expression will better satisfy experimental data outside the range of Lee's measurements.

In the same year, 1971, Radcliffe[282] suggested that the oxidation rates of soot and pyrolytic graphite should be approximately equal and demonstrated a different interpretation of the apparently conflicting data. Park[269] argues that Magnussen's different conclusion arose because the basis of the comparison was carbon of more isotropic structure than pyrolytic graphite, e.g. the 'Reactor' graphite.

In view of these findings, data from solid-based oxidation studies should be used with care[113]. Such studies are very numerous and are reviewed by **Laurendeau**[204] and others[113]. Most of this work has concentrated on determination of the activation energy for oxidation. The study of **Nagle**[249] is of particular interest and has been widely used in the context of engine modelling.

Nagle[249] developed the theoretical model of surface reaction rate proposed by Blyholder. It is assumed that there are two types of reaction site on the solid surface, namely an 'A-site' which is more reactive, and a less reactive 'B-site'. An equation for reaction rate can then be defined:

$$\frac{dm_{soot}}{dt} = A\, m_{soot}\left[\left(\frac{k_A p_{O_2}}{(1+\frac{p_{O_2}}{k_Z})}\right)X + k_B p_{O_2}(1-X)\right] \qquad (3.35)$$

where, X, the fraction of the surface covered by A-sites, is defined as follows:

$$X = \frac{1}{1+\frac{k_T}{p_{O_2} k_B}} \qquad (3.36)$$

and, k is a simple Arrhenius term:

$$k = K e^{-\frac{E_o}{RT}} \qquad (3.37)$$

At low temperatures, active sites dominate, and the rate is controlled by the fraction of sites not covered by surface oxides. Thus, the rate is exponential with temperature and the equivalent activation energy is that of k_A/k_Z, i.e. 34.1 kcal/mol. Beyond a certain temperature, thermal rearrangement favours the formation of unreactive B-sites and the overall rate will decrease because of the lower reactivity (desorption is rapid); eventually when B-sites dominate, the order in oxygen partial pressure tends to unity and rises again with temperature.

In the original work, the values of the constants were determined for the experimental range $10^{-5} < p_{O_2} < 1$ atm and temperatures between 1100 and 2500 K. Several authors have provided further empirical validation and extended the temperature range of the expression. The work of Park[269] is most comprehensive, and the summary plot given in that paper has become the standard for comparing oxidation rates. It is shown in Fig. 3.2 below.

The plot includes the data of Tesner[344], Lee[207], and Fenimore[70] as well as Park's own shock-tube measurements extending the temperature range to 4000 K and the oxygen partial pressure to 13 atm. Park[269] concludes that the Nagle rate is approximately a factor of two too low at high temperature, and further confirmation is provided by the measurements of Walls[359] and Lundell[219]. Mullins extended the analysis to include the low-temperature data of Chan[41] and the correlations of

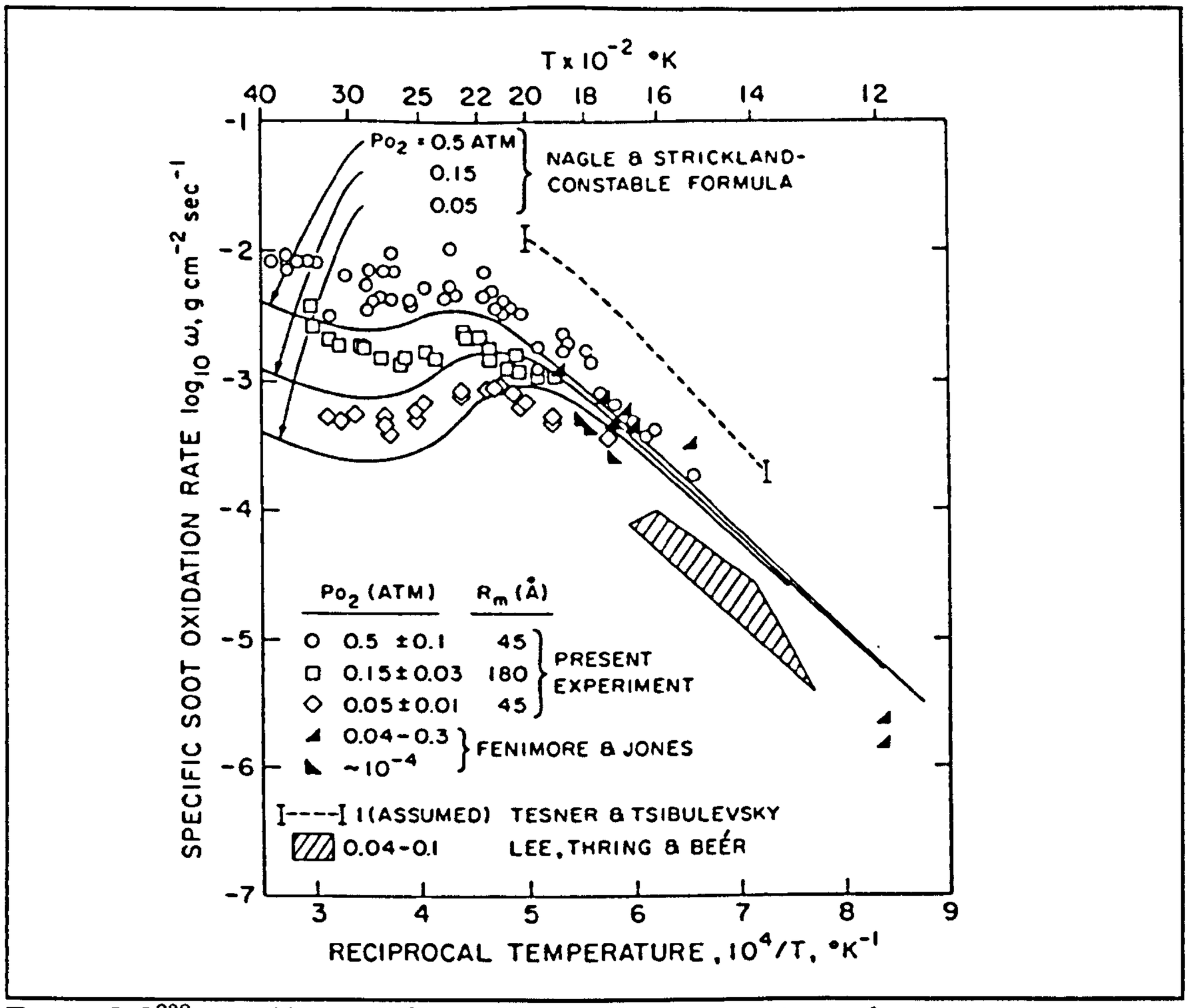

Figure 3.2[238] - Park's plot of soot oxidation rate v reciprocal temperature

Garo[85], Smith[326] and Hargreave[109]. On the basis of all of the available data, the following relationship was obtained as a best fit at flame temperature conditions:

$$\frac{dm_{soot}}{dt} = A\, m_{soot}\, p_{O_2}^{\frac{1}{2}}\, e^{-\frac{E_a}{RT}} \qquad (3.38)$$

The activation energy value is 38.2 kcal/mol.

Najjar[251] modified some of Nagle's constant values and obtained good agreement with data from a model combustor. The original form of the correlation has also been successfully applied in a variety of combustion systems, including the jet-stirred combustor[69], gas turbine[251] and diesel engine[124].

Tesner[344] and Wilson[371] are unique in including an equivalence-ratio dependency in the oxidation-rate correlation. **Tesner**[344] derived the following relationship from measurements in a laminar diffusion flame:

$$\frac{dm_{soot}}{dt} = A\, X_{O_2}\, p\, \phi^{-1}\, T^{-\frac{1}{2}}\, e^{-\frac{E_{ox}}{RT}} \qquad (3.39)$$

This expression is otherwise similar to that of Lee. The effect of the additional term is to increase the order of the oxygen dependency to two or more; this is not consistent with Nagle's expression[249].

Wilson[371] proposed the following expression for use with a quasi-dimensional diesel combustion model:

$$\frac{dm_{soot}}{dt} = A\, p\, \phi^{-1}\, T^{\frac{1}{2}}\, e^{-\frac{E_o}{RT}} \qquad (3.40)$$

Fenimore[71] is the only researcher to have determined an oxidation expression in terms of the hyrdoxyl concentration. A linear dependence was obtained:

$$\frac{dm_{soot}}{dt} = \frac{A\, m_{soot}\, X_{OH}\, e^{-\frac{E_o}{RT}}}{d} \qquad (3.41)$$

The measurements were made in a diffusion flame at oxygen partial pressures of between 0.04 and 0.3 atm. An order of magnitude increase in the rate was observed as the pressure increased from 1 to 3 atm. Park[269] considers that the apparent dependence on temperature and oxygen partial pressure obtained by other authors may be mainly accounted for by changes in equilibrium OH concentration.

3.4.3.2 Turbulent rate

The important effects of turbulence on oxidation rate have been described (section 3.1.6). Magnussen expressed the consumption rate as first order in soot concentration and oxygen mass fraction[223]:

$$\frac{dm_{soot}}{dt} = A\, m_{soot} X_{O_2} \frac{\varepsilon}{k} \qquad (3.42)$$

ε/k is the reciprocal of the timescale for turbulent mixing. Many variants have since been proposed representing different models of the segregation of the reactants and products[102].

The model has been successfully applied to the prediction of turbulent diffusion flames, enclosed premixed flames and premixed diffusion flames[226].

Despite the success of this model[1,223], Mullins[243] argues against the necessity of incorporating turbulent-mixing steps in gas-turbine models, stating that turbulent mixing is not a controlling factor in gas turbine situations, which are lean. Turbulence levels are generally higher in the gas turbine than the diesel, and it has been shown that diesel smoke can be well-correlated in terms of the turbulent timescale[55]. Thus, this assertion is not well-supported.

3.4.3.3 Conclusions

The most popular soot-oxidation expressions are those of Nagle[249] and Lee[207]. In fact the former is more generally applicable and is supported by many other measurements (see plot of Park[269], Fig. 3.2). Despite evidence of the importance of hydroxyl radicals and turbulent mixing in controlling the oxidation rate, considerable success has been reported in the application of these expressions to practical combustion devices. The activation energies are relatively well-established. However, in the case of the diesel engine, the conditions are different from those of most of the expression derivations. In particular, the average partial pressures of oxygen are generally higher; also, because conditions are often fuel-rich and the temperatures are high, oxidation by hydroxyl radicals is likely to be more significant. For these conditions, the quantitative accuracy has not been clearly shown.

Soot oxidation

Researcher	Year	Combustion system	Fuel	E_{ox} (kcal/kmol)	T range (K)	p_{o_2} range (atm)
Feugier[73,74]	1972	Laminar diffusion	ethane	20000	2000-2300	<0.56
Nishida[260]	1979	Turbulent diffusion	propane	14000 (much scatter)	830-1350	0.07
Shibayama[311]	1968	Spray flame	fuel oil	37000	650-1650	0.08
Hiroyasu[124]	1982	Spray flame[12]	kerosine[12]	14000[260]	1000-1300[12]	0.04-0.12[12]
Lee[207]	1962	Laminar diffusion	propane	39300	1300-1680	0.05-0.1
Khan[171]	1971	Diesel engine (motoring)	diesel	39300	1600	-
Magnussen[221,75,270,352,93,249]	1971	Laminar diffusion[207], solid carbon[75,270,352,93,249]	propane[207], carbon	35700	1000-2500	0.05-0.1
Park[269]	1973	Shock-tube	carbon black	n/a	1700-4000	0.05-13
Laurendeau[204]	1978	Solid	coal char etc	Many, 25000-80000	700-2200	10^{-6}-0.2
Mullins[243,70,207,269,85,41,344]	1987	Many	many	38240	770-3300	0.1
Chan[41]	1987	Laminar diffusion	propane	34300	770-1250	0.01-0.2
Nagle[249]	1962	Solid carbon	pyrographite	34100 low T-limit; 15200 high T-limit	1000-2000	0.1-0.6
Tesner[344]	1967	Laminar diffusion	acetylene-H_2, acetylene-H_2O	40000[3371]	1400-1870	<0.003
Fenimore[71]	1969	Laminar diffusion	ethane	n/a	<2200	-
Magnussen[223]	1976	Turbulent diffusion	acetylene	n/a	300-2000	n/a

Table 3.7 - Soot oxidation expressions

3.5 DIESEL MODELS

Most of the diesel engine models used for soot emission prediction have been of the zonal phenomenological type, but simple thermodynamic simulations, stochastic models and multi-dimensional techniques have also been employed. Several different soot formation and oxidation expressions have been examined, but no comparative study has been undertaken. The techniques used and progress reported in these works are reviewed below.

Table 3.8 presents summary information on model types and the related soot expressions. Every unique combination of soot and combustion model is listed, though a number of related works which did not incorporate soot calculations are omitted. Models deriving from a common source are grouped together, including later work which was done by independent authors, and each group of models is classified by a chosen main author (this author is used in later references to the models). All the soot models used have been previously discussed in section 3.4 and the expressions are also set out in Appendix B.

3.5.1 Review

The earliest application of a soot model in the diesel was the work of **Khan**[170] in 1971. In this study a formation expression was postulated and a thermodynamic simulation was used to fit the model constants by matching to exhaust values for different injection timings (equ. 3.3). The combustion model describes the temperature and equivalence ratio of the jet, but does not represent the variation of these quantities within the jet. However, the calculated mass of micromixed fuel-air mixture is used to estimate the equivalence ratio and temperature in the soot formation region, so that the emission model has an element of dimensionality.

The original work neglected oxidation[170]. Nevertheless, predictions of soot variation with injection parameters showed excellent agreement with the experimental data. On the other hand, for different engines and running speeds, variations of up to an order of magnitude were found. A later work[173] incorporated Lee's oxidation model[207], but this was found to make little difference to the quantity exhausted.

Main author	Year	Eng.	Model type	Authors	Soot formation	Soot oxidation
Khan	1971	DI	Quasi-D	Khan[170]	Khan[170]	-
				Khan[173]	Khan[173]	Lee[207]
Wilson	1974	DI	Multizone	Wilson[371]	Khan[170]	-
				Kau[164]	Khan[170]	Lee[207]
Hiroyasu	1976	DI	Multizone	Hiroyasu[121]	Hiroyasu[121]	Lee[207]
	1982	IDI	Multizone	Hiroyasu[124]	Harmadi[110]	Nagle[249]
	1982	DI	Multizone	Hiroyasu[126], Kuo[197]	Hiroyasu[125]	Hiroyasu[125]
	1989	DI	Multizone, multi-D diff.	Nishida[262]	Hiroyasu[125]	Hiroyasu[125]
Dent	1981	DI	Quasi-D	Dent[57], Kyriakides[198]	Tesner[344]	Magnussen[223] + Lee[207]
	1986	DI	Multizone	Mehta[104,105,237]	Tesner[344]	Magnussen[223]
Mansouri	1982	IDI	Stochastic	Mansouri[227,228]	equilibrium	Nagle[249]
				Kittelson[174]	(Khan) Harmadi[110]	Nagle[249] + Fenimore[71]
	1987	DI	Stochastic, multiple comp. zone, multi-D flow	Brown[37]	Wang[363]	Nagle[249]
Kono	1985	DI	Multizone	Kono[184]	Hiroyasu[125]	Hiroyasu[124]
Kouremenos	1987	DI	Quasi-D	Kouremenos[191]	Hiroyasu[125]	Hiroyasu[125]
	1989	IDI	Multizone	Kouremenos[192]	Hiroyasu[125]	Hiroyasu[125]
Wade	1987	DI	Zero-D, 3 comp. zone	Wade[356]	Hiroyasu[125]	Hiroyasu[125]
Zhou	1989	DI	Multizone	Zhou[389]	Hiroyasu[125]	Hiroyasu[125]
Lapuerta	1990	DI	Multizone	Payri[271]	Hiroyasu[125]	Hiroyasu[125]
Nakakita	1990	IDI	Multi-D	Nakakita[254]	Tesner[344] + Farmer[69]	Magnussen[223] + Nagle[249]
Zellat	1990	IDI	Multi-D	Zellat[386,387]	Tesner[344]	Magnussen[223]
Xiao	1991	DI	Multizone, stochastic	Xiao[378]	Khan[173]	Nagle[249] + Fenimore[71]
Bazari	1992	DI	Multizone	Bazari[19,20,327]	Hiroyasu[125]	Hiroyasu[125]

Table 3.8 - Diesel simulation soot models

Wilson[371,164] simply applied a modified version of Khan's expression (equ. 3.4), but this time in a zonal model. No results were given.

Hiroyasu incorporated soot prediction in the first version of his multizone combustion model[121]. Soot formation is expressed in terms of the fuel burn rate using a simple expression proposed by the same author (equ. 3.6), and Lee's expression was used for oxidation. Parametric predictions were mixed. For the model applied to an IDI diesel[124], the soot-formation expression of Harmadi was used, in conjunction with the Nagle[249] oxidation correlation. Poor results were briefly reported, but this may have been due to weaknesses in the combustion model. However, as with the earlier simple formation expression, the Harmadi model was abandoned in subsequent work[126,262].

Also in 1982, Hiroyasu postulated a pair of expressions for soot formation and oxidation[125] (equs. 3.7, 3.29) which have since been used by five other research groups (see below)*. These expressions are calibrated by fitting to exhaust data, which related to a heavy-duty DI diesel engine in the case of the original work. Excellent predictions of exhaust soot were obtained for varying injection timing, engine speed and swirl ratio. However, in applying the same model to two open-chamber diesel engines, Kuo[197] found much poorer results, particularly in the case of the smaller light-duty engine.

Hiroyasu's model was further developed by super-imposing a multi-dimensional calculation of diffusion processes[262]. A full description of the distribution of soot in the chamber of a light-duty DI diesel was obtained, though no in-cylinder data was available for validation. However, the limited results for exhaust data show that predictions of variation with piston-bowl diameter are relatively poor.

In 1982, **Dent** added a soot emission model to the phenomenological combustion model described in the previous year[56,57]. Soot formation was represented by the Tesner formation model, thus defining both soot and nuclei number densities. Nuclei oxidation was described using the turbulent mixing rate expression of Magnussen, taking into account both injection and swirl processes. A modified form of the Lee oxidation model was used for the overall soot mass reduction. This

---

* All further references to Hiroyasu's soot expression refer to this model, rather than the 1976 model mentioned above.

was based on the assumption that soot burn-out takes place only in the fine-structure level of the turbulent eddies. The average spray composition and temperature values were taken as inputs to these expressions. The results demonstrated the correct trends with engine operating variables and revealed the relationship of the sooting phenomena to the combustion process. In this work the calculated exhaust smoke levels were much too low. However, later work in which the soot particle size was set to 50 nm produced a good quantitative agreement with experiment[198].

In an independent development of the original model, **Gupta** added a multizone representation of the spray[104]. Mehta implemented a soot model derived from Magnussen's original work[224]. This simply uses the Tesner mechanism for formation and a turbulent mixing rate for oxidation, but these are applied within a thermodynamic structure which accounts for two regions of mixture - heated fine structure and surrounding fluids. However, as described by Mehta, the heated fine structure region is not defined according to Magnussen's model of turbulence structure, but rather is expressed in terms of the combustion rate. Also, the spray which is not burning during a timestep is described using a single temperature value, implying infinitely fast mixing of the products. Nevertheless, choosing a particle size of 2000 nm but adjusting no other constants gave an excellent agreement with experiment. For a dataset encompassing fuel, speed, load, swirl ratio and injection parameter variation, predictions matched experimental values with a correlation coefficient of 0.9 ± 0.1. However, no justification is given for choosing such a large particle size.

Mansouri predicted soot emission using a stochastic model[227,228]. The details of the formation mechanism were neglected and the initial soot mass loading in each element was assumed to be the amount of solid carbon obtained from a chemical equilibrium calculation. Nagle's correlation was used for oxidation. The results provided qualitative insights into the emission process, but the quantitative sensitivity to combustion model assumptions was unacceptable. For example, changing the rich-limit for elements allowed to burn from 3 to 4 resulted in an order of magnitude increase in the initial soot loading.

Kittelson further developed this combustion model and used it to study soot emission[174,175]. Preliminary calculations were made using Khan's formation expression, but it was found necessary to increase the activation energy to at least

80 kcal/mol (from 40 kcal/mol) in order to match the location of the soot peak. All subsequent calculations used the formation expression of Harmadi[110] in conjunction with the oxidation expressions of Nagle[249] and Fenimore[71]. The exhaust value was found to increase roughly in proportion to the assumed initial diameter of the soot particles. The best match was obtained with a particle size of 22 nm, which is very close to typical empirical values. Also, inclusion of the OH oxidation mechanism had a significant effect, giving a reduction in exhaust soot of up to twenty-fold. However, parametric effects were poorly represented, with a predicted reduction in exhaust soot for injection advance and reduction in peak soot for doubling of load. Both trends are the opposite of those determined experimentally and the poor performance is attributed mainly to the lack of spatial resolution in this purely stochastic model.

Brown[37] developed this model in order to simulate DI diesel engine combustion. The stochastic model was used to post-process the output of the KIVA multi-dimensional code. Multiple composition zones were used to characterise different regions of the spray since the mixture distribution is more heterogeneous than in the IDI engine. Excellent NO_x predictions were given, demonstrating the utility of the model in calculating slow emissions chemistry. For soot, the formation expression of Wang was used together with Nagle's soot oxidation expression. A calibration constant was used for the formation rate and this was set by matching to experimental data for a single operating condition. However, predictions of soot concentrations at 80° aTDC were very poor for other operating conditions. This was attributed to weaknesses in the combustion model.

Kono[184], **Kouremenos**[191,192], **Wade**[356], **Zhou**[389] and **Lapuerta**[271] all applied Hiroyasu's expressions for prediction of smoke in DI diesel engines. In a multizone model[184], Kono demonstrated a good representation of the smoke trends with swirl and various injection parameters, but the constant values used are not given. Kouremenos first incorporated soot emission prediction in a simple two-zone combustion model. The values used for activation energy were higher than those proposed by Hiroyasu (see Table B.1). Results showed an excellent representation of the effects of injection timing, load and speed variation. This model was later developed for the IDI diesel engine, using separate zones for the main chamber and the prechamber[192]. In this case the results followed the experimental data less closely, though the correct trends were still shown. Wade used simple thermodynamic simulation[356] which includes separate thermodynamic descriptions

of premixed, diffusion and surrounding fluids combustion regions. The correct trends with injection timing and boost pressure were demonstrated. Zhou showed that the correct trend with injection timing was given and also states that the predicted in-cylinder distribution was validated by sampling measurements[389]. Lapuerta's results are not validated experimentally[271].

In 1990, **Nakakita** became the first to publish soot results from a multi-dimensional simulation[254]. Soot rates are based on ensemble-averaged properties so that, at least in this respect, the model is similar to a simple zonal model, differing mainly in degree of spatial resolution. The formation mechanisms of Tesner and Farmer are used and equations are proposed which represent the variation of two of the Tesner model constants with pressure. Magnussen's turbulent mixing rate and the Nagle expression are used for oxidation. For both formation and oxidation processes, the minimum calculated rate is selected. Detailed soot predictions are given which are supported qualitatively by combustion photography and good agreement with exhaust data is achieved. A breakdown of the rate components shows that the Tesner and Magnussen expressions are rate-limiting initially, but at 20-30° aTDC the Farmer and Nagle expressions take over. In both cases, the chemical rate becomes important once the temperature has dropped; thus the Farmer and Nagle expressions supplement the Tesner and Magnussen models in their temperature-deficiency. If this form of hybrid model had not been used the results would have been very poor. Even so, the universality of the expressions remains questionable. In particular, the Farmer rates are so temperature-sensitive that they are effectively acting as a switch - at lower temperature the rate suddenly drops to zero.

Zellat has also applied the Tesner and Magnussen models in a multi-dimensional environment[387]. The KIVA code was used for simulation of an IDI diesel engine. Again, a simple approach appears to have been taken, with no interaction between soot and other combustion phenomena. Encouraging qualitative results are demonstrated by comparison with combustion photography for the early burning phase[386], but oxidation is over-predicted such that exhaust levels are negligible under some conditions[387].

In 1991, **Xiao** became the first to introduce a variable particle size in diesel soot modelling[378]. This was done by the addition of a coagulation model. An advanced multizone combustion model was used including a stochastic mixing model and

accounting for 12 chemical species. Soot formation is given by Khan's expression, and Khan's empirical constant for the Smoluchowski equation has been adopted. Coagulation calculations also require the assumption of an initial particle size, which was taken as 1 nm, and specification of a critical surface area beyond which no new particles are generated. These constants were selected to give the expected exhaust levels. Oxidation by O_2 and OH is accounted for using the Nagle and Fenimore expressions. Unfortunately, only limited results are presented and no empirical validation is given.

Finally, **Bazari** has also included soot models in a multizone combustion simulation[19,327]. Hiroyasu's correlations are again employed and calibrated by exhaust data. The model predictions show a wide variation between soot levels in different parts of the jet, with very little present towards the edges. Soot concentration is found to peak at about $5\,g\,m^{-3}$, dropping rapidly to about 10% of that level, and changing little beyond 50° aTDC when temperatures have fallen below 1500 K. Empirical validation of exhaust level trends has also been undertaken; good results are shown[20].

Discussion

The performance of the different soot models described above is now considered in general, and the issue of matching soot and combustion models is addressed. The analysis is divided up between soot models of similar type.

The simplest models are the calibrated semi-global expressions of **Khan**[170], **Hiroyasu**[121] (1976), **Harmadi**[110] and **Hiroyasu**[125] (1982). The constants for each of these are determined by applying the models in engine simulation and matching exhaust values to empirical data. There are two important consequences of this procedure. The first is that fitting to exhaust data cannot guarantee an accurate representation of the in-cylinder levels. Khan attempted to get round this problem by fitting to exhaust data for different injection timings. However, this is a very crude method and the resulting expression was found to be quantitatively inaccurate at other operating conditions. Moreover, the constants fitted include the equivalence-ratio exponent as well as the pre-exponential constant. Thus, uncertainty in the overall form of the correlation may be as important as uncertainties in the overall rate-scaling factor. In the case of Hiroyasu's expressions, in-cylinder levels will be poorly defined, because the pre-exponential constants have not been defined and experimental data is not generally available.

The second consequence of using a model fitted to exhaust data is that the resulting correlation is expressed in terms of model parameters rather than measured properties. Typically, these parameters are the representative averaged variables of zero-D and zonal models, such as the averaged concentrations and temperatures. Thus, the approach attempts to describe the sooting processes in terms of accessible parameters and neglects the detailed description of local phenomena. In principle, it may be expected to be better suited for use in zonal models than the expressions derived from measurements in idealised combustion systems, and the Khan and Hiroyasu (1982) correlations have in practice been applied almost exclusively in simple zero-D and zonal models (see Table 3.8).

The results for these models are mixed, with good trend predictions achieved by Hiroyasu[126], Kono[184], Kouremenos[191], Wade[356] and Zhou[389], but poorer comparisons shown by Khan[170], Hiroyasu[121], Kittelson[174], Nishida[262] and Kuo[197]. Thus, the usefulness of these models is perhaps limited and their quantitative accuracy is not guaranteed.

The correlations of **Farmer**[69], **Lee**[207], **Nagle**[249] and **Fenimore**[71] are typical of the expressions derived from measurements in simplified combustion systems. They have been applied in conjunction with combustion models of different types, ranging from zero- to multi-dimensional. However, in these cases it is harder to separate out the effects of formation and oxidation, and little indication is given of the quantitative accuracy of the expressions. The most useful comparison is that of Nakakita[254] in a multi-dimensional simulation involving the Farmer and Nagle rates. This suggested that the chemical rates only become important once the temperature has dropped, but the quantitative accuracy of the expressions was not established. Reasonable exhaust values were obtained though this seems to have been rather fortuitous in view of the unphysical predictions of the Farmer and Tesner expressions early and late in combustion respectively.

Finally, the more detailed models of **Tesner**[344] and **Magnussen**[223] have been applied in zero-dimensional, zonal and CFD models. The models derive from fundamental studies, but seem to have been most successfully applied in the simplest model - the quasi-dimensional model of Dent. Mehta's results are remarkably accurate, but an unphysical particle size of 2000 nm was used. In the CFD models of Zellat and Nakakita, realistic exhaust levels could not be predicted by use of these expressions alone.

3.5.2 Sources

To assess their applicability in the diesel-engine environment, the sources of the models discussed above are summarised in Tables 3.9 & 3.10 (in addition, information is included for the Feugier[73] and Magnussen (laminar)[207] expressions implemented in this work). Amongst the formation expressions, only those of Khan and Hiroyasu relate to high pressure conditions and diesel-like fuels. Also, even in the case of Hiroyasu's expression, the pressure term seems to be more of an approximation and is not directly related to the data source. The other expressions were derived at atmospheric conditions using simple fuels. With oxidation, the partial pressure of oxygen is more significant than the total pressure. Only the study of Nagle[249], as extended by Park[269], covers the range of conditions found in the diesel. On the other hand this is the only study which did not measure oxidation rates of flame-produced soot *in-situ*.

Researcher	Combustion system	Fuel	T range (K)	p range (atm)
Khan[170]	Diesel engine model	diesel	1000-2000	40-100
Harmadi[110]	Open diffusion flame	-	-	-
Hiroyasu[125]	Single droplet combustion[155], spray flame[12]	paraffins[155], kerosine[12]	-[155], 1000-1400[12]	1-10[155], 1[12]
Tesner[344]	Diffusion flame	acetylene	1900	1
Farmer[69]	Jet-stirred combustor	ethylene, toluene, isooctane	1650-1850	1
Wang[363]	Shock tube	toluene, benzene, acetylene	1400-2500	2.5-10

Table 3.9 - Soot formation expression sources

Researcher	Combustion system	Fuel/soot type	T range (K)	Total p range (atm)	p_{O_2} range (atm)
Lee[207]	Laminar diffusion flame	propane	1300-1680	1	0.05-0.1
Nagle[249] (Park[269])	Solid carbon	pyrographite (carbon black)	1200-2700 (1700-4000)	0.1-0.6 (1.4-35)	10^{-5}-1 (0.05-13)
Hiroyasu[125]	Spray flame	kerosine	1000-1300	1	0.04-0.12-
Magnussen[223]	Turbulent diffusion flame	acetylene	300-2000	1	n/a
Fenimore[71]	Laminar diffusion flame	ethane	<2200	1	n/a
Feugier[73]	Laminar diffusion flame	ethane	2000-3000	1	<0.56
Magnussen[207]	Laminar diffusion flame[207]	propane[207], carbon	1000-2500	1	0.05-0.1[207]

Table 3.10 - Soot oxidation expression sources

3.5.3 Conclusions

The above review reveals that none of the models proposed for soot modelling has been found to be completely satisfactory. The semi-global soot models of Khan, Harmadi and Hiroyasu are quantitatively poor, and even the form of the expressions must be uncertain. The quantitative performance of the Nagle, Lee and Fenimore models is hard to assess and no comparisons have been made with the semi-global expressions. The Farmer correlation seems unsuited to diesel engine use. Finally, the Tesner-Magnussen model has performed well in a zero-dimensional model, but very poorly in the context of CFD simulations.

Despite this, some reasonable predictions of exhaust trends and in-cylinder distribution have been obtained using particular model types. Satisfactory predictions of parametric effects have been demonstrated using Hiroyasu's correlations[126,184,356] and a Tesner-Lee combination[198], and realistic predictions of spatially-resolved soot were given by Nakakita[254] and Zellat[387]. However, with these respective model types, predictions of in-cylinder and exhaust levels are weak.

Examination of the sources for these expressions is not encouraging. The only formation expressions established under high pressure conditions using diesel-like fuels are the tentative and relatively unproven expressions of Khan and Hiroyasu. Of the oxidation correlations, only that due to Nagle has been validated at high values of oxygen partial pressure, such as may be found in a diesel engine, and this study did not use flame-produced soot.

Because none of the soot models proposed is entirely satisfactory, more work is required, this being the motivation for the current study.

3.5.4 Strategy for the current study

In this work, computer simulation has been used to make a comprehensive analysis of various soot models and modelling techniques. For the first time, quantitative rate comparisons are made and most of the models previously applied in diesel work have been implemented. Exceptions are Fenimore's hydroxyl oxidation model[71], the early model of Hiroyasu[121] and Wang's expression[363] which is very similar to that of Farmer[69]. The models used are listed in Table 3.11 and full details are set out in Appendix B. In most cases, zonal averages have been used for the soot expression inputs, but in the accounting for composition, oxidation is preferentially taken from the combustion products subzone. Also, special treatment has been given to the Tesner-Magnussen soot model, and the related thermodynamic structure model developed by Magnussen[223] has also been implemented (see section 4.4 and Appendix B).

A multizone combustion model has been used in this study, which may seem to restrict the applicability of the findings to models of similar type. However, it is possible to extract information of a more fundamental nature from the simulation results. This is because a wide range of thermodynamic conditions are represented by the various model zones over the whole combustion period, and soot rates are calculated for each. Thus, interesting information may be revealed by plotting rates against other parameters, such as equivalence ratio and temperature, giving more generally useful conclusions.

Formation	Oxidation
Khan[170], 1971	
Harmadi[110], 1982	
Hiroyasu[125], 1982	Hiroyasu[125], 1982
Tesner[344], 1971	Magnussen (turbulent)[223], 1976
Farmer[69], 1981	
	Lee[207], 1962
	Nagle[249], 1962
	Feugier[73], 1972
	Magnussen (laminar)[221], 1971

Table 3.11 - Soot models implemented in this study

CHAPTER 4 - THE COMBUSTION MODEL

This chapter gives details of the work done on each constituent of the engine combustion model and presents results illustrating the overall performance of the simulation program. The description of the development work is divided into four sections describing the spray model, the evaporation model, the turbulence model and combustion and thermodynamics. In each section or subsection, previous work is reviewed and the methods chosen for the current work are outlined. The results are discussed and conclusions drawn. The overall performance of the model and all work done on soot modelling are described in chapter 5.

4.1 THE SPRAY

Diesel combustion is strongly influenced by the mixture formation process occurring in the fuel spray. This is a very complex transient two-phase flow phenomenon involving atomization, evaporation and mixing on micro and macroscopic scales. These processes depend upon the structure of the spray and rates of air entrainment, which in turn are controlled by the characteristics of the injector and the air motion in terms of gross structure and of turbulence. The relationship of the spray behaviour to these and other parameters has been the subject of extensive investigations including in particular the work of Reitz[289-292,377], Shimizu[312], Bracco[33], Hiroyasu[130], Iiyama[143], Nishida[263], Kuo[195], Soteriou[329] and Singal[322].

4.1.1 Spray structure

The basic features of the diesel spray have been described by Hiroyasu[130] and Heywood[116]. Markedly different spray structures are found according to the Reynolds number associated with the injection process. Under typical diesel-engine operating conditions, the spray structure may be classified as either 'incomplete' or 'complete' (Fig. 4.1(a))[130]. The structure of the incomplete spray may be divided into three sections - a smooth liquid column is followed by a break-up region which finally gives rise to a fully-developed spray. Several factors influence jet break-up, though their significance varies according to operating conditions[33]. Important mechanisms include the aerodynamic interaction at the liquid-jet interface and cavitation in the nozzle hole[329].

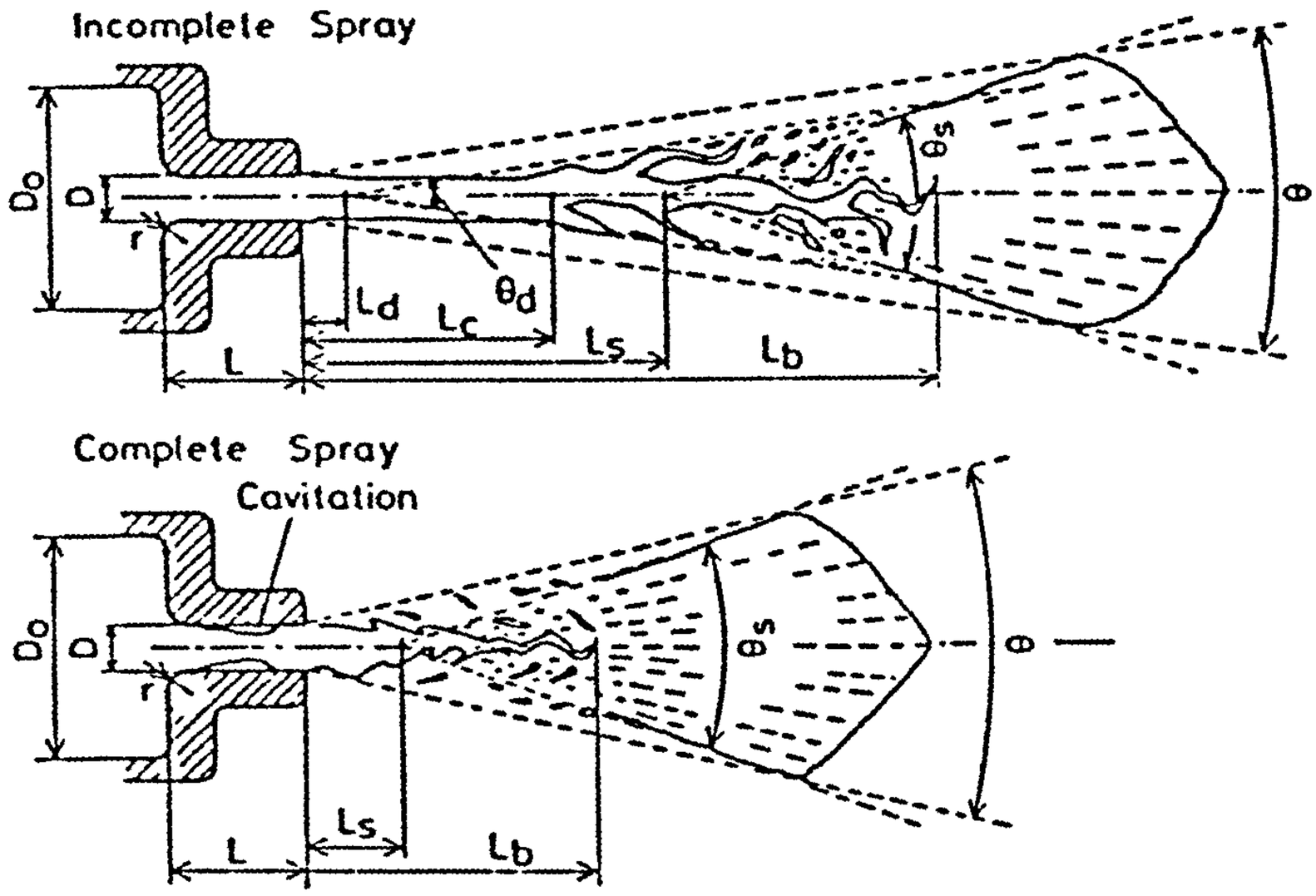

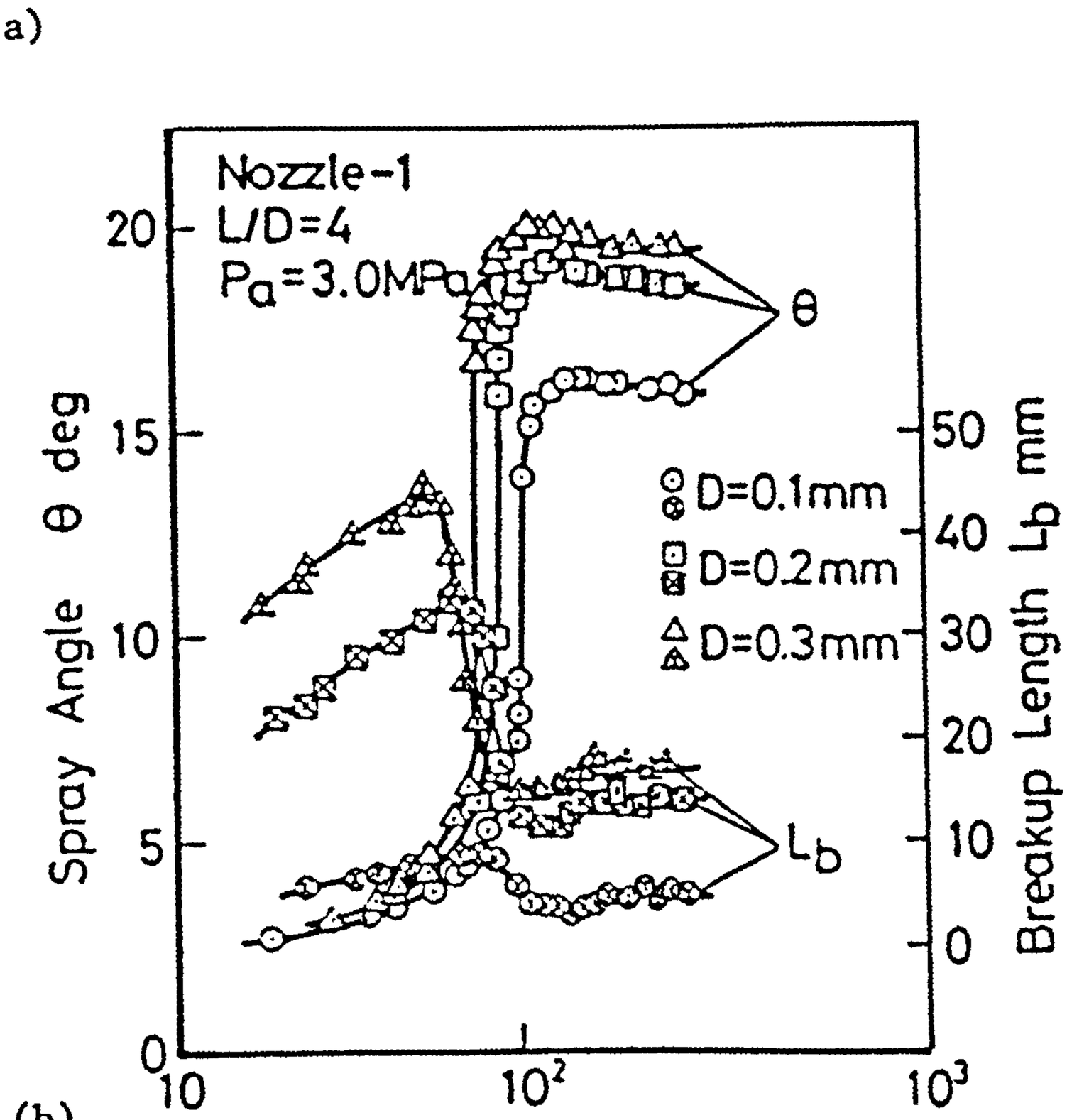

Figure 4.1[130] - Structure of diesel spray

As injection velocity is increased, the onset of disintegration moves back to the nozzle. At the transition velocity, cavitation expands out to the exit of the nozzle, and the resulting highly turbulent internal flow gives a discontinuity in spray angle and break-up length (Fig. 4.1(b)). Beyond this speed the spray is said to be 'complete'.

Entrainment of air from the surroundings has been examined by Ricou[293] and Sato[106,301]. Sato used a smoke plume to demonstrate that air is taken up at the

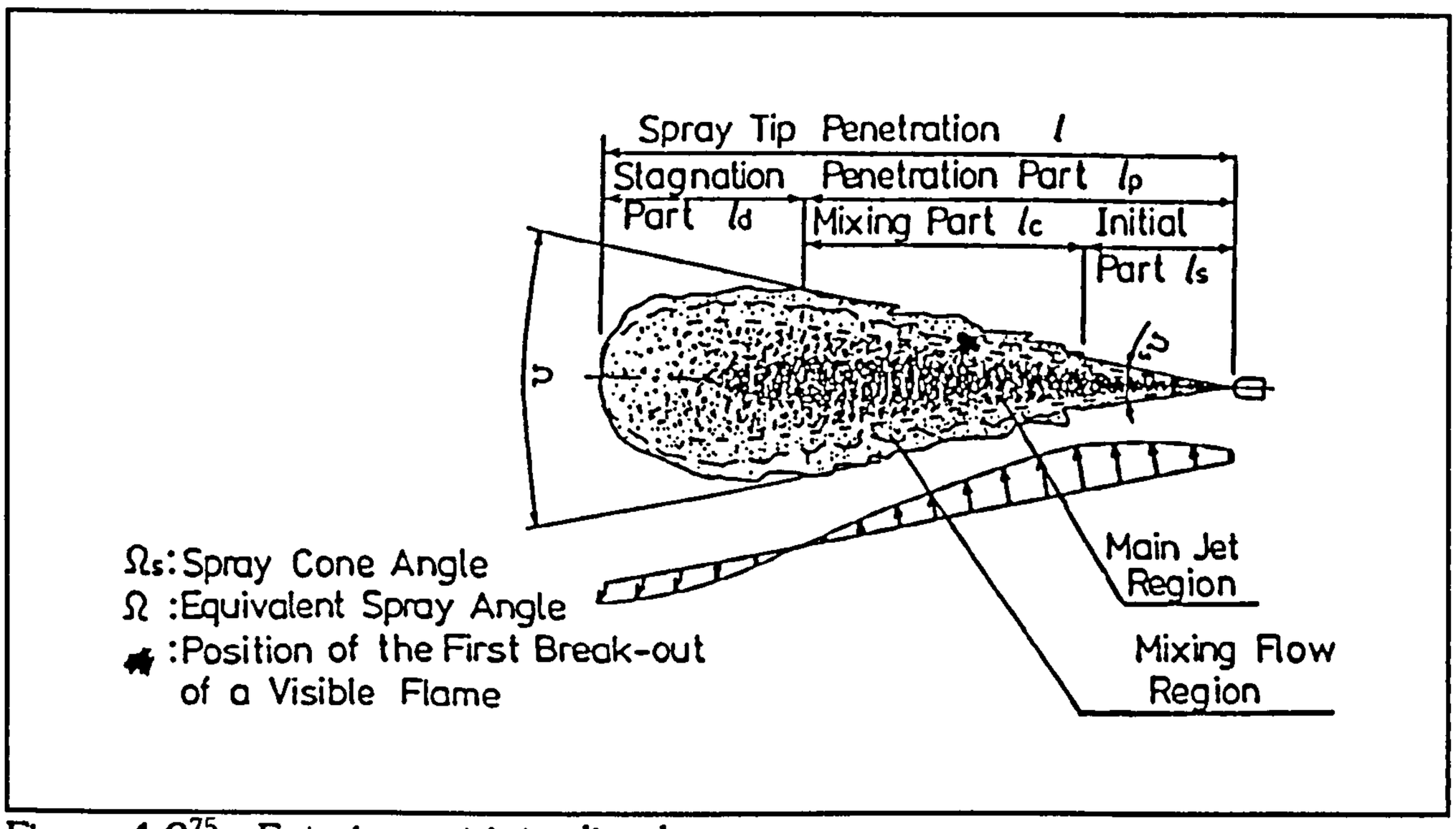

Figure 4.2[75] - Entrainment into diesel spray

back of the jet (Fig. 4.2)[106]. A further insight has been provided by Kobayashi[179] who investigated the effect of combustion on entrainment using a rapid compression machine. The ignition delay was artificially increased over the range 0.8 - 2.0 ms and total entrainment was doubled in the late ignition case by the end of the injection period. This was attributed to the effect of large-scale eddies in the lower temperature peripheral zones, resulting from the more rapid thermal expansion in the jet core. Thus it seems that in certain circumstances, entrainment occurs via vortical gas-flows of the order of the spray half-width in size.

The process of entrainment observed in transient jets differs greatly from that observed in steady-state sprays. The first fuel to be injected slows down rapidly as it entrains air. Thus a vortex or puff is formed at the head of the jet. Later-injected fuel encounters less resistance and pushes through to the tip, where it in turn is

slowed by aerodynamic resistance. Therefore the head vortex is maintained as the droplets at the front are continually replaced by those which were injected later and have high momentum.

Consequently, some of the fuel which is injected first remains as small drops and fuel vapour distributed along the length of the jet, particularly at the periphery of the spray. In a study of jet transience, Kuo[195], concluded it is best to describe the spray as a steady-state jet following a small head vortex. In transient laminar jet experiments of Abramovich[2] and in fuel-spray experiments of Borman[31] and Taylor[342], the velocity of this head vortex has been determined as 70% and 68-72% of the centreline steady-state velocity respectively.

4.1.2 Spray modelling

The most sophisticated spray models are those used in conjunction with multidimensional models of in-cylinder gas motion. The conservation equations governing the two-phase flow are solved within the computational mesh and droplet motion is tracked either individually (continuum droplet model) or using a statistical representation following parcels of identical droplets (discrete droplet model). Phenomenological models lack an exact geometric description, so other means of representing spray motion must be found. A wide variety of models have been developed based on the correlations and assumptions derived from a multitude of theoretical and experimental spray studies. Important contributions are summarised briefly below.

Phenomenological spray models have been built on two different premises: those which calculate spray motion according to the solution of governing conservation equations, which will be termed 'fundamentally-based', and those in which the spray motion is fully specified using empirical correlations, termed 'geometrically-based'. Each type has received approximately equal attention in the field of diesel combustion modelling.

Generally diesel spray models are represented as quasi-steady and axisymmetric. However, as has been noted, the transient behaviour of diesel spray is important[284,195] and in some cases an attempt has been made to account for this effect[45,234].

Another basic assumption is that the spray can be represented as a gaseous jet, i.e.

ignoring droplet ballistics (Ramos, 1989)[284]. This approximation has been used in all phenomenological models applied to diesel combustion simulation and comprehensive justification has been given by Lipkea[213] amongst others.

4.1.2.1 Fundamentally-based models

Fundamentally-based models are summarised in Table 4.1. In this case, the jet motion, size and centreline velocity are calculated by solving the conservation equations for mass and momentum. In addition, an expression to describe the rate of air entrainment is required. In 1961 Ricou[293] determined an expression relating jet mass flow rate to penetration in the case of an axisymmetric jet. Hoult, 1969[136], first proposed an equation relating the entrainment rate to the velocity difference between the jet and the surrounding atmosphere and the jet surface area. The model was applied to a jet growth in a cross-flow and contains two empirical constants. In 1972, Escudier[64] extended applicability to flows of large density variation using the density-scaling factor of Ricou[293]. In the same year Hoult[137] determined the values of the empirical constants, and the resulting expression is commonly referred to as 'the turbulent-entrainment expression of Hoult and Weil' (equ 4.1).

$$\frac{dm_a}{dt} = 2\pi r \rho_j \rho_a \left[\alpha (u - u_{a,tan}) + \beta u_{a,nor}\right] \qquad (4.1)$$

Rife[294], 1974, calculated diesel spray behaviour using a model of this type. Sinnamon[323] extended this model to a two-dimensional representation for calculation of fuel sprays in swirling flows. Hiraki[118] further extended this to the three-dimensional case and Kobayashi[180] made some modifications to Sinnamon's model to achieve a better match with experiment. Kono[184] included the turbulent intensity as a factor in the entrainment expression, though Ramos[284] considers this expression to be dimensionally inconsistent.

In each of these fundamentally-based models, solution is for spray centreline values. Thus, in order to define cross-jet velocities and concentrations, recourse is often made to the expressions of Abramovich[2] which were derived from a theoretical analysis of two-phase flow. Most models of this type allow for the effects of air swirl and impingement of the jet on the chamber wall. The latter is a major topic in itself[236,59] and will not be dealt with here. The model of Meguerdichian[234] also attempts to account for the transient nature of the jet. Kono's model[184] is unique in that it uses multiple cross-jet zones, so that assumed cross-jet profiles are not

required. The model of Wilson,M.[370] is the most detailed phenomenological model yet developed. Cross-section distortion is taken into account and the velocity and scalar profiles are allowed to vary independently.

Fundamentally-based		
	Cross-jet profile assumed	Multiple cross-jet zones
	Wilson,R. 1974[371,165]	*Kono 1985*[184]
	Meguerdichian 1978[234]	
	Hiraki 1980[118]	
	Wilson,M. 1986[370]	
	Kobayashi 1986[180]	
	Lapuerta 1988[271]	
	Singal 1990[321]	
Geometrically-based		
	Fuel-air distribution imposed	
	Khan 1971[170]	
	Shahed 1975[45]	
	Zhou 1989[389]	
	Fuel-air distribution calculated	
	Cross-jet profile assumed	Multiple cross-jet zones
	Hodgetts 1974[132]	*Hiroyasu 1976*[125,262,124]
	Dent 1981[56]	*Lipkea 1987*[213]
	Watson 1985[365]	*Bazari 1992*[19]
	Kouremenos 1986[189]	

Table 4.1 - Spray model classification

4.1.2.2 Geometrically-based models

Geometrically-based models are summarised in Table 4.1. In this approach, spray motion is specified directly by use of correlations for penetration and spreading rate. Twenty such expressions are summarised by Hiroyasu[128], roughly half derived from theory and half from experiment. Those applied to diesels include the expressions due to Dent[52] and Hiroyasu[126]. The latter author has also determined a correlation to describe the effect of swirling airflow in reducing jet penetration[126].

Different approaches have been taken to determination of air entrainment and prediction of fuel concentrations within the jet. In the models of Khan[170], Shahed[309,45], Watson[365], Kouremenos[189] and Lipkea[213] the air entrainment is obtained directly from the total size of the jet. It is then necessary to make an assumption regarding the fuel distribution within the jet. Shahed assumes a hyperbolic distribution along the spray axis and normal distribution across the spray. The inaccuracy of this approximation was demonstrated by comparison with results of a two-dimensional thick-spray 'discrete droplet model'[196]. Suggestions were made for modification of the radial and centreline vapour distribution. The simple 1-D model of Watson defines the axial fuel-air distribution using axially divided zones. Lipkea's model uses axial and radial profiles from classic jet theory, including the work of Abramovich[2].

Ricou's simple entrainment correlation relates the flow rates of air and fuel at any cross-section to the jet penetration[293]. Dent[56] applied this expression in the case of a quiescent-chamber diesel, and used the correlations of Abramovich[2] to specify cross-jet profiles. In the presence of swirl, a different approach was adopted using the turbulent-entrainment equation of Hoult and Weil described above.

Finally, all other geometrically-based models rely on an assumption of momentum conservation for calculation of the fuel-air distribution. The simplest is that due to Hodgetts[132], which again assumes the cross-jet profiles of Abramovich[2]. The remaining models of Hiroyasu[126,262,124] and Bazari[19] use the approach first set out in Hiroyasu[124]. Multiple cross-jet zones are used and momentum conservation is applied to each so that fuel-air distribution is fully specified. In such geometrically-based models, this approach has an advantage over use of the turbulent entrainment equation due to Hoult and Weil because the zonal surface areas needed for the latter are poorly defined.

All geometrically-based models make some attempt to describe the effect of wall impingement. It has also been argued by Shahed[309] that in using penetration expressions derived from transient-jet studies an advantage is achieved over the majority of the fundamentally-based models which are quasi-steady. However, this depends upon the validity of the assumptions for calculation of the axial fuel-air distribution. Certainly for direct application of Hiroyasu's model[124], no such benefit is possible, since the motion of all spray zones is described by a jet-tip expression.

4.1.2.3 Other approaches

In some cases the models described above have been extended using different concepts. Dent[56] has employed an entrainment expression which is more directly related to the turbulent structure than that of Hoult[137]:

$$\left(\frac{dm_a}{dt}\right)_{ent} = C\frac{m_a}{\tau_{mix}} \tag{4.2}$$

Here, τ_{mix} is the turbulent mixing time for break-down of large-scale eddies. The expression is employed beyond the end of the injection period and the constant C determined by matching to the entrainment rate calculated using Ricou's correlation[293]. Hiroyasu has employed a similar expression for entrainment rate calculation in an IDI diesel[124]:

$$\left(\frac{dm_a}{dt}\right)_{ent} = C(m_a + m_f)\,u_{throat} \tag{4.3}$$

where u_{throat} is the velocity of the mixture through the pre-chamber throat

Finally, Brown[37], Nishida[262] and Lapuerta[203] have superimposed multidimensional calculations on top of zonal spray models. For example, in Nishida's model, rates of fuel vaporisation and heat transfer are computed for the spray-model zones and distributed to the cells of the computational mesh. Thereafter rates of dispersion of the gaseous components, soot and enthalpy are calculated, giving a full description of the species and temperature fields.

4.1.2.4 Conclusion

The approach followed most closely in the current work is that embodied in the geometrically-based model of Hiroyasu[124,126,262]. Hiroyasu's own spray penetration equations are used[122] and entrainment is calculated on the basis of conservation of momentum. It is instructive to see where this fits into the range of alternative strategies. On the one hand it represents a more comprehensive approach than the geometrical-based spray models which do not follow zone masses, but merely impose axial and cross-jet fuel-air distributions. On the other hand, because zone motion is specified externally rather than calculated from first principles, the adopted model is unlikely to provide as general a description as the fundamentally-based models which employ zones. Compared to these models, though, the current approach is considerably more flexible, allowing, for instance, straight-forward representation of the transient nature of the spray. It is also less computationally-intensive and easier to control. Therefore, the method used can be seen as a compromise. It follows individual mixture elements through the chamber, but according to a motion which is specified and hence well-behaved. Thus, the sound foundation to the calculations of fuel-air distribution is backed-up by a flexible and controllable overall jet structure.

4.1.3 Spray model

The spray model developed in the current work is presented in this section. First the model is described and the model equations are set out in section 4.1.3.1; then in section 4.1.3.2 some of the modelling assumptions are discussed.

4.1.3.1 Description

Details of the spray model implemented in this study are given below. The model is based on the approach of Hiroyasu[124] and the penetration expressions used are those previously obtained by the same author[122]. The spray is represented in terms of the simplified structure shown in Fig. 4.3.

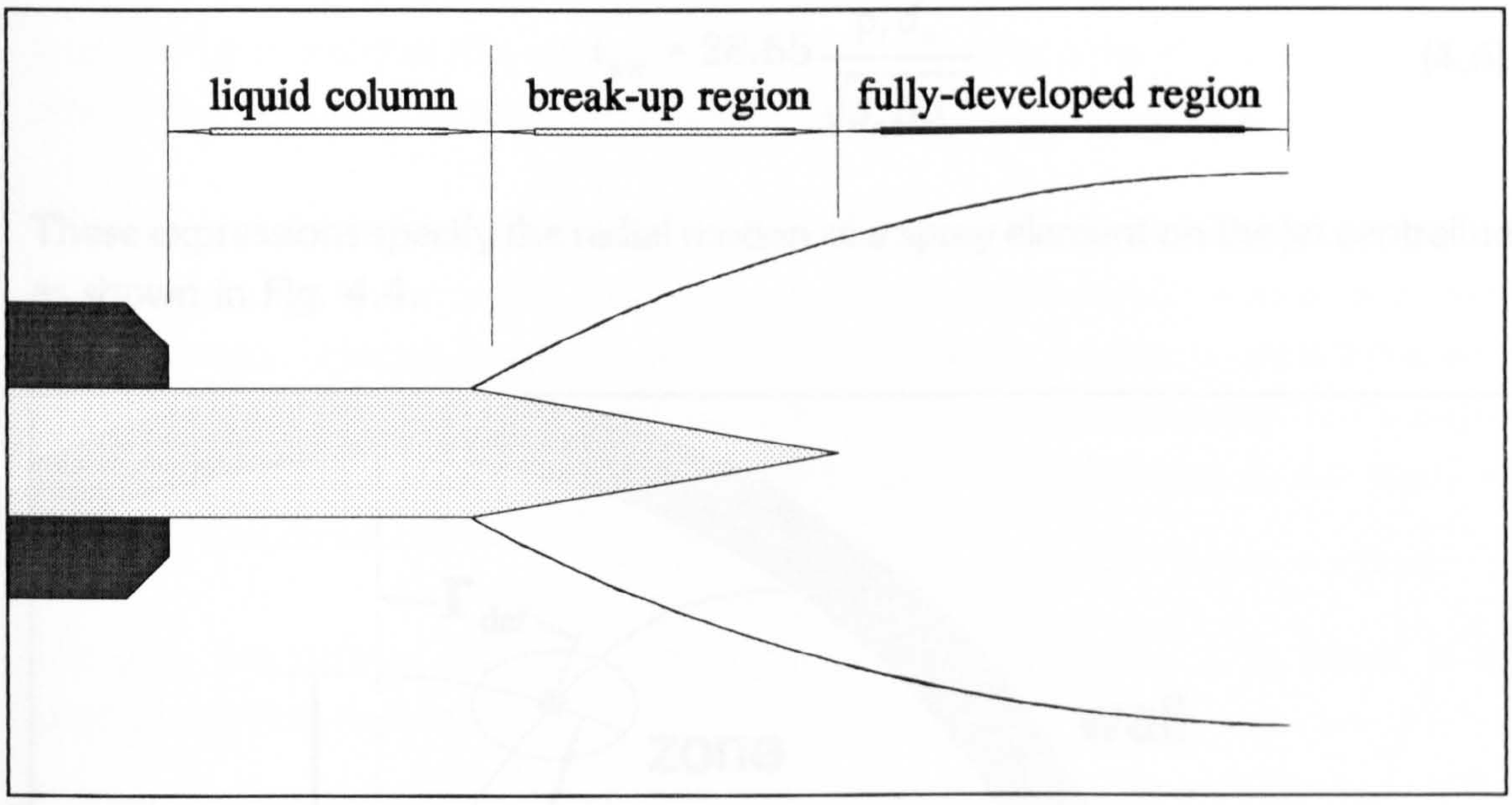

Figure 4.3 - Model spray structure

Axially-divided sets of zones are injected successively according to an empirical injection profile. The motion of the zones within the jet is described largely by use of correlations and assumptions. Conservation of momentum is applied in the radial direction to determine air entrainment. The key element of the spray-motion model is the pair of spray-tip penetration equations as follows:

for $0<t<t_{break}$:

$$S = 0.39 \sqrt{\frac{2\Delta p}{\rho_f}}\, t \qquad (4.4)$$

for $t>t_{break}$:

$$S = 2.95 \left(\frac{\Delta p}{\rho_a}\right)^{\frac{1}{4}} \sqrt{d_o t} \qquad (4.5)$$

where:

$$t_{brk} = 28.65 \frac{\rho_l d_o}{\sqrt{\rho_a \Delta p}} \qquad (4.6)$$

These expressions specify the radial motion of a spray element on the jet centreline, as shown in Fig. 4.4.

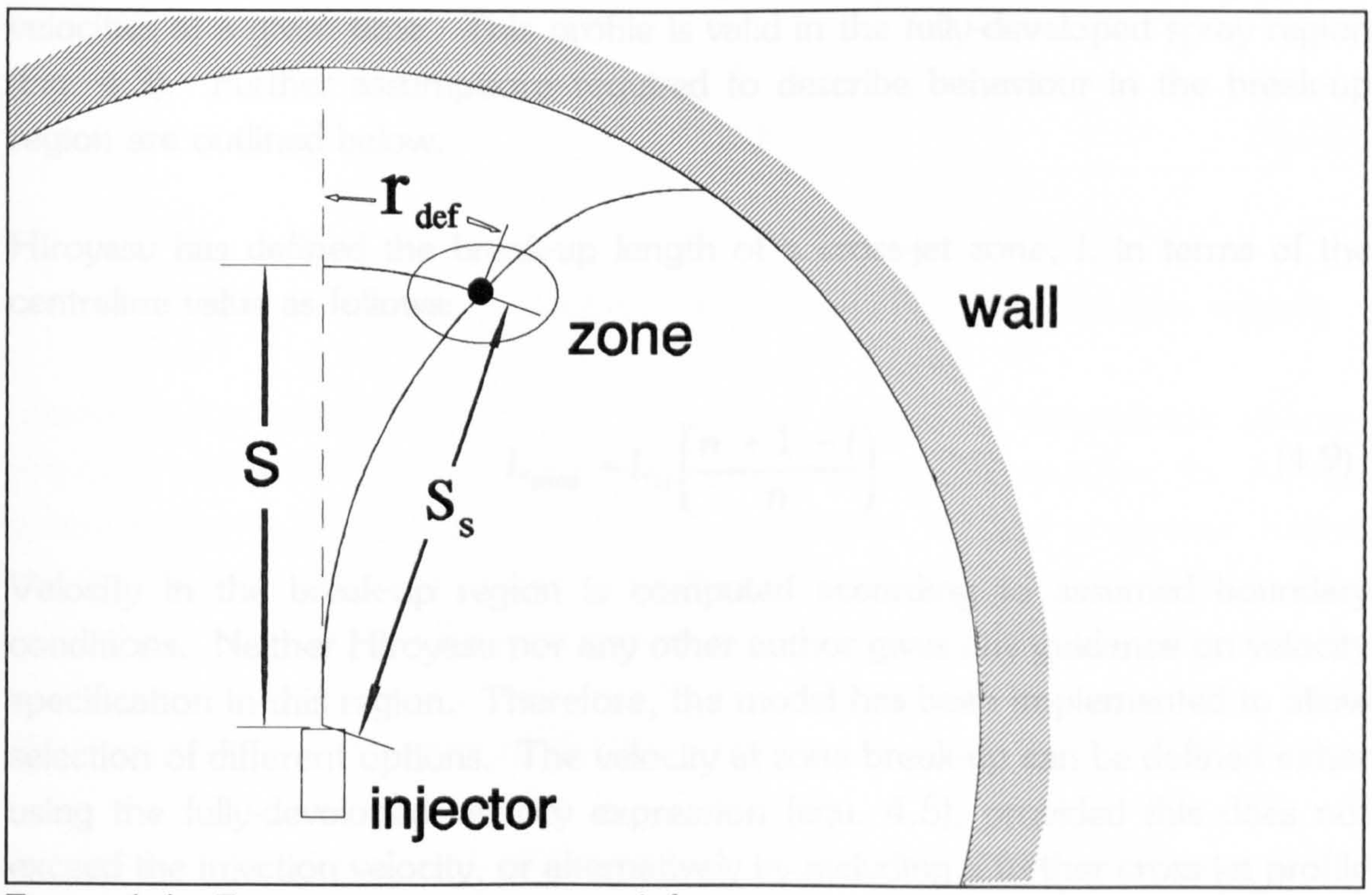

Figure 4.4 - Zone motion parameter definitions

For the case of off-centreline zones further correlations are necessary. Hiroyasu defines the cross-jet penetration variation in terms of the centreline penetration:

$$S_l = S\,e^{-8.557\times10^{-3}(l-1)^2} \tag{4.7}$$

The current model requires a cross-jet velocity distribution and a velocity coefficient consistent with equ. 4.7 is simply obtained (see Appendix C):

$$C_f = 2.0^{-\left(\frac{l-1}{n-1}\right)} \tag{4.8}$$

where l is the zone number in the radial direction.
n is the total number of cross-jet zones

It should be noted that this expression does not describe a velocity profile since the size of the individual zones is undefined.

This description is for a jet cross-section which contains fluid injected at different times, while the spray model follows the position of individual zones at successive time intervals. Hence, a numerical technique must be applied to determine zone velocities at a given time. This profile is valid in the fully-developed spray region (Fig. 4.3). Further assumptions required to describe behaviour in the break-up region are outlined below.

Hiroyasu has defined the break-up length of a cross-jet zone, l, in terms of the centreline value as follows:

$$L_{zone} = L_{cl}\left(\frac{n+1-l}{n}\right) \tag{4.9}$$

Velocity in the break-up region is computed according to assumed boundary conditions. Neither Hiroyasu nor any other author gives any guidance on velocity specification in this region. Therefore, the model has been implemented to allow selection of different options. The velocity at zone break-up can be defined either using the fully-developed velocity expression (equ. 4.5), provided this does not exceed the injection velocity, or alternatively by including a further cross-jet profile to factor down this velocity, provided that the result exceeds the corresponding zone

velocity at onset of the fully-developed region. A linear variation is assumed between the two boundary values and, using these, an expression for the penetration can be derived by integration (Appendix C):

$$S = \left(\frac{U_{cl}C_f L_{zone} - U_{zone}L_{cl}}{U_{cl}C_f - U_{zone}}\right)\left[1 - \left(\frac{U_{cl}C_f(L_{cl} - L_{zone})}{U_{zone}L_{cl} - U_{cl}C_f L_{zone}}\right) e^{\frac{(t - t_{brk})(U_{cl}C_f - U_{zone})}{L_{cl} - L_{zone}}}\right] \qquad (4.10)$$

where U_{zone} and L_{zone} are the zonal velocity and penetration at the position of the zone breakup,

U_{cl} and L_{cl} are the centreline velocity and penetration at the position of the centreline breakup

Hence, the general expression for the zone velocity is:

$$\frac{dS}{dt} = U_{cl}C_f \; e^{\frac{(t - t_{brk})(U_{cl}C_f - U_{zone})}{L_{cl} - L_{zone}}} \qquad (4.11)$$

The effect of air swirl on jet penetration is described by a further correlation due to Hiroyasu, for the case of an injector placed centrally in the flow.

$$S_s = \frac{S}{\left(1 + \frac{\pi N_s S}{30 U_o}\right)} \qquad (4.12)$$

where N_s is the overall swirl ratio in rpm and U_o is the injection velocity

However, this expression cannot be applied directly in determining reduced velocities and penetrations. This is because the velocity variation for the off-centreline zones is fixed by the boundary conditions, so that in general, further variation in velocity cannot be permitted if a consistent physical description is to be maintained. Hence full calculations must be made for the no-swirl case while the swirl behaviour is computed in parallel by application of equ. 4.12. Meguerdichian[234] has used a similar approach.

Swirl also affects the circumferential motion of the spray, represented by r_{def} in Fig. 4.4. Hiroyasu has correlated this behaviour by the following expression:

$$r_{def} = S_s\left(\frac{m_a}{m_a + m_f}\right)\left(\frac{\frac{N}{60} r_s 2\pi S_s}{\frac{U_o + \frac{dS_s}{dt}}{2}}\right) \qquad (4.13)$$

However, initial work established that use of this expression does not guarantee matching of zone and air-swirl velocity at conditions of large entrainment. In fact, because each zone follows its own trajectory, it was shown that it is impossible to meet this condition for all zones with this type of spray model. Hence an alternative approach was adopted, based on the conservation of angular momentum. This requires a model to describe the air motion and a simple uniform swirl model was adopted:

$$U_a = \omega_s(S)\, S_s \qquad (4.14)$$

The effect of squish has been neglected by Hiroyasu, but the current model attempts to account for it, in view of its potential significance. Fitzgeorge[76] has determined the following expression for the instantaneous squish velocity, v_{sq}, in a bowl-in-piston chamber:

$$v_{sq} = \frac{S_p D_b}{4z}\left(\left(\frac{B}{D_b}\right)^2 - 1\right)\frac{V_b}{A_c z + V_b} \qquad (4.15)$$

where S_p is the instantaneous mean piston speed
D_b is the bowl diameter
B is the cylinder bore
V_b is the bowl volume
A_c is the cross-sectional area of the cylinder
z is the distance from the crown top to the cylinder head

The following expression was derived (Appendix C) to describe the effect of squish on the radial velocity:

$$\frac{dS_s}{dt}_{sq} = \frac{U_o + v_{sq}}{U_o} \frac{dS}{dt}_s - \frac{\Sigma \delta m_a v_{sq}}{m_{tot}} \qquad (4.16)$$

The transient nature of the jet is easily accounted for by simply post-processing the velocities. Since the penetration expressions used are for jet-tip motion, the velocity of later zones can be scaled-up according to an empirical profile.

Another consequence of the use of tip-motion expressions is that a correction factor must be applied in the spray model since zonal motion is tracked using the centre of gravity. Thus the time variable in equs. 4.1 and 4.2 is replaced by an equivalent time, t':

$$t' = t - t_{inj,\,m} \qquad (4.17)$$

where t is time and $t_{inj,\,m}$ is the time at which the centre of gravity of the zone was injected

Likewise, in the fully-developed region, where non-centreline zone motion is described solely by the assumed cross-jet velocity profile (equ. 4.8), penetration determination involves a corrected timestep, $\delta t'$:

$$S = \Sigma u \, \delta t' \qquad (4.18)$$

where:

$$\delta t' = \delta t - \delta t_{inj,\,m} \qquad (4.19)$$

The spray must be represented three-dimensionally, and therefore the zones of the model are in fact conical elements. Each element is of equal thickness, such that fuel division between elements in a set is specified according to:

$$m_{f,zone} = m_{f,tot}\left(\frac{2l-1}{n^2}\right) \tag{4.20}$$

where $m_{f,\,tot}$ is the total fuel mass in the current set.

Air entrainment is calculated by use of a simple momentum assumption:

$$\Delta m_a = \left(\frac{u_o}{u} - 1\right) m_f - m_{a,last} \tag{4.21}$$

where u is radial velocity.

Hiroyasu recommends scaling of zonal entrainment rates by a factor of 1.5 following impingement on the chamber wall and by 0.7 following ignition[126]. Again, these effects were included by use of a parallel calculation, since with direct implementation a consistent physical description cannot be maintained.

Because the model does not compute interzone mixing, final zonal compositions may be misrepresented. The values for the end of entrainment are maintained, whereas there is in reality a convergence towards the average spray composition. This has important consequences, not least for soot modelling, so in order to get round the problem a simple post-processing procedure has been adopted. Zonal average compositions are increasingly weighted to the spray average as described in Appendix F. The resulting composition is used only as an input to the soot model.

4.1.3.2 Discussion

The uniform model described above and shown in Fig. 4.3 is clearly a very simplistic representation of the complex structure of the diesel fuel spray (Fig. 4.1). Therefore, the validity of a number of the modelling assumptions is considered briefly below.

An area of particular interest is the transition region between the liquid core and the broken-up jet. This has been represented simply as a discontinuity of velocity at a straight-line boundary, whilst in reality, jet break-up is progressive. The most

important effect resulting from this simplification is a slight delay in the onset of air entrainment. This occurs because entrainment is calculated on a zonal basis according to the velocity for the centre of mass. However atomisation occurs progressively in each zone as fuel passes the calculated break-up length and evaporation and ignition delay are not directly affected by the air entrainment. This ensures that the model representation is sufficiently accurate for the current purpose, helped by the fact that the zones cover relatively large regions of space, and hence do not need to describe local conditions.

Another concern is the potential inconsistency arising from the independence of the thermodynamic calculations which give zone volumes, and the geometrical description. In fact the trajectory calculations completely neglect physical interaction between zones and there is no allowance for mixing of composition. There is therefore no guarantee that the evolution of the zone size and shape will be consistent with the assumed cross-jet profile, and though zonal boundaries cannot be properly defined, some overlap is implicit. However, in the no-swirl case we do have some confidence that the basis of the geometrical calculations is reasonable. Fuel sprays have been extensively studied and are known to grow steadily, giving an almost constant spray angle (Hiroyasu, 1990)[130]. Though there will be mixing between adjacent zones and maybe even large-scale eddies, these will represent perturbations from the uniform continuous flow described by the model, and should average out over relatively short time-scales.

The geometric description is likely to be less accurate when there is air swirl. In this case the jet cross-section will be deformed and there will be a large discrepancy between conditions on each side. In particular, a substantial proportion of the small droplets and fuel vapour will be blown out of the spray and left behind nearer to the injector. Thus the model concept of adjacent conical zone elements is far from true. Nevertheless, there are reasons to believe that the description of jet behaviour is reasonable. Despite the change in jet structure, in overall terms there certainly exists a strong analogy with the no-swirl case. The main difference is the reduction in penetration because of swirl and this is known with confidence. The differences due to a change in cross-jet structure can be neglected in the current model, since conical elements are used so that averages are sufficient. However, this does call attention to the general problem of neglect of fuel-air ratio variations in the spray due to use of zonal averages. It is possible to model this phenomenon separately, using Monte-Carlo methods. However, such techniques are highly computation

intensive, and due to this factor and time limitations, no attempt has been made to implement such a scheme in the current model. The effect of such neglect on the soot predictions is discussed in section 5.2.2.

Finally the momentum-entrainment assumption needs to be examined. As detailed in the above review, several spray models are based on the turbulent entrainment equation of Hoult and Weil (equ. 4.1) while the current model uses a simple momentum equation (equ. 4.21). It is worthwhile considering the consistency of these two approaches. The Hoult and Weil expression gives one insight into the entrainment process. It sets entrainment rate proportional to zone area and to the velocity difference between the jet and the surroundings. Therefore, at the start of the cycle, small zone size limits entrainment, while at large penetrations, low relative velocities counteract the increase in volume. With the momentum-based expression, on the other hand, air is entrained to maintain the zone momentum while the velocity is reducing. The rate is entirely dependent on velocity and increases at large penetrations according to the square root of time. Thus, the potential for similar behaviour exists. Since the zone surface area is not well defined in a multizone model, it is difficult to make a fair comparison of these approaches in the context of the current work.

The validity of the momentum conservation equation may still be questioned. Implicit is the assumption that there are no resultant forces operating on the zone, for example due to pressure gradients or frictional shear. It is clear that this is a much better approximation near to the injector than further away as body and frictional forces increase with zone size, while the inertia remains roughly constant. Thus entrainment later in the cycle may be over-predicted by this model.

Ultimately, the air-entrainment assumptions will be assessed by comparison with empirical data. The following section presents some information on the performance of the spray model and is followed by a discussion of the results.

4.1.4 Results

This section describes performance of the model. It is desirable that air entrainment predictions are independent of the number of zones chosen to represent the jet. The sensitivity to the number of axial sets of zones and to the number of cross-jet zones is shown below in Figs. 4.5 and 4.6 respectively.

Fig. 4.5 shows that variation in number of axial sets has minimal effect on the air entrainment. The curves for 4 sets and 8 sets are virtually indistinguishable, while that for 2 sets is only marginally higher. The latter effect is to be expected, since if a single zone is divided into two, the slower-moving component will tend to overcompensate for the other, and overall entrainment will be higher than if a single average velocity is used.

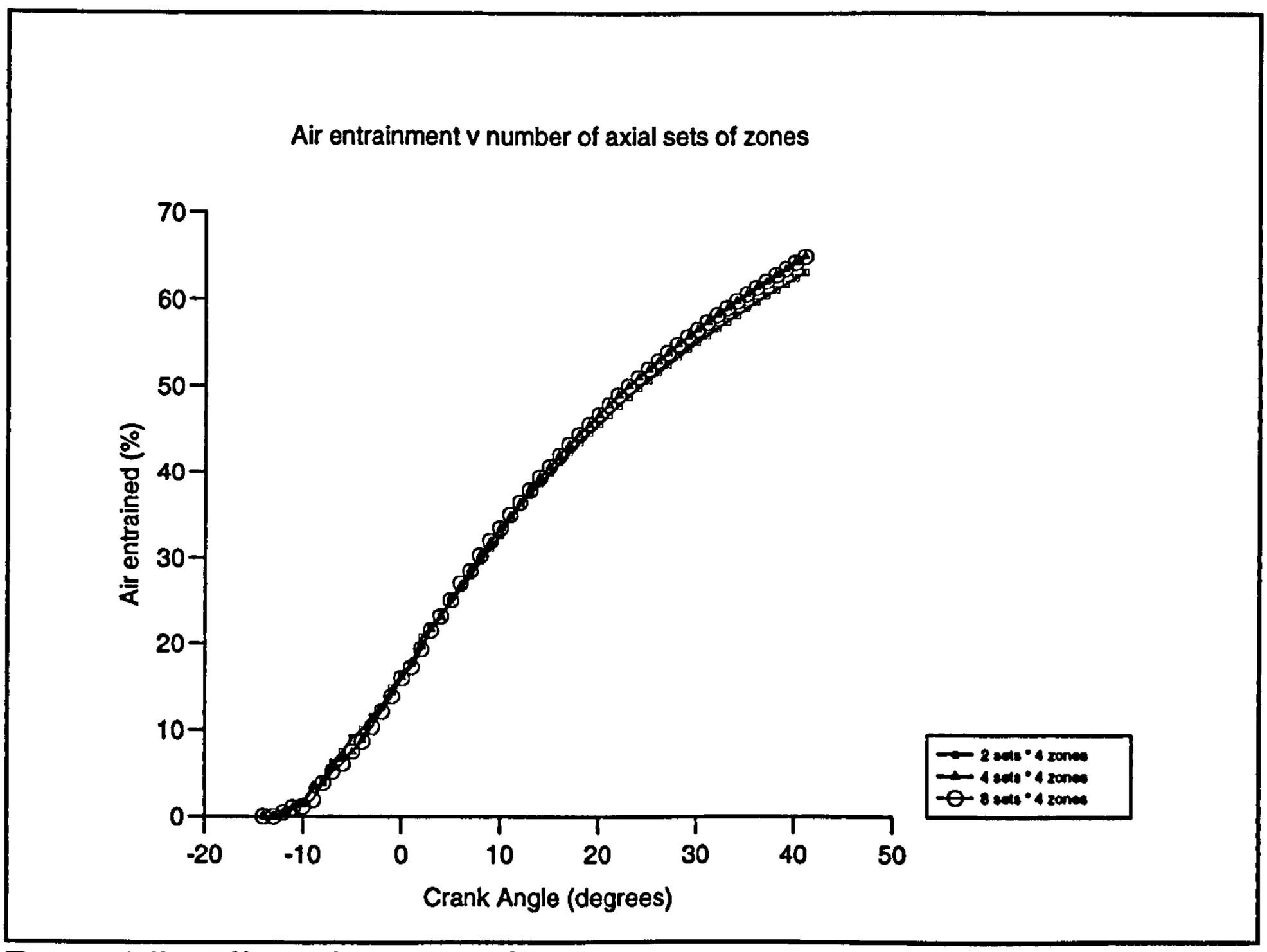

Figure 4.5 - Effect of number of axial zone sets on air entrainment

Fig. 4.6 shows that variation in the number of cross-jet zones has a more significant effect on entrainment. However, the major part of this discrepancy is due to the use of a simple method of jet subdivision which renders the model inaccurate for

very small numbers of cross-jet zones. For example, if only two cross-jet zones are used, the inner takes the velocity of the centreline, while the outer takes the velocity of the edge of the jet. It would have been more accurate to integrate the velocity profile over the region of space each occupies, but the model was designed for multizone use and the inaccuracy will be very small when several cross-jet zones are used. This is demonstrated by the convergence of curves for higher numbers of cross-jet zones in Fig. 4.6.

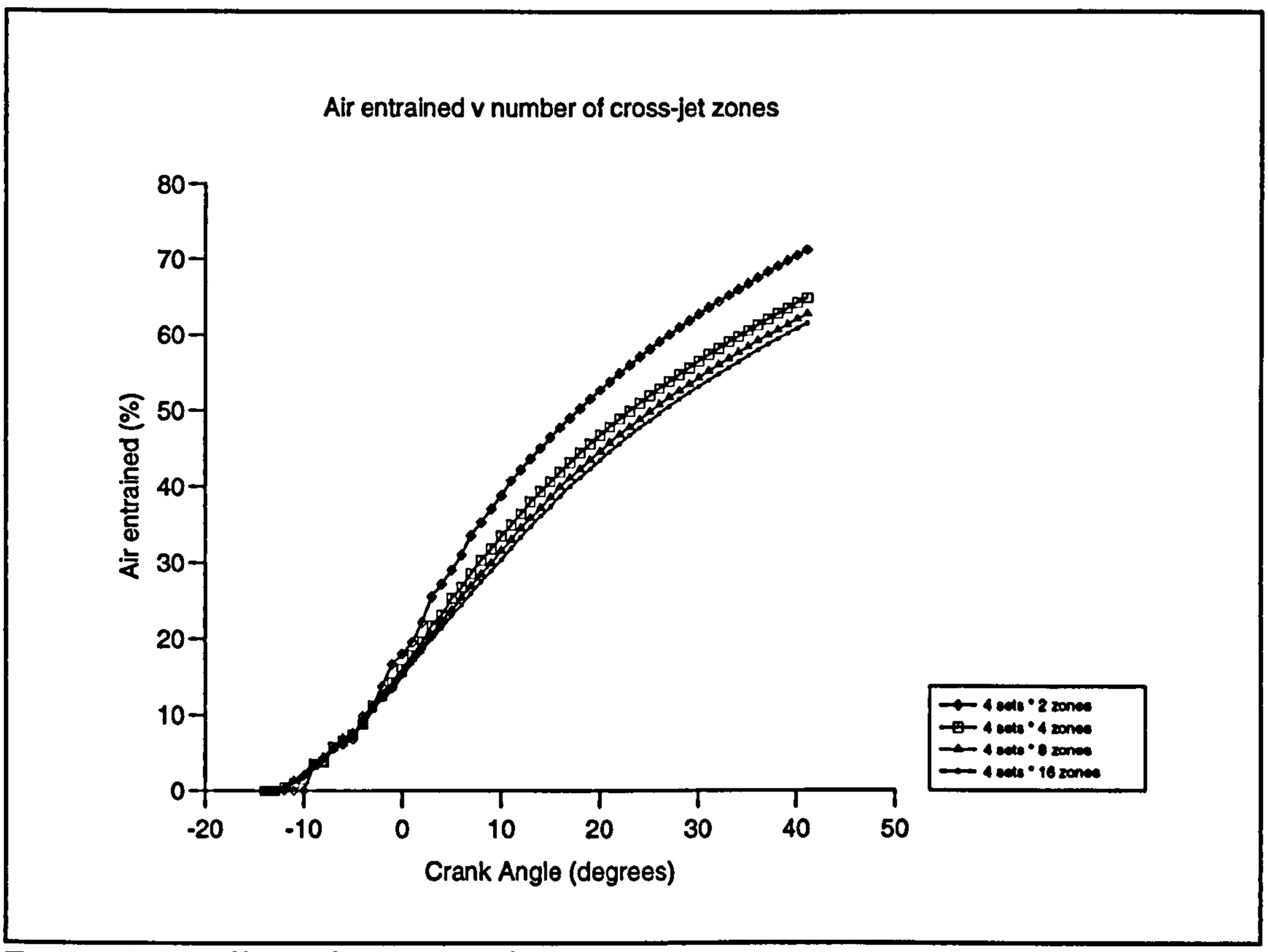

Figure 4.6 - Effect of number of cross-jet zones on air entrainment

In the light of this satisfactory performance, together with some investigation of the combustion model as a whole, the case of four axial sets and four cross-jet zones was chosen as the standard setup for all other modelling work.

There are a number of ways of assessing the accuracy of the predicted entrainment rates. The simplest is to compare the model results directly with entrainment rate data from the chosen experimental case. In addition, general data on rates of entrainment in jets can be utilised, for instance by comparison of experimental entrainment coefficients with a value calculated from the model predictions.

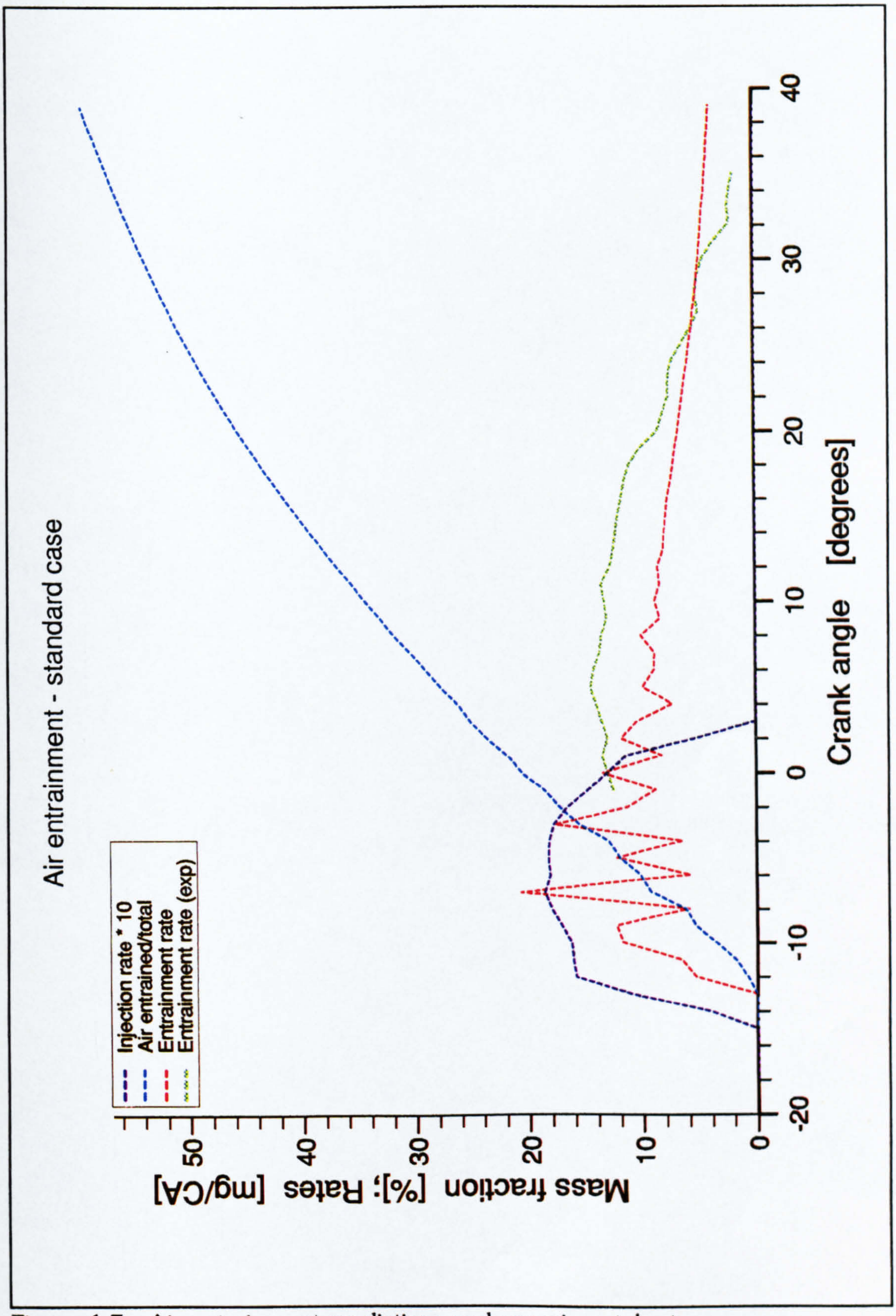

Figure 4.7 - Air entrainment predictions and experimental rate

Fig. 4.7 plots the model predictions for the standard case of the Kamimoto dataset[159], together with the experimentally measured air-entrainment rate. Agreement over the bulk of the range is very good, though the calculated rate does not fall off as rapidly as the experimental values. Also, the simulation results show some large oscillations in the entrainment during the early phase while injection is still continuing. This phenomenon may be simply attributed to the zonal division of the jet in the axial direction, with peaks in entrainment when each successive set breaks up. This is not a problem if the average rate in the region is accurate. However, direct assessment of rate in the early phase is not permitted, since the experimental curve does not extend to the point of onset of entrainment. Nevertheless, it was found that the heat-release diagram (see section 5.1) does give a good guide as to the adequacy of the predictions in this region, as outlined below.

The premixed part of the heat-release curve is very sensitive to the total amount of air entrained up until ignition. Initial results showed that this quantity was insufficient, since even if all of the air was allowed to burn in premixed mode, the heat-release rate fell short of the experimental levels. Thus, some modifications to the spray model were necessary. Due to the requirement of satisfactory performance over the full range of operating conditions, this modification was carried out in conjunction with the parametric study. It is therefore described fully in that context, in section 5.1.

Fig. 4.8 is a plot of an entrainment coefficient against axial position in the jet. The entrainment coefficient, α_e, is defined by the following equation:

$$\frac{m_a + m_f}{m_f} = \alpha_e \left(\frac{S}{d_o}\right)\left(\frac{\rho_a}{\rho_f}\right)^{\frac{1}{2}} \qquad (4.22)$$

This equation was derived by Ricou[293], who obtained a value of 0.32 for the entrainment coefficient. Ha used hot-wire anemometry to measure actual rates of entrainment into a diesel-like spray[106]. Fig. 4.8 includes data points from this study, together with values computed from the model predictions. The injection conditions for each case are given in Table 4.2.

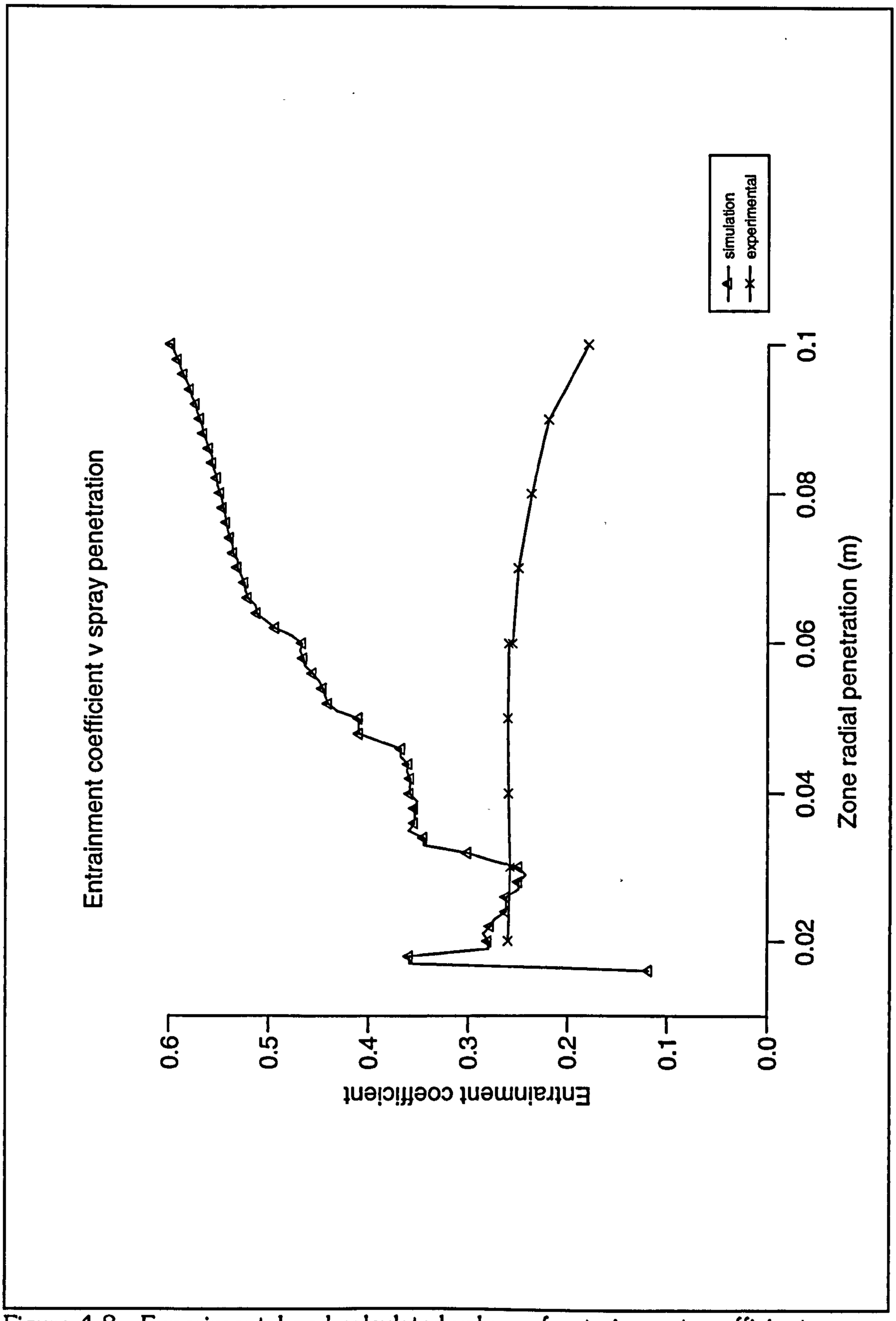

Figure 4.8 - Experimental and calculated values of entrainment coefficient

Injection conditions	Nozzle diameter (mm)	Injection pressure (MPa)	Ambient pressure (MPa)
Ha[106]	0.32	22.6	1.35
Simulation	0.4	17	2.6 - 4.8

Table 4.2 - Injection conditions for Fig. 4.8

The values computed by the model rise to more than double the experimental values at large penetrations. Fig. 4.7 may give some indication of this, since the entrainment rate is dropping less rapidly than the experimental level from the end of injection onwards. A possible reason is that the momentum basis begins to break down at high levels of entrainment, since body forces due to friction and the pressure gradient can no longer be neglected. In order to overcome this difficulty, entrainment at higher penetrations could be calculated by use of the turbulent entrainment equation of Hoult and Weil[137] (equ. 4.1). This model was implemented, but the predicted entrainment levels were found to be no lower than the momentum-based values. The difficulty of estimating the zonal surface area in this type of multizone model was probably the main source of the error.

Conclusion

A geometrically-based spray model has been implemented which uses the penetration equations of Hiroyasu and calculates air entrainment according to momentum conservation. The model takes into account the effects of air swirl, combustion and wall impingement. The spray behaviour is fairly independent of the number of model zones. Experimental data has been used to validate the predictions of entrainment rate, though some overprediction at higher penetrations is suggested. Reasons for the latter effect are suggested. Though some modifications have been necessary, the sufficiency of the model as a basis for the combustion and emissions model has been established.

4.2 EVAPORATION

4.2.1 Introduction

Droplet evaporation may have an important influence on the combustion process in a diesel engine. Though combustion is usually limited primarily by mixing, not evaporation (Kuo, 1983[196]), the amount of fuel mixed to within the flammability limits is dependent upon the preceding evaporation process. This, in turn, is related to the atomisation of liquid fuel. Thus, if these processes are inaccurately described, there will be a knock-on effect on the simulation of the main combustion process, and hence emission predictions. The outcome will mirror the effect of varying the injection timing. Therefore, the evaporation model is an important element of a combustion simulation.

In a diesel engine, evaporation rates will vary markedly according to local operating conditions. On a fundamental level, heat and mass transfer are the controlling processes, affected by the thermodynamic state and property gradients in neighbouring regions. Due to the temperature rise, evaporation rates are generally greatly increased following the start of combustion. In this case, the position of the flame is important. When droplet-containing regions burn, the flame may enclose groups of droplets and rich mixture (group combustion), or a flame may surround each individual droplet. Another rate-enhancement effect occurs via increase of the heat-transfer coefficient due to convection. With both combustion and convection, the transport properties of the mixture surrounding the drop are altered and the temperature gradient increased.

Both atomisation and evaporation rates are affected by the chamber conditions. However, because these conditions change over fairly long timescales, it is sufficient to neglect changes in the rates over the short period of a calculation timestep. This is of great benefit to the engine modeller, since it allows isolation of the atomisation and evaporation processes from other combustion phenomena.

A considerable amount of research has been concentrated on the theoretical and empirical analysis of droplet evaporation over a wide range of thermodynamic state conditions. The basic governing equation was determined empirically over a century ago[333]:

$$r^2 - r_o^2 = \beta t \qquad (4.23)$$

The core of the basic theory consistent with this equation was established by the 1950s[330]. Based on the work of Williams[369], Kadota[154] and Faeth[66], Jin[152] (1985) considers the vaporisation characteristics of single component droplets to be reasonably well-understood, both at atmospheric and elevated pressures.

Phenomenological diesel combustion models have generally made use of the standard theoretical approach (Nishida[262], Gupta[105,237], Dent[56,198], Payri[271]), though in others either a simple empirical correlation (Hodgetts[132,317]), or an alternative theoretical approach have been applied (Hiroyasu[126,124], Kuo[197], Wang[361]). In some cases evaporation has been completely neglected[196,310,184]. The current work follows the established basic theory.

4.2.2 Atomisation

As has been observed in the description of spray structure, the liquid core of the fuel jet rapidly breaks up into a spray of fine drops. The extensive studies of Reitz & Bracco[33,289-292,377] identified several factors contributing to jet break-up and concluded that interaction at the liquid-gas interface is the major mechanism[33]. However, in a recent study, Soteriou[329] found that cavitation originating inside the nozzle hole was the predominant mechanism. Following breakup, secondary breakup and droplet collision occur[66], yielding a continuously-evolving distribution of droplet size. For the purposes of the current work, modelling must be confined to the specification of the initial droplet-size distribution. Usually this is achieved by specifying the Sauter Mean Diameter* (SMD) and a related distribution for size. Hiroyasu has reviewed measurement of SMD and listed four empirical correlations whilst Aigal[5] lists seven correlations. Those chosen for study in the current work are as follows:

---

* This is the droplet size which gives an area-to-volume ratio equivalent to the average over the whole distribution range.

Tanasawa & Toyoda[341]; 1955:

$$D_{32} = 3.98x10^{7}\frac{d_o}{V}\left(\frac{\sigma}{\rho_a}\right)^{0.25}\sqrt{g}\left(1+3.34.10^{-2}\frac{\mu_f\sqrt{g}}{\sigma\rho_f d_o}\right) \qquad (4.24)$$

Knight[178]; 1955:

$$D_{32} = 1.605x10^{6}\Delta p^{-0.458}Q^{0.209}\nu_f^{0.215}\left(\frac{A_{orf}}{A(t)_{eff}}\right)^{0.916} \qquad (4.25)$$

Hiroyasu & Kadota[120]; 1974:

$$D_{32} = 2.33x10^{3}\Delta p^{-0.135}\rho_a^{0.121}Q^{0.131} \qquad (4.26)$$

Elkotb[63]; 1982

$$D_{32} = 3.08x10^{6}\nu^{0.385}\sigma^{0.737}\rho_f^{0.737}\rho_a^{0.06}\Delta p^{-0.54} \qquad (4.27)$$

Hiroyasu, Arai & Tabata[129]; 1989

$$D_{32} = \max(D_{32_{incomp}}, D_{32_{comp}}) \qquad (4.28)$$

where the complete spray and incomplete spray SMD expressions are:

$$D_{32_{incomp}} = 4.12\,Re^{0.12}\,We^{-0.75}\left(\frac{\mu_l}{\mu_a}\right)^{0.54}\left(\frac{\rho_l}{\rho_a}\right)^{0.18} \qquad (4.29)$$

$$D_{32_{comp}} = 0.38\,Re^{0.25}\,We^{-0.32}\left(\frac{\mu_l}{\mu_a}\right)^{0.37}\left(\frac{\rho_l}{\rho_a}\right)^{-0.47} \qquad (4.30)$$

Hiroyasu (1967)[119] examined several of the mathematical expressions proposed to describe droplet-size distribution in a liquid spray, and correlated spray behaviour for conditions which simulate those in diesel engines using a Chi-square distribution[120]. The correlation applies to sprays injected through three types of nozzle (the hole nozzle, the Pintle nozzle, and the throttling Pintle nozzle)[128]:

$$\frac{dV}{V} = 13.5\left(\frac{D}{D_{32}}\right)^2 e^{-3\left(\frac{D}{D_{32}}\right)} d\left(\frac{D}{D_{32}}\right) \qquad (4.31)$$

Typical values of SMD are in the range 5 - 100 μm (Hiroyasu[128], Heywood[116]) and they are generally reduced with increasing injection pressure.

4.2.3 Evaporation modelling

4.2.3.1 Evaporation theory

Evaporation calculations are based on theory of evaporation and burning of a single fuel droplet, neglecting any group-combustion effects. This theory was developed by Spalding[137] (1950) and is presented in a more general form by Williams[369] (1965). Wise[374], Chigier[44], Faeth[66] and Sirignano[324] have reviewed the subject.

Assuming spherical symmetry and quasi-steady state conditions, the following basic evaporation-rate equation has been derived*:

$$\dot{m} = \frac{1}{\int \frac{dr}{4\pi\rho D}} \log_e(1+B) \qquad (4.32)$$

where:

$$B = \frac{\int_{su}^{\infty} c_{p_g}(T_\infty - T_B)}{L} \qquad (4.33)$$

This expression holds for both non-combusting and combusting conditions, though in the case of the latter, the mass-transfer number is modified as follows:

---

* The derivation of this equation ignores radiation effects. Previous studies have shown that radiative heating is relatively unimportant in sprays[66]. The ratio of radiative to convective heat transfer rates was 0.02 - 0.2 in a furnace[135].

$$B = \frac{\left(\Delta H F Y_{O_2 \infty} + \int_{su}^{\infty} c_{p_g}(T_\infty - T_B)\right)}{L + \Delta H F Y_{O su}} \qquad (4.34)$$

These equations may be simplified and modified in various ways. By assuming that the Lewis number is unity, ρD can be replaced by λ / c_{pg}. Making the further assumption that this term is invariant with temperature*, even during species change as combustion occurs, the integral term in the above equation is simplified as follows:

$$\frac{1}{\int_{su}^{\infty} \frac{dr}{4\pi\rho D}} = \frac{2\pi\lambda r}{c_{p_g}} \qquad (4.35)$$

Thus, equ. 4.32 is usually written:

$$\dot{m} = \frac{4\pi r\lambda \log_e(1+B)}{c_{p_g}} \qquad (4.36)$$

By use of the continuity expression, the following equation can be derived:

$$r^2 - r_o^2 = \beta t \qquad (4.37)$$

where β, the evaporation or burning constant, is:

$$\beta = \frac{2\lambda \log_e(1+B)}{c_{p_g}\rho_l} \qquad (4.38)$$

The form of equ. 4.37 is confirmed experimentally. Kanury[162] summarises the values obtained by several researchers for the burning of twenty different hydrocarbons in air at atmospheric pressure. The theoretical results range from 0.85×10^{-6} to 1.44×10^{-6}, whilst measured values average slightly lower at 0.66×10^{-6}

---

* This result is given to a first approximation by the kinetic theory of gases[90].

to $1.14 \times 10^{-6}\ m^2\ s^{-1}$. For diesel fuel the value is about 0.8×10^{-6}. Though these empirical values have been determined for droplets typically of order 1mm in diameter, Gokalp (1988)[92] considers that the experimental and numerical results existing in the literature do not show any strong dependency of the burning-droplet characteristics with the initial droplet diameter. In agreement with this, experimental work by Borman (1967)[31] shows that the evaporation times of individual fuel droplets 25 μm in diameter injected into air at typical diesel conditions are usually less than 1 ms, corresponding to an evaporation constant of more than 0.6×10^{-6}.

If the integral term in equ. 4.32 is to be evaluated numerically, rather than approximated as above (equ. 4.35), then the thickness of the thermal boundary layer or position of the flame front must be known.

Following Kanury, given that heat flux can be expressed:

$$q = h\,(T_\infty - T_{su}) = k\frac{(T_\infty - T_{su})}{\delta_T} \qquad (4.39)$$

where δ_T is the thickness of the thermal boundary layer

and Nusselt number is:

$$Nu = \frac{h\,D}{\lambda} \qquad (4.40)$$

then the thermal boundary layer thickness is:

$$\delta_T = \frac{D}{Nu} \qquad (4.41)$$

Hiroyasu[121] quotes the following result from Kadota[153]:

$$\delta_T = \frac{D}{Nu - 2} \qquad (4.42)$$

and Faeth[66] gives an identical expression for film thickness.

Since the Nusselt number is commonly expressed:

$$Nu = 2 + 0.6 Re^{\frac{1}{2}} Pr^{\frac{1}{3}} \tag{4.43}$$

equ. 4.41 suggests that the boundary-layer thickness is always less than the droplet radius, whereas equ. 4.42 suggests that it becomes very large under conditions approaching quiescent.

In the droplet-burning case, the position of the flame front must be known. Theoretically, it is given by[162]:

$$\frac{r_{fl}}{r_{su}} = \frac{\log_e(1+B)}{\log_e\left(\frac{FY_{O\infty}}{Y_{f_s}} + 1\right)} \tag{4.44}$$

In air, the term $FY_{O\infty}/Y_{fsu}$ is very small so that the expression can be simplified to:

$$\frac{r_{fl}}{r_{su}} = 14.5 \log_e(1+B) \tag{4.45}$$

Typically, combustion mass-transfer numbers are of order 10, so that predicted flame positions are several droplet diameters from the droplet surface. However, Williams (1965)[369] states that in droplet-burning experiments, the value of flame radius, r_{fl}, is too large by roughly a factor of two, because of convection effects[369]. Faeth[66] considers that flame-position expressions of this type are meaningless in convection conditions, and that they overemphasise dependency on droplet diameter. In fact, data published by Gokalp[92] (1988) shows that for droplet diameter of order 1 mm, r_{fl}/r_{su} is roughly constant at a value of between 5 and 10 during the whole burning time.

4.2.3.2 Mass-transfer coefficient

The mass-transfer number, B, can be approximated in various ways. If c_{pg} is assumed constant in the gas, equ. 4.34 is simplified as follows:

$$B = \frac{\Delta H F Y_{O\infty} + c_{p_g}(T_\infty - T_B)}{L + \Delta H F Y_{O\,su}} \qquad (4.46)$$

In studies on drop burning, it is assumed that $Y_{O\,su} = 0$ since nearly all of the oxidant is consumed before diffusing to the droplet surface. This has been verified numerically[218], with typical $Y_{O\,su}$ values found to be of order 10^{-8}.

Alternatively, following Kanury[162], B is expressed as :

$$B = \frac{\Delta H F Y_{O\infty} + c_{p_g}(T_\infty - T_B)}{L + c_f(T_B - T_d)} \qquad (4.47)$$

In this case, the droplet temperature, T_d, must be estimated.

4.2.3.3 Convection effects

The basic equation of the above analysis, equ. 4.32, applies to evaporation in quiescent conditions. In the case of a moving droplet, the heat-transfer coefficient is increased due to convection, giving a corresponding increase in the evaporation rate. Conventionally, this effect is allowed for via a Nusselt-number correction term, though significant differences are found between the various methods of application. Because of this variation, the correlations used are first set out below in original form. This is followed by a summary table, where the equations have been re-expressed on a standard basis to allow a more meaningful comparison.

The original and most popular Nusselt-number correlation is due to Frößling[80] (1938):

$$Nu = 2 + 0.552 Re^{\frac{1}{2}} Sc^{\frac{1}{3}} \qquad (4.48)$$

and Ranz[285,286] (1952):

$$Nu = 2 + 0.6 Re^{\frac{1}{2}} Pr^{\frac{1}{3}} \qquad (4.49)$$

The Schmidt number is used interchangeably with the Prandtl number.

With the Reynolds number set to zero for quiescent conditions, equating the evaporation-rate ratio to the Nusselt-number ratio yields the following expression:

$$Nu = \left(1 + 0.39 Re^{\frac{1}{2}} Pr^{\frac{1}{3}}\right) \frac{\log_e(1+B)}{B} \qquad (4.50)$$

This is the equation given by Godsave (1953)[91], Williams (1965)[369] and Law (1977)[205].

Glassman (1987)[90], however, gives the Nusselt-number correlation as:

$$\frac{\dot{m}}{\dot{m}_o} = 1 + 0.3 Re^{\frac{1}{2}} Pr^{\frac{1}{3}} \qquad (4.51)$$

stating that the term $(\log_e(1+B))/B$ has been used as an empirical correction for higher Reynolds number problems.

Natarajan[256] defines Nusselt number in the presence of mass transfer as:

$$Nu = \frac{\rho_l c_p \beta}{4\lambda B} \qquad (4.52)$$

where β is as defined in equ. 4.38.

This can be re-expressed:

$$Nu = \frac{2\log_e(1+B)}{B} \qquad (4.53)$$

An empirical correlation applying to both non-combusting and burning drops is derived:

$$Nu = \frac{1.46 Re^{\frac{1}{2}}}{1+B} \tag{4.54}$$

Eisenklam[62] also correlates Nusselt number to mass-transfer number for intense mass-transfer conditions:

$$Nu = \frac{2\log_e(1+B)}{B} \tag{4.55}$$

Separate correlations are given for the non-combusting case:

$$Nu = \frac{2+1.6 Re^{\frac{1}{2}}}{1+B} \tag{4.56}$$

and for burning drops:

$$Nu = \frac{4.9 Re^{0.4}}{1+B} \tag{4.57}$$

Faeth's (1977) review[66] states that the Ranz correlation[285,286] can be interpreted as a convection correction:

$$\frac{h}{h_{Re=0}} = 1 + 0.3 Re^{\frac{1}{2}} Pr^{\frac{1}{3}} \tag{4.58}$$

on the assumption that the form of the expression is unchanged in the presence of mass transfer. In general, heat and mass transfer can be correlated by a multiplicative correction for convection:

$$\frac{Nu}{Nu_{Re=0}} = 1 + f(Re, Pr, Sc) \tag{4.59}$$

For the non-convective case, Faeth[66] derives the following equation for Nusselt number:

$$Nu = \frac{2\log_e(1+B_Y)}{B_Y} \tag{4.60}$$

where:

$$B_Y = \frac{(Y_{fsu} - Y_{f\infty})}{(1 - Y_{fsu})} \tag{4.61}$$

Under low mass-transfer conditions, B_Y tends to zero, such that the Nusselt (and Sherwood) numbers tend to two. Faeth[66] goes on to derive a synthesised correlation for Nusselt number which approaches limiting values at low and high Reynolds numbers (at the limit $B_Y = 0$):

$$Nu = 2 + \frac{0.555 Re^{\frac{1}{2}} Pr^{\frac{1}{3}}}{\left(1 + \frac{1.232}{RePr^{\frac{4}{3}}}\right)^{\frac{1}{2}}} \tag{4.62}$$

The equation is modified as follows when B_Y is not small:

$$Nu = \frac{\log_e(1+B_Y)}{B_Y}\left(2 + \frac{0.555 Re^{\frac{1}{2}} Pr^{\frac{1}{3}}}{\left(1 + \frac{1.232}{RePr^{\frac{4}{3}}}\right)^{\frac{1}{2}}}\right) \tag{4.63}$$

Faeth[66] states that various experimental and property value uncertainties have led to confusion, with the term $(\log_e(1+B))/B$ replaced by $1/(1+B)$ by some authors[62,369]. This procedure is undesirable, since it does not asymptotically approach the correct behaviour at the limit of a motionless drop.

Frößling (1938)[80]	$\frac{\dot{m}}{\dot{m}_o} = 1 + 0.276 Re^{\frac{1}{2}} Sc^{\frac{1}{3}}$
Ranz (1952)[285,286] (Godsave (1953)[91], Williams (1965)[369], Law (1977)[205])	$\frac{\dot{m}}{\dot{m}_o} = 1 + 0.3 Re^{\frac{1}{2}} Pr^{\frac{1}{3}}$
Glassman (1987)[90]	$\frac{\dot{m}}{\dot{m}_o} = 1 + 0.39 Re^{\frac{1}{2}} Pr^{\frac{1}{3}}$
Natarajan (1970)[256]	$\frac{\dot{m}}{\dot{m}_o} = \frac{0.73 Re^{\frac{1}{2}} B}{(1+B)\log_e(1+B)}$
Eisenklam (1967)[62] (non-combusting case)	$\frac{\dot{m}}{\dot{m}_o} = \frac{(1 + 0.8 Re^{\frac{1}{2}}) B}{(1+B)\log_e(1+B)}$
(combusting case)	$\frac{\dot{m}}{\dot{m}_o} = \frac{2.45 Re^{0.4} B}{(1+B)\log_e(1+B)}$
Faeth (1977)[66]	$\frac{\dot{m}}{\dot{m}_o} = \left(1 + \frac{0.277 Re^{\frac{1}{2}} Pr^{\frac{1}{3}}}{\left(1 + \frac{1.232}{RePr^{\frac{4}{3}}}\right)^{\frac{1}{2}}}\right)$

Table 4.3 - Convection correlations

Following Faeth's suggested approach, it is assumed that equ. 4.53 holds in all cases and that the non-convective Nusselt number is specified by equ. 4.60 when not

explicitly mentioned. Therefore, the correlations for Nusselt number can be summarised in terms of ratio of mass-transfer rate as above (Table 4.3). These expressions have been standardised by appropriate application of the correction factor for high mass-transfer rate, thus allowing direct comparison.

Finally, Sirignano[324] gives an approximate expression for the relaxation time of a droplet moving through air in a diesel environment (equ. 4.64). It may be important to take this effect into account, since it will have a big impact on convection effect via the Reynolds number term.

$$\tau = \frac{r_{drop}^2}{10^{-7}} \qquad (4.64)$$

4.2.3.4 Other approaches

Hodgetts (1975)[132,317] applied a correlation given by Benson[22] in his phenomenological model:

$$\frac{dm}{dt}_{eva} = \frac{K_7 \zeta p_{O_2}^{0.4}}{B} (\rho_f X_f)^{\frac{1}{3}} (\rho_f X_f - \rho_g X_{eva})^{\frac{2}{3}} \qquad (4.65)$$

The factor ς was added to the original expression to allow for the effect of turbulence.

Hiroyasu presents an alternative theoretical approach[154]. The first equation in his analysis implies that there is zero net mass transfer across a surface due to diffusion. From this condition alone, it is possible to derive the relationship:

$$\dot{m}_{su} = \frac{4\pi r \lambda B}{c_p} \qquad (4.66)$$

This is consistent with the more complex result given by Hiroyasu, in lacking the dependency on the logarithm of *(1+B)* found in the more conventional analysis. Thus, a much higher temperature sensitivity is predicted, and evaporation rates are greatly increased during combustion. It is interesting to note, however, that the conventional approach has been used in the most recent version[262] of Hiroyasu's phenomenological combustion model.

4.2.3.5 Pressure effects

Various theoretical works (Spalding[331], Rosner[297], and Chervinsky[43]) and experimental studies (Faeth[65], Williams[368] (review)) have examined droplet evaporation and combustion under high pressure and supercritical conditions. More recently, investigation has been made into the phenomena of micro-explosion, in which a droplet heated through its critical point is rapidly fragmented by internal gasification. Wang[362] highlighted the importance of the stability of droplet generation in determining the likelihood of micro-explosion, though without attempting to quantify this process. Various studies[5] have examined the phenomena in pure liquid compounds, but it is generally accepted that micro-explosion only occurs when the volatilities of the droplet components are sufficiently different. On the other hand, Jin[152] has calculated that high pressure reduces both the likelihood of a multicomponent droplet reaching its critical point and the potential for microexplosions. For octane-decane mixtures, Lazar[206] calculated a critical burning pressure of 36 - 57 atm, and obtained empirical values in the range 44 - 47 atm. These value are more than double the equivalent single component values. It therefore seems likely that this mechanism is of importance in diesel engines, though apparently it has never been fully quantified or incorporated into any phenomenological models.

4.2.3.6 Radiation

Previous studies of burning drops have indicated that radiative heating is relatively unimportant for drop sizes representative of most sprays[66].

4.2.4 Results

4.2.4.1 Atomisation

Spray atomisation has been described by equ. 4.31 and a choice of one of equs. 4.24-28. The resulting SMD's are given in Table 4.4 (over) and the size distribution for the case of the Hiroyasu, Arai & Tabata correlation (equ. 4.16) is illustrated in Fig. 4.9. The latter aimed to establish a more general correlation than the earlier works, and was the first to be derived from experiments on high-speed diesel sprays. Also, the predicted SMD is within the range of the other results. Thus, it seemed reasonable to select this expression for default use in the model. The effect of this choice on evaporation rate is illustrated in Fig. 4.10.

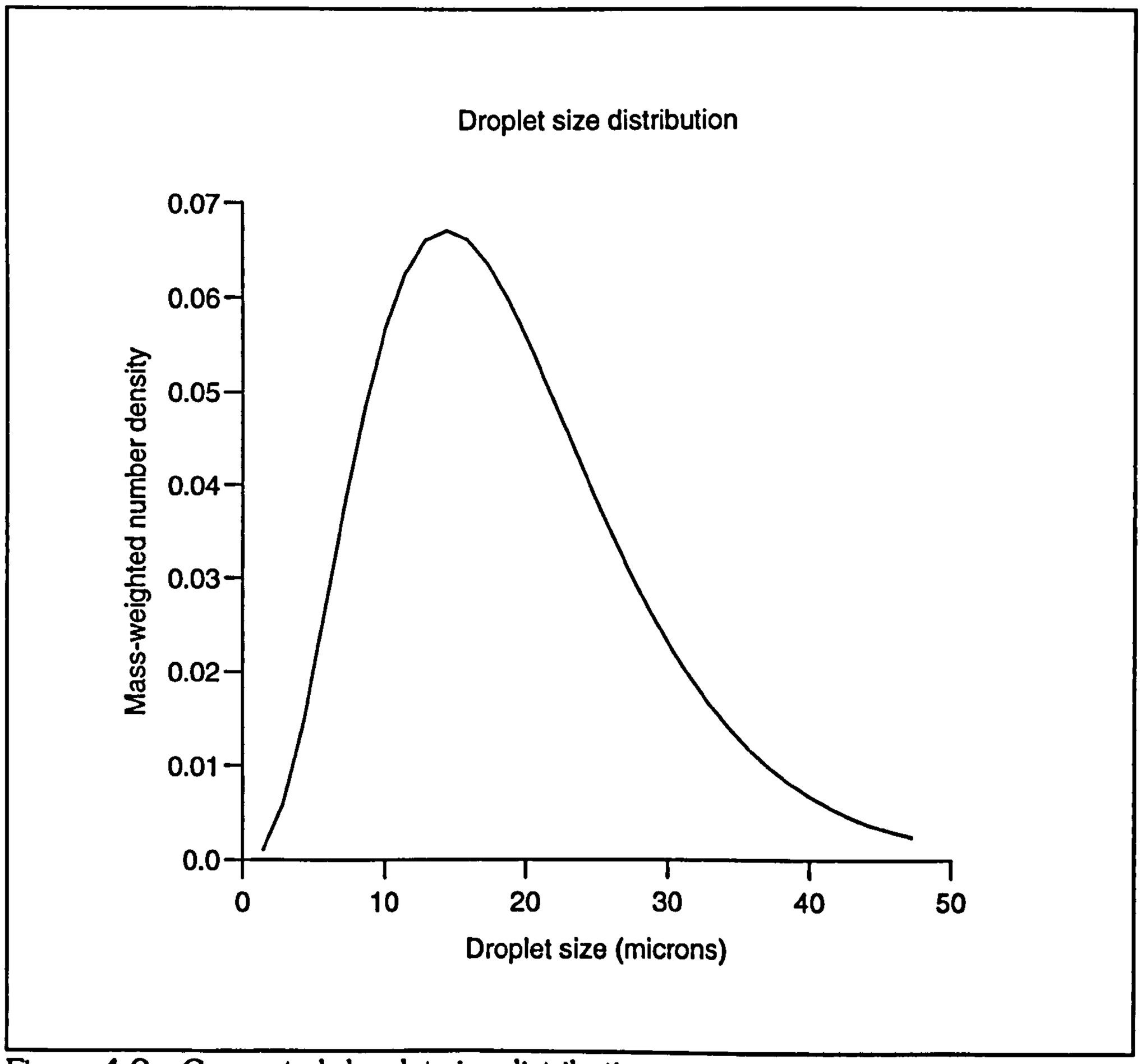

Figure 4.9 - Computed droplet size distribution

Researchers	Year	Calculated SMD (μm)
Tanasawa & Toyoda[341]	1955	55.6
Knight[178]	1955	6.7
Hiroyasu & Kadota[120]	1974	28.4
Elkotb[63]	1982	5.0
Hiroyasu, Arai & Tabata[129]	1989	7.6

Table 4.4 - Calculated SMD values

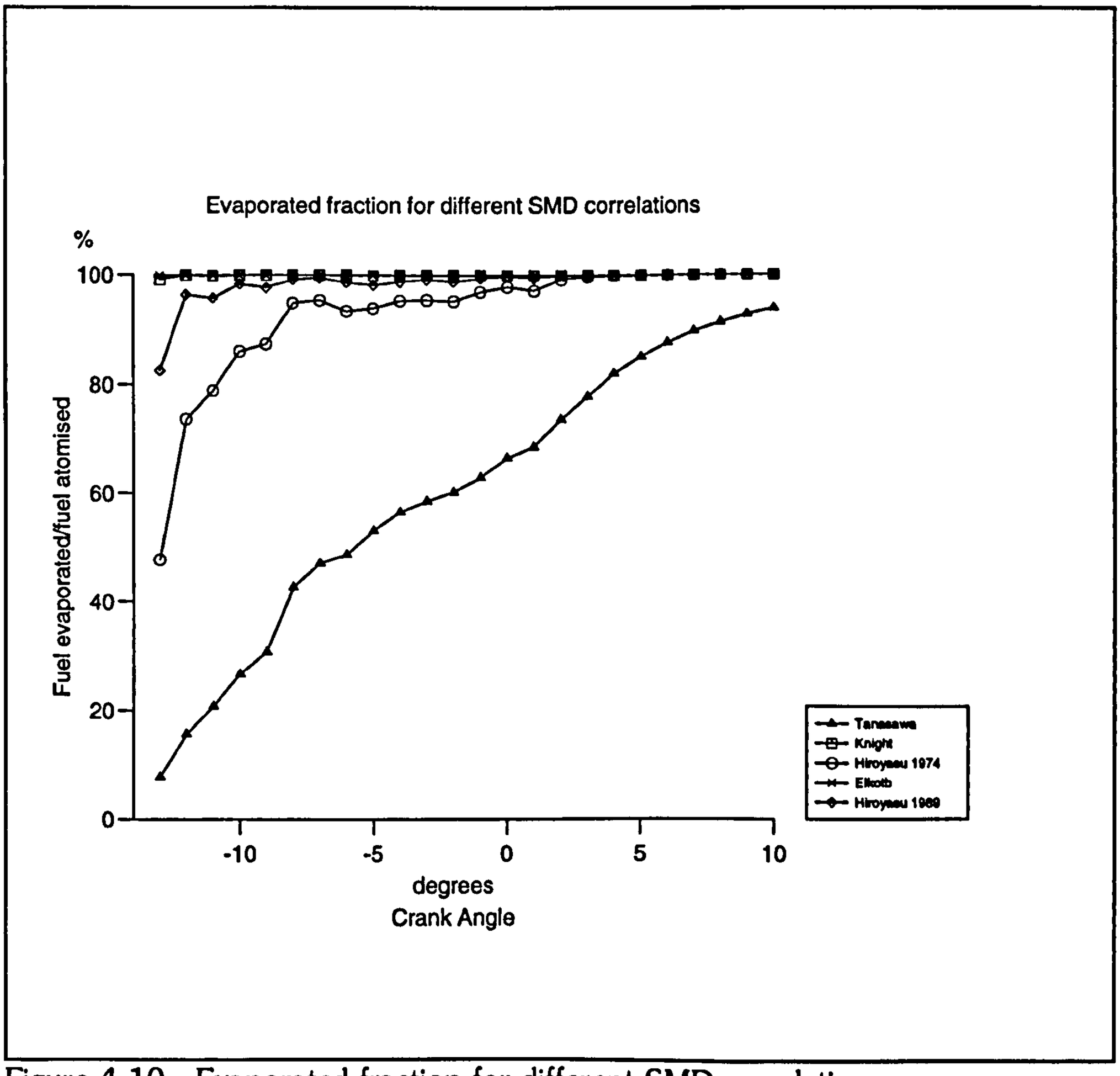

Figure 4.10 - Evaporated fraction for different SMD correlations

4.2.4.2 Evaporation rate

The evaporation rate has been determined by use of equ. 4.32. A choice is provided between the convection factor corrections of Ranz[285,286], Natarajan[256] and Eisenklam[62]. With the Ranz correlation, an additional correction factor for high mass-transfer rates has been included (equ. 4.60); in the other cases this factor is implicit in the Nusselt-number expression (equs. 4.52-57). A plot of evaporated fraction (as a percentage of the atomised fuel mass), according to each of the correlations, is shown in Fig. 4.11.

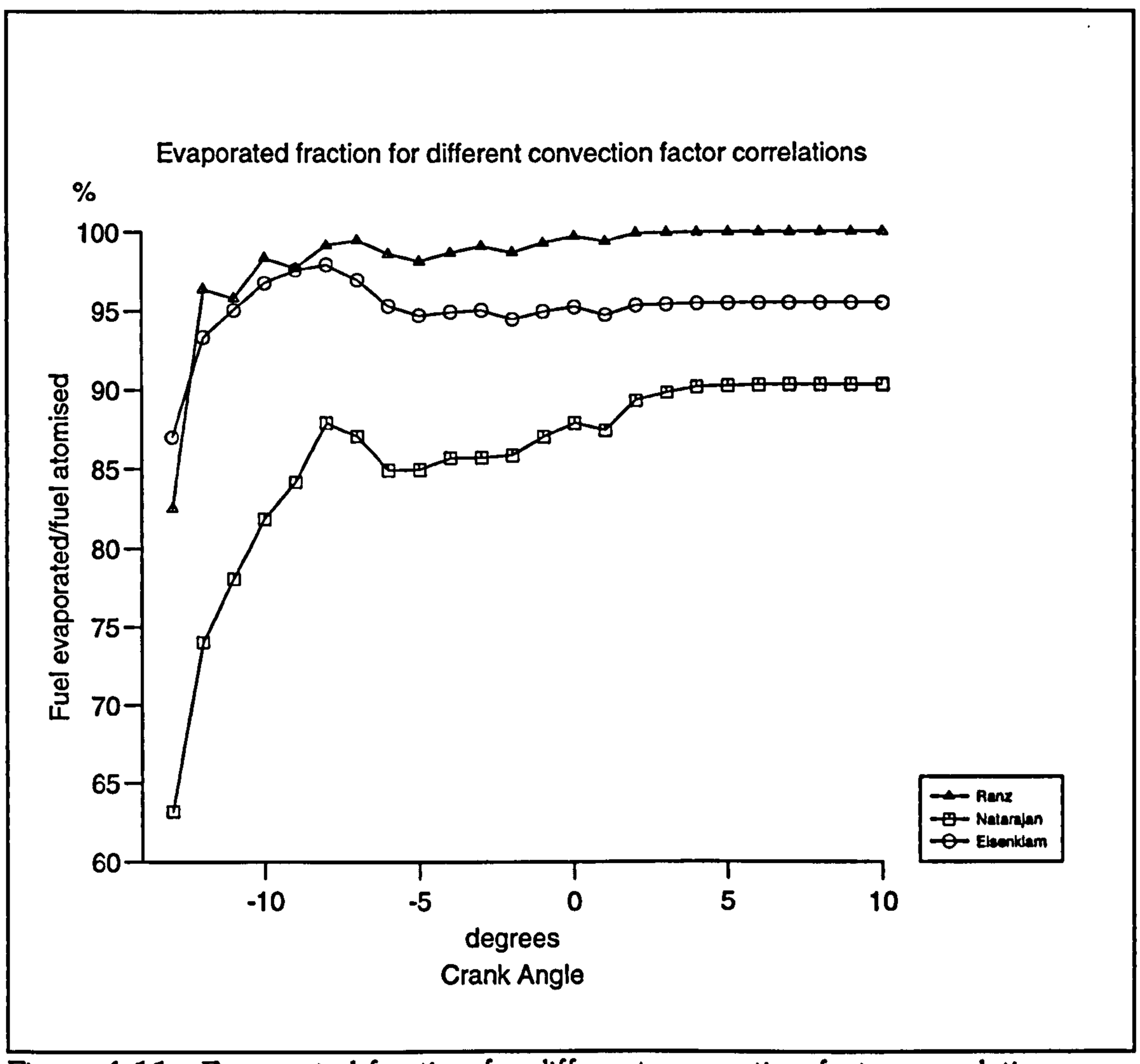

Figure 4.11 - Evaporated fraction for different convection factor correlations

The figure shows good agreement between the correlations of Ranz and Eisenklam during the first phase, but a divergence later with the total evaporated fraction of the latter not rising above 95%. The Natarajan correlation yields a slower rate, and a final value of 90% evaporated. Incomplete evaporation occurs because the correlations of Eisenklam and Natarajan are both functions of Reynolds number in the combustion regime, and velocity has dropped to zero according to Sirignano's relaxation expression. When droplet velocity was forced to follow that of the spray, the predicted evaporated fractions rose to over 98% at TDC and 100% before 10° aTDC. The Ranz correlation was chosen for default use because of its satisfactory performance, and all other comparisons illustrated are made on this basis.

The overall rate predicted is very high with most of the small droplets evaporating almost instantly. Virtually all of the fuel (98%) has evaporated by the start of combustion (8° bTDC). Using a comprehensive multidimensional model, Kuo[196] obtained a value of 70 - 95% vaporization by ignition with an SMD of only 5 μm, so the current result seems rather high.

The magnitude of the Ranz-based convection factor was found to be typically about 10 though rising as high as 18 in certain cases. Thus it has a marked effect on the evaporation rate, and it is important to use the correct velocity input to the Reynolds number of the convection correlation. Sirignano's relaxation-time expression has been implemented to allow for slowing of droplets by drag. The effect of this assumption is illustrated in Fig. 4.12, by comparison with rates calculated with the droplet relative velocity set to zero and to the speed of the spray. Since evaporation is very rapid in the case shown, the effect of allowing relaxation is very small as velocities have not fallen much below that of the spray. Under different operating conditions, the effect might be much more noticeable.

There are some other variable parameters in the evaporation model. Rather than approximating the value of the integral term in equ. 4.32 using equ. 4.35, it has been evaluated numerically. The thickness of the thermal boundary layer is estimated according to the expression of Hiroyasu (equ. 4.60), and the ratio of flame-front radius to droplet radius is taken as 10, following Gokalp[92]. It was shown that virtually identical evaporation rates are obtained if a constant radius factor (bulk condition over droplet radius) of 1.1 or 1.3 was assumed for the non-combusting case, and if the flame radius was determined according to equ. 4.45. Thus, selection of these parameters is not critical. It was also demonstrated that the

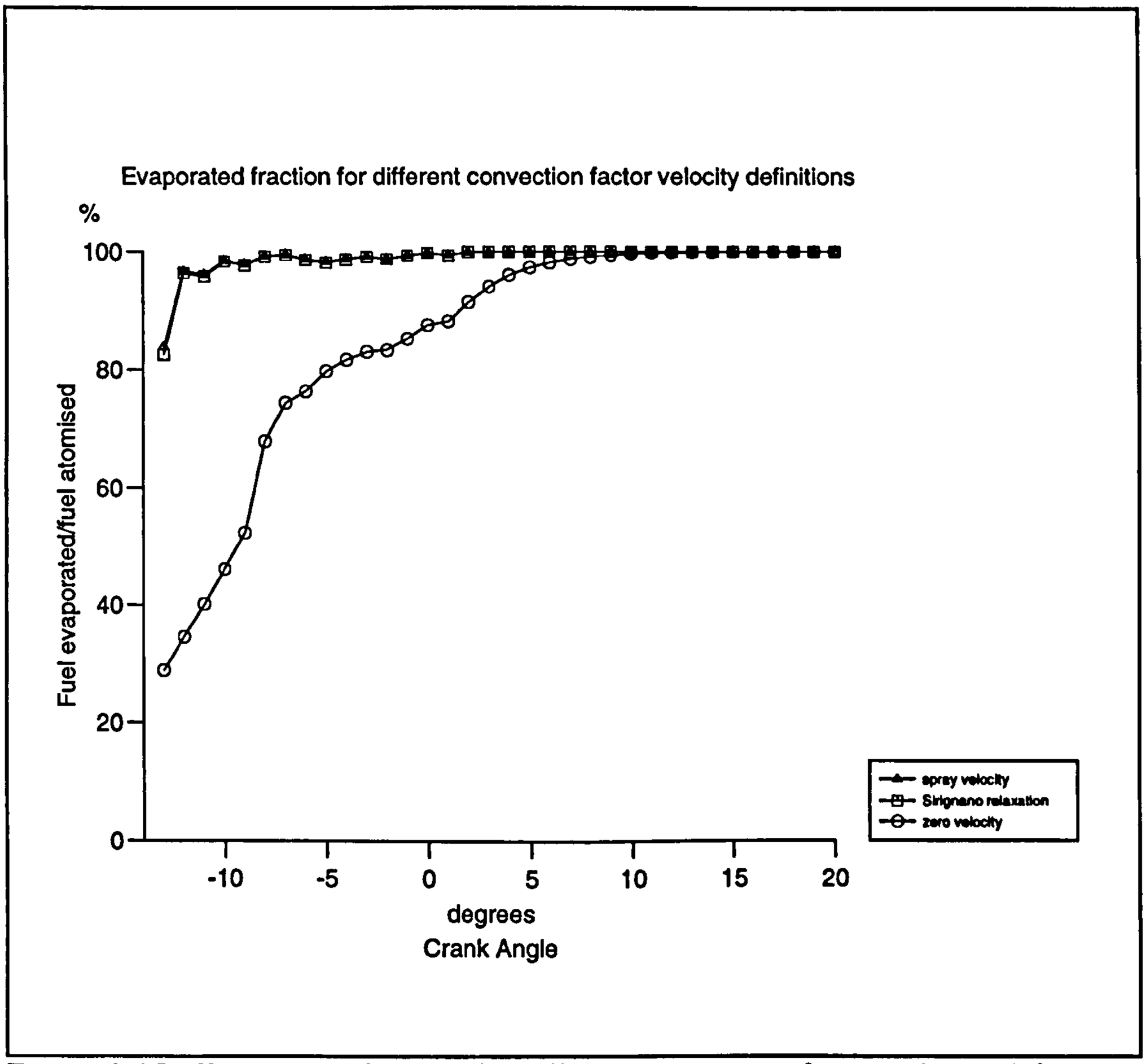

Figure 4.12 - Evaporated fraction for different convection factor velocity definitions

result did not vary significantly with number of integration steps used. Overall values of the integral term of equ. 4.32 were found to be 1.5 - 1.7 times the value of the simplified term of equ. 4.35 justifying use of the numerical method.

Finally, the composition of the atmosphere surrounding the combusting droplet has been shown to have a negligible effect on the evaporation rate. Thus, estimation of chemical composition in the droplet surroundings is not important.

The values of the evaporation and burning constants for 25 μm diameter droplets are tabulated in Table 4.5. Borman's value was measured under conditions typical of those in a diesel[317], whilst the Godsave[91] value was obtained at one atmosphere, and in the absence of convection. The latter is in good agreement with the typical

value of 10^{-6} given by both Kanury[162] and Williams[369]. All values are of the same order of magnitude, but the lack of standard conditions does not allow any further conclusions to be drawn.

Source	Evaporation constant	Burning constant
Borman[31]	$> 0.6 \times 10^{-6}$	-
Godsave[91]	-	0.8×10^{-6}
Simulation	2.6×10^{-6}	3.3×10^{-6}

Table 4.5 - Experimental and calculated evaporation and burning constants

4.2.4.3 Conclusion

An evaporation model has been implemented and validated. The most important influences on the calculated rate of evaporation are the initial droplet size and convection effects. A choice of five expressions has been provided for the former and three for the latter. Hiroyasu's SMD correlation was selected, because it was determined by the most comprehensive experimental analysis and lies within the range of the other values. Use of the Ranz correlation for convection is important if droplet relative velocities are allowed to drop to zero, since with the other expressions the predicted rate drops to zero. Overall, the calculated rates of evaporation seem rather high compared with other computational values[196], but the evaporation and burning constants are of the right order of magnitude.

4.3 TURBULENCE MODEL

4.3.1 Turbulence modelling

4.3.1.1 Introduction

The turbulence field in the diesel combustion chamber has a major impact on combustion rates and will also directly affect sooting processes. In internal combustion engines, the description of the turbulent properties of the fluid has been achieved almost exclusively by use of the k-ε model due to Launder and Spalding[116]. Here, the parameters k and ε are the turbulent kinetic energy and the rate of dissipation of this energy respectively. The definition of the turbulence properties and measurement techniques have been comprehensively reviewed by Tabaczynski[338] and Heywood[116], and the relevant details are summarised below. This section focuses mainly on methods used for estimation of the turbulence properties in phenomenological-type engine models.

The turbulent velocity is the small fluctuation around the mean, and is generally defined by its rms value, the turbulence intensity, u'. Estimation of this value in engines is complicated by the variation of mean velocities. This leads to use of ensemble-averaging techniques, where the turbulent intensity is defined as the average fluctuation from a mean summed over many cycles. Since this includes cycle-by-cycle fluctuation in the mean velocity, it may be up to double the individual turbulence intensity[116].

Having obtained an estimate of the turbulence intensity, it is possible to define the turbulent kinetic energy per unit mass, k, as

$$k = \frac{3u'^2}{2} \tag{4.67}$$

Isotropic turbulence is assumed, and this has been shown to be a good approximation at the end of the compression stroke, the cycle position of most interest[116,212]. The turbulent intensity is taken as applying to the largest scale of the turbulence structure. A simple equilibrium consideration allows definition of the macroscale of turbulence, l_I, in terms of k, ε and a universal constant C_D[182]:

$$l_l = \frac{C_D k^{\frac{3}{2}}}{\varepsilon} \tag{4.68}$$

l_l is usually known as the integral lengthscale, and is the average maximum distance separating points whose velocities can be correlated. Equ. 4.68 is the key relationship of the k-ε model. Estimation of the integral lengthscale together with either k or ε allows determination of the other desired property. Methods of determining these properties are reviewed below.

4.3.1.2 Estimation of turbulence parameters

Multidimensional models generally follow k and ε values according to transport equations, though ε may be simply determined from the above integral lengthscale equation (equ. 4.68). The source terms representing production, dissipation and diffusion are usually expressed in terms of velocity and pressure gradients[116]. This technique has also been adapted for use in phenomenological models by Mansouri[228] and Kono[184].

A simple alternative is to correlate k or ε directly in terms of the properties of the flow. **Nishida**[262] relates the turbulent kinetic energy to the mean flow velocities. Within the spray boundary, the velocity fluctuation of the turbulence is assumed to be 30% of the local penetrating velocity of the spray, whilst outside it is taken as 11% of the mean velocity of the swirling gas. Thus:

$$\begin{aligned} k &= \frac{3}{2} u'^2 \\ &= \frac{3}{2} 0.3^2 u_{spray}^2, \ \frac{3}{2} 0.11^2 u_a^2 \\ &= 0.135 u_{spray}^2, \ 0.018 u_a^2 \end{aligned} \tag{4.69}$$

Murakami[244] derives an empirical equation for the decay of turbulent intensity in the compression process. Defining a parameter, G_{ed}:

$$G_{ed} = \frac{D\bar{\varepsilon}^{\frac{1}{4}}}{\nu^{\frac{3}{4}}} \tag{4.70}$$

this is then correlated to Reynolds number, giving:

$$G_{ed} = 1.459 R_e^{0.578} \tag{4.71}$$

Therefore:

$$\varepsilon = \frac{4.531\, V_\theta^{2.312}\, \nu^{0.688}}{D^{1.73}} \tag{4.72}$$

Following Corrsin[48] and Broadkey[35], **Dent**[55] expresses the turbulent energy dissipation ε by a power input term multiplied by a factor representing the fraction of input energy appearing as turbulence. Thus:

$$\varepsilon_q = C\left(\frac{N}{\theta_{lp}}\right)\left(\frac{Q}{n d_o^2}\right)^2 \tag{4.73}$$

This expression applies for operation under quiescent conditions. In the high-swirl chamber, an additional term is used to account for the effect of swirl on the turbulent mixing rate[57]:

$$\varepsilon_s = \left(\frac{\omega^3 d^2}{32}\right) \tag{4.74}$$

The rates are assumed to act in parallel[198] so that:

$$\varepsilon = \frac{\varepsilon_q \varepsilon_s}{\varepsilon_q + \varepsilon_s} \tag{4.75}$$

In a slightly different approach, **Mehta**[105,237] relates the turbulent eddy dissipation rate to the kinetic energy change in the system:

$$\varepsilon = \eta_t \dot{K} \tag{4.76}$$

The constant of proportionality represents the efficiency of the conversion of kinetic energy to turbulence energy. According to Corrsin[48] it has a value of 0.2. However, Mehta equates the rate of the change of kinetic energy to that resulting from energy change due to air motion, viscous dissipation, fuel injection and heat release[105]. The latter in particular makes no physical sense, since energy liberated in combustion is not converted entirely to kinetic energy. It would seem that some modification is necessary if this model is to be successfully implemented.

Given a value of k or ε, the other parameter may be determined from equ. 4.68 provided C_D and l_I are known. C_D is an empirical constant and most authors have used the best fit value of 0.09 obtained by Rodi and Spalding in 1970[296]. In fact, equ. 4.68 has been fairly loosely used with a variety of lengthscale definitions and C_D values. Those used for the diesel are shown in the summary Table 4.6:

Researchers	Value of C_D (equ. 4.68)	l_I expression
Nishida[262]	0.09	$0.07D$, $0.05B$
Ikegami[144]	0.54	$(\rho_f/\rho_a)^{1/2} d_o$
Kyriakides[198]	1	$(\rho_f/\rho_a)^{1/2} d_o$
Mansouri[227]	0.54	h
Morel[240]	0.09	$0.1h$

Table 4.6 - Turbulence model parameter definitions
(D - bore, B - jet width, d_o - nozzle diameter, h - instantaneous clearance height)

Part of this variation in C_D value will be due to the use of different integral lengthscales. As mentioned above, the integral lengthscale can be seen as the size of the largest eddies in the flow. It will vary according to engine operating conditions and position in the cycle. Heywood states that it is of the order of the intake-jet diameter during the intake stroke, and this in turn is of the order of the valve lift (≈ 10 mm). However, Tabaczynski[338] points out that the correspondence with valve lift is a function of measurement location since the intake jet expands as air is entrained. Thus, use of estimated jet width is recommended.

Tabaczynski[338] further states that the integral lengthscale varies little throughout the intake and compression strokes. Heywood[116], though, considers it to be proportional to the clearance height at the end of compression, reaching a value of about $0.2h$ at TDC ($\approx$ 2 mm). The values used in various phenomenological models are given below and summarised above in Table 4.6.

Nishida[262] relates l_I to the piston diameter in regions outside the spray:

$$l_I = 0.07D \tag{4.77}$$

and to the spray width within the spray:

$$l_I = 0.05B \tag{4.78}$$

Kyriakides[198] equates l_I to the nozzle equivalent diameter d'_o, which is typically much smaller than the clearance height. Ikegami uses the same relationship. Mansouri uses the instantaneous clearance height while Morel[240] uses 10% of this value.

In view of the variety of approaches to turbulence modelling, each of the models described above has been implemented in the simulation program, with the exception of the Mehta model[105,237] which was deemed physically unrealistic.

4.3.2 Evaluation

There are many sets of engine measurement data which can be used to assist in evaluation of model performance. A selection of experimental results are given in Table 4.7. All the values relate to conditions at the end of the compression stroke.

Researcher	u' (ms^{-1})	u'/u_{mean} (-)	l_I (mm)	τ_I (ms)	u'/S_p (-)	Speed (rpm)
Tindal[350]	1-2	10-20%	-	-	0.3-0.6	1000
Murakami[244]	1	-	-	-	0.96-0.24	250-1000
Brandtl[34,35]	4-12	-	0.8-1.3	0.1-0.3	-	1100-2400
Dent[53]	0.05-2	10-20%	0.2-3.5	-	0.02-0.17	900-3500
Semenov[307,338]	0.3	20%	2	-	-	600-1200
Windsor[373,53]	-	-	1.2-2.5	-	-	-
Rask[288]	1	20%	-	-	1.3	300
Hamamoto[107]	0.5-2.2	7-11%	10-7	1.3-6	0.23-0.31	750-2500
Karimi[163]	3	20%	-	-	0.71	1000
Catania[39]	2-4	-	-	0.4-0.7	0.3	1600-3000
Arcoumanis[14]	1.6	-	-	-	0.5	1000
Ikegami[146]	2	-	2-3	-	0.4	400-1200
Amato[8]	0.8-2	-	1-4	-	-	-
Lancaster[201,338]	1-2.5	-	4	1.2-0.6	-	1000-2000
Liou[212]	0.5-7	-	-	-	0.25-1.25	-

Table 4.7 - Experimental values of turbulence parameters

The overview indicates that typical turbulence intensities are between 1 and 10 ms^{-1}, integral lengthscales are between 1 and 10 mm, and integral timescales are about 1 ms. Turbulence intensities are approximately 10 to 50 % of mean flow velocities, excluding the values for very low running speeds.

The values given for integral timescale are in agreement with the typical value given

by Heywood of 1 ms at 1000 rpm. Tabaczynski[338] and Hamamoto[107] have shown a reduction at higher engine speeds. Tabaczynski states that turbulence intensity scales with mean flow velocities when the latter are significant, again in accordance with the above data. Also, the results of Liou[212] show a linear correlation between turbulent intensity and mean piston speed. Heywood reports a consensus that in the absence of swirl, turbulence intensity has a maximum value of about half the mean piston speed[116]. Slightly higher values apply in swirling flows. Finally, though it cannot be measured directly, Tabaczynski gives a typical value for ε of 2000 m^2s^{-3}.

There are other turbulence scales, and the Kolmogorov scale should be mentioned as it is an important input to the Magnussen eddy-dissipation model used in the combustion rate and soot-oxidation calculations. At the smallest level of the turbulence structure, molecular viscosity acts to dissipate small-scale kinetic energy into heat. It is related to the kinematic viscosity, υ, and the energy-dissipation rate by:

$$l_K = \left(\frac{\nu^3}{\varepsilon}\right)^{\frac{1}{4}} \tag{4.79}$$

The Kolmogorov timescale is similarly defined as:

$$\tau_K = \left(\frac{\nu}{\varepsilon}\right)^{\frac{1}{2}} \tag{4.80}$$

A typical value of this lengthscale at TDC is 0.01 mm[116].

4.3.3 Results

The simulation program was run for the current case of a 2-litre 4-cylinder direct-injection diesel with zero swirl at 1250 rpm[11]. Since the Murakami model is invalid in the absence of swirl, in this case alone the swirl ratio was set to 2 to allow a comparison. Computed average values at TDC are given in Table 4.8 below. The value of the constant C_D was taken as 0.09 in all cases, since this was found to give the most satisfactory results.

Author (equ.)	l_I (mm)	ε (m^2s^{-3})	k (m^2s^{-2})	τ_I (ms)
Nishida[262], (4.69)	1.0	30110	61	2.0
Murakami[244], (4.70)	1.0	32	0.59	18.4
Dent[55,57], (4.73)	1.6	112	1.68	14.4

Table 4.8 - Calculated turbulence parameters

Conclusions

The model of Nishida[262] gives rather large values of turbulence intensity. This is because the magnitude is set to 30% of the spray velocity, which in this case is initially 78 ms^{-1}. A reasonable upper limit would be the mean piston speed[116] of 4.85 ms^{-1}. On the other hand the Murakami model[244] seems to underestimate the dissipation rate leading to a low turbulence intensity value and an integral timescale which is rather high. The Dent model[55,57] performs much more satisfactorily, and each of the calculated values is well in line with expectations. This model was therefore chosen for use in the simulation program.

4.4 COMBUSTION AND THERMODYNAMICS

4.4.1 Introduction

This section covers a number of model components related to the determination of the combustion rate and thermodynamic state. These issues are key to the determination of the heat-release rate which is the critical element of any engine simulation. The preceding three sections have outlined the model representation of macroscopic fuel-air mixing (spray model), microscopic mixing (turbulence model) and evaporation. These are the 'physical' processes which set bounds on the heat-release rate and together with knowledge of combustion chemistry allow determination of combustion rates. Heat release is in turn the dominant process affecting evolution of the thermodynamic state. The thermodynamic properties of the mixture feed back into the mixture preparation and combustion processes. Thus, the thermodynamic model underpins and ties together the other model components. The accurate description of the thermodynamic state is also essential for emission prediction and this is the overall aim of the combustion model.

Combustion cannot begin until an ignition delay period has been completed. Though this is known to depend on both physical and chemical processes, it is generally determined in engine simulations by use of a single simple correlation. The combustion process itself is influenced by the rates of chemical reaction and the physical mixing rates and evaporation mentioned above. The thermodynamic model is centred around determination of the temperature of the mixture in the spray zones and subzones. This is achieved by estimating the temperature change during each time-step according to the calculated values of chemical energy release, heat transfer, compressive work and mixing-process energy transfers occurring in each zone or subzone. Essential inputs are the internal energy and specific heat capacity of the mixture. Since these are themselves affected by temperature, some degree of iteration is necessary.

Details of the thermodynamic state estimation are given in the author's MSc thesis[366] so are covered only briefly here. More attention is given to the estimation of combustion rates, the new thermodynamic structure of the zones and the calculation of heat-transfer rate.

4.4.2 Ignition delay

Hiroyasu[128] sets out ten ignition delay correlations which have been proposed for diesel-engine use. Heywood[116] examines use of three of these and others. Many of these correlations have the general form:

$$\tau_{id} = A\, p^{-n}\, e^{\frac{E_a}{RT}} \tag{4.81}$$

Hardenberg proposed a more detailed expression[108]:

$$\tau_{id} = (0.36 + 0.22\bar{S}_p)\, e^{\left[\left(\frac{618840}{CN+25}\right)\left(\frac{1}{RT} - \frac{1}{17190}\right)\left(\frac{21.2\times10^5}{p - 12.4\times10^5}\right)^{0.63}\right]} \tag{4.82}$$

The three expressions in common between Hiroyasu and Heywood were implemented in the simulation program together with Hardenberg's correlation. Results for the 'standard' case of the experimental dataset chosen for model validation are summarised in Table 4.9.

Source	End of ignition-delay timing (°CA bTDC)	Ignition delay (ms)
Stringer correlation	6.17	1.04
Wolfer correlation	5.55	1.13
Hiroyasu correlation	6.25	1.03
Hardenberg correlation	11.8	0.29
Kamimoto experimental value	c. 9.9	c. 0.72

Table 4.9 - Ignition delay correlations

Injection begins at c. 15.3° bTDC and if it is assumed that evaporation starts simultaneously, the experimental delay period is about 0.72 ms. In practice, there may be a short delay before evaporation begins, but lack of knowledge concerning the initial jet behaviour makes it difficult to determine this.

In the simulation, fuel becomes available at 14° bTDC, though evaporated fuel does not appear until the following crank angle. For the three simple expressions, calculated delays all exceed 1 ms, whilst the Hardenberg value is less than a third as long at 0.31 ms. Thus, none gives a good match to the experimental value. This is probably due to the uncertainties in defining the start of the delay period in the simulation and the error in estimating the experimental delay.

Heywood cautions against use of correlations for conditions outside the range for which they were derived[116]. The Stringer correlation was derived for pressures above 30 atmospheres, the experimental temperature range for the Wolfer correlation extended only to 782 K and the Hiroyasu correlation was obtained using kerosine. In the simulated case, pre-ignition pressures never exceed 30 atm and the temperature has reached c. 990 K by ignition. Thus, none of the simple expressions seems to be well-suited to use in this environment. The Hardenberg correlation alone was derived from diesel engine measurements and it was selected as the best available by Dent[56].

In view of the high sensitivity of the heat-release rate and temperatures to the ignition timing, all model output illustrated in this thesis was obtained with the ignition delay set to the experimental value. This is to provide an ideal basis for comparison the other model predictions.

4.4.3 Combustion rate

4.4.3.1 Introduction

Analysis of combustion in diesel engines is traditionally divided into two main phases: the initial rapid 'premixed' burning and later 'diffusion' burning. However, when consideration is given to modelling these processes, the need for a more fundamental description of the burning mechanism becomes apparent. Most mixture consumed during the premixed phase has attained a fairly uniform composition during mixing in the ignition-delay period. Burning of the first fraction of the charge is controlled by an autoignition process, according to chemical reaction rates. Still within the premixed combustion period, the flame propagation process begins to make a contribution. Finally during the diffusion-burning phase, physical mixing of the reactants is the dominant combustion process. Thus, the combustion regimes may be more usefully classified as homogeneous premixed, homogeneous diffusion and heterogeneous[165].

Modelling techniques have been developed to describe each of these processes. For instance, the standard CFD representation of diesel combustion uses a rate-limit expression which selects between chemical and mixing rates. This technique has also been employed in a phenomenological model[262], while others employ flame-propagation rates, several use only chemical rates and the remainder assume infinite rates of combustion (Table 4.10).

Rate expression	Researcher
Chemical-mixing limit	Nishida[262]
Chemical	Hodgetts[132], Meguerdichian[234], Watson[365], Lipkea[213], Bazari[19]
Infinite	Kau[164], Shahed[309], Hiroyasu[126], Dent[56], Payri[271]
Flame propagation	Kono[184], Hiraki (stratified charge)[118]

Table 4.10 - Reaction-rate definitions

In most cases reasonable predictions of the combustion rate have apparently been

achieved. Despite this success, there are certain difficulties in using such techniques in zonal models. For instance, it may be necessary to integrate the rate expression over a calculation timestep. A method for doing this is described in section 4.4.3.5 below. Other problems are identified in the discussion (section 4.4.3.6). First, the expressions proposed for reaction rate are briefly reviewed.

4.4.3.2 Chemical rate

In virtually all diesel CFD models, chemistry is described by a greatly simplified reaction scheme with a single rate equation. The only exceptions are chemical models of several steps which have been used for the autoignition process[386,274,347,384,385] and these are not appropriate for use at higher temperatures. It is possible to incorporate fairly detailed chemistry into phenomenological-type models but it is usually deemed unnecessary. The chemical rate is usually expressed in the following form[116,262]:

$$\left(\frac{dm_f}{dt}\right)_{chem} = A\rho^2 X_f^m X_{ox}^n e^{-\frac{E_A}{RT}} \qquad (4.83)$$

The constants A, m, n and E_A are calibrated by experimental data to give acceptable results over a limited range of engine operating conditions[116]. Typically, *m* and *n* are taken to lie between 0.25 and unity[116,112,94,337]. In two cases, the values of all constants were specified; these are shown in Table 4.11:

Author	m	n	A ($m^3kg^{-1}s^{-1}$)	E_A ($Jmol^{-1}$)
Nishida[262]	1	5	$5x10^{10}$	$1.0x10^5$
Meguerdichian[234]	1	1	$5x10^7$	$1.25x10^8$

Table 4.11 - Chemical reaction rate parameters

A further difference is that Meguerdichian's rate is proportional to density rather than the square of the density. Also, the activation energy given by Meguerdichian is such that the exponential term vanishes for all realistic temperatures, and it is assumed to be a misprint for $1.25x10^5$.

The expression used in the original version of the simulation program[185] was taken from Benson[22]:

$$\frac{dm_f}{dt}_{chem} = \frac{10^{11} p_{O_2} e^{-\frac{1.5x10^4}{T}}}{NT^{\frac{1}{2}}} \min\left(m_{fuel}, \frac{m_{air}}{AFR_{stoich}}\right) \qquad (4.84)$$

4.4.3.3 Flame propagation

The models used by Kono[184] to describe both premixed and diffusion burning are expressed in terms of flame speeds. For the premixed burn phase, an expression originally developed for the spark ignition engine[339] is used:

$$\frac{dm_f}{dt}_{flame,pm} = \frac{C_{pre}\, m_{stoich}}{\tau_{chem}} \qquad (4.85)$$

where m_{stoich} is the mass of stoichiometric mixture

τ_{chem} is the chemical timescale, given by:

$$\tau_{chem} = \frac{\lambda}{S_{lam}} \qquad (4.86)$$

where S_{lam} is the laminar flame speed and λ the Taylor microscale[339]

The rate of diffusion burning is also related to the laminar flame speed, using an entrainment equation due to Dent, 1981[56]:

$$\frac{dm_a}{dt}_{ent} = C\left(\frac{m_{ent}}{\tau_{mix}}\right) \qquad (4.87)$$

where:

$$\tau_{mix} = \left(\frac{l_I^2}{\varepsilon}\right)^{\frac{1}{3}} \qquad (4.88)$$

The burning rate is given by:

$$\left(\frac{dm_f}{dt}\right)_{flame,diff} = \frac{\frac{dm_a}{dt}_{ent}}{\tau_{chem}} \tag{4.89}$$

where τ_{chem} is the chemical timescale, defined as above

4.4.3.4 Mixing rate

Most diesel CFD models have employed Magnussen's eddy-dissipation model to describe mixing-controlled combustion[94,96,274,299,316,364,387]. This model is based on a theoretical representation of the transfer of mixture through the levels of turbulence structure existing in the fluid, known as the eddy-dissipation concept[226]. The theoretical analysis leads to the following equation:

$$\left(\frac{dm_f}{dt}\right)_{diff} = \dot{m}\,\frac{\chi}{1-\gamma\chi}\,m_{min} \tag{4.90}$$

where χ is the mass fraction burnt

γ is the mass fraction of mixture in the fine structure regions

m_{min} is the smaller of the fuel mass and the air mass divided by the stoichiometric air-fuel ratio

$\dot{m}$ is the non-dimensionalised exchange rate of mass with fine structures

Also, the fine structure mass fraction and the mass-transfer rate may be expressed in terms of turbulence parameters as follows:

$$\gamma = 9.7\left(\frac{\nu\varepsilon}{k^2}\right)^{\frac{3}{4}} \tag{4.91}$$

$$\dot{m} = 23.6\left(\frac{\nu\varepsilon}{k^2}\right)^{\frac{1}{4}}\frac{\varepsilon}{k} \tag{4.92}$$

This model has been developed and re-expressed in a variety of forms. Drawing distinctions between different combustion regimes, Magnussen[223] obtained the following expression which has been adopted by most subsequent authors[94,96,274,299,316,364,387]:

$$\frac{dm_f}{dt}_{diff} = A \min\left(\bar{m}_f, \frac{\bar{m}_{O_2}}{AFR_{sto}}, \frac{B\bar{m}_{pro}}{1+AFR_{sto}}\right)\frac{1}{\tau_{mix}} \qquad (4.93)$$

where the turbulent mixing scale, τ_{mix}, is:

$$\tau_{mix} = \frac{k}{\varepsilon} \qquad (4.94)$$

Magnussen[223] states that the equation is assumed to be generally applicable to diffusion and premixed flames. In an extension of the original expression (equ. 4.90), Grimsmo[102] provides a complex expression for χ which is redefined as the 'reaction progress factor'.

Different values have been employed for the constants A and B in the above equations. Magnussen obtained good results with A=4 and B=0.5 in the case of the atmospheric diffusion flame[223]. Gosman[94] had to change these to A=20 and B=2.5 to give plausible predictions of the heat-release rate in an axisymmetric direct-injection diesel engine. Pinchon[274] found that A=16 and B=2 gave a good match with experimental data for a prechamber diesel, though A=20 and B=2.5 gave very similar trends. Equ. 4.93 has also been used in the multizone model of Nishida[262], though the combustion-product term is omitted. In this case, the value of A is set to 1.

4.4.3.5 Integration over calculation timestep

In all cases the reaction rates are related to the concentration of unburnt fuel. Thus, when reaction rates are high, a simple model may predict elimination of the fuel in a calculation timestep. This is unphysical, since the reaction rate drops as the concentration falls, and zero fuel concentration should be approached asymptotically. In order to solve this problem Watson[365] used a first-order relaxation equation which was first proposed by Blizard[24] for SI engine use:

$$\tau \frac{dm_f}{dt} + m_{pro} = m_{f,tot} \qquad (4.95)$$

The relaxation parameter, τ, can be related to chemical and mixing processes and Watson used a simple chemical reaction expression. Zeleznik derived a generalisation of the Blizard model allowing use of time-dependent relaxation parameters[383]. This expression was implemented in the current work in conjunction with a simple numerical integration technique.

4.4.3.6 Discussion

Interest in rate of combustion has been greatest for CFD-type models, as is apparent from the above review. Typically, the limiting rate is selected between chemical and eddy break-up mixing. In considering whether such a procedure is appropriate for use in zonal models some general difficulties become apparent.

Description of 'premixed' combustion presents a unique problem, since determination of the dominant mechanism of combustion is not straightforward. The first element of fuel is consumed in the autoignition process, in which the rate limit is purely chemical. Subsequent burning will tend to be by the flame-propagation process, which is more appropriately described by a mixing rate or flame speed. Empirically, it is hard to distinguish between these phenomena and no quantitative information is available relating to the process.

It may appear that the rate-selection procedure used in CFD models will supply a theoretical solution to this problem by providing a break-down of the process.

However, this is not the case because microscopic mixing has already taken place during the ignition-delay period. It is therefore inappropriate to use the mixing-rate expression described above to determine the limiting mechanism during this phase of combustion. This difficulty was identified by Shirakawa[316], who proposed to solve the problem by modifying the rate-selection criteria. Chemical rates are used only when the chemical timescale is greater than 10^4 - 10^5 times the mixing timescale. This markedly reduces the proportion of chemically-limited burning. Saad[299] has adopted an alternative strategy, in which the procedure of selecting limiting rates is confined to those mixture elements where the temperature exceeds 1500 K. At lower temperatures chemical rates are assumed.

Considering now phenomenological models, most do not draw any distinction between the chemical and mixing controlled parts of the combustion process. However, Li[215] has proposed that all fuel evaporated prior to ignition should be allowed to burn infinitely fast, while subsequent combustion is controlled by a chemical rate. This is contrary to the empirical observation that most of the fuel injected before ignition burns in the diffusion mode[277] since only 10-35% is mixed to within the flammability limits[196]. Kono[184] has separated the 'premixed' and diffusion-flame processes by using the rate of the former during the first 0.5 ms of the combustion period, following experimental findings. If chemical rates are to be used, it may be possible to implement the modifications proposed by Shirakawa or Saad. However, this is complicated by the fact that the criteria for rate change-over are rapidly exceeded, so that an iteration procedure is required. Simply allowing all mixture prepared to burn at chemical rates during the first calculation timestep may lead to serious over-estimation of the quantity burnt.

Another possibility would be to allow only a certain fraction of prepared mixture to burn during the first calculation timestep. Ideally the parameter used should be linked to the ignition delay time and turbulent mixing parameters. This approach was adopted in the current work, but for simplicity a constant value of the 'premixed burn factor' was assumed. The value was selected to give a good match to the experimental heat-release rates (see section 5.1).

4.4.3.7 Results

Chemical rates were calculated using the constant values proposed by Nishida[262] and Meguerdichian[234]. The original form of Magnussen's eddy-dissipation combustion model was used to determine mixing rates[223]. Typical values for premixed burning and the diffusion phase are shown in Table 4.12. Note that in order to determine a value for the Magnussen mixing-rate during premixed phase, an initial value of 0.1 was set for the fraction of fuel burnt.

Author, rate	Premixed phase rate ($kgm^{-3}s^{-1}$)
Nishida[262], chemical	$2.2x10^6$
Meguerdichian[234], chemical	27.8
Magnussen[223], mixing	$11.4x10^3$

Table 4.12 - Calculated reaction rates

Nishida[262] plotted reaction rate against fuel mass fraction for low-temperature premixed burning. The peak value obtained is $2x10^7$ kg m^{-3} s^{-1} confirming the above result. Meguerdichian's values are much lower and provide a finite rate for the premixed phase.

If Nishida's values are assumed to be accurate, chemical rates reach very high levels once the temperature has begun to rise. Thus, the rate of burning is only really chemically-limited during the precursive auto-ignition reactions, and this phase of combustion is at least partly included within the ignition delay period. However, since the rate is so high, the combustion rate is in practice rapidly limited by lack of fuel. In this work, the small fuel concentration remaining is obtained by numerical integration, as described in section 4.4.3.5. Subsequent combustion is limited by mixing rates and Magnussen's eddy dissipation combustion model was used to describe this phase.

4.4.3.8 Chemistry

Most previous phenomenological models have used a simple one-step description of the combustion chemistry, though some of the more recent models have included up to 12 species[19,193,262,389]. In this work, a single-step chemical description is used in the interests of simplicity.

4.4.3.9 Conclusions

A variety of approaches have been used for the prediction of combustion rates in diesel combustion models. The expressions used can be classified according to the predominant controlling rate: chemical, flame propagation and mixing. However, empirical data on the importance of each mechanism are lacking. In practice, chemical rates rise very rapidly so that they are never limiting. A much more important issue is the quantity of mixture allowed to burn in premixed mode. Several crude methods have been proposed to define the transition to diffusion burning. In the current work a constant 'premixed burn factor' is used, the value of which is determined by fitting to experimental data. Magnussen's eddy dissipation concept has been successfully applied to the determination of the rate of diffusion burning. The original form of this model (equ. 4.90) was used in this work.

4.4.4 Thermodynamic state

This section gives details of model elements that contribute to determination of the thermodynamic state. The thermodynamic structure and method of temperature estimation are described.

4.4.4.1 Thermodynamic structure

The model described thus far consists of a set of zones containing fuel and air which represent different regions of the diesel spray. Methods of following the evolution of the average zonal composition, in terms of liquid fuel, vapour and air have been described. Following ignition, hot products of combustion are formed and these will tend not to be uniformly distributed initially but rather confined to separate regions of the mixture. The fluid can be visualised as consisting of eddies of fairly uniform composition which are steadily breaking down and mixing. It has long been appreciated that a better description of the thermodynamic state may be obtained by recognising this subdivision, and describing 'reactant' and 'product' regions independently. A number of simple 'two-zone' thermodynamic models have been developed, which have even been used for emissions work[151,245,356,359], and some multizone phenomenological models have also incorporated some representation of the two regions[193,271]. Such a structure falls far short of modelling the full range of states existing in the mixture, but it does represent a major advance on the use of zonal averages, and has therefore been implemented in the current work.

The cost of partitioning the model zones is the introduction of great complexity into the determination of composition and thermodynamic state, due to the transfers between subzones. Several processes are modelled which affect the composition at a zonal level: air entrainment, evaporation, combustion and soot formation and oxidation. The effects of some or all of these must be accounted for in each subzone independently. Moreover, though the combustion-products region may be taken simply as the fraction of mixture which has burnt stoichiometrically, a more realistic estimate is obtained by calculating a rate of transfer through a burning region. Thus, excess air or fuel will be found in the products region when the zone is globally rich or lean.

The process of determining the component of unburnt air in each subzone provides

a good example of the complexity. Physically, most entrainment will be to the reactants region, but at the same time air from this region is being consumed in combustion and sooting processes, and in lean zones, some may be passing into the products region unburnt. The scale of the consumption processes depends in turn on the evaporation which is also occurring in parallel. Some of the methods used to describe these interrelated processes are outlined briefly below.

The basic rate of combustion was given by equ. 4.90 for diffusion-phase burning. This may be re-expressed as:

$$\left(\frac{dm_f}{dt}\right)_{diff} = R_{xfer}\, m_{min} \qquad (4.96)$$

where m_{min} is the smaller of the fuel mass and the air mass divided by the stoichiometric air-fuel ratio

R_{xfer}, the rate of transfer through heated fine structure, is:

$$R_{xfer} = \dot{m}\,\frac{\chi}{1-\gamma\chi} \qquad (4.97)$$

where χ is the mass fraction of mixture burnt

γ is the mass fraction of mixture in the fine structure regions

This rate cannot be applied directly to determination of the amount of mixture which burns, because the reactant concentration is changing according to the evaporation, air entrainment, sooting and combustion processes mentioned above. For example, considering only the latter, the rate may be sufficiently high that all fuel would be consumed according to the average rate multiplied by the calculation timestep. In fact, as fuel is consumed, the rate would drop to zero. Thus, some sort of numerical integration is necessary in order to follow the species concentrations. One limit on the average burn rate can be approximated as follows.

Consider a mass of reactant subzone mixture, m^-, to which is entrained a mass of air given by $(dm_a/dt)_{ent}\ \delta t$, and which loses a mass $(dm_f/dt)_{soot}\ \delta t\ (1+AFR_{sto})$ in oxidation of soot during a small time interval δt; at the end of the timestep Δt, mass m^+ of mixture remains (Fig. 4.13).

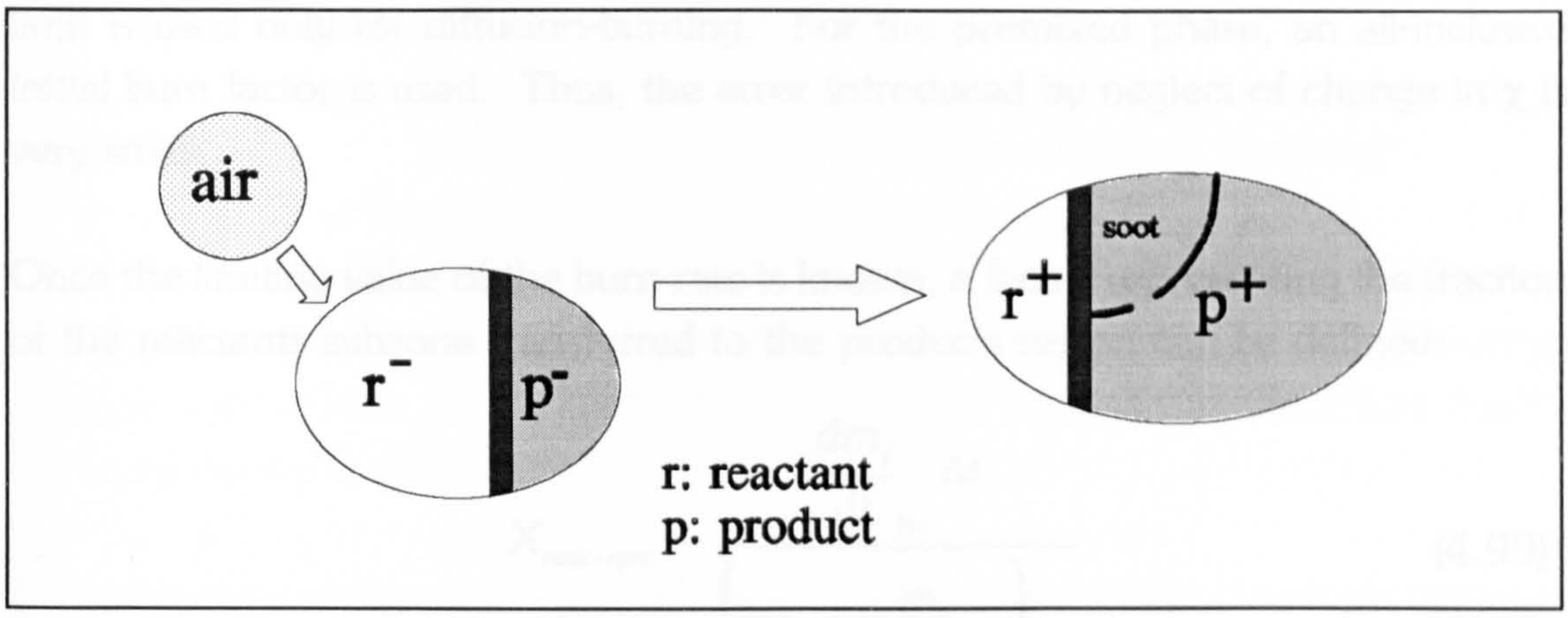

Figure 4.13 - Change in subzone composition during a timestep

By balancing the mass consumed in burning during the timestep with the change in mass of the reactants subzone, a limit on the average rate of consumption of fuel can be set:

$$\frac{dm_f}{dt}_{\lim} \delta t\,(1+AFR_{sto}) \;<\; -\left[m^{+}_{reac} - \left(m^{-}_{reac} + \frac{dm_a}{dt}_{ent}\delta t - \frac{dm_f}{dt}_{soot}\delta t\,(1+AFR_{sto})\right)\right]$$

$$\Rightarrow \frac{dm_f}{dt}_{\lim} < \frac{-\sum\left(\dfrac{\dfrac{dm_a}{dt}_{ent}}{(1+AFR_{sto})} - \dfrac{dm_f}{dt}_{soot} - \dfrac{R_{xfer}\,m_{reac}}{(1+AFR_{sto})}\right)\delta t}{\Delta t} + \frac{\dfrac{dm_a}{dt}_{ent}}{(1+AFR_{sto})} - \frac{dm_f}{dt}_{soot} \qquad (4.98)$$

where m_{reac} is the instantaneous mass of reactants, which is followed during the evaluation of the numerical integral

Similar limiting rates can be derived by considering the processes affecting the mass of air and the mass of evaporated fuel individually. These equations are set out in Appendix C. Note that the transfer rate, R_{xfer}, is a function of the mass fraction burnt, χ, and the latter is also changing during the calculation timestep. To properly allow for this change, iteration would be required, and this would add considerably to the complexity and computational time. However, the only time when χ is changing rapidly is during the premixed burn phase, and the above rate

limit is used only for diffusion-burning. For the premixed phase, an all-inclusive initial burn factor is used. Thus, the error introduced by neglect of change in χ is very small.

Once the limiting value of the burn rate is known, a factor representing the fraction of the reactants subzone transferred to the products region can be defined:

$$X_{reac \rightarrow pro} = \frac{\left(\frac{dm_f}{dt}\right)_{\lim} \Delta t}{\left(m_{eva}, \frac{m_a}{AFR_{stoich}}\right)_{\min}} \qquad (4.99)$$

Use of this equation is only necessary for the reactant component which is not limiting (i.e., air in lean mixtures and fuel in rich mixtures). The value obtained for the limiting component should be identical to that obtained by summing the individual mass-transfer components.

4.4.4.2 Temperature estimation

Having established the composition of the subzones, the thermodynamic state may be determined. The basic principle used is to estimate the pressure at the end of the timestep according to the rate of change on the previous timesteps. The temperature changes in all zones are then computed by taking into account heat release, heat transfer, compressive work and mixing, and a check on the consistency is made by comparing the sum of the zonal volumes with the cylinder volume. It was demonstrated that the resultant error is small, and this procedure is more computationally-efficient than iterating for pressure.

The basic equation for change of temperature is as follows:

$$\Delta T = \frac{\left(\frac{dm_f}{dt}\right)_{comb} \Delta H_{fuel} + \left(\frac{dm_f}{dt}\right)_{soot,ox} \Delta H_{soot,ox} + \left(\frac{dm_f}{dt}\right)_{soot,for} \Delta H_{soot,for} + \left(\frac{dQ}{dt}\right)_{wall} - p\Delta V}{m c_p} + \Delta T_{mix} \qquad (4.100)$$

where dQ/dt_{wall} is the total heat-transfer rate to the wall
ΔT_{mix} is the change in temperature due to the change in internal energy occurring on mixing between two elements
m is the mass of the zone or sub-zone

Each of the numerator terms represents a component of the internal energy change, and the sum can be defined as ΔU_{tot}. The temperature reduction due to fuel evaporation is neglected.

The estimation of temperature is greatly complicated by transfer processes between subzones. For example, where an element of mixture contains components which originated in two different subzones (or the air zone) on the last time-step, the overall volume change and average specific heat must be considered in determining the temperature change. Also, due to the rapid change in state, particularly during premixed burning, it is not sufficient to calculate rates based on the conditions existing at the start of the calculation timestep, and iteration is necessary. Special attention must be paid to the specific heat capacity, c_p, since its value may change rapidly during a calculation timestep and the temperature change estimate is very sensitive to its value. The following equation was used to give a more accurate estimate of the temperature change (the derivation is given in Appendix C):

$$\Delta T = \frac{\Delta U_{tot} \log_e \left(\frac{c_{p_2}}{c_{p_1}} \right)}{c_{p_2} - c_{p_1}} \qquad (4.101)$$

where *1* applies to conditions at the start of a calculation timestep
2 applies to conditions at the end of a calculation timestep

However, the rate of combustion and the sooting processes are not included within the iterative loop in order to reduce complexity. This omission is not serious, as the combustion rate is fixed and sooting processes are unimportant when conditions are changing fastest during the premixed burn phase.

The simulation follows the temperature in every zone and subzone in the mixture and in most cases the latter equation is used since the temperature change is significant. Iteration is performed until the temperature converges both for the zone

and the component subzones.

The methods used for evaluation of the terms in equ. 4.100 are now briefly considered. The rates of heat release and soot formation and oxidation are dealt with elsewhere. The heats of combustion, ΔH, are given in Appendix D; that for soot formation was obtained by difference (the other values are easily measured) thus balancing energy release between the sooting processes and direct fuel combustion. This is a fairly crude approximation, but using more detailed chemistry adds greatly to the complexity.

The compressive work term is determined using the total pressure and the following expression for ΔV:

$$\Delta V = \left(V_2 - \frac{N_2}{N_1} V_1 \right) \tag{4.102}$$

where N is the number of moles of gas

The volumes are obtained from the perfect gas law according to the known mass components, the chamber pressure and the instantaneous temperature and gas constant values. The expressions for gas constant are given in Appendix D. The chamber pressure is determined according to the following approximate equation:

$$p_{cyl} = \frac{m_{cyl} \sum \frac{R_{zone} m_{zone}}{m_{cyl}} \sum \frac{c_{v_{zone}} m_{zone} T_{zone}}{\sum \frac{m_{zone} c_{v_{zone}}}{m_{cyl}} m_{cyl}}}{V_{cyl}} \tag{4.103}$$

The summation terms, reading left to right, represent average gas constant value, the average temperature and the average specific heat capacity in the cylinder. The most accurate estimate is obtained using subzone values as inputs.

The specific internal energy of the mixture is computed according to Krieger's polynomial expression[194], given in Appendix D. An error in the original expression

was corrected in MSc thesis work[366]. Additional terms to account for the effects of dissociation, which becomes important above about 2100 K, have been included in the current work. Overall, the polynomial expressions are claimed to be accurate to within 2.5% for temperatures up to 3000 K at the precombustion pressure, and the limit rises to over 3200 K at peak pressures. The specific heat capacity is obtained simply by differentiating these equations.

In order to calculate the component of temperature change due to combination of two elements of mixture with different compositions, ΔT_{mix}, an internal energy balance is applied. The total internal energy of the two components at the last calculation timestep is equated to the internal energy of the resulting mixture, and the corresponding temperature is obtained using an iterative technique. Due to the large change of internal energy during combustion, these calculations must be based on conditions existing before any combustion has occurred on the current calculation timestep.

Finally, determination of the rate of heat transfer is dealt with in the next section, 4.4.5.

4.4.4.3 Initial conditions

It is very important to provide an accurate estimate of the conditions existing in the chamber at the start of the injection process. Determination of initial temperature is particularly important, since all subsequent temperatures are set according to incremental changes. It would be possible to use the above temperature change equation to follow the thermodynamic state from the time of inlet valve closure, but an alternative method which is simpler and well-established is use of the polytropic relationship:

$$pV^n = constant \tag{4.104}$$

The constant value is set according to the thermodynamic state at inlet valve closure. The pressure and temperature at this position are related via the volumetric efficiency, η_{eff}:

$$p_{ivc} = \frac{\eta_{eff} p_{ntp} T_{ivc}}{T_{ntp}} \qquad (4.105)$$

where *ntp* is normal temperature and pressure (Appendix D)

The temperature, T_{ivc}, will vary according to atmospheric conditions and the quantity of combustion residuals remaining from the previous cycle. Estimation of the latter was considered to be beyond the scope of this work, and a constant value was used (293K).

The volumetric efficiency is typically about 90% in a diesel[116] but it will vary with engine speed. In the current work a value of 0.82 was taken from the chosen experimental dataset[159] and an approximate speed correction was incorporated[116].

The polytropic exponent, *n*, is affected by heat transfer and consequently will also vary with engine speed, tending to unity as speed tends to zero. However, for normal operating speeds, there is broad agreement on a value of 1.3 (± 0.05)[116]. Analysis of curves published for the chosen experimental dataset[159] yields a surprisingly high value of c. 1.47, but the author of that work recalls obtaining a value of 1.35 from the original pressure diagrams (Kamimoto, personal communication). Hence, the later value was used in the simulation program, and an approximate speed correction was incorporated (see Appendix C).

For the standard case of the chosen experimental dataset, a temperature of 907 K and pressure of 23.8 atm were calculated for start of injection conditions. Examination of the published curves[159] yields values of c. 880 K and c. 28 atm, though there is reason to doubt these values as mentioned above.

4.4.5 Heat transfer

4.4.5.1 Review

Heat transfer in engines has been extensively studied and reviewed by various authors, including Spalding[332], Heywood[116], Markatos[229] and Hiroyasu[128]. Hiroyasu[128] describes a total of fifteen heat-transfer correlations, from a variety of sources, and plots calculated heat-transfer coefficients against crank angle. Yet more correlations are given in the diesel combustion modelling literature. Besides choice of correlation, the method adopted for distributing heat loss between the model zones must be considered.

Heat transfer from diesel engines is primarily convective, but radiative losses are not negligible, contributing 20 to 40 % to the total[116,228,241,86]. Considerable variation would be expected in the radiative component, since it is dominated by emission from soot particles, and the concentration of the latter varies widely between engines. Most of the proposed correlations do not account for radiative transfer explicitly, and of the fifteen expressions listed by Hiroyasu[128], only those of Nusselt and Annand[9] include a separate radiative term. Also, heat transfer within the mixture is generally neglected.

Some of the expressions applied to heat-transfer prediction in diesels are summarised in Table 4.13 (over). The most popular correlations are those of Annand[9,10] and Woschni[376]. Hohenberg's expression[133] is a development of the latter[116]. Hiroyasu's comparative plot of calculated heat-transfer coefficients shows that the Annand expression gives values which are generally higher than those of the other correlations, and typically double the Woschni predictions[376]. However, the original form of the Annand correlation does not explicitly account for soot, so it is unlikely to provide a reliable estimate of the radiative heat loss. Bazari[19] has attempted to remedy this by accounting for the influence of soot as follows:

$$\left(\frac{dq}{dt}\right)_{rad} = \sigma \varepsilon (T_{zone}^4 - T_{wall}^4) f \qquad (4.106)$$

where q is a heat flux per unit area
ε is the emissivity
f is a shape factor

Author	Correlation(s)	Comments
Hodgetts[132], 1974	Woschni	Includes additional turbulence factor
Shahed[309], 1975	Annand	
Hiraki[118], 1980	Woschni	
Dent[56], 1981	Woschni	Two-zone model
Mansouri[228], 1982	Woschni	IDI, stochastic model
Hiroyasu[124], 1982	Woschni, main chamber Dent, swirl chamber	IDI
Hiroyasu[126], 1983	Woschni	
Kono[184], 1985	Woschni	
Gupta[105], 1986	Woschni	
Lipkea[213], 1987	Annand	
Xiao[378], 1991	Woschni	Stochastic model Interzone transfer allowed
Zahdeh[382], 1991	Hohenberg	Single-zone model
Bazari[19], 1992	Annand	Radiative term includes soot
Jiang[151], 1992	Annand	Single-zone model
Li[215], 1993	Assanis[15], convection Li[214], radiation	
Rocco[295], 1993	Hohenberg	Single-zone model

Table 4.13 - Heat transfer correlations used in combustion simulations

The emissivity, ε, is calculated assuming that the zonal soot cloud acts as a grey body:

$$\varepsilon = 1 - e^{fK_a L_{cloud}} \tag{4.107}$$

where L_{cloud} is the cloud dimension

K_a, the overall absorption coefficient is related to soot density by:

$$K_a = 1200\,\rho_s \tag{4.108}$$

f is taken to be unity, and L_{cloud} is set to the diameter of an equivalent sphere of equal volume to the zone. The overall heat-transfer rate is determined by multiplying the heat flux by the surface area of the soot cloud.

$$\frac{dQ}{dt}_{rad} = \frac{dq}{dt}_{rad} A_{cloud} \tag{4.109}$$

Since it is well-proven, the Woschni correlation has been chosen to describe convective heat transfer in the current work. The particular form of the expression used is that obtained by Woschni in 1979[376], as given by Heywood[116]. The radiation follows the above Annand-based approach of Bazari[19].

There is no consensus on the method of distributing heat transfer between the model zones. Most authors either make no mention of it or simply state that the division is made according to zonal temperature and mass. Shahed[309] and Gupta[105] give the following expression:

$$\frac{dQ}{dt}_{zone} = \frac{m_{zone} T_{zone}}{\sum m_{zone} T_{zone}} \frac{dQ}{dt}_{total} \tag{4.110}$$

Bazari[19] replaces the zonal temperatures in the above by the zonal temperature relative to the wall temperature, which seems more realistic.

Mansouri extends this approach by accounting for the zonal surface area too, deriving the following equation[227]:

$$\frac{dQ}{dt}_{zone} = \frac{\frac{T_{zone} - T_{wall}}{(\rho_{zone})^{\frac{2}{3}}}}{\sum \frac{T_{zone} - T_{wall}}{(\rho_{zone})^{\frac{2}{3}}}} \frac{dQ}{dt}_{tot} \qquad (4.111)$$

However, in Mansouri's stochastic model, zones are of equal mass, so mass-dependency is not accounted for. For use with a multizone model, Xiao[378] gives a modified version of this equation, replacing $1/\rho$ by zonal volume to include mass. The latter equation has been adopted in the current work to describe partitioning of convective heat transfer between the model zones.

Equations of this type appear to be unsuitable for describing the division of the radiative component between spray zones. The temperature dependency differs greatly to that found in radiative transfer, and in the case of convective heat transfer, surface-area terms are involved since they are representative of an estimated wall contact area. With radiation, partitioning in terms of zonal surface areas is not possible because the process can only be meaningfully described in terms of the whole soot cloud. Since no alternative approach could be found in the literature, the following expression is proposed for use in the current work:

$$\frac{dQ}{dt}_{zone} = \frac{\varepsilon_{zone}\left(T_{zone}^4 - T_{wall}^4\right)}{\sum \varepsilon_{zone}\left(T_{zone}^4 - T_{wall}^4\right)} \frac{dQ}{dt}_{tot} \qquad (4.112)$$

Interzone radiative heat transfer has been neglected in the interest of simplicity.

4.4.5.2 Results

Initial results gave a ratio of radiative to total heat transfer of only 3.7% over the full cycle in the standard case of the experimental dataset (mid-load, ϕ=0.5). Kamimoto's calculated value for the same engine is about 33% during the main combustion period[159]. Moreover, the simulation result was obtained for a predicted mean temperature which exceeded the experimental value by 200 to 300 K. Since the method of convective heat-transfer estimation is probably more reliable than the radiative calculation, an additional model parameter was used to scale up the radiative term so that the ratio of the predicted values lay in the typical experimental range. With a multiplicative factor of ten, the total calculated heat loss at exhaust valve opening was 433 J, equivalent to 37.7% of the fuel energy. Heywood[116] gives a range of 8 to 41% for the maximum power condition, and the contribution of the heat loss is expected to increase towards lower loads. Thus, the calculated values are not unreasonable.

4.4.5.3 Conclusion

A heat transfer model has been implemented using the convective heat transfer correlation of Woschni and a radiative correlation which is expressed in terms of soot concentration, following Bazari. Initial results showed that the radiative component is underpredicted and it was found necessary to include an additional scaling parameter. With this modification, reasonable values of the overall heat loss were obtained.

The overall performance of the thermodynamic models and further model development that was necessary are described in the context of the combustion model validation in section 5.1.

CHAPTER 5 - RESULTS

5.1 COMBUSTION MODEL RESULTS

The fundamental requirement of the combustion model is the accurate prediction of thermodynamic state over as wide a range of operating conditions as possible and it is important that this is achieved without any variation of the parameters that relate only to the model. For validation, performance can be examined on a number of levels, including the overall engine efficiency, the time-dependent variation of properties, i.e. the progress of the combustion process and the in-cylinder distribution of temperature and composition. Depending on the parameter being assessed, different methods of evaluation will be appropriate and the criteria for satisfactory performance will also vary. In this work, though, the bulk of the validation is carried out by means of comparisons with experimental data from the chosen data-set (Kamimoto[159], see section 3.2). Following the above breakdown of performance measures, the analysis is split into four sections, the first three dealing with thermodynamic performance in terms of global, time-dependent and spatially-dependent behaviour, and the fourth being comparison with results of a parametric study. In view of the need for general applicability, the final values of some of the key model parameters were selected in the context of the latter.

5.1.1 Overall performance

The most basic level of model evaluation is to check that the overall efficiency and the distribution of the fuel energy lie in the range which is typical for the engine type. Heywood gives performance data for a range of engines, including a 0.82 l/cylinder Deutz DI diesel which is the closest match to the 0.781 engine chosen for the simulation. Table 5.1 gives the brake specific fuel consumption (bsfc) of this engine for the standard case of the simulation data-set, and the corresponding fuel conversion efficiency. The value of mechanical efficiency used in evaluating the simulation result was obtained by comparing the imep values given by Aoyagi[11] with the corresponding bmep values of Kamimoto[159]. Averaging over the eight data points, and applying a correction factor to the imep values (see discussion on pressures below) yields an efficiency of 85.8%; the highest value was 88.7% and the lowest 82.3%.

Performance parameter	Deutz engine[116]	Simulation
bsfc (g $kWhr^{-1}$)	240	188
fuel conversion efficiency (%)	33.5	41.8

Table 5.1 - Comparison of engine performance parameters

The comparison shows that the calculated efficiency is too high; part of the discrepancy may be in the assumed mechanical efficiency, but more likely the calculated pressures are too high. Comparison with the corrected experimental pressure curve shows that this is the case since the simulation value is approximately 10% higher in absolute terms (see Fig. 5.9). Relative to the motoring pressure, the discrepancy is more like 20% and this is a better guide to the expected difference in the work output. Fundamentally, the higher pressure may result from overestimated temperatures. These issues will be dealt with more fully in subsequent sections.

Other useful information can be obtained by examining the distribution of the fuel energy. Heywood gives typical data values for the maximum-power condition in a range of diesel engines. These are shown in Table 5.2 and compared with the nearest simulation case of 0.67 equivalence ratio.

% of fuel energy	Experiment[116]	Simulation
Brake work	34-38	40.1
Heat loss	18-41	34.6

Table 5.2 - Comparison of fuel energy breakdown

Again the brake work is rather high, but the heat-transfer value lies within the range of the empirical values. Though the latter relates to quiescent conditions, the empirical values include swirl-chamber DI engines in which heat transfer rate will be markedly increased. However, for the equivalent simulation case with a swirl ratio of 4 the calculated value is only 42%, which is not unreasonable.

5.1.2 Combustion process

Kamimoto[159] has used various means to investigate the combustion process in the test engine. By application of a simple two-zone thermodynamic model, air entrainment rates were calculated and the mean equivalence ratio in the burning regions was determined. The flame temperatures were estimated using the two-colour method[158] and pressures were measured using both a strain gauge and a pressure transducer[159]. Also, detailed measurements of the chemical composition were made[11].

An important conclusion of the analysis was that during the early part of the diffusion phase the burning mixture was rich and air entrainment was limiting. A parameter representing the efficiency of air utilisation in the flame was defined by taking the ratio of the entrainment rate times the heat of combustion at the mean flame equivalence-ratio to the heat-release rate. It was found to have a value of unity from the start of the diffusion burn phase at 5° bTDC up to about 10° aTDC. During this period the mean equivalence ratio in the burning region was greater than 1.5. After 10° aTDC, the air utilisation gradually declines from unity, i.e. some air escapes the burning process. Nevertheless, the mean equivalence ratio remains above 1.0 until about 25° aTDC. Consistent with this is the fact that the flame temperature is above 2000 K from the start of the diffusion-burning phase.

The predictions of the current model calculations also indicate that early diffusion burning is air-limited. Air-entrainment rates were examined in section 4.1 in the context of the spray model. Figs. 5.1 - 5.3 illustrate the evolution of the zonal mixture composition and the mean equivalence ratio in the spray for the standard experimental case. Comparison with the estimated empirical value of equivalence ratio in Fig. 5.3 shows a generally good agreement considering the expected uncertainties in each value; the model may slightly over-estimate the richness of the mixture during the main diffusion-burning period. The model calculations indicate that the equivalence ratio remains rich until at least 40° aTDC.

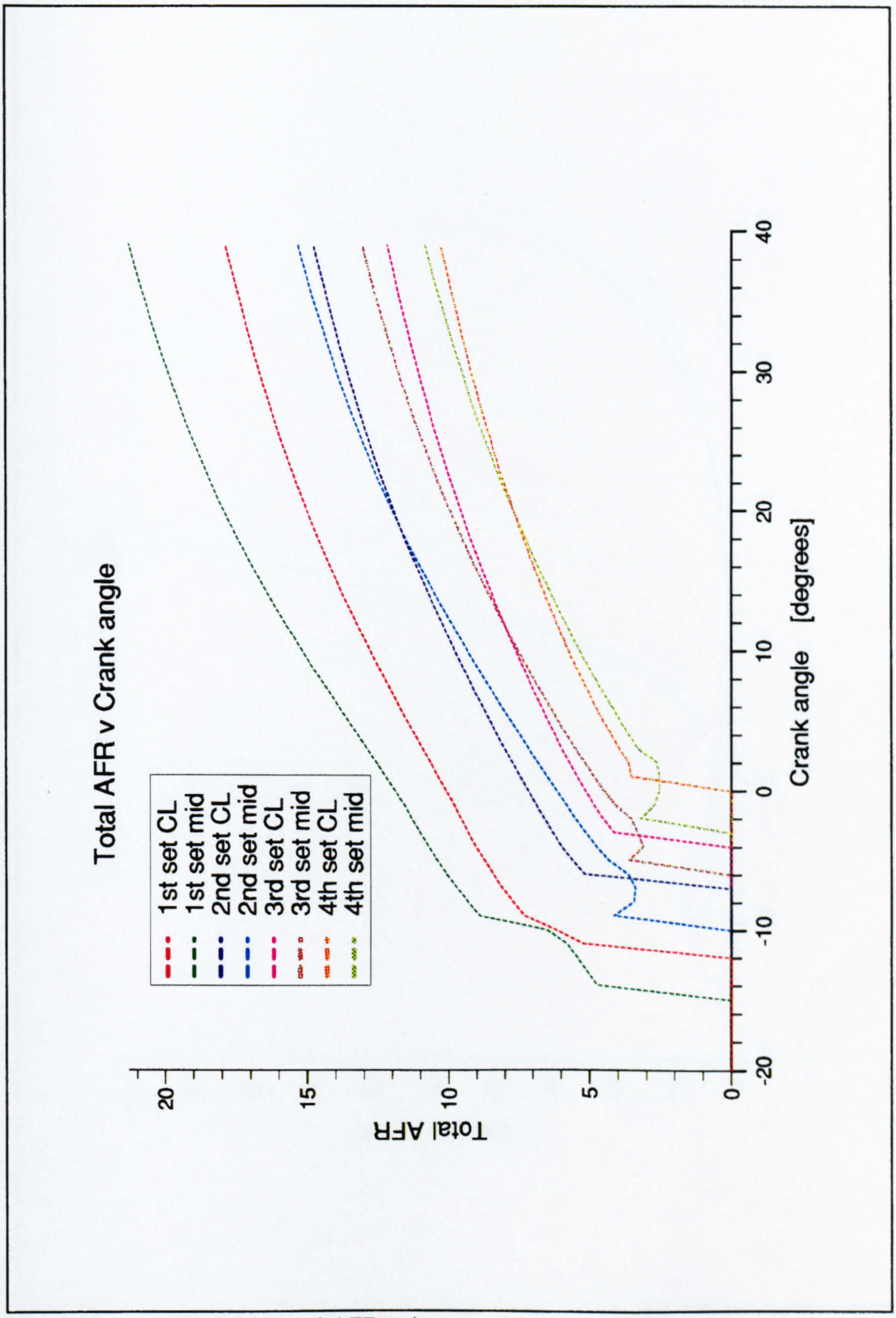

Figure 5.1 - Calculated zonal AFR values

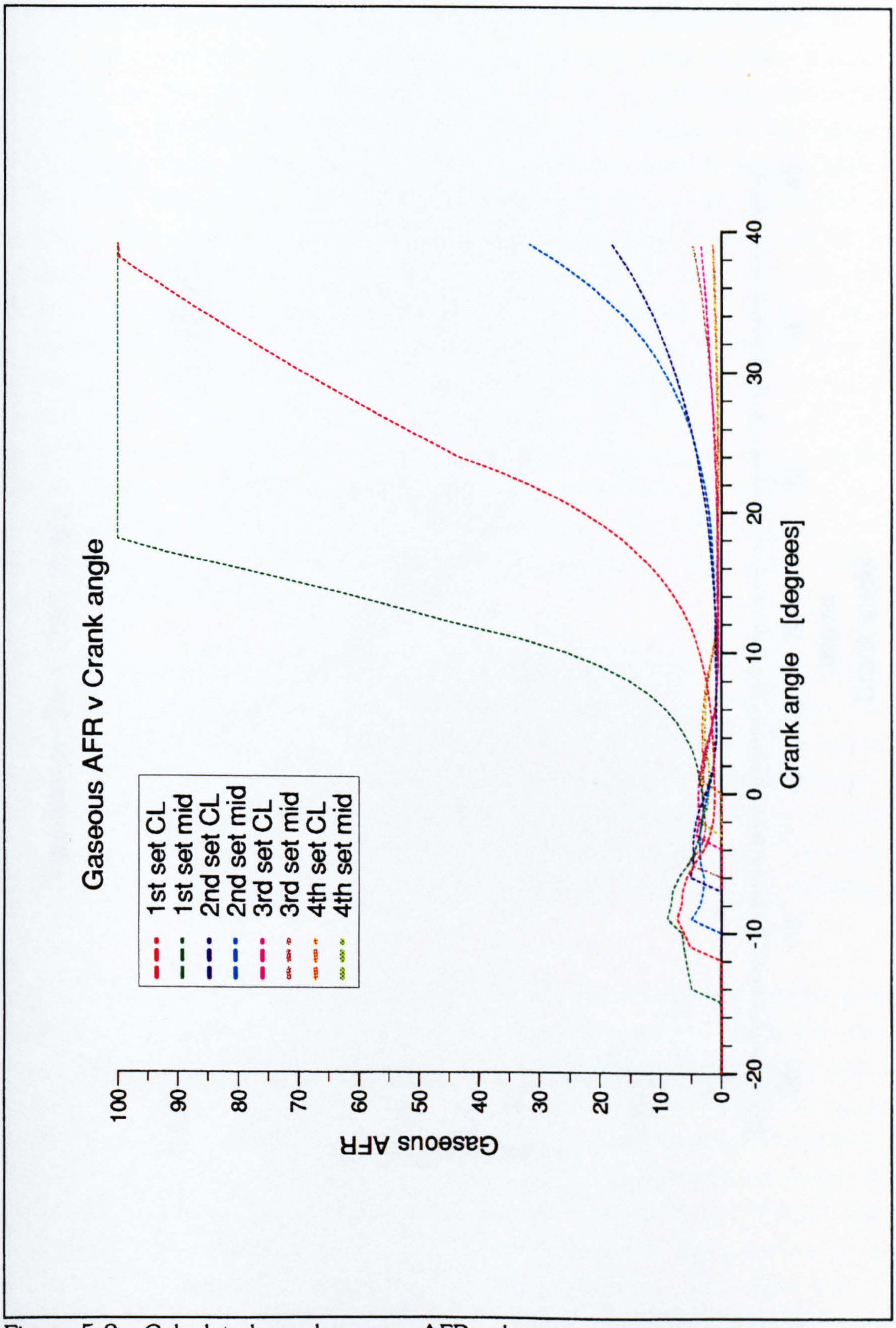

Figure 5.2 - Calculated zonal gaseous AFR values

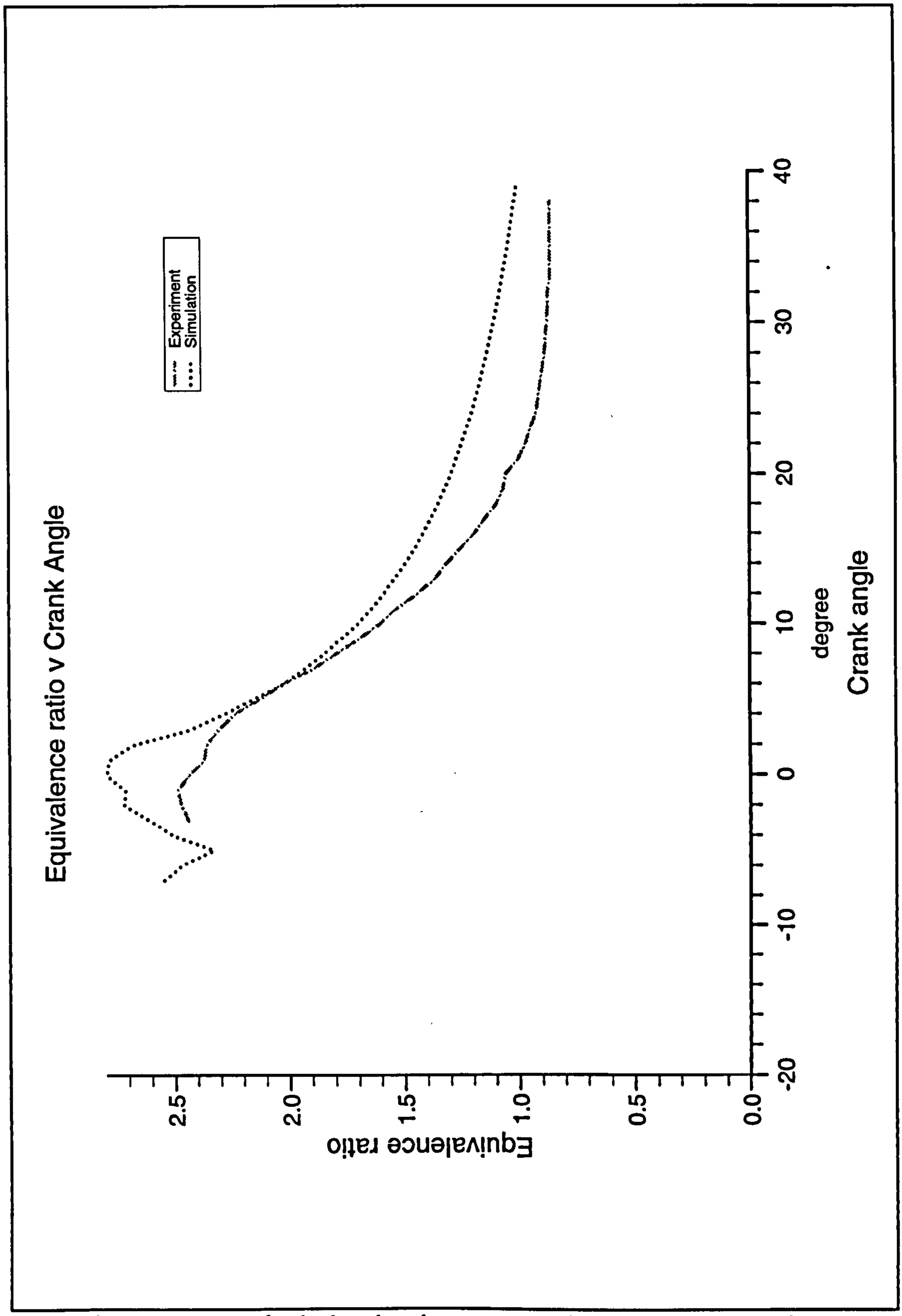

Figure 5.3 - Variation of calculated and experimental overall spray equivalence ratio

Because the bulk of the diffusion burning occurs at rich conditions, the heat-release rate is very sensitive to the predicted air-entrainment rates so that accurate estimation of the latter is essential. In the course of optimising the model performance through appropriate choice of premixed burn factor and the constant for the diffusion burning rate (see 'Parametric Study' below), it was found that overall entrainment rates were a little high. Using the original model developed by Hiroyasu, Kuo reached a similar conclusion and proposed the use of modified air-entrainment coefficients[197]. Kuo's study involved engines of 0.52 l and 2.0 l capacity, whilst Hiroyasu first applied the model to a 1.8 l engine. In the case of the smaller engine, Kuo achieved a satisfactory match with experiment only by reducing the coefficient which scales down the air-entrainment rate in burning mixture from 0.7 to 0.4. Since the current engine is of 0.78 l capacity, it is not unrealistic to use this lower value. The coefficient which scales up entrainment after wall impingement was also modified in accordance with Kuo's recommendation of a reduction from 1.5 to 1.4. Khan[170] and Dent[56] have also adjusted entrainment coefficients to obtain satisfactory heat-release rates; in the latter case, Ricou's constant value of 0.32 was increased to 0.7.

Fig. 5.4 shows the heat-release rate for the standard experimental case. Kamimoto calculated heat-release rates for each set of experimental conditions, but unfortunately, the curves published do not yield the correct totals for heat release when integrated. However, following his own recommendation (personal communication), the experimental heat-release diagrams were scaled up in the y-axis direction such that the total heat release matches the fuel energy. The figure shows that the curve modified in this way agrees very well with the calculated results.

Figs. 5.5 - 5.8 show the calculated temperatures of every model zone and the spray average. Each plot applies to all zones at a particular position across the spray width, starting with the spray centreline zones and finishing with the edge zones. Also included on the plots are the flame temperatures measured by the two-colour method. These are seen to be typically a few hundred degrees below the calculated temperatures of the combustion products in the main diffusion-burning phase. As indicated in the discussion of 'Overall Performance' in section 5.1.1, the predicted temperatures are probably a little high. However, the two-colour method is not known to be particularly accurate[380]. Some limitations are described by Kamimoto[159].

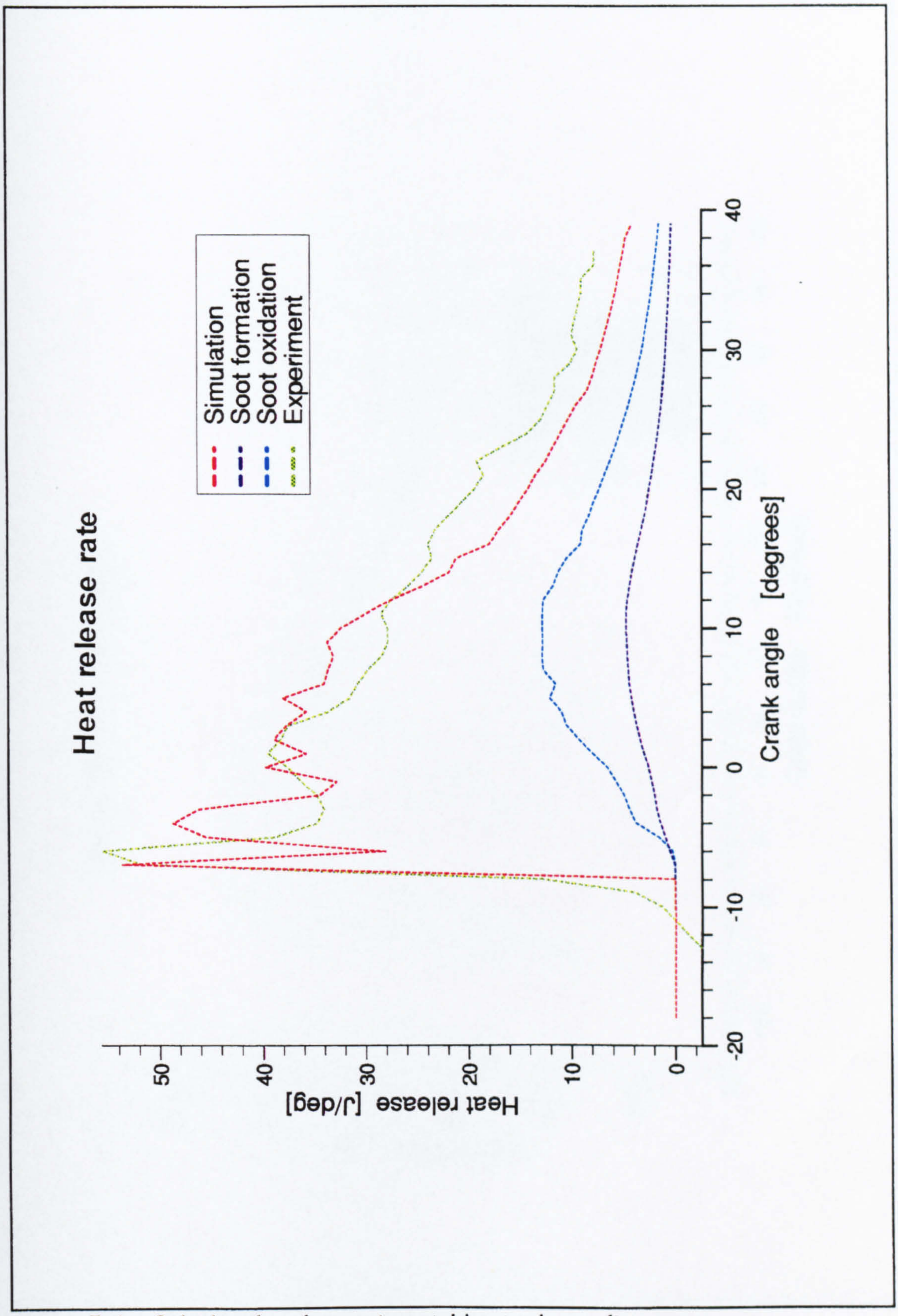

Figure 5.4 - Calculated and experimental heat-release diagrams

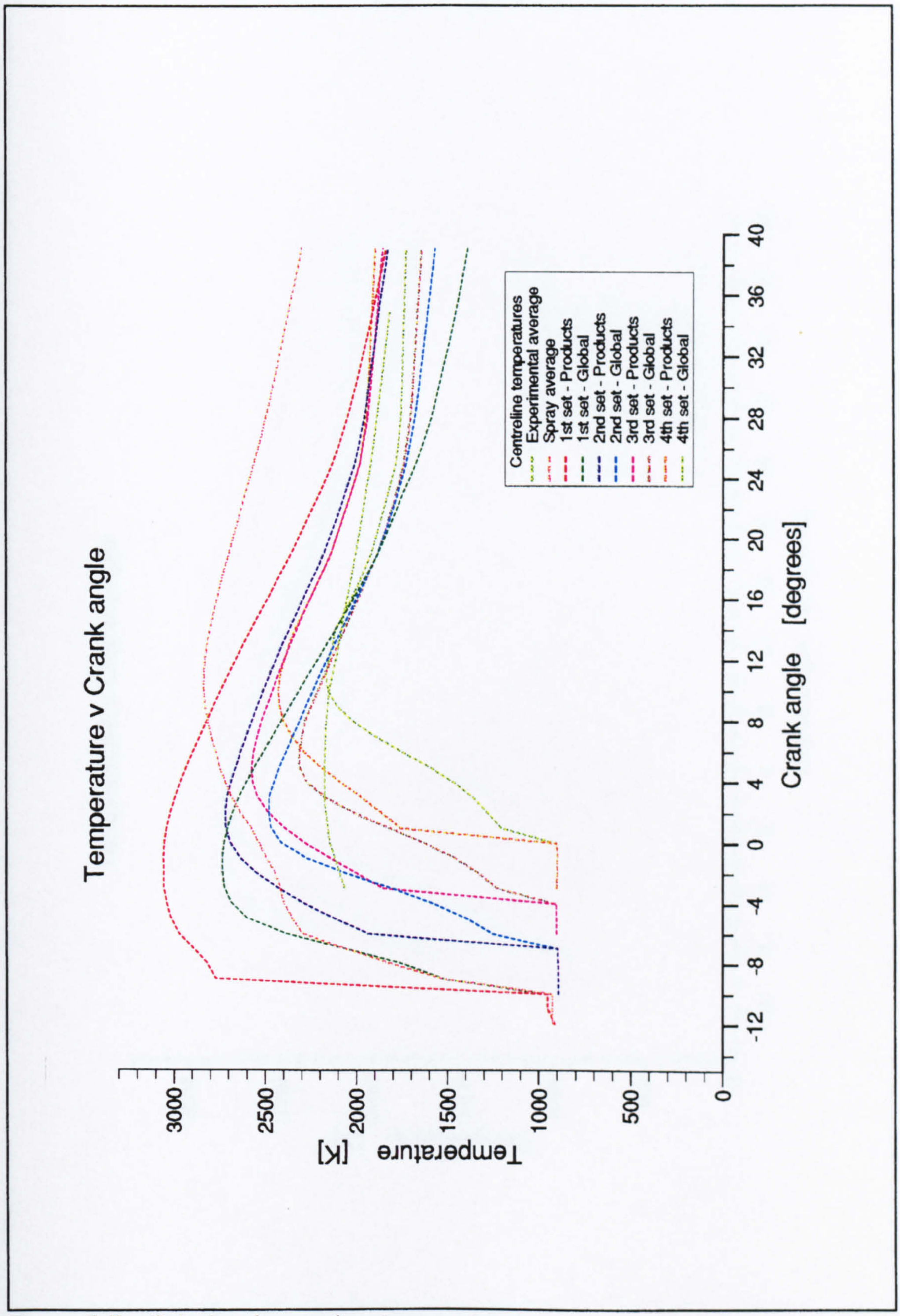

Figure 5.5 - Calculated centreline temperatures

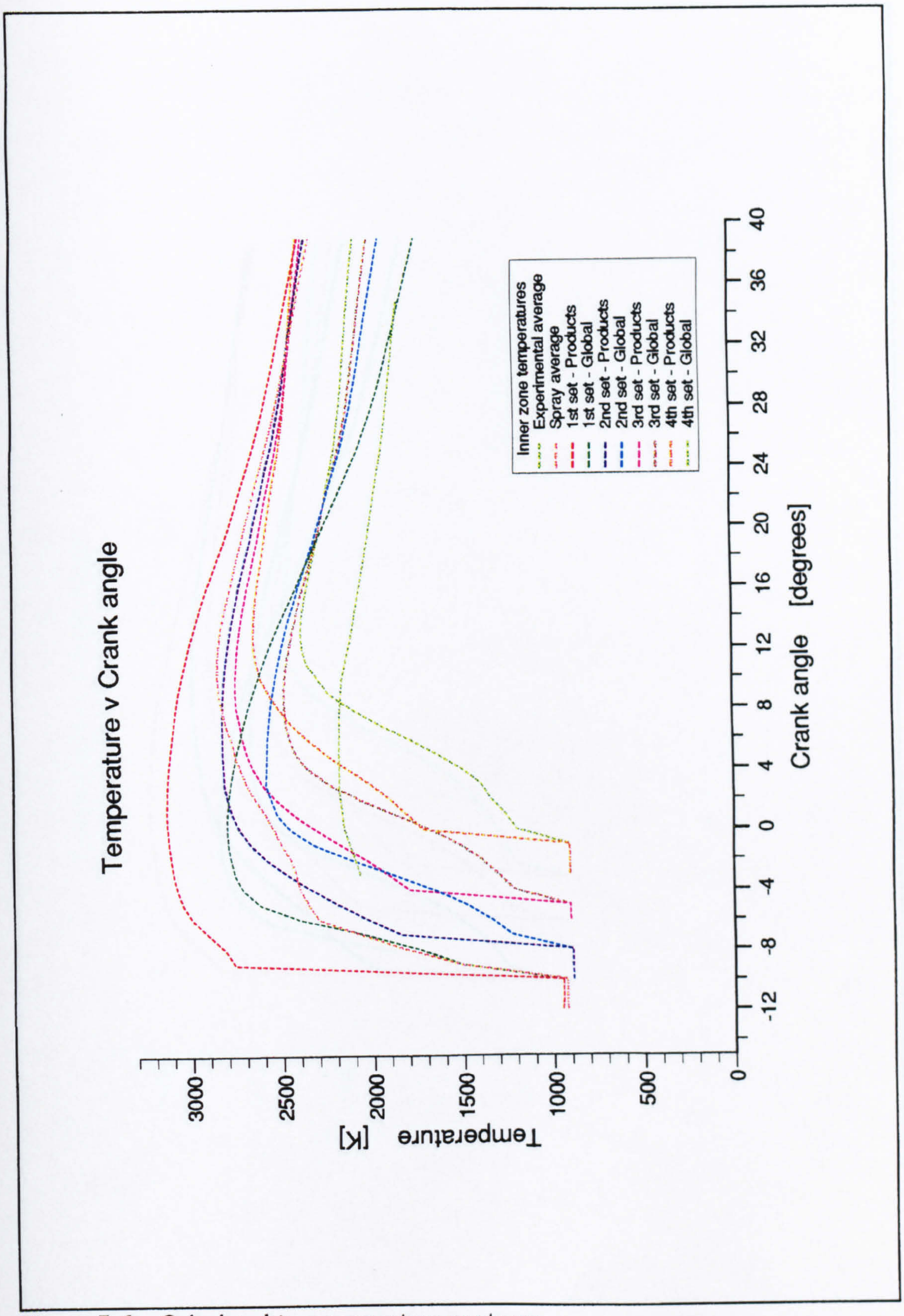

Figure 5.6 - Calculated inner zone temperatures

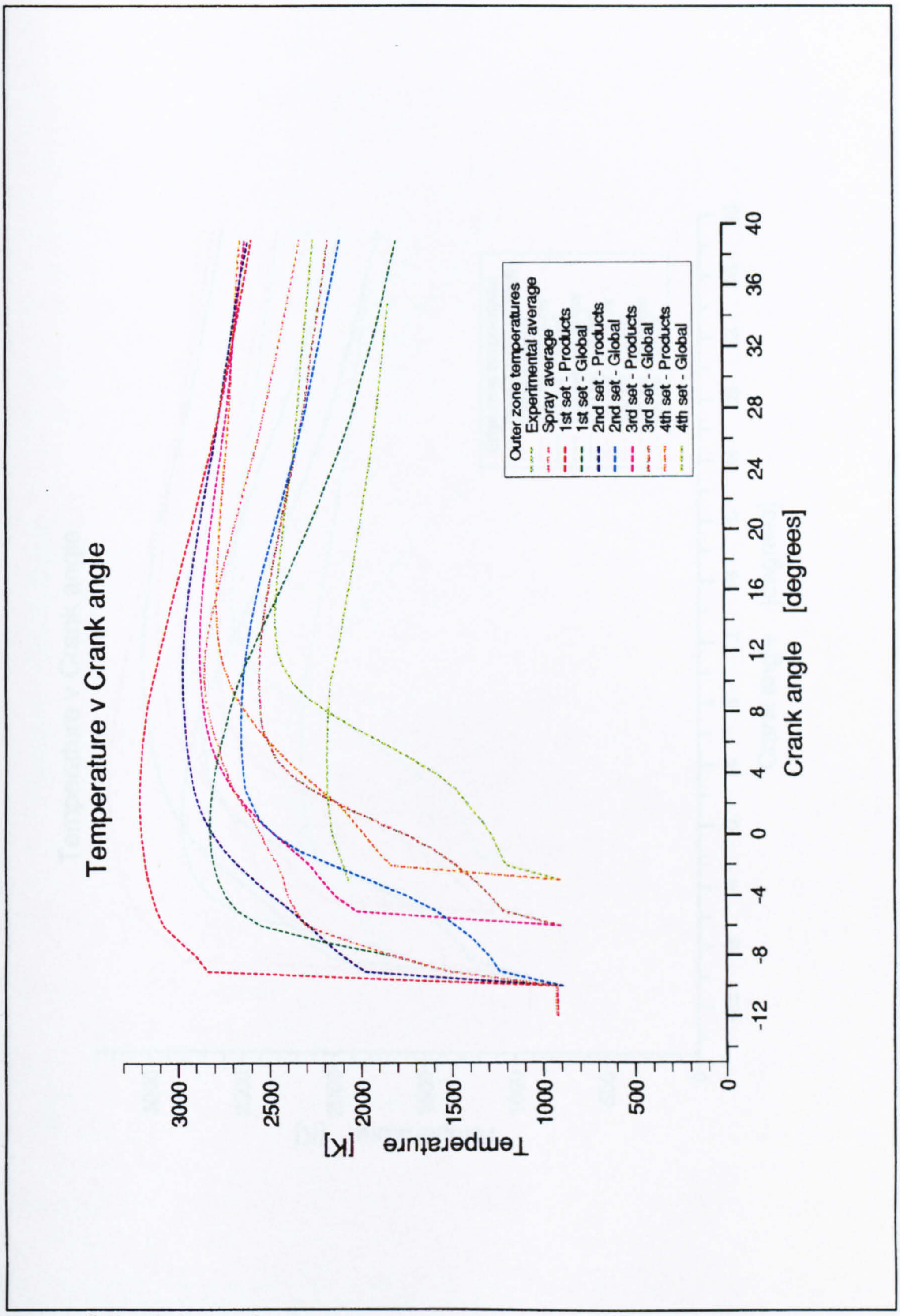

Figure 5.7 - Calculated outer zone temperatures

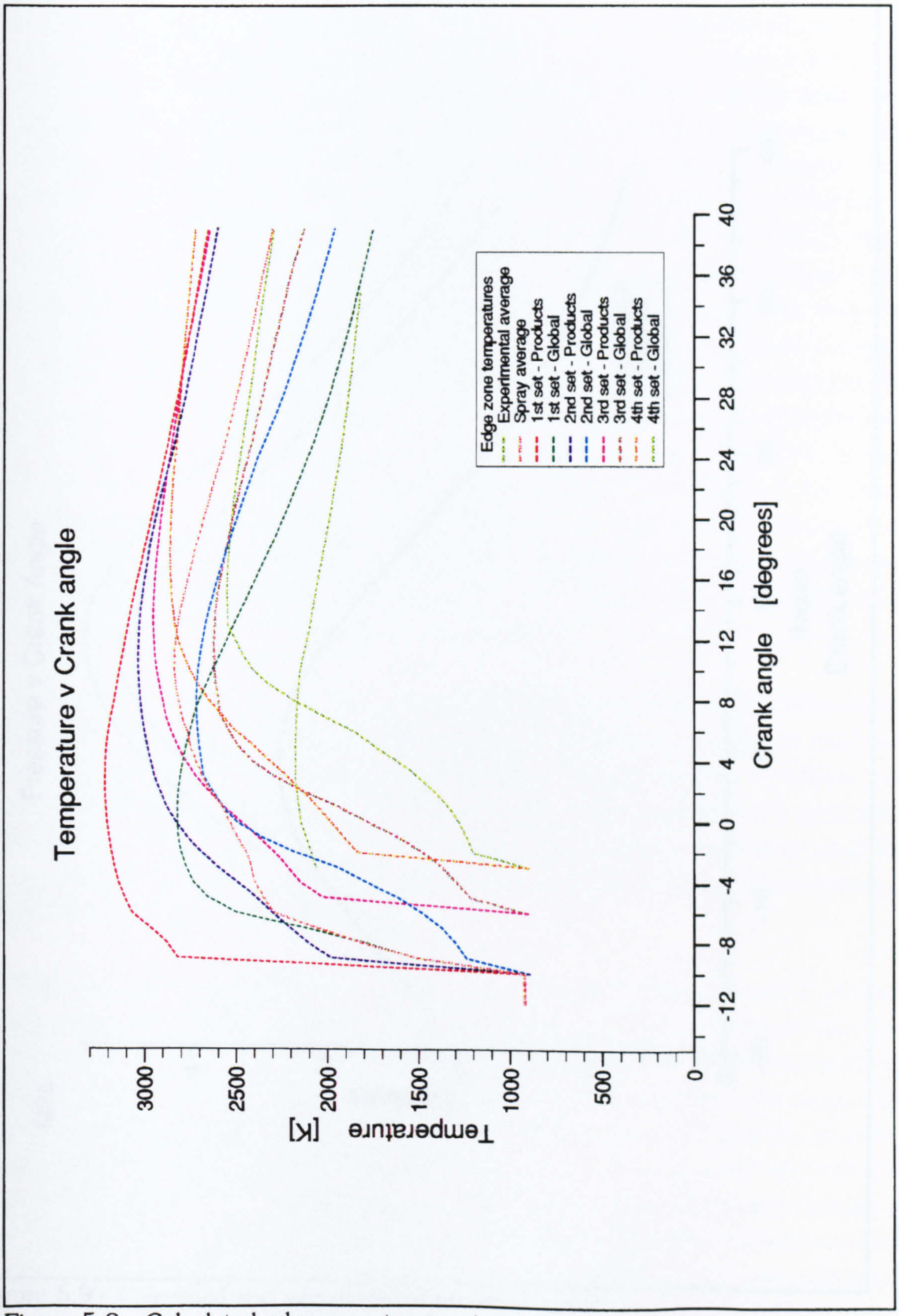

Figure 5.8 - Calculated edge zone temperatures

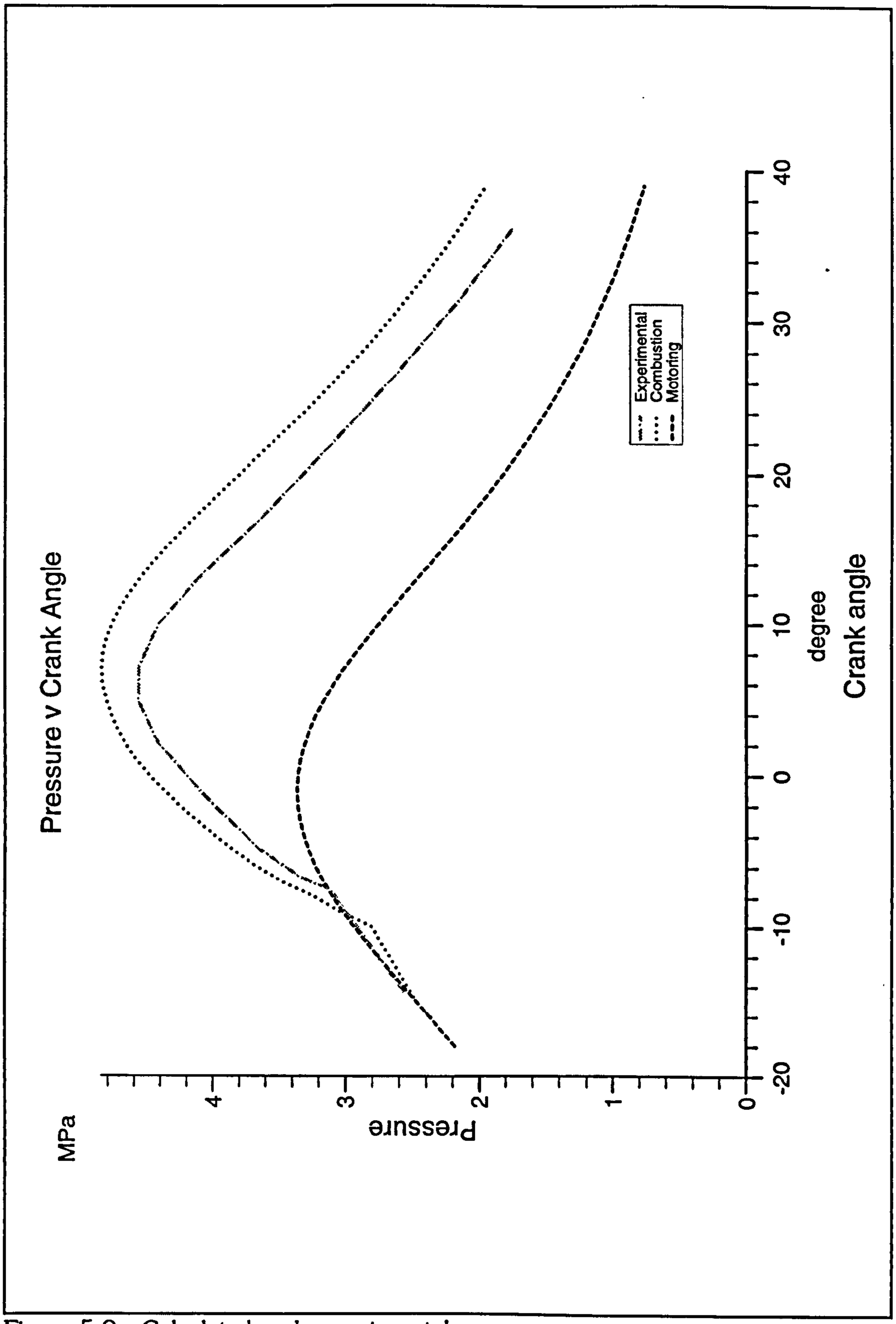

Figure 5.9 - Calculated and experimental pressure curves

In fact, estimation of the zonal temperatures is one of the most difficult aspects of the combustion simulation. The methods used are outlined in section 4.4.4.2. In particular, two factors contribute to uncertainty in the calculated temperatures. The first is the fact that the temperature change is determined on the basis of the total rate of change of energy and the specific heat in each element of mixture. The specific heat in particular is not constant during the time step, and at first burn, when the subzone temperature may rise by nearly 2000 K (see Fig. 5.8), its value is more than doubled. Because of the changing values, improved estimates of the temperature change may be obtained by integrating the rate equation over the timestep. For instance, the variation of c_p is partially accounted for by use of equ. 4.101. However, in reality, the relationship of the specific heat value to the physical mechanisms contributing to the change in energy is far from simple, and it is a gross simplification to assume an average specific heat value which applies to the whole zone and simply rises linearly. However, the details of the actual mechanisms are unknown and it is not possible to construct a model taking any of these effects into account. Thus, some uncertainty in temperature is inevitable and it would not be unrealistic if the magnitude were around 10% of the calculated temperature change. This amounts to nearly 200 K at first burn.

The second contribution to temperature uncertainty is the incremental method used to follow the temperatures. The zonal temperatures at each timestep are obtained from the temperature change, and the other thermodynamic properties are determined from the temperature. Thus, any errors are cumulative and systematic errors are not corrected for. Again, no alternative method is available, and the overall accuracy of the thermodynamic calculations is directly limited by the accuracy of the temperature-change estimate.

The computed pressure for combustion and motoring conditions together with an experimental pressure curve were shown in Fig. 5.9. Using the perfect gas law, the latter was found to be inconsistent with the corresponding mean temperature. Since the values of pre-ignition temperature given in Kamimoto's paper agree well with the calculated value, it may be assumed that the pressure curves are in error. By dividing all experimental pressures by a factor of 1.2, good agreement with the pre-ignition calculated values was obtained in all cases. Thus, all pressure curves in this thesis show the corrected values. In comparison to this experimental pressure curve, the computed values are rather high. This is consistent with over-estimated model temperatures.

5.1.3 In-cylinder variation

A more severe test of the simulation is the prediction of the spatial distribution of temperature and species in the chamber. For the chosen experimental case, an abundance of detailed measurements is available for model validation, including in particular the measurements reported in 1980 by Aoyagi[11]. This paper illustrates the results of a gas-sampling study in which N_2, O_2+Ar, CO_2, CO, CH_4, NO, NO_2 and unburnt hydrocarbons were measured. Most of the data is presented as time histories for a given point in the chamber, though some distribution maps have been constructed from this information (see Figs. 5.10 & 5.11). However, because the composition varies three-dimensionally, even the maps can only give an indication of the range of conditions existing in the spray. Also, because the simulation program is based on a quasi-dimensional spray model, conditions at a given position in the chamber are not well-defined. Whilst the location of the centre-of-gravity of each zone is followed in the simulation, the exact size and degree of overlap of the model zone is not known. Moreover, the model does not compute detailed chemistry. Notwithstanding these limitations, some useful information can be obtained from the maps of the history and spatial distribution of equivalence ratio and temperature shown in Figs. 5.10 & 5.11.

The upper plot in Fig. 5.10 shows a steadily increasing equivalence ratio on the jet centreline moving away from the injector and a reduction following the injection period. This behaviour is in accord with our knowledge of the evaporation and mixing processes. The lower plot shows that the overall equivalence ratio does not vary in a regular manner across the spray width at the position 29 mm from the injector along the spray axis. This is somewhat surprising in view of the standard conceptual model of a spray with a fuel-rich core, and the predicted local value of spray width of only 8.8 mm at TDC (according to Hiroyasu's spray width correlation[130]).

Model results were illustrated in Fig. 5.1. It was seen that there is no convergence in the zonal composition with time, and because the model allows no mixing between the zones, the overall zonal compositions are fixed once entrainment is complete. This is a model deficiency which is imposed by the method used to calculate air entrainment. In practice it probably has a small effect on the overall thermodynamic predictions, but the effect on emissions would be much more serious. Therefore, the zonal compositions and temperatures have been post-

processed using a simple averaging technique to give better estimates for the soot-model inputs (see Appendix F). Fig. 5.1 also shows that at a given time there exists a range of air-to-fuel ratios along the length of the spray and across the jet. Generally, the composition of zones injected simultaneously is seen to evolve in a similar fashion; this gives a fuel-rich core since the centreline zones move faster. As mentioned above, this distribution is not borne out by the measurements. The only realistic way of ensuring a similar result from the model calculations would be to neglect the cross-jet velocity variation and this is in turn would render use of multiple cross-jet zones unnecessary (to allow interzone mixing is not feasible with this type of model). However, there is plenty of evidence elsewhere that concentrations do vary across the jet[2,301,312], so the original form of the model was retained.

Fig. 5.11 shows that the flame temperature is remarkably uniform at all points in the spray at a given time. Providing that radiative heat transfer from soot is unimportant, this is to be expected, since flames will be found predominantly in regions of near-stoichiometric mixture. The model predictions were shown in Figs. 5.5-5.8. Careful examination shows that the temperatures of the products regions are fairly uniform, especially after the main diffusion-burning period. The largest discrepancy occurs between edge zones at the end of the injection period. At this point, the edge zones from the fuel injected last are very rich, and consequently about 25% of the mass of the combustion products region is excess unburnt air; the value for the first zone set is less than 5%. Hence, the temperature of these regions is not expected to approximate well to the flame temperature.

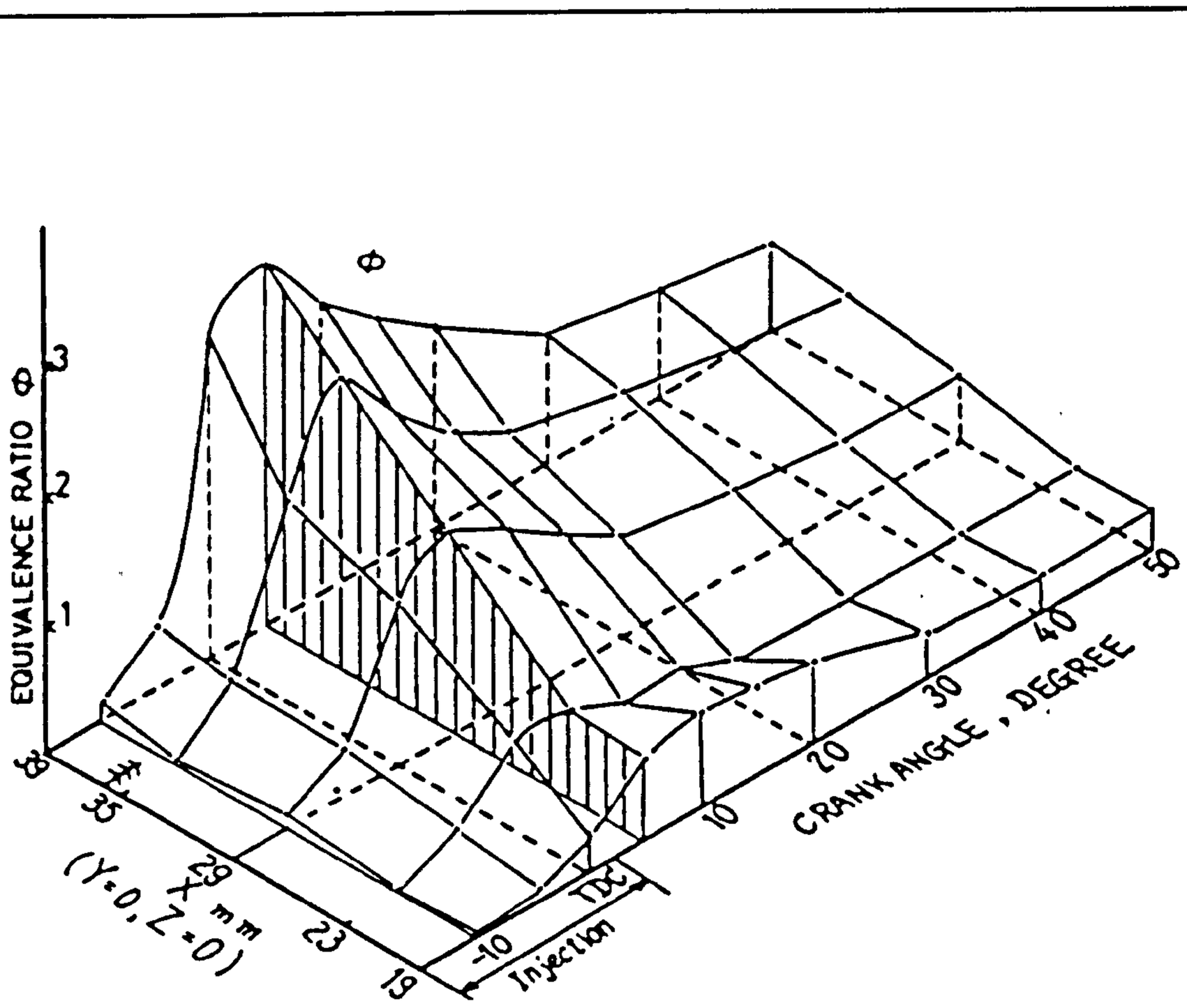

(a) - Along X axis

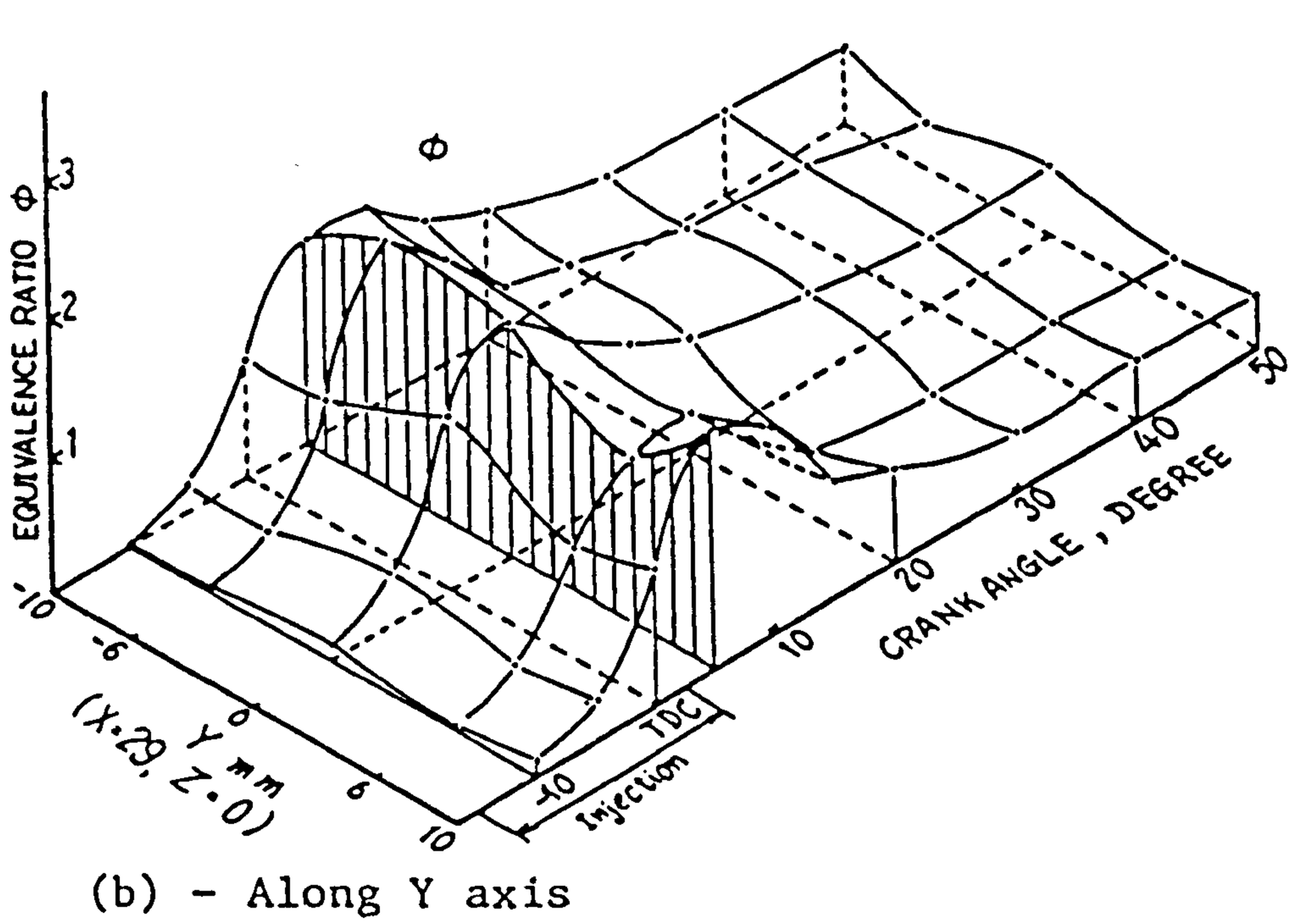

(b) - Along Y axis

Figure 5.10[11] - Experimental equivalence ratio maps

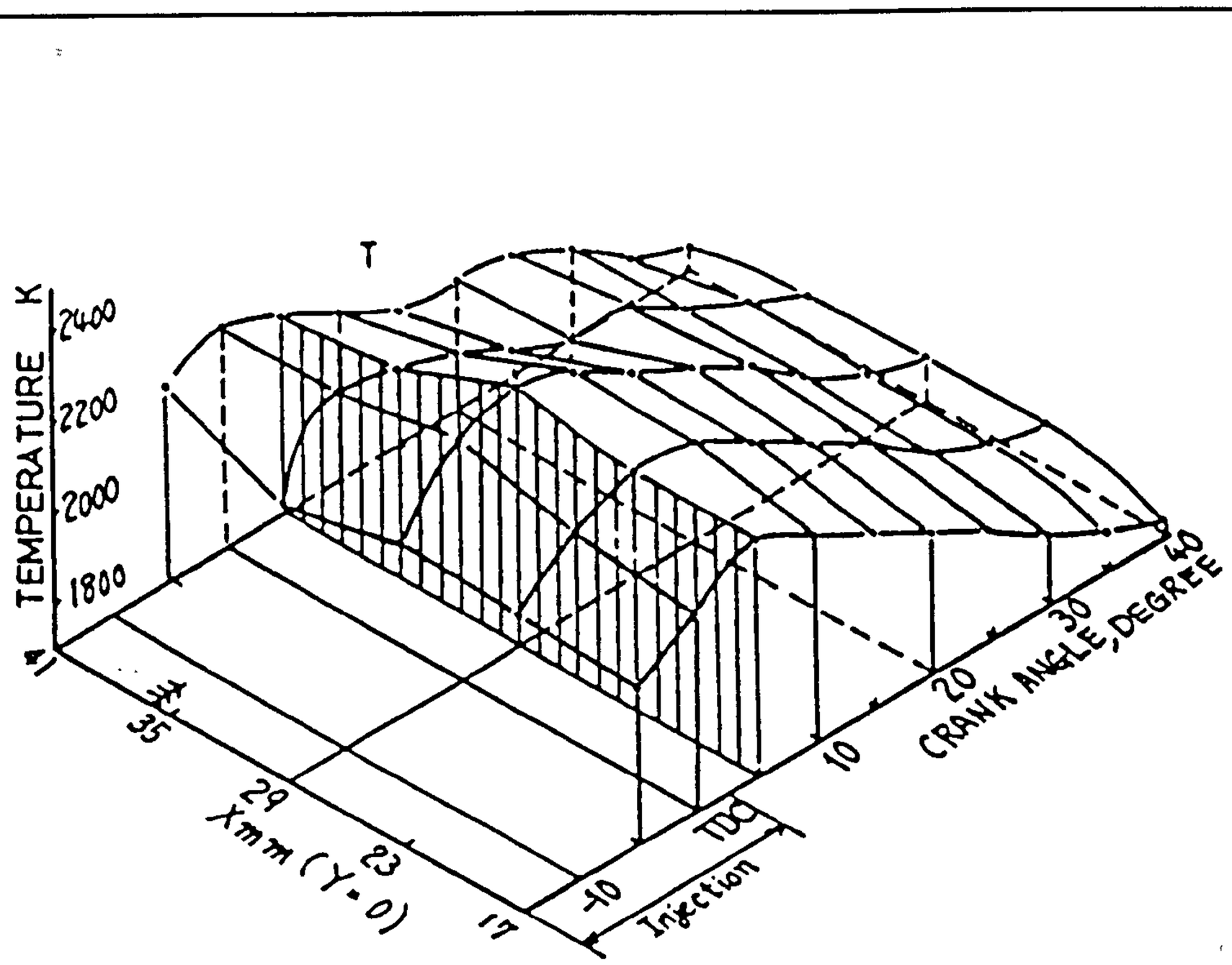

(a) - Along X axis

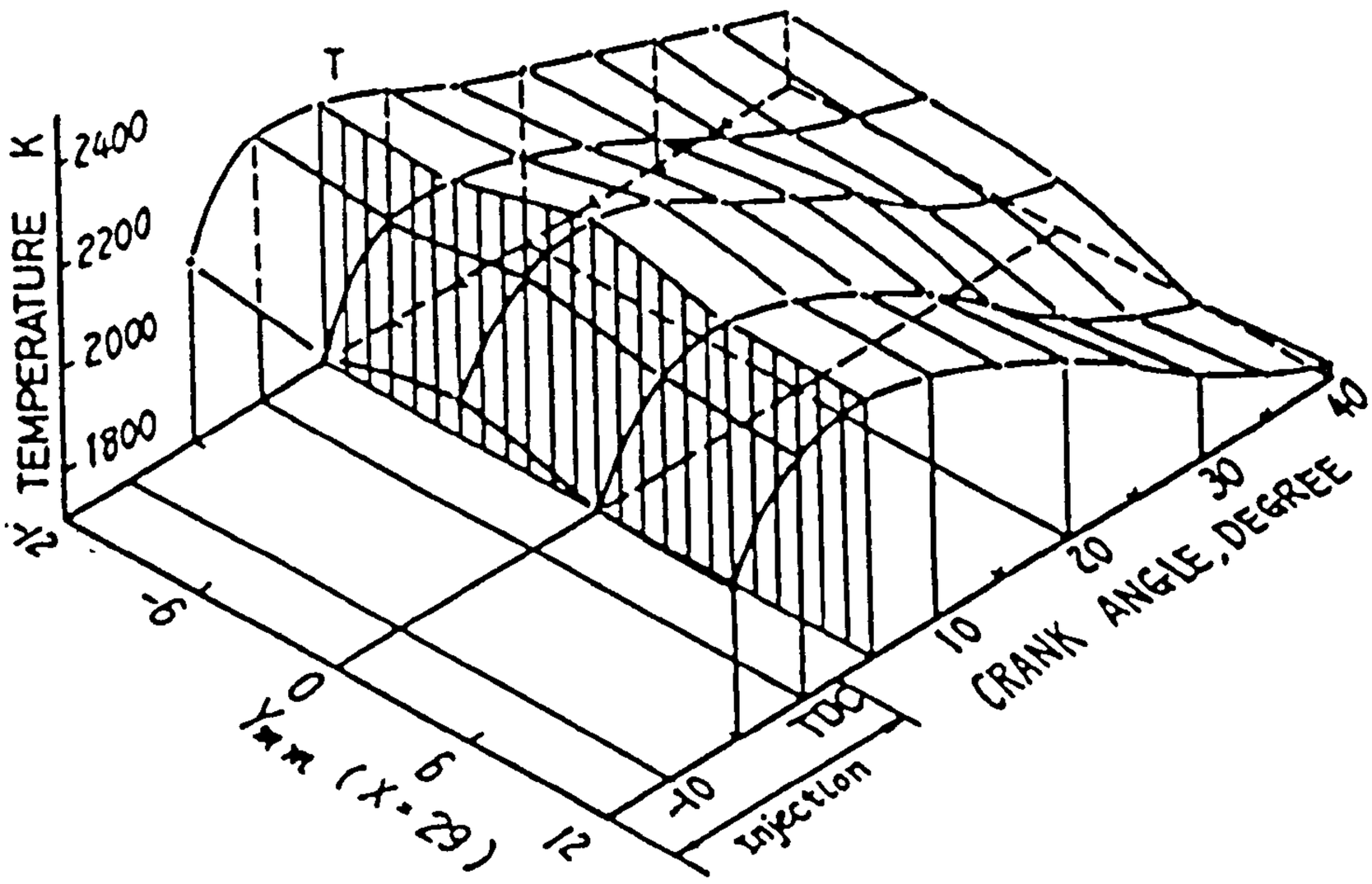

(b) - Along Y axis

Figure 5.11[11] - Experimental temperature maps

5.1.4 Parametric study

Phenomenological models usually contain a number of adjustable parameters which allow some degree of "tuning" of the output to give a better match with empirical data. The existence of these parameters is undesirable since they generally represent approximations made necessary by a lack of understanding of the phenomenon in question, and a long-standing goal in the development of such models has been the elimination of as many as is feasible[371]. This should result in models which are more generally applicable, i.e. that can accurately represent combustion processes at a range of operating conditions and in a variety of engines, without the need of empirical calibration. There is still much to do before this goal is achieved[280].

A parametric study provides an opportunity to investigate the general applicability of a given model and parameter set, and also allows the value of some of the adjustable constants to be established with more certainty. The latter is achieved by identifying the choices which give satisfactory model output over the whole range of conditions investigated. The particular experimental case being used for validation of the current model was chosen in large part because of the provision of an extensive data-set from a parametric study. The engine parameters varied and conditions covered are shown in Table 5.3:

Parameter	Conditions	Normal
injection pressure	17 MPa, 25 MPa	17 MPa
swirl ratio	0,2,4,8	0
load	ϕ = 0.34,0.45,0.5,0.67	0.45
injection timing	25° bTDC, 15° bTDC, 5° bTDC	15° bTDC
piston shape	shallow bowl, deep bowl	shallow
fuel type	n-tridecane, gas oil	n-tridecane

Table 5.3 - Parameter variation details

For each set of conditions a plot of measurements was included, illustrating variation of the following parameters:

mean flame temperature
cylinder pressure
mean flame-zone equivalence ratio
heat-release rate
air-entrainment rate
injection rate

To facilitate model development, graphics routines have been developed using Uniras AGL and FGL libraries to allow interactive display of the model predictions and experimental data. Predictions and experimental values of all of the above parameters can be compared, though as noted earlier, the combustion-products temperature from the model may not always correspond to that of the flame. The effect of varying any of the engine parameters shown in Table 5.3 can be examined, and the simulation program has been set up to allow easy choice between thirteen representative data-sets, which are specified in Table 5.4 below. The engine running speed was 1250 rpm and corresponding volumetric efficiency 0.82. Other engine specification details are given in Appendix E.

Case	Value of varied engine parameters
Standard	Gas oil, ϕ=0.56
Swirl	0
	2
	4
Injection timing	25° bTDC
	15° bTDC
	5° bTDC
Injection pressure	Gas oil, 17 MPa
	Gas oil, 25 MPa
Load	$\phi = 0.67$
	$\phi = 0.34$
Bowl shape	$\phi = 0.67$, deep bowl
	$\phi = 0.34$, deep bowl

Table 5.4 - Conditions for each case of parametric study

5.1.4.1 Results

There is not space in this thesis to include comparative plots for all of the model predictions and operating conditions. However, as has been noted previously, accurate prediction of the heat-release rate is key to satisfactory model performance and development work focused upon this parameter. Therefore, plots illustrating predicted and experimental data points are given for all of the above model conditions (Figs. 5.12-5.17). Any error in the calculated heat-release rates will be due in part to inaccuracy in determining air entrainment, and further, it will result in an incorrect estimate of the thermodynamic state properties. In order to look at these effects and their interrelationship, plots showing the flame-zone equivalence ratio and chamber pressure are also included for each experimental case (Figs. 5.18 -5.29). The variation shown between the pressure plots also gives an indication of the general applicability and reliability of the model.

The pressure plots can be analysed further since Kamimoto gives a value of bmep for each experimental condition and Aoyagi provides several imep values. A realistic estimate of imep and bmep can be obtained from the model since pressure is followed between inlet valve closing and exhaust valve opening. Table 5.5 (over) gives all experimental and calculated values and also includes peak pressure data from the pressure plots (Figs. 5.18-5.29) to facilitate the analysis. A discussion of the development work and results follows.

Case	Condition	bmep (MPa)		Peak pressure (MPa)	
		Simulation	Experiment	Simulation	Experiment
Standard*		0.261	0.344	4.92	4.57
Swirl	0	0.258	c. 0.344	4.93	4.83
	2	0.242	0.394	4.91	5.20
	4	0.232	0.336	4.98	5.14
Injection timing	25° bTDC	0.221	0.359	5.43	6.15
	15° bTDC	0.258	c. 0.344	4.93	4.73
	5° bTDC	0.276	0.294	4.10	3.51
Injection pressure	17 MPa	0.261	0.304	4.92	4.64
	25 MPa	0.265	0.314	5.48	5.33
Load	$\phi = 0.67$	0.305	0.416	5.27	4.86
	$\phi = 0.34$	0.165	0.140	4.13	4.18
Bowl shape (deep)	$\phi = 0.67$	0.339	0.485	5.49	5.42
	$\phi = 0.34$	0.182	0.162	4.16	4.65

Table 5.5 - Comparison of calculated and experimental bmep and peak pressure

---

* swirl = 0, injection @ 15° bTDC, injection pressure 17 MPa, $\phi = 0.5$, shallow bowl, gas oil

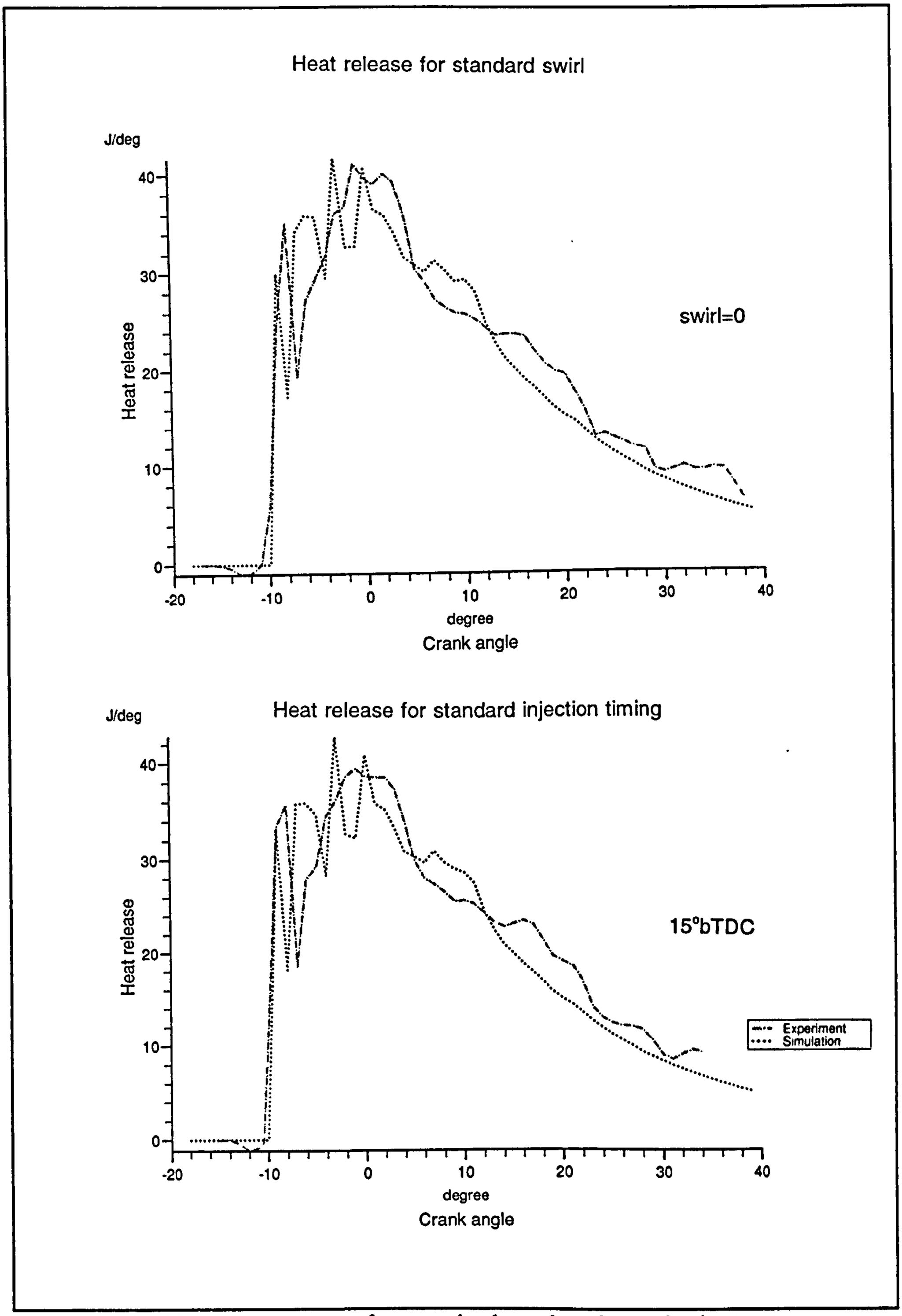

Figure 5.12 - Heat-release rates for standard swirl and standard injection timing

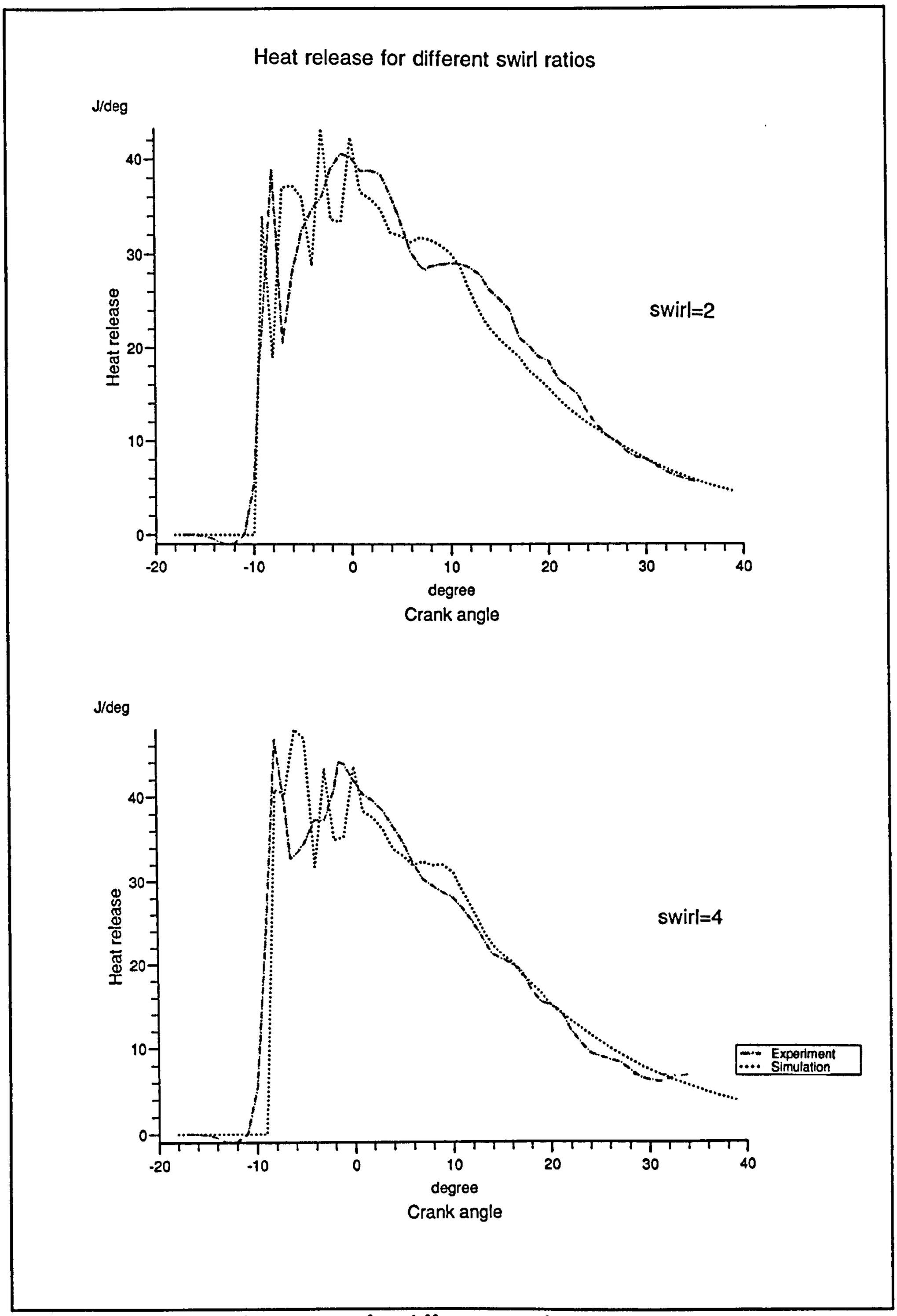

Figure 5.13 - Heat-release rates for different swirl ratios

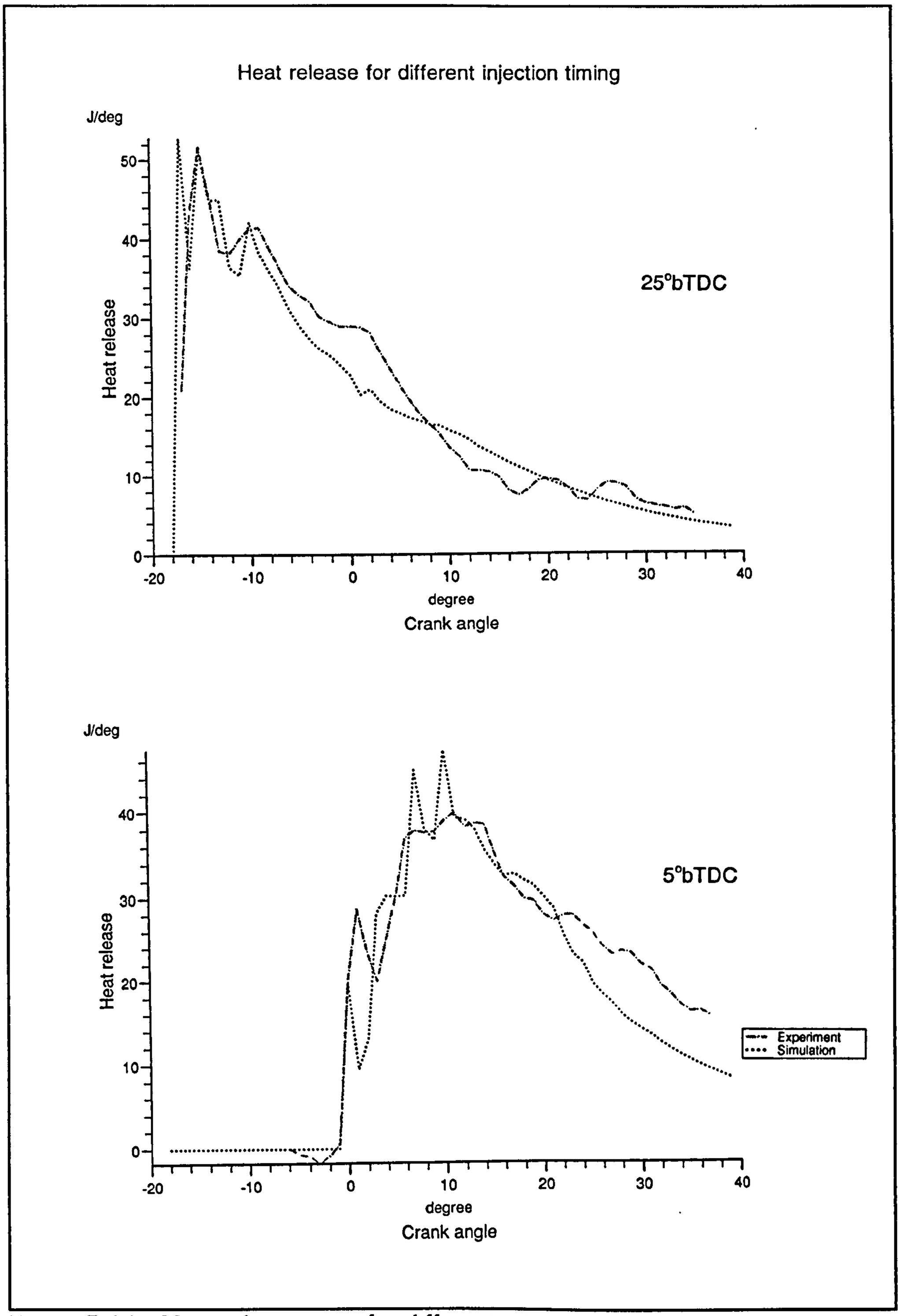

Figure 5.14 - Heat-release rates for different injection timing

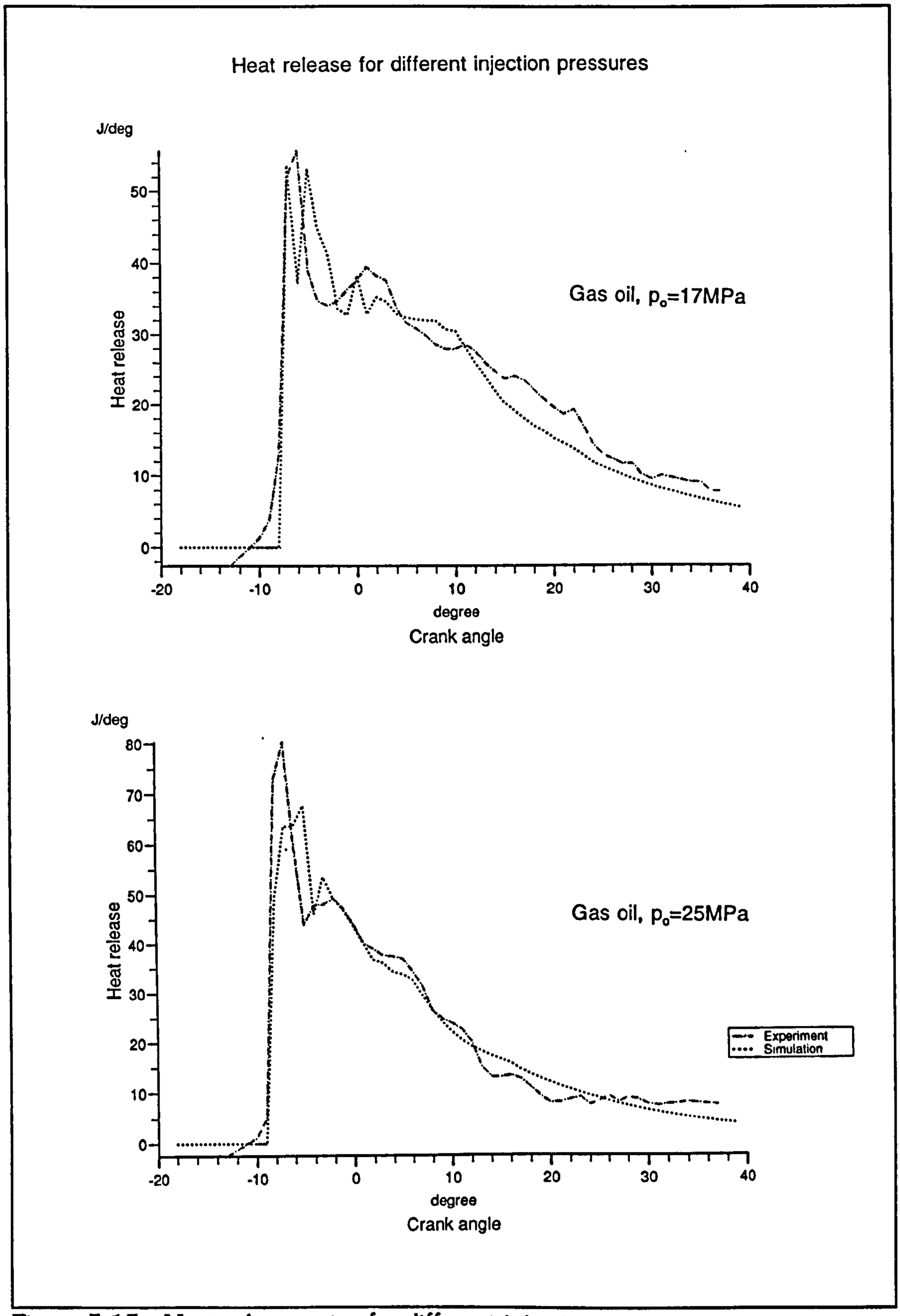

Figure 5.15 - Heat-release rates for different injection pressures

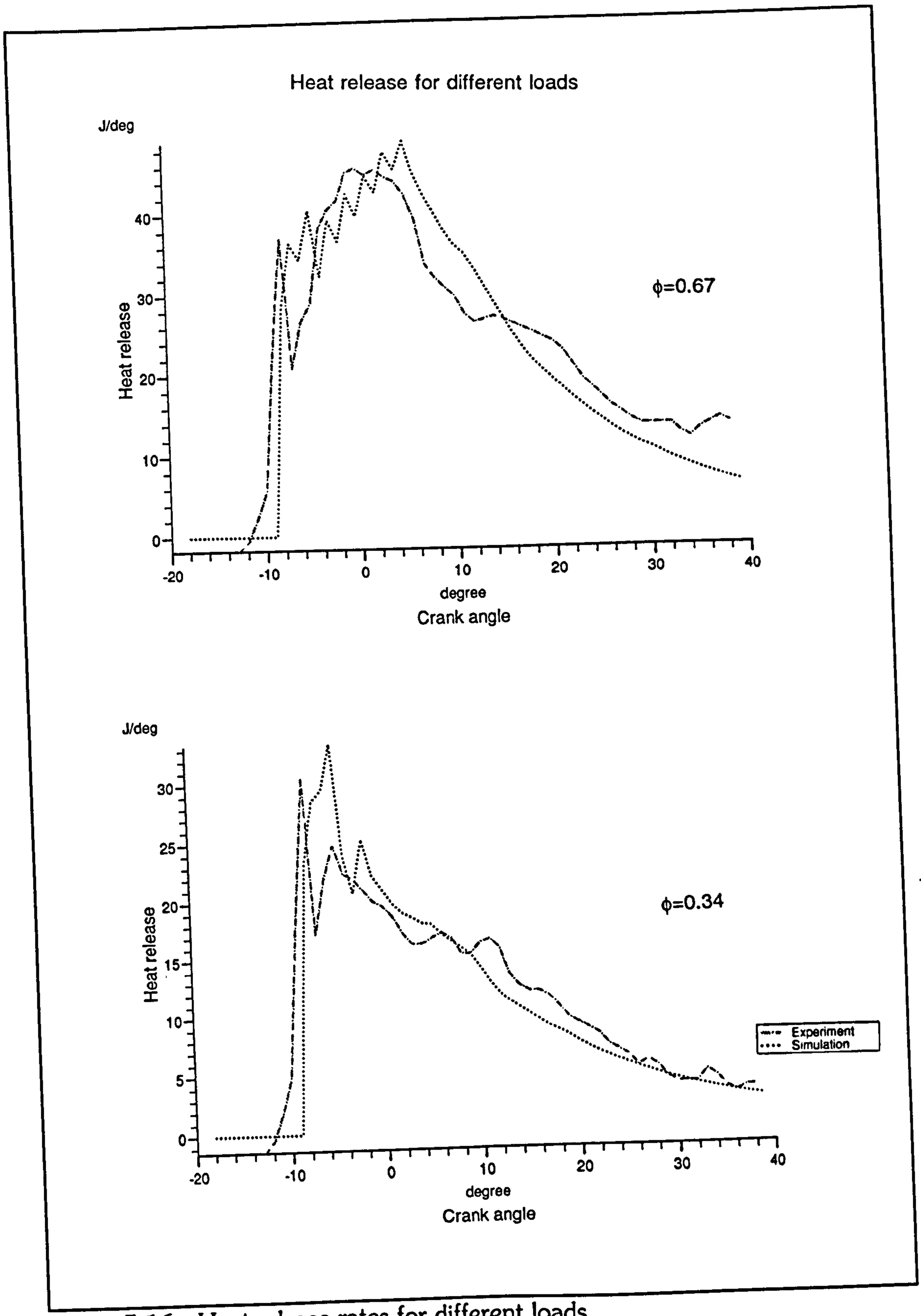

Figure 5.16 - Heat-release rates for different loads

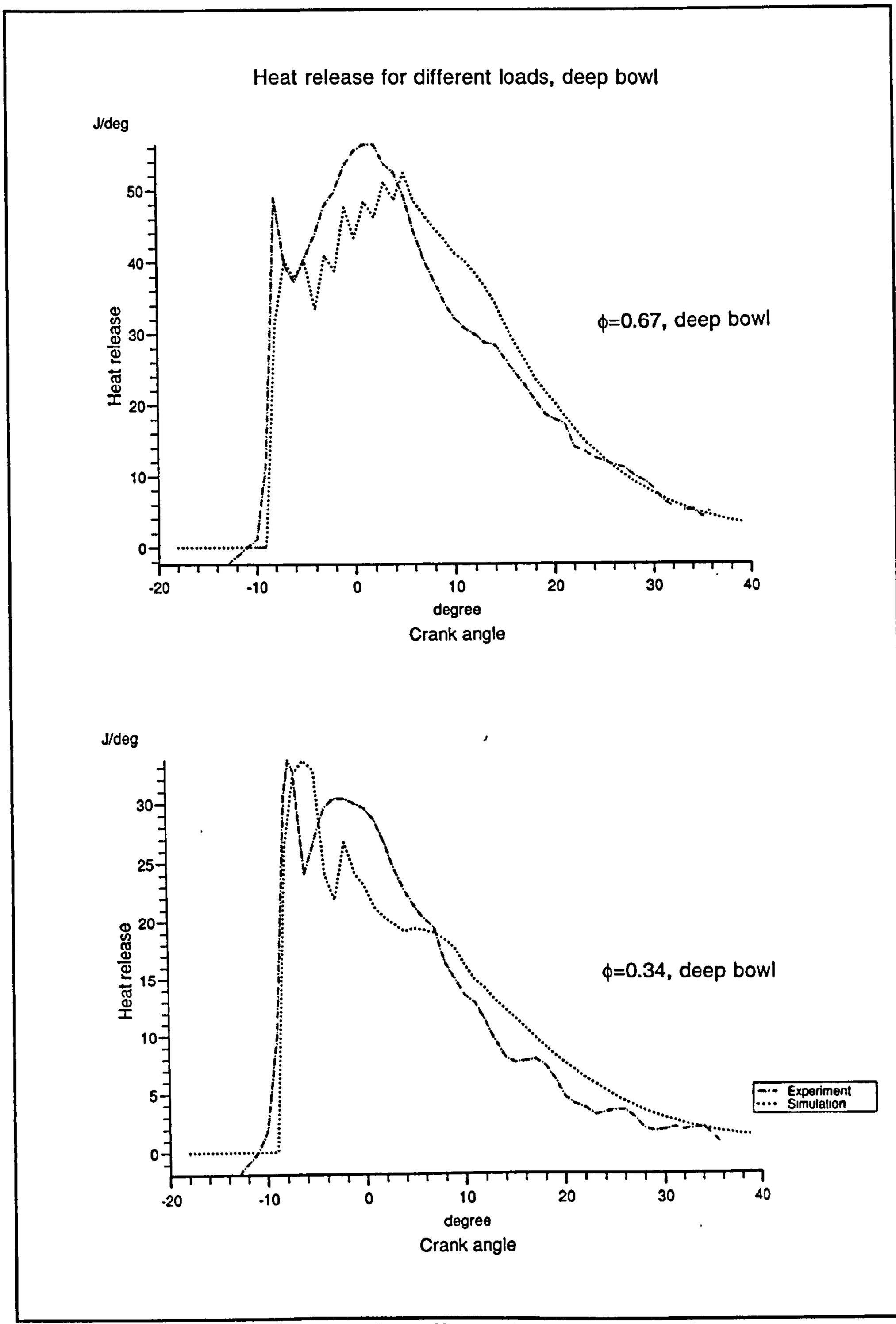

Figure 5.17 - Heat-release rates for different loads, deep bowl

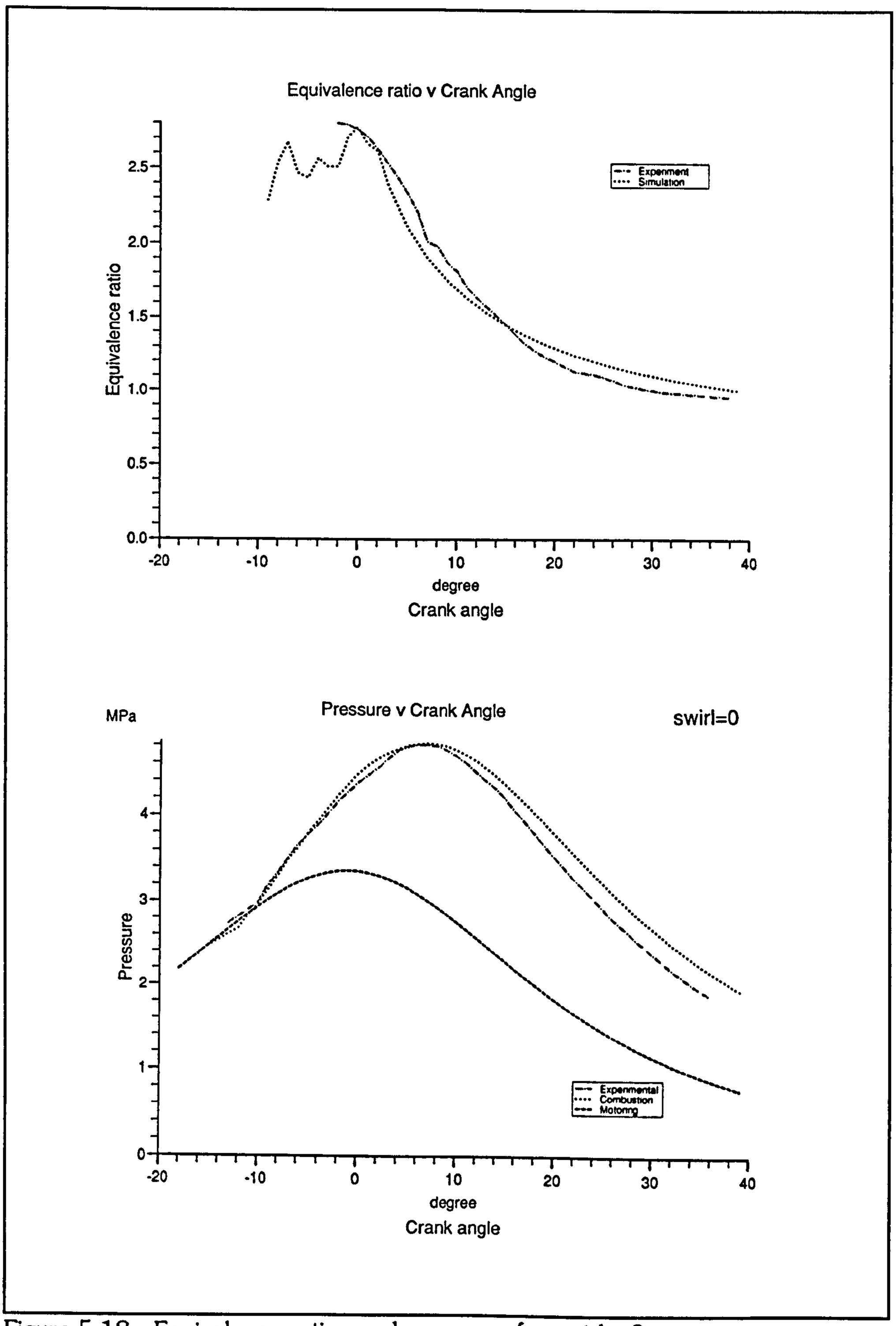

Figure 5.18 - Equivalence ratios and pressures for swirl = 0

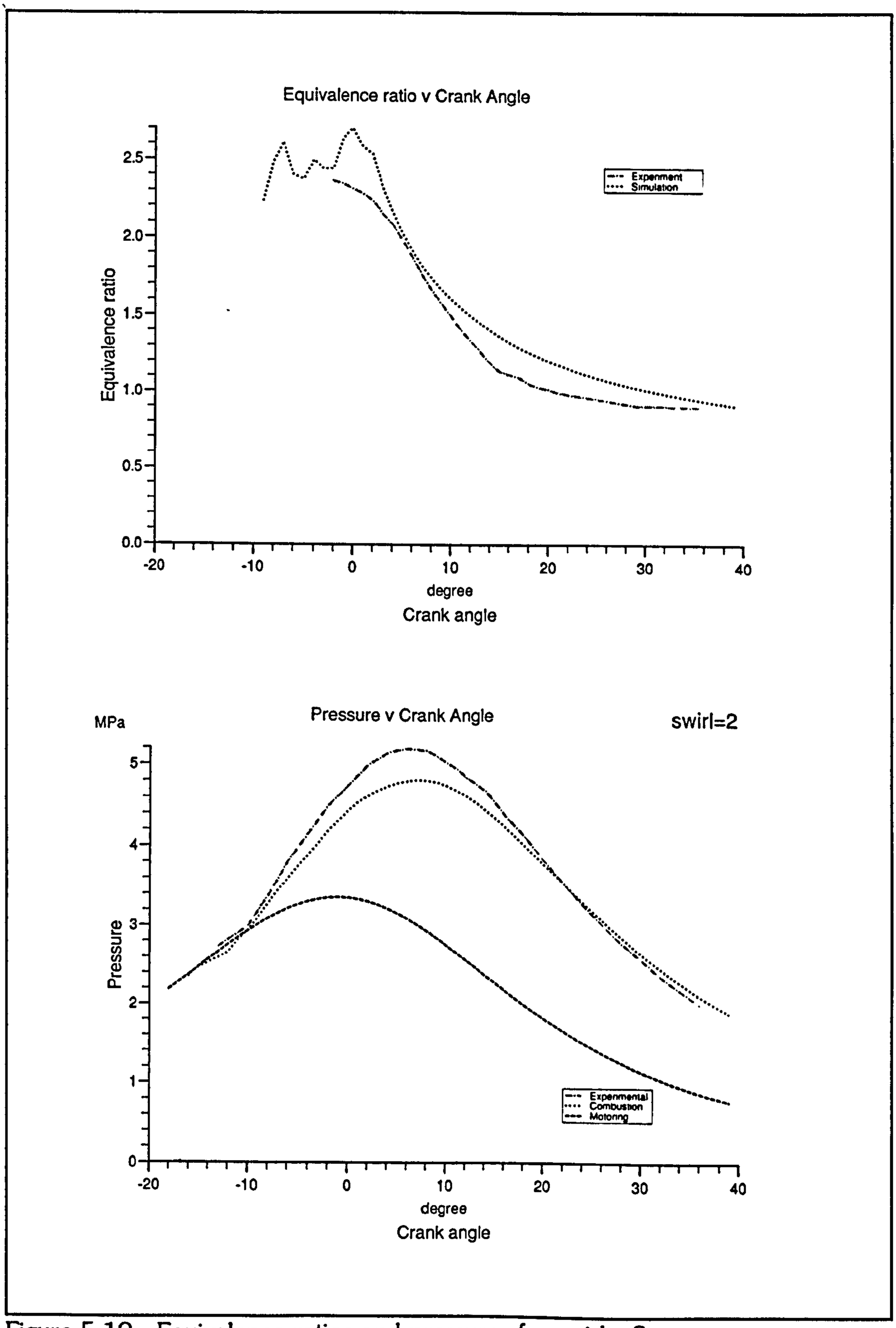

Figure 5.19 - Equivalence ratios and pressures for swirl = 2

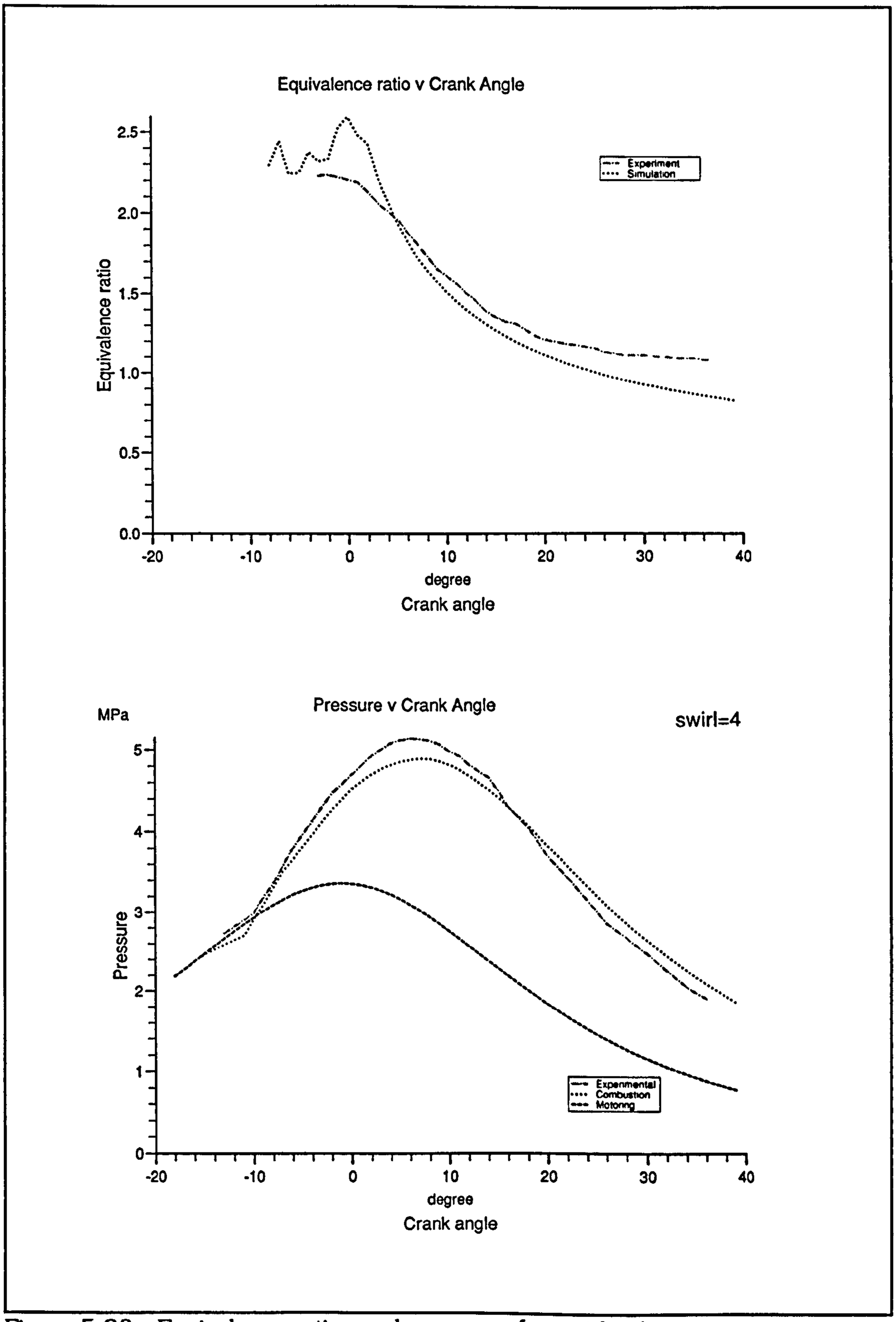

Figure 5.20 - Equivalence ratios and pressures for swirl = 4

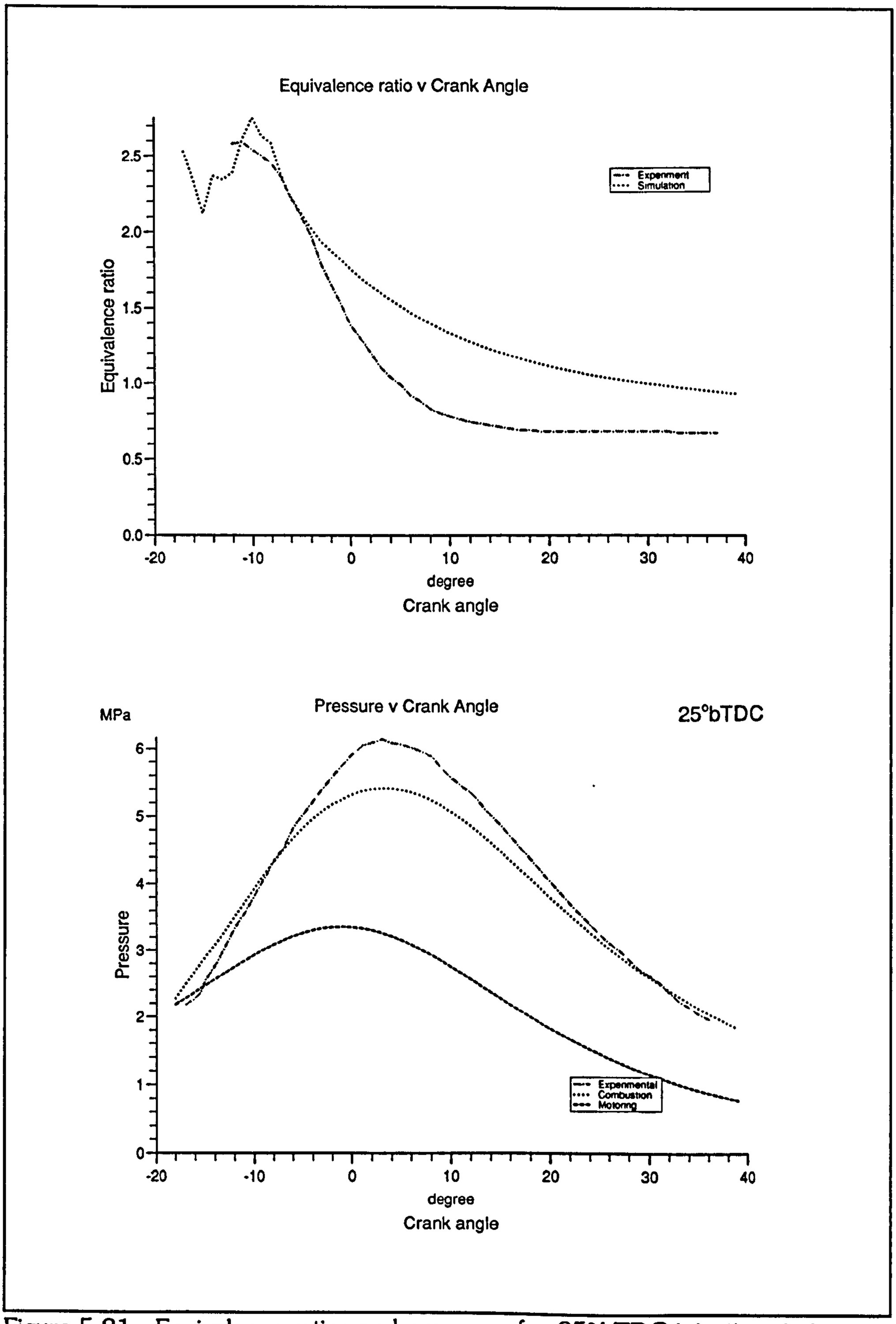

Figure 5.21 - Equivalence ratios and pressures for 25° bTDC injection timing

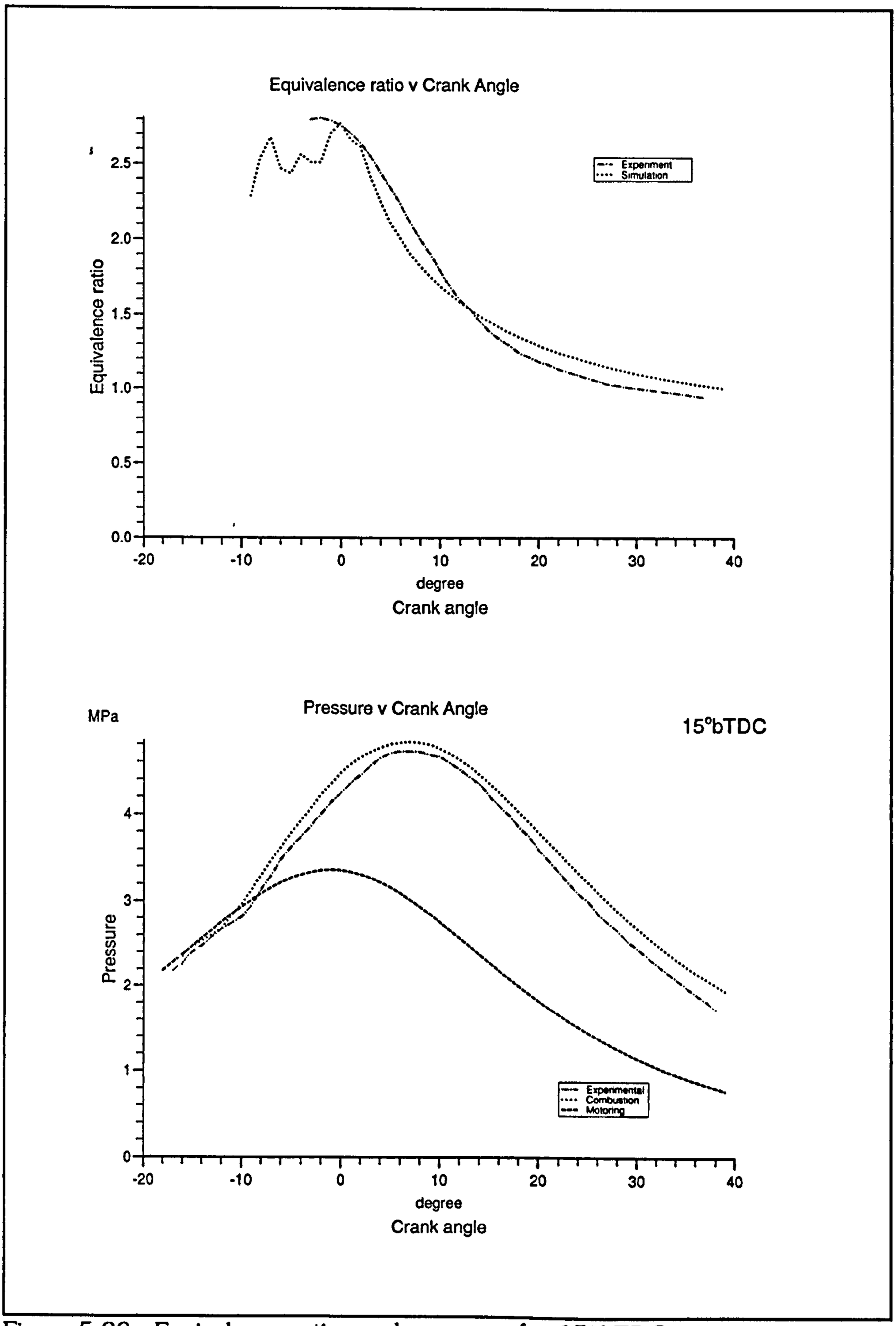

Figure 5.22 - Equivalence ratios and pressures for 15° bTDC injection timing

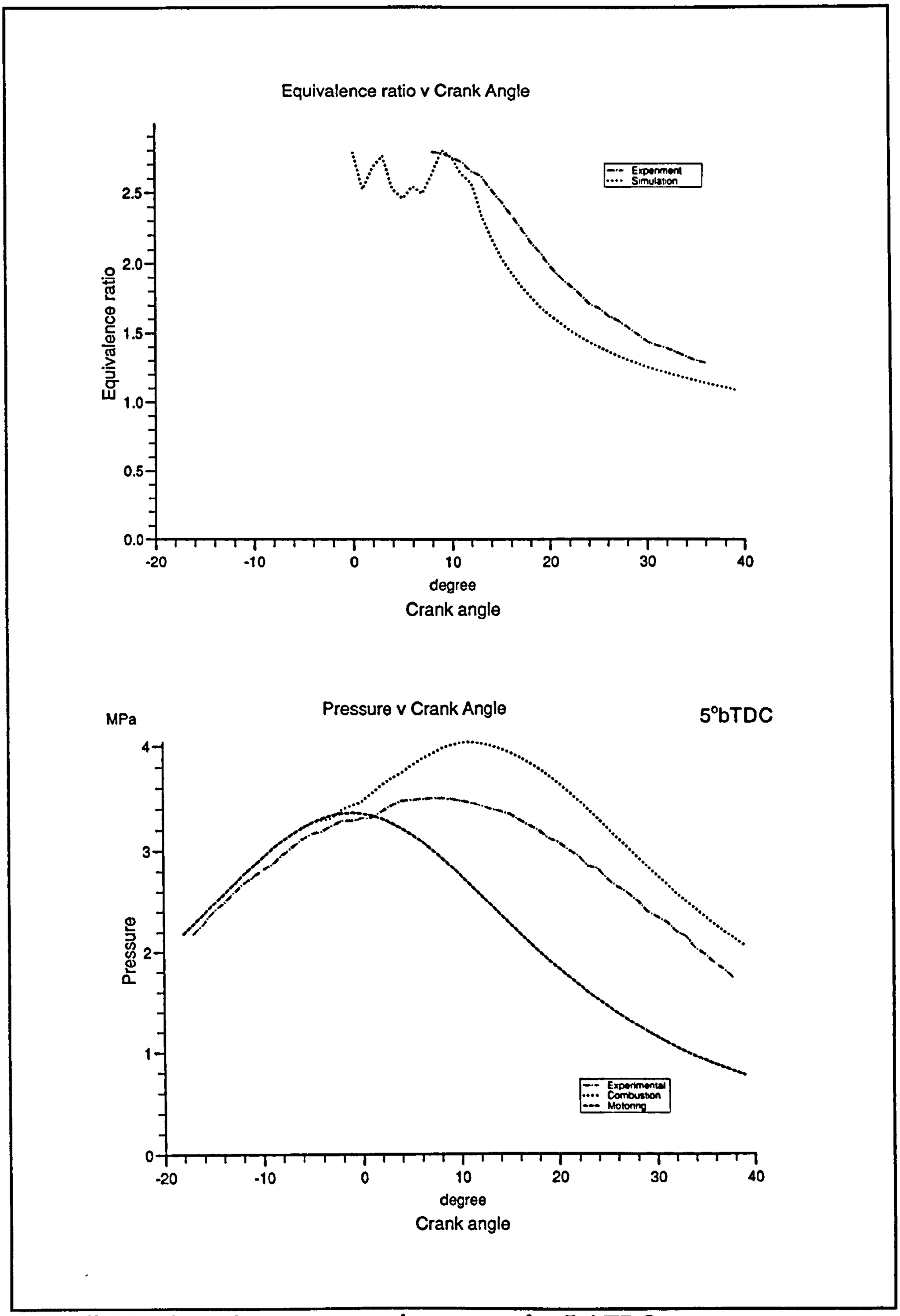

Figure 5.23 - Equivalence ratios and pressures for 5° bTDC injection timing

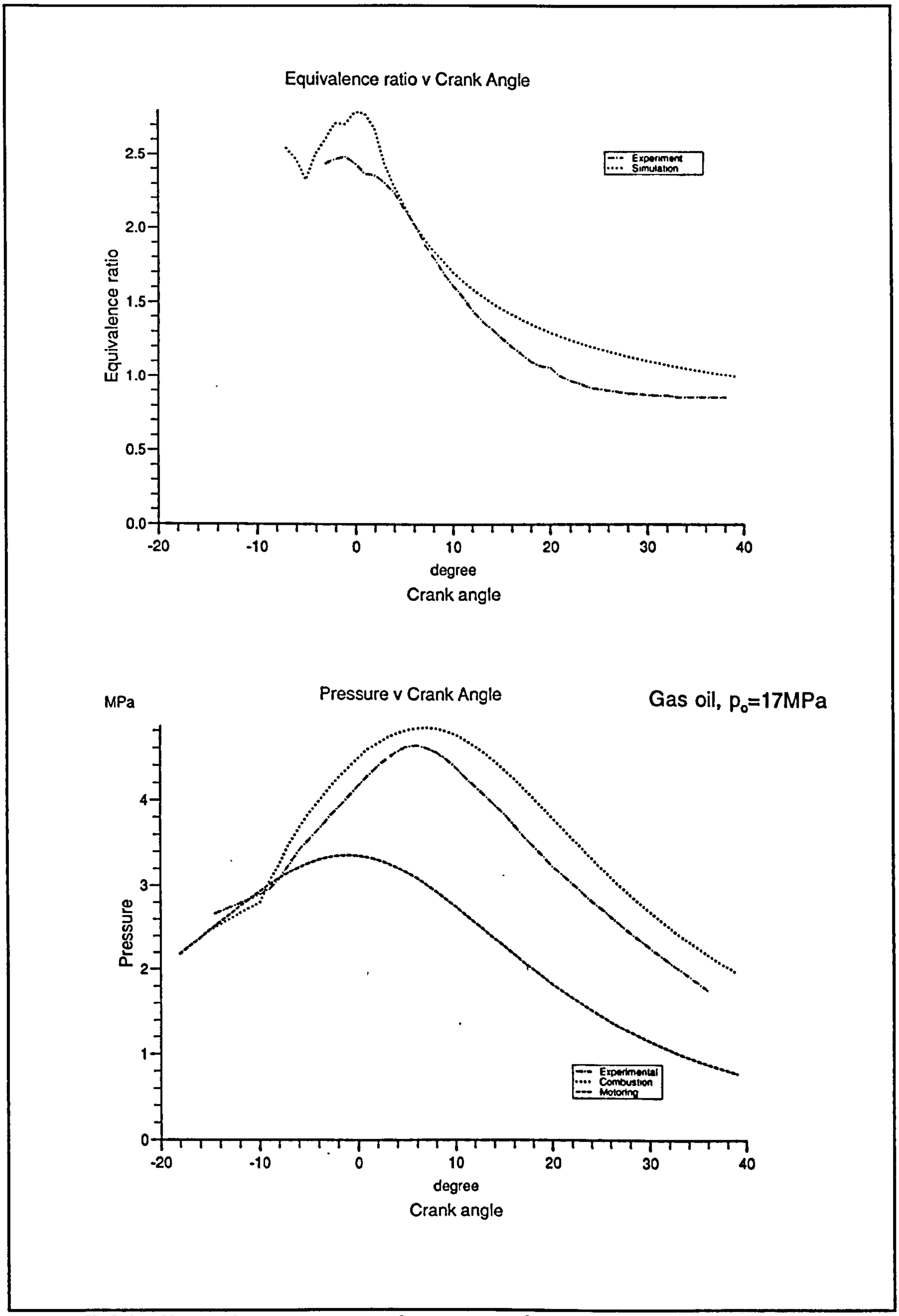

Figure 5.24 - Equivalence ratios and pressures for 17 MPa injection pressure

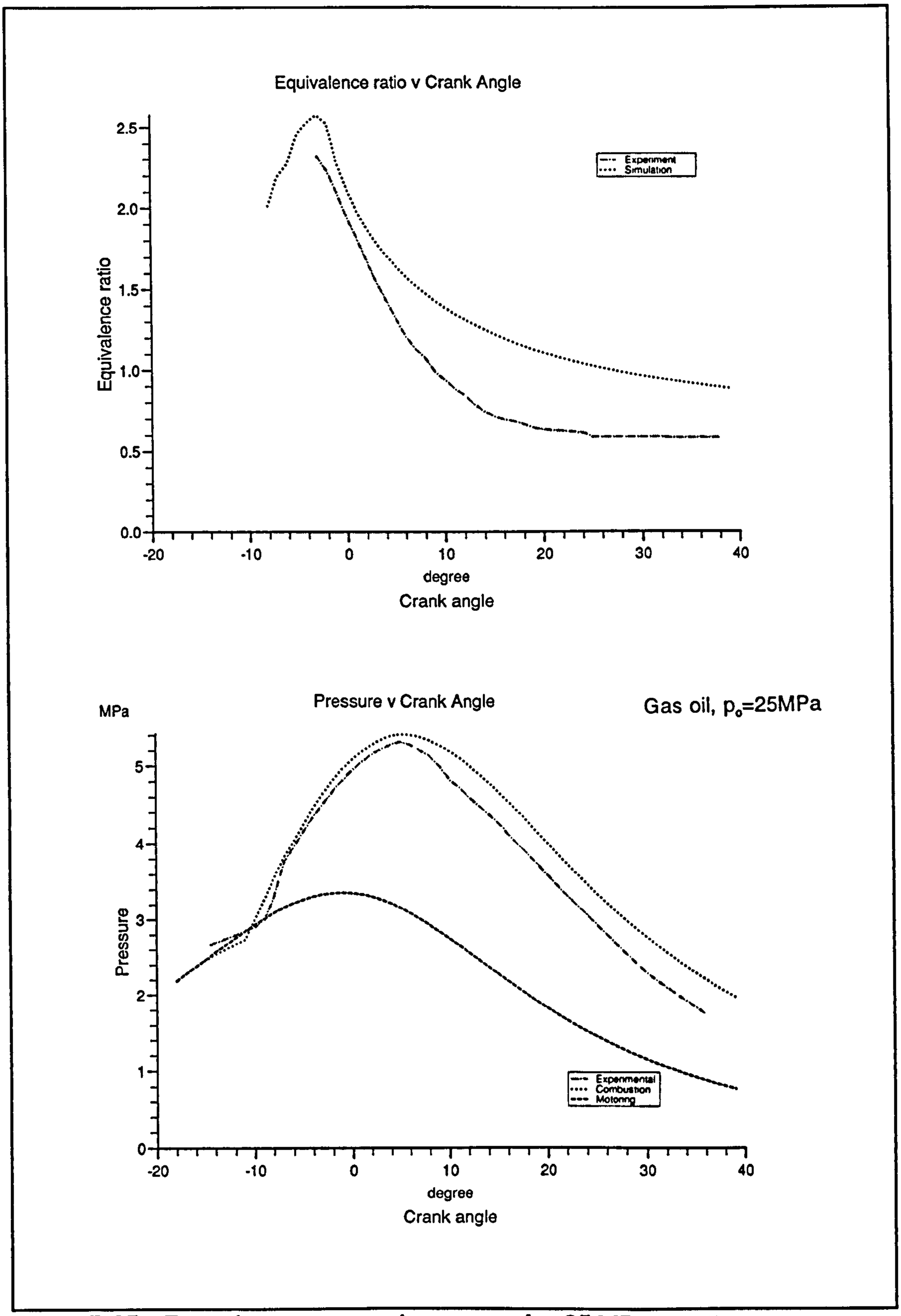

Figure 5.25 - Equivalence ratios and pressures for 25 MPa injection pressure

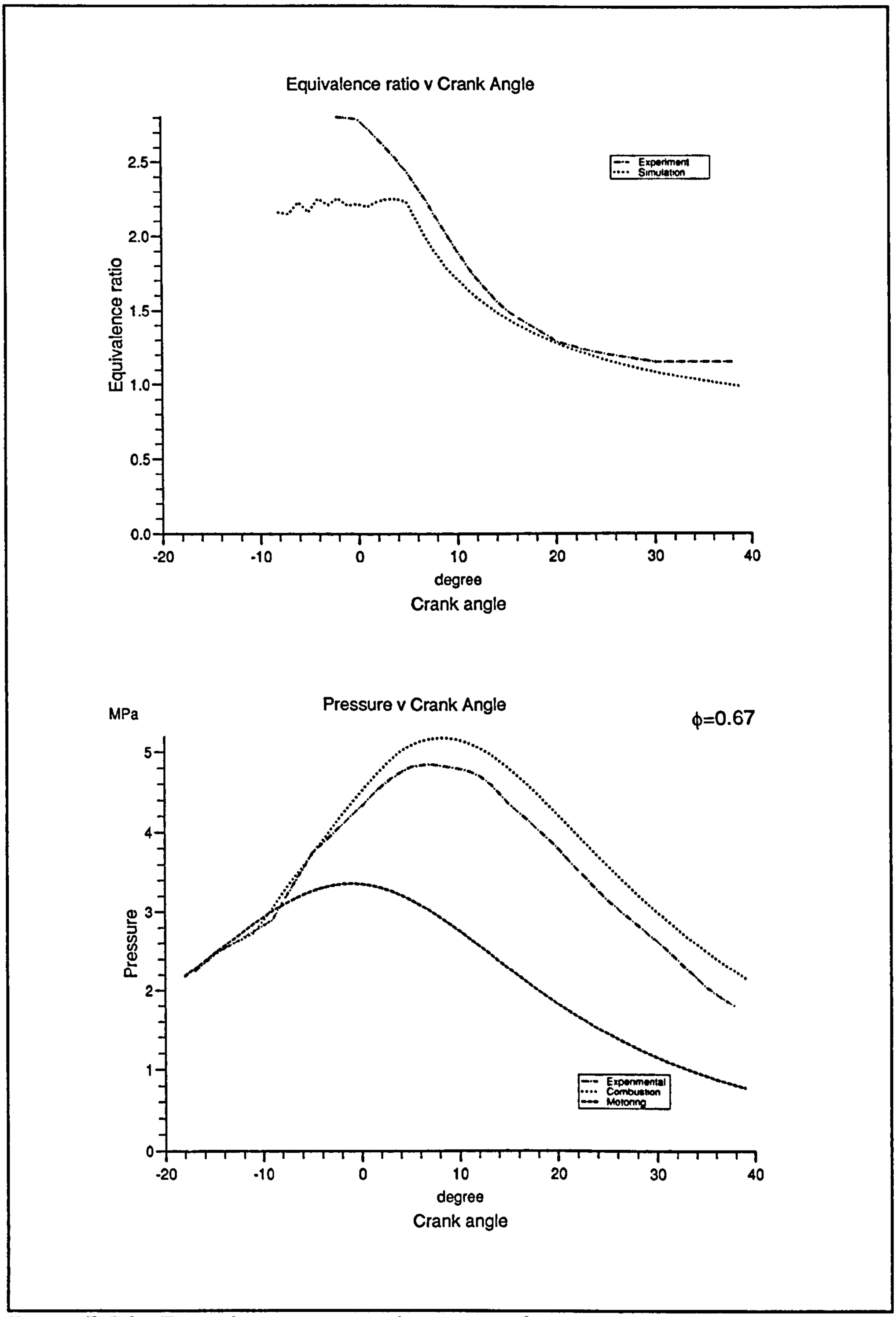

Figure 5.26 - Equivalence ratios and pressures for $\phi = 0.67$

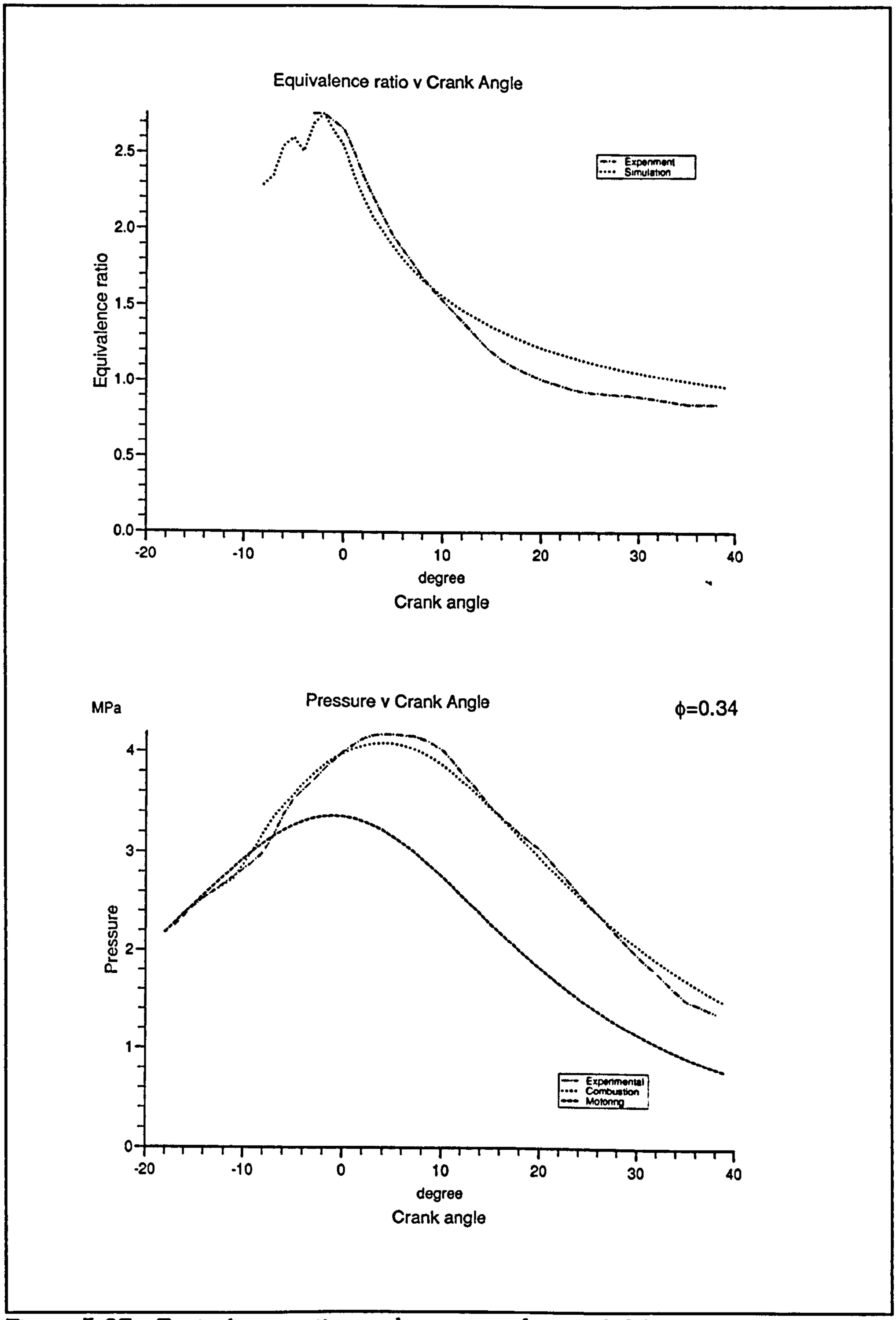

Figure 5.27 - Equivalence ratios and pressures for $\phi = 0.34$

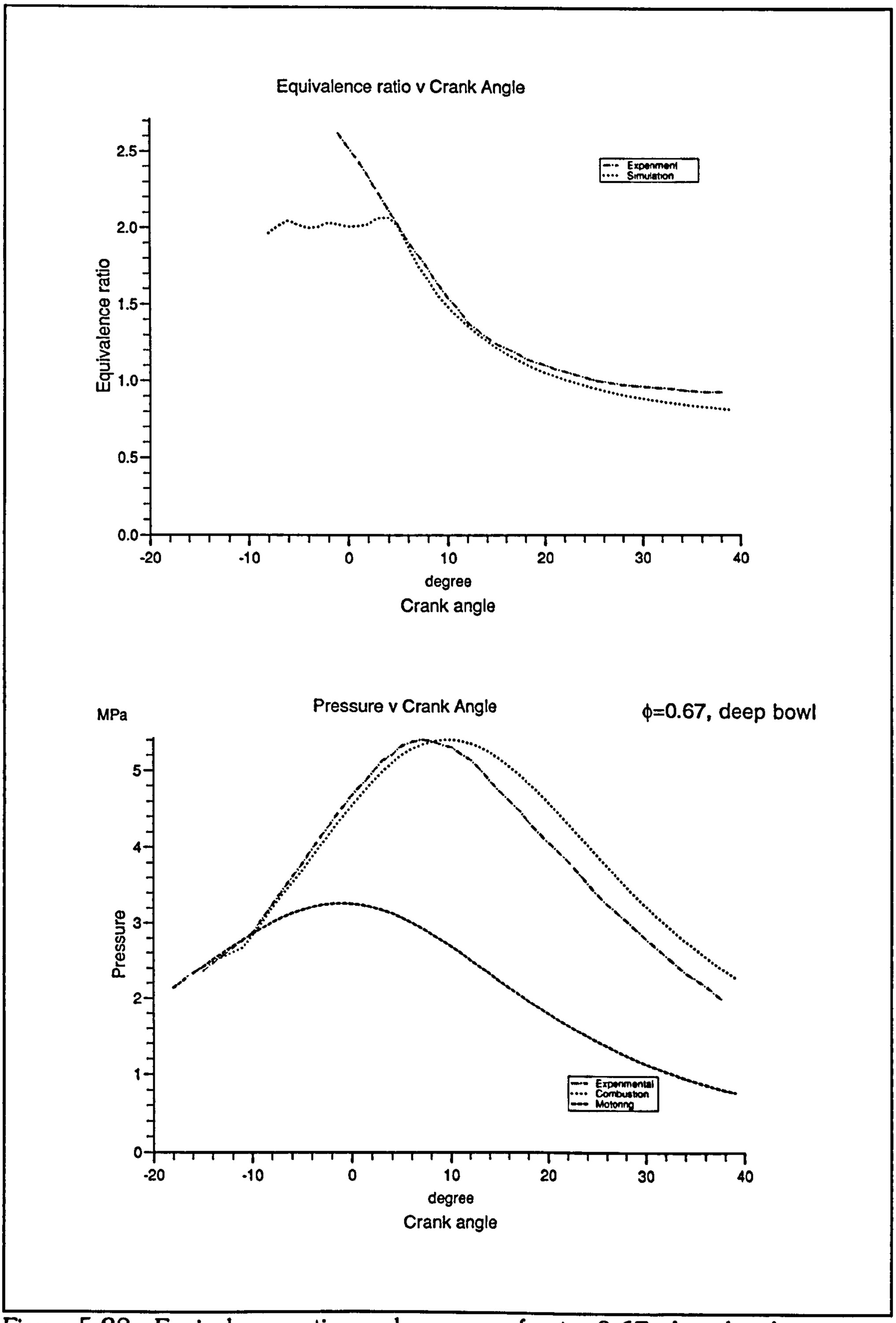

Figure 5.28 - Equivalence ratios and pressures for $\phi = 0.67$, deep bowl

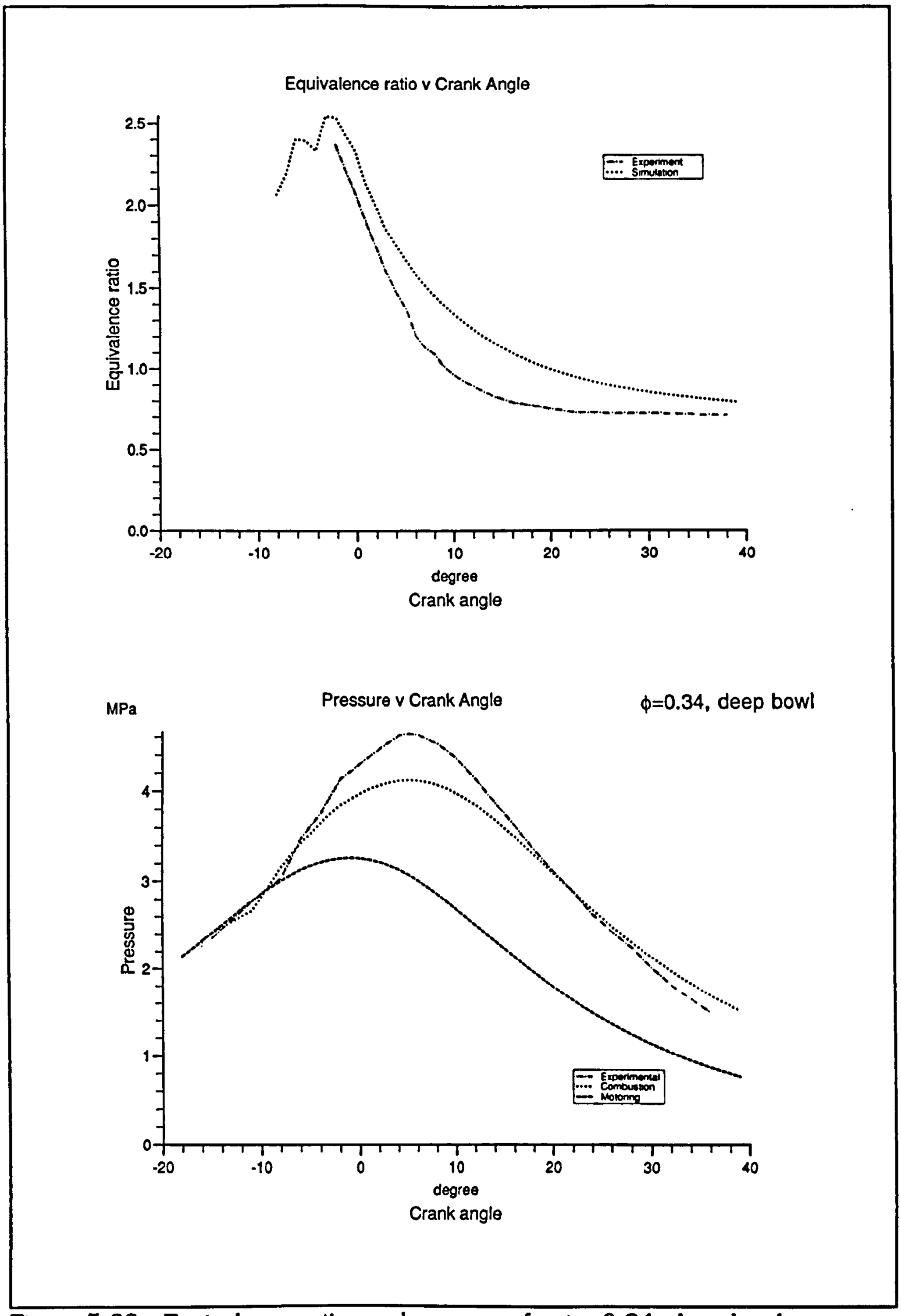

Figure 5.29 - Equivalence ratios and pressures for $\phi = 0.34$, deep bowl

5.1.4.2 Development work and discussion

In this section, the selection of adjustable model parameters is considered and the results of the parametric study are analysed.

Having selected suitable air-entrainment model constants and obtained satisfactory predictions of entrainment rates, the main adjustable parameters affecting heat-release rate are those pertaining to the combustion rate. For the first of these, the amount of premixed mixture which is allowed to burn during the initial combustion, no value is given in the literature. The second is the constant used in Magnussen's burn-rate expression (equ. 4.92). Magnussen has provided a theoretical value of this constant and at first sight there seems to be no justification for changing it. However, initial work showed that whatever the value of the premixed burn factor, the diffusion-burning rates were too low during the early phase. If air-entrainment rates were artificially increased to compensate, late diffusion burn was too rapid and the diffusion-burn phase was completed too early. Also, when Magnussen's eddy dissipation concept has been applied in CFD models, a variety of constants have been used in order to obtain satisfactory burn rates (see section 4.4.3.4 - Diffusion burning). Therefore it is not unrealistic to allow some modification to the value of the Magnussen model constant.

The mixing burn-rate equation (equ. 4.90) can be re-expressed in a form analogous to 4.93 by setting $\nu = \nu_{turb}$ and assuming that γ is small. This gives a theoretical value of A equal to 12.9, which can be compared with values used by others[94,112,223,262,274] in the range from 1 to 20. In this study, the effect of setting $\dot{m}$ using a constant value or a further multiplicative factor was investigated. Considering all cases of the parametric study, the best balance was obtained using a premixed burn factor of 0.27 and multiplying the combustion rate by 50. The plots illustrated in this chapter were obtained with $\dot{m}$ actually set to a constant value of 15000, but this choice gives a virtually identical result. The universality of these constants is questionable, but it was beyond the scope of this work to extend analysis to different engines. However, the premixed burn factor is probably the least well-established and it is encouraging to see that satisfactory results have been obtained for a range of operating conditions including fuel of widely different cetane numbers (n-tridecane - 81, gas oil - 57).

Having established the combustion-rate constants, some further model deficiencies could be identified. The simplest was that for the high-load cases ($\phi = 0.67$), the heat-release diagram was dominated by premixed spikes corresponding to the ignition of each successive set of zones. The effect is pronounced in this case due to the extended period of fuel injection, nearly double the value for the case of 25 MPa injection pressure. The solution was simply to double the number of axially-injected sets to eight in this case alone.

The second problem was more serious. In the variable swirl cases, combustion was much too rapid due to an excessive rate of air entrainment. The latter is a strong function of swirl, since the penetration velocity is reduced according to Hiroyasu's recommendation (equ. 4.12). The effect of using lower swirl ratios for the air-entrainment model was investigated, and surprisingly the best match of the heat-release diagram was obtained when swirl was set to zero. This implies that swirl has a much smaller effect on entrainment than suggested by Hiroyasu. The satisfactory performance of his own model[126,127] is hard to explain. Therefore, the effect of swirl on air entrainment was neglected, though it was maintained as an input to the heat-transfer and turbulence calculations.

However, even with this modification, the model does not show the correct trends in bmep or maximum pressure. The pressures are reduced in the case of swirl ratio equal to 2, rather than increased. The reason for this can be deduced from the plots of measured air-entrainment rates[159]. These show that as the swirl ratio increases, the initial rate of entrainment does in fact increase, but that during combustion it drops to a lower level than was obtained in the absence of swirl. The cause of this behaviour can be understood by referring to the turbulent entrainment equation Hoult and Weil (equ. 4.1). This equation simply relates the entrainment rate to the velocity difference between the jet and the swirling air. Under higher swirl conditions, this difference is progressively reduced as the jet becomes deflected and begins to follow the motion of swirling air. The momentum-based entrainment equation due to Hiroyasu used in the current work (equ. 4.21) cannot account for this effect and an attempt to implement the Hoult and Weil expression met with little success (see sections 4.1.3.2 and 4.1.4). The multizone spray model used is not well-suited to use of the latter expression, and a major change in the spray model would probably be necessary to achieve a better representation. This was not possible in the time available.

The plots shown in Figs. 5.12 - 5.29 were obtained with identical sets of model parameters, apart from the justifiable use of more axial sets for the high-load case. Overall the agreement with experiment is very good for all parameters, and excepting the swirl case mentioned above, the correct trends in variation of peak pressure are shown. However, there are some remaining discrepancies, and consideration is now given as to whether there are any underlying systematic errors, with a particular focus on pressure.

Table 5.5 earlier in this section shows that the calculated bmep values are generally lower than the measured data. Peak pressures on the other hand, are more often higher than lower, but are a better match with experiment. However, both low-load cases contradict these generalisations, with significantly higher calculated bmep values even though the peak pressures are lower. These examples serve to illustrate that there is no obvious correspondence in the discrepancies between measured and calculated values of bmep and overall pressure. A clue to the explanation lies in the fact that the low-load cases show the poorest match of bmep. This implies that insufficient allowance is being made for the overhead of frictional work, i.e. a lower mechanical efficiency should have been used. This is confirmed by Heywood who states that the coefficient drops from about 0.9 at full load to 0.75 at part load[116]. If realistic bmep values are to be obtained, a way of representing this variation in the model must be determined.

In view of this uncertainty, the calculated cylinder pressures alone give a better measure of model performance (the bmep includes an extra efficiency factor). The biggest discrepancies here are illustrated by the case of variation in injection timing. For the 25° bTDC injection start, the calculated pressure is too low at the peak, whilst for 5° bTDC, calculated pressure is always too high. Careful examination of the experimental curves reveals part of the explanation - the rise in pressure in the 25° bTDC case begins about 2° CA after the heat release has taken off, and longer ignition delays give higher pressures. Perhaps the pressure trace was not measured simultaneously to the heat-release estimate (which has been used to determine the end of the ignition delay period). The flame-zone equivalence ratio gives a further insight. For 25° bTDC injection timing, the degree by which the diffusion-phase equivalence ratio is over-estimated matches the greatest of all the cases studied, while for 5° bTDC the opposite is true. The reason for this may be a consequence of some inaccuracy in the turbulence or squish models. Further work will be necessary to determine and resolve the problem.

5.1.5 Conclusions

Overall performance of the combustion model compares reasonably well with typical experimental measurements. The most noticeable difference is the higher power output obtained from the simulation. This is directly related to calculated pressure values, which are slightly higher than those of the experiment. This in turn is a consequence of over-estimated zonal temperatures. Accurate estimation of temperatures is extremely difficult (see explanation in section 5.1.2) and there is little scope for improving this aspect of the simulation. Generally, a good match between calculated and experimental values of the flame-zone equivalence ratio is obtained, resulting in satisfactory predictions of heat release.

In-cylinder measurements show a very small variation of equivalence ratio across the spray. This is contrary to the model predictions and the bulk of experimental evidence from elsewhere. The model could be modified in a simple manner to represent this behaviour, but in view of the otherwise satisfactory performance, there seemed insufficient justification for doing so.

Finally, model combustion-rate parameters have been selected which give satisfactory predictions of heat-release rate for every condition of the parametric study. This resulted after initial work had revealed a serious over-prediction of air-entrainment rate in the swirl case when Hiroyasu's penetration correlation was implemented in its original form. Much improved behaviour was shown when the swirl effect on entrainment was neglected, though the trend in peak pressures was still incorrect. This is due to a weakness in the method of calculating the air entrainment rate. Hiroyasu's momentum-based approach cannot represent the reduction in entrainment following large deflection of the jet and a major change in the spray model would be necessary to obtain accurate predictions in all cases. Otherwise, peak pressures were generally well-represented and the overall thermodynamic performance of the model has been shown to be satisfactory.

5.2 SOOT MODEL RESULTS

This section presents the results of the soot-modelling work. As described in chapter 3, five soot-formation expressions and six soot-oxidation expressions were chosen for study in the context of the simulation. These are listed in Table 3.11 of section 3.5. The equations and constant values are detailed in Appendix B. The performance of the models is demonstrated in terms of predictions of soot formation and oxidation rates and also the calculated soot mass, which is known as the yield. Validation is made using empirical data, particularly the measured yields and exhaust values given by Kamimoto[159], together with the results of other comparative studies. Model sensitivities are examined and applicability in different combustion model types is discussed. The section is divided into two halves: in section 5.2.1, the model results are presented and described and the main discussion is give in section 5.2.2. Final conclusions are summarised in chapter 6.

Most of the comparative analysis which follows is made on the basis of predicted rates, though the yields are also examined in specific cases. This strategy is followed in order to simplify the analysis, since yields vary according to the expressions used and there are many possible combinations of soot formation and oxidation rate. However, two sets of expressions are normally used together: the formation and oxidation expressions proposed by Hiroyasu, and the Tesner formation and Magnussen EDC oxidation expressions. The standard case used for the yield predictions is the Hiroyasu expression pair, since these expressions may be calibrated to give a realistic estimate of the yield. This value is then used as a basis of all other calculations of oxidation rate, with the exception of the Magnussen EDC rate which generally uses the yield set according to the joint Tesner-Magnussen model. The use of a common soot yield is important because all of the oxidation expressions include a soot-concentration term.

The soot calculations have a significant effect on the combustion-model predictions. In the model cases examined, empirical data shows that up to 30% of the fuel carbon may exist in the form of soot[11]. Thus, an important part of the heat release is due to the formation and oxidation of soot. Also, the predictions of thermodynamic state are also strongly influenced by the sooting processes because the radiative heat loss is very sensitive to soot concentration. Therefore, to provide a uniform basis for comparison, the Hiroyasu-expression yield has been used in all cases illustrated in this thesis.

5.2.1 RESULTS

5.2.1.1 Hiroyasu soot model

The Hiroyasu expressions are the most popular of those applied in diesel emission modelling and the results obtained from this model are examined first. The yields and rates obtained for the standard case of the experimental data-set are shown in Figs. 5.30 & 5.31. Following Kamimoto, the yield is expressed as a percentage of the total number of moles of gas and the carbon-to-hydrogen ratio is assumed to be three to one[348]. The Hiroyasu expression pre-exponential constants used in these cases were chosen to give average in-cylinder and exhaust levels matching the Kamimoto data. This procedure is described further in the "Parametric study" results section below.

In-cylinder soot

Fig. 5.30 shows that during the main combustion period there is a considerable variation in yield between zones. This is followed by a progressive convergence towards the time of the exhaust valve opening. In fact, the convergence results from allowing some mixing between the zones, as described in Appendix F; the zonal yields obtained directly from the Hiroyasu expressions do not tend to converge.

It can be seen that there is a tendency for more soot to be formed in the zones injected later. This is in-line with expectations, since temperatures and pressures increase in early diffusion burning, whilst the oxygen concentration is reduced. Kamimoto presented plots of in-cylinder measurements[11] (Fig. 5.32), but these are not well-suited to validation of the zonal data. Most zones move through the measurement region (X = 19 - 39 mm) in less than ten degrees of crank angle, so only a small section of the zonal history can be traced. Perhaps more significantly, the engine spray impacts on the piston bowl at a radius of 36 mm (shallow bowl case), and reaches the chamber wall at 47.5 mm. The mixing and quenching occurring on impingement are not represented directly in the model. Nevertheless, a general increase in yield during the injection period is shown for the Kamimoto measurement region, as predicted by the model.

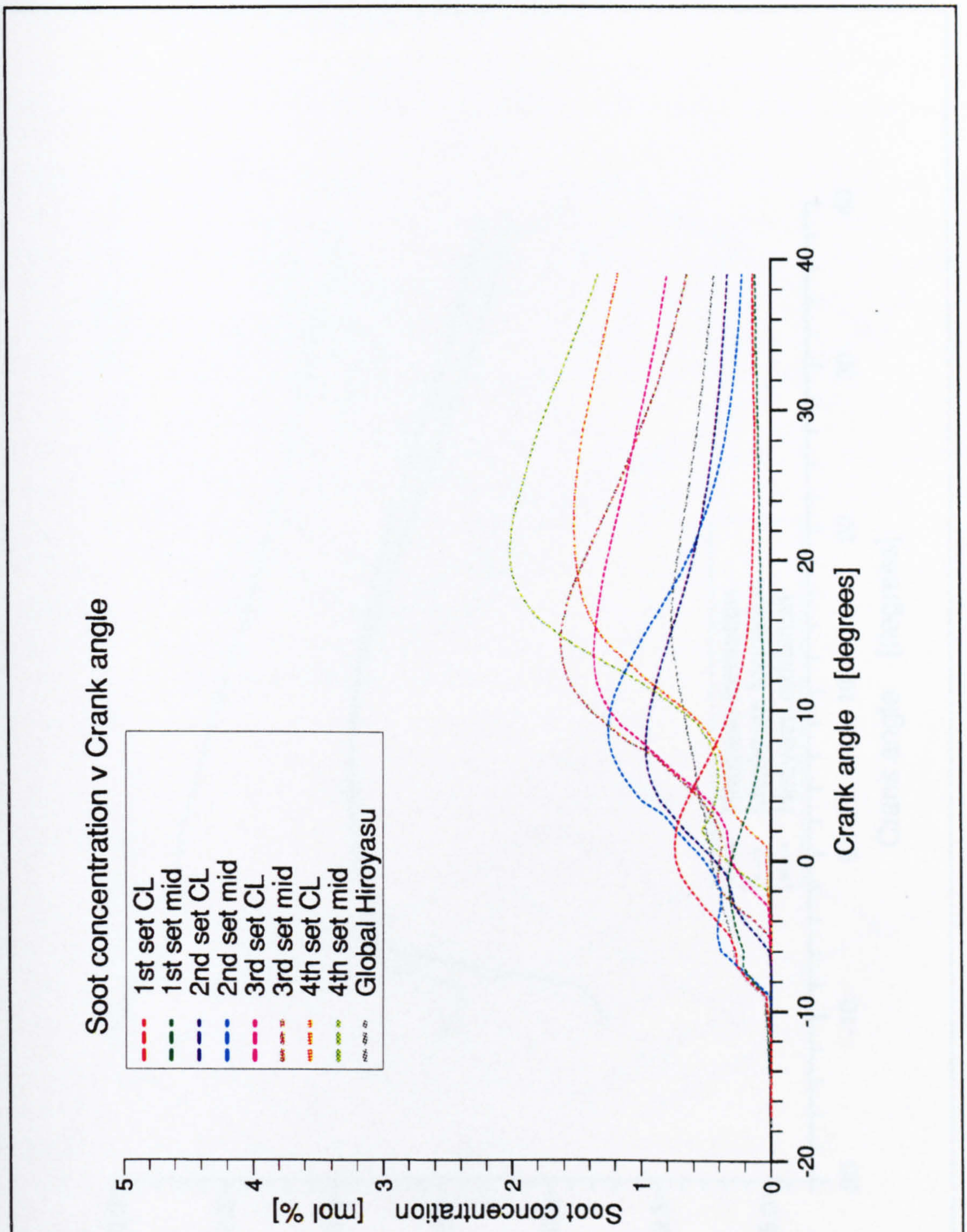

Figure 5.30 - Zonal soot concentrations from Hiroyasu model

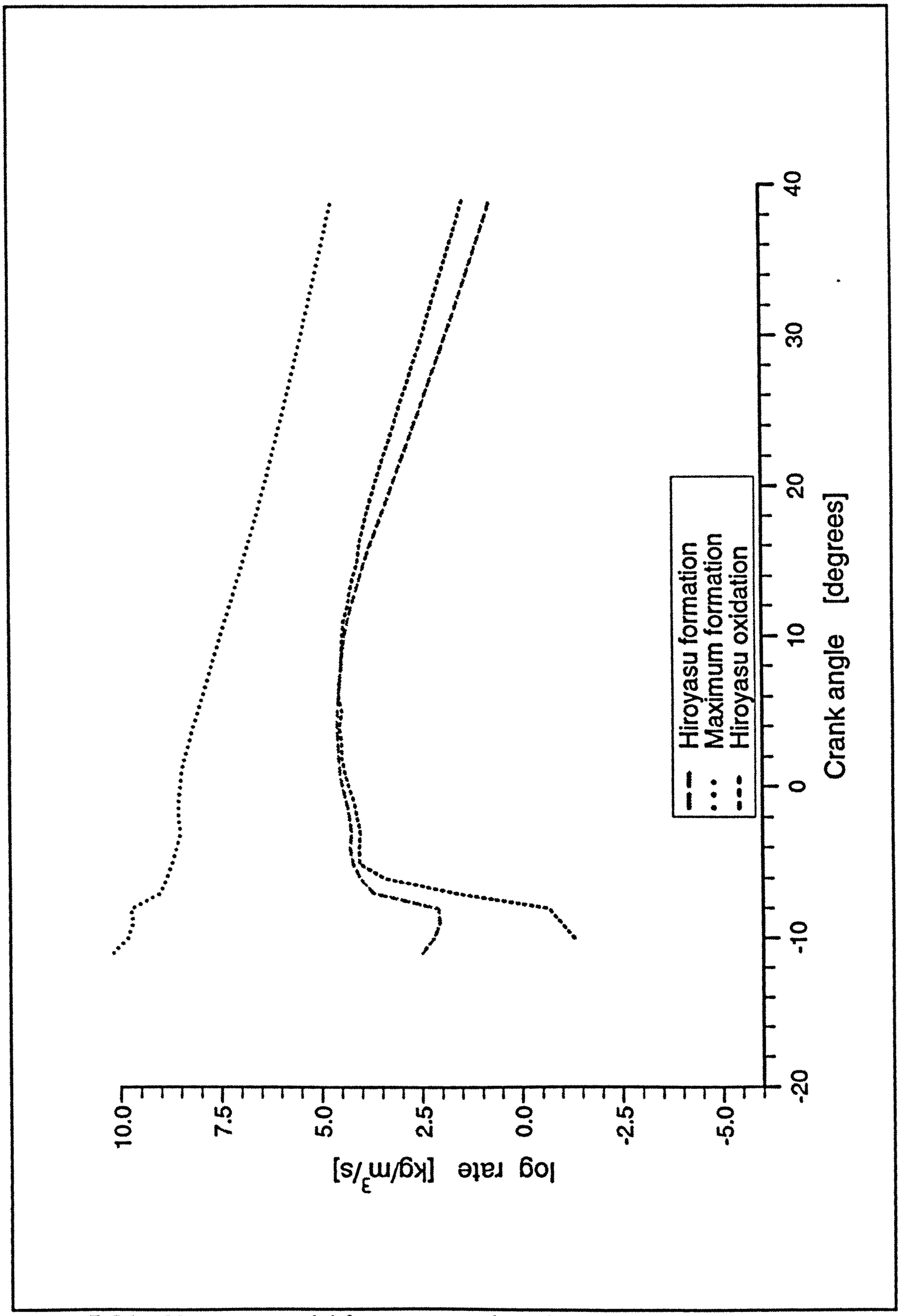

Figure 5.31 - Hiroyasu model formation and oxidation rates

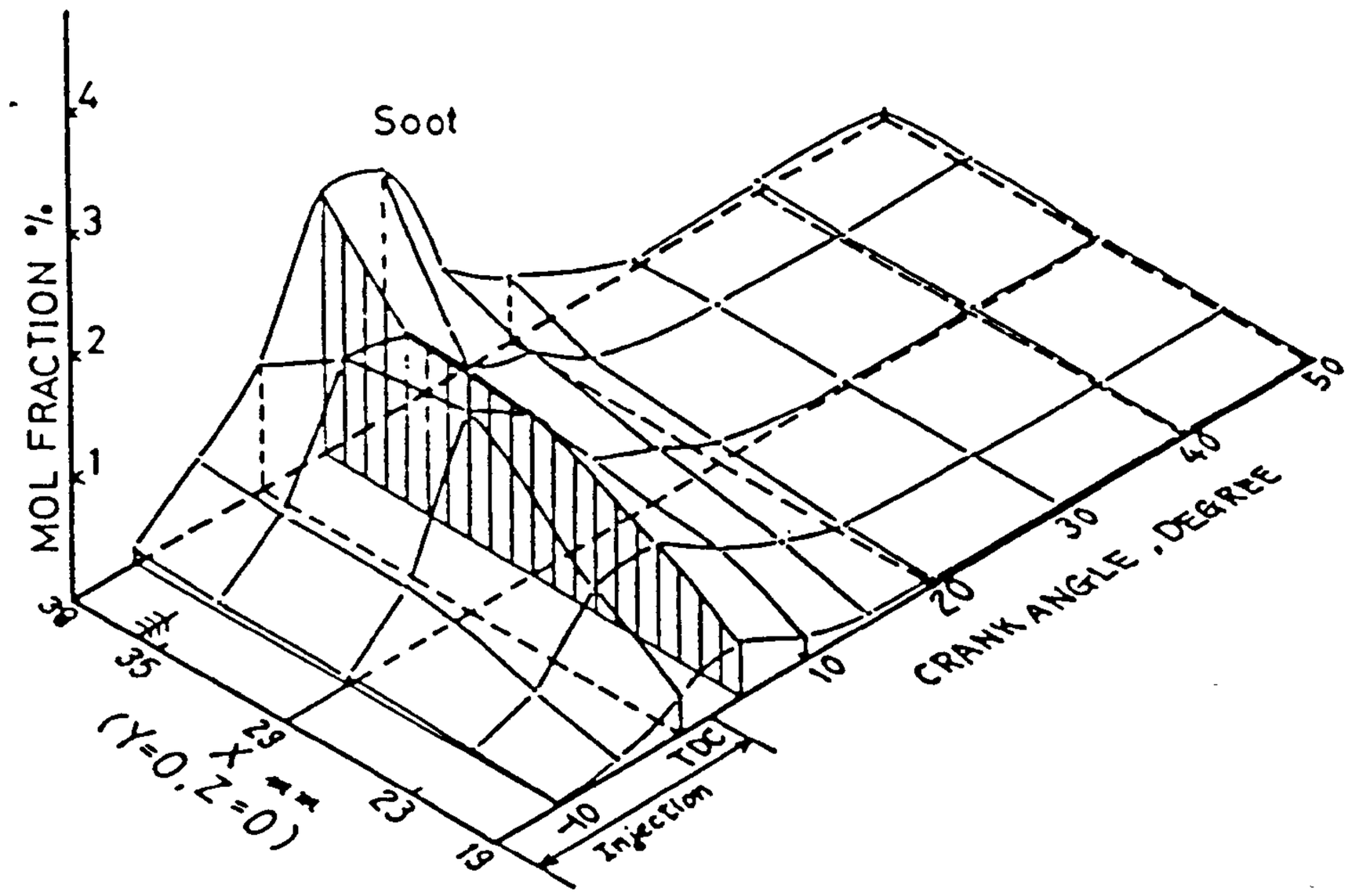

(a) - Along X axis

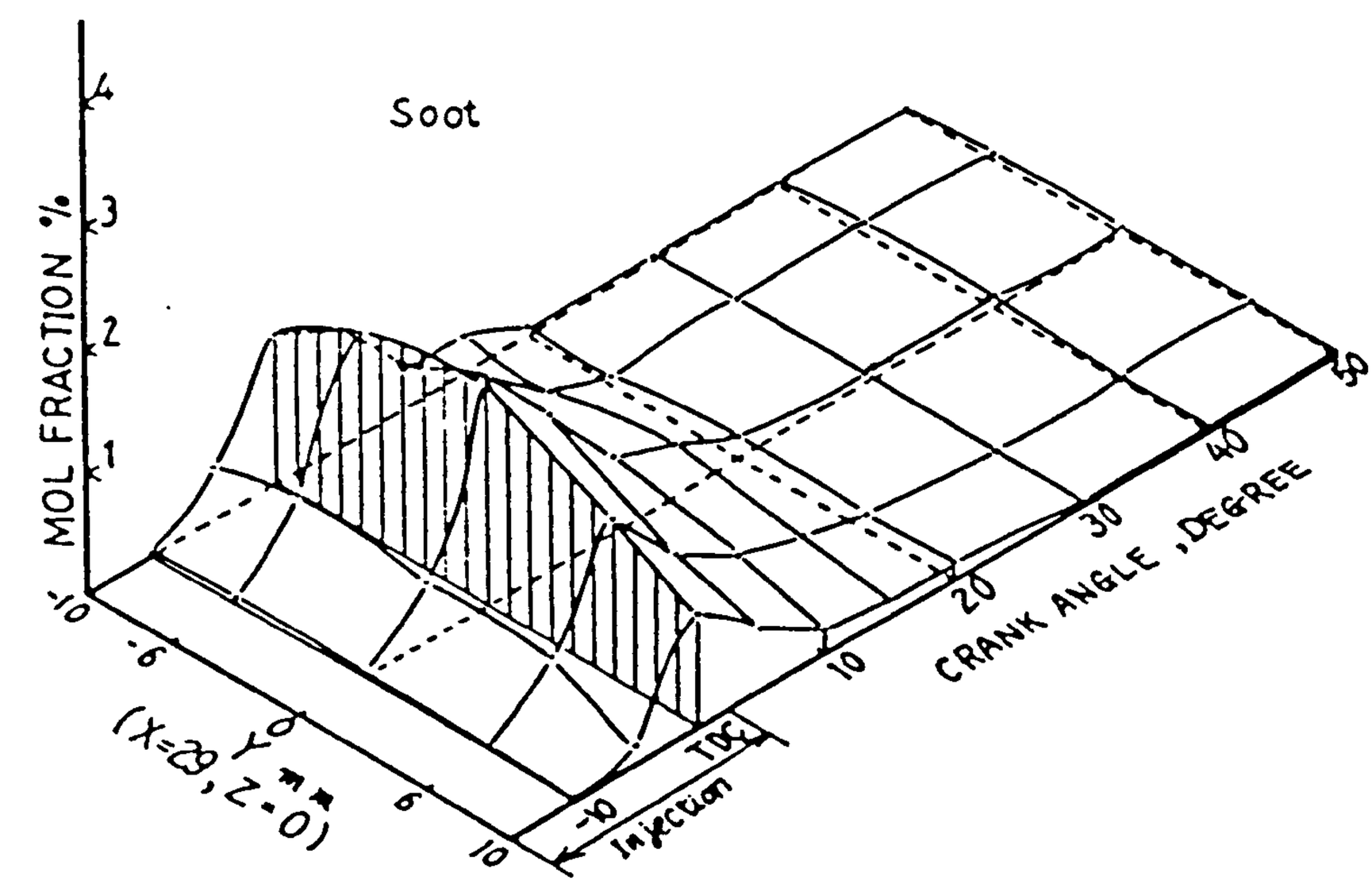

(b) - Along Y axis

Figure 5.32[11] - Experimental soot maps

Cross-jet variation is also hard to verify, due to the difficulty in estimating the model values relating to a single axial plane. At the measurement position X = 29 mm in Fig 5.32 (b) the zones injected at the rear of the spray have not begun combustion.

However, Fig. 5.30 shows that during the main combustion period, the variation in soot concentration between most sets is not much greater than the factor of two shown in Fig. 5.32 (b). The zones of the first set are an exception, showing a rapid fall-off to a value of about 10% of that of the later-injected sets. It is difficult to say whether this is borne out by the experimental data and in practice the phenomenon is likely to be obscured by wall-impingement effects.

The total yield calculated by the model begins to rise at 9° bTDC and peaks at around 17° aTDC. No chamber-average data is given for the experimental case, but the point data and soot maps indicate a peak at between 5 and 10° aTDC[11,230]. Kittelson[175] found peak concentrations at 20 - 30° aTDC in a very similar engine operating with a start of injection delayed by 5° relative to the standard Kamimoto case. However, assuming the accuracy of the Kamimoto data, there is a significant discrepancy with the model value. Unfortunately, it was found that there is very little scope for adjustment of the position of the peak within the constraints of matching the peak and exhaust concentrations. Thus, there is a weakness in representing in-cylinder soot; this is considered further in the discussion below (section 5.2.2).

The results from other in-cylinder studies provide further interesting comparisons. In particular, Kittelson's measurements[175] were made in a DI diesel similar to that of the Kamimoto study. The engine capacity was 0.70 l/cylinder compared with 0.78 l/cylinder in the latter. During the main soot formation period, the measured overall rate ranged from 0.26 to 0.30 g s^{-1} and was found to vary little with speed or load (1000-1500 rpm, $\phi = 0.4 - 0.7$). For the standard case of the Kamimoto data-set, the calculated net value is 0.36 g s^{-1} in the period between TDC and 10° aTDC (see Fig. 5.30). Thus, agreement is good (however, see the following section for details of the variation in predicted soot formation rates with operating conditions).

Finally, the calculated soot formation and oxidation rates are shown in Fig. 5.31 on a $\log_e$ scale. To a first approximation it may be said that these rates have been validated indirectly, since they correspond to the computed yield (Fig. 5.30) which

has been set to match empirical data. However, this assumes the ratio of the rate magnitudes is also correct, since it is possible to obtain accurate yield predictions from overall higher rates with a smaller discrepancy or lower rates with a greater difference between them. Kamimoto[160] has also computed oxidation rate from the in-cylinder measurements, assuming that the formation process has terminated by 15° after the end of injection. The peak values are about $1.5\,g\,cm^{-2}\,s^{-1}$ and allowing for use of a slightly larger particle size, this is about five times lower than the peak calculated rates (see Fig 5.44 in section 5.2.1.3). Thus, the model predictions are probably on the high side.

Parametric study

Table 5.6 presents the soot yield results obtained using the Hiroyasu expressions for all cases of the parametric study. Peak and exhaust predictions are given together with experimental values from the Kamimoto study. The Kamimoto values were converted from Bosch smoke number units using the Alkidas' formula for conversion to particulate concentration[6].

Overall, the experimental values show a greater variation than the model results. The experimental concentration range is $0.028 - 0.376\,g\,m^{-3}$, whilst the simulation results range from 0.115 to $0.363\,g\,m^{-3}$. More seriously, it is found that the predictions of parametric variation are generally poor. Only the variation with injection pressure and bowl shape are well-represented.

Besides exhaust values, it is important that in-cylinder levels are accurately described. Kamimoto provides in-cylinder measurements only for the standard case, and these were used as a basis for the selection of the pre-exponential constants in Hiroyasu's correlations (equs. B.5 & B.13 in Appendix B). In practice it was found that only a very narrow range of values gave acceptable predictions for any given case. Thus, the values chosen for default use were those which gave accurate values for the standard case, i.e. $A_{for} = 2$, $A_{ox} = 6 \times 10^{-6}$.

Case	Condition	Smoke (g m^{-3})			
		Simulation			Experiment
		Exhaust	Peak	Pk/exh ratio	Exhaust
Standard*		0.363	1.579	4.35	0.304
Swirl	0	0.346	1.459	4.21	0.304
	2	0.247	1.069	4.33	0.155
	4	0.181	0.697	3.85	0.292
Injection timing	25° bTDC	0.359	1.573	4.37	0.132
	15° bTDC	0.346	1.459	4.21	0.304
	5° bTDC	0.363	1.341	3.69	0.376
Injection pressure	17 MPa	0.359	1.573	4.37	0.292
	25 MPa	0.185	1.315	7.12	0.132
Load	$\phi = 0.67$	0.300	1.311	4.37	0.351
	$\phi = 0.34$	0.299	0.794	2.66	0.105
Bowl shape (deep)	$\phi = 0.67$	0.151	0.513	3.40	0.179
	$\phi = 0.34$	0.115	0.418	3.64	0.028

Table 5.6 - Comparison of calculated and experimental soot concentrations

Other useful comparisons are provided by the results of other in-cylinder studies (see chapter 3.2). For example, Kittelson measured peak and exhaust soot concentrations in a DI diesel engine similar to that of the Kamimoto study. Data for medium and high-load cases are shown in Table 5.7:

Case	Smoke (g m^{-3})		
	Exhaust	Peak	Pk/exh ratio
$\phi = 0.4$	0.06 - 0.12	0.47 - 0.79	6.6 - 7.6
$\phi = 0.7$	0.32 - 0.59	0.48 - 0.92	1.2 - 1.6

Table 5.7 - Exhaust and peak soot concentrations measured by Kittelson[175]

---

* swirl = 0, injection @ 15° bTDC, injection pressure 17 MPa, $\phi = 0.54$, shallow bowl, gas oil

Despite approximately equal peak values, the medium-load exhaust level is about five times lower than that for the high load. This trend is not shown by the simulation results.

It is possible that inaccuracies in the model predictions stem from deficiencies in the underlying combustion model. However, it has been established in section 5.1 that the predictions of the combustion model are good, with heat-release rates and the mean equivalence ratio in the spray showing a reasonable match with experiment. Only the swirl effect is poorly represented. Thus, it is unlikely that any deficiency in the overall description of the combustion process is the only source of error. The detailed predictions of in-cylinder processes must therefore be examined.

A good insight into the model deficiency is obtained by a careful analysis of the effect of load variation. Table 5.6 shows that almost identical exhaust values are predicted for the lowest and highest loading cases, though empirical findings show that exhaust smoke is very sensitive to load[116]. However, comparison of calculated zonal compositions and temperatures for the low ($\phi = 0.32$) and high ($\phi = 0.67$) load cases of the Kamimoto data-set reveal remarkable uniformities. Temperatures are very similar despite the higher pressure in the high-load case (see Table 5.5 and Figs. 5.26 & 5.28 in section 5.1.4). Overall zonal compositions are also found to be very similar during the main combustion period, such that the major difference between the two cases is simply the overall size of the jet. Since the temperatures and compositions are key inputs to the soot model expressions, it is not surprising that the predicted soot concentrations are very similar during the main combustion period. In the low load case, about twice as much air is mixed into the jet by the time the exhaust valve opens, but the slightly higher temperatures at the higher load enhance the oxidation rate overcompensating for this effect. Thus the resultant exhaust levels are almost identical.

In practice, though, other factors give rise to much higher soot levels in the high-load case. Since a greater amount of air is consumed by the fuel injected early in the combustion, fuel injected towards the rear of the spray encounters a much reduced availability of air. In fact, much of the mixture this fuel entrains will consist of combustion products from the burning of spray-tip mixture, and this naturally gives rise to greater soot-production rates. In the model, air entrainment is assumed to be entirely from the surrounding pure air zone, and no distinction can be made between zones injected early and late in the process. Transfers between spray zones are neglected, and the global mixing procedure (see Appendix F) has a similar

effect on composition whatever the jet size. Thus, there is a weakness in the model representation. However, to incorporate interzone transfers is extremely complex, since an iterative procedure is required. This adds greatly to the computational costs and implementation was considered beyond the scope of this work.

The crude representation of air entrainment no doubt affects the predictions of other parametric effects. For instance when the air-swirl ratio is increased, there will be a different distribution of entrainment, with more air from the surroundings being taken up at the rear of the jet. However, in this case the major cause of the discrepancy between predictions and measurements can be attributed directly to a combustion model deficiency. As described in section 5.1.4.2 the spray model used is unable to correctly represent the reduced entrainment when the jet is deflected. Thus, the lowest predicted soot concentration is for the high-swirl case, whilst the experimental data gives a minimum for the medium-swirl condition. The model reduction with swirl corresponds to a marginal increase in aeration of the jet which gives enhanced oxidation, whilst the experimentally observed increase in smoke at high swirl is due to the reduced air-entrainment rate during diffusion burning following jet deflection.

The remaining parametric effect which is not well-represented is that of variation of injection timing. The experimental variation shows a rapid reduction in smoke with injection advance, but this is not matched by the simulation values, which vary little. However, the measurements of air entrainment revealed a greatly enhanced rate with early injection, giving reduced average equivalence ratios in the jet (see Figs. 5.21 - 5.23). This behaviour is not represented in the model, and may be due to a steady reduction of air velocities and turbulence towards TDC.

Conclusion

The analysis of the parametric study results reveals the need for a more sophisticated spray model. In particular, the method of representing mixing between fresh charge and combustion products must be improved and the reduction in entrainment following large deflection of the jet must be accounted for. Other deficiencies may be due to the assumption of constant turbulent parameters and an inadequate description of bowl and wall impingement effects. Despite these difficulties, the results shown are encouraging because they indicate that, given a sufficiently detailed spray model, zonal-averaged information may be sufficient for the prediction of parametric trends.

5.2.1.2 Tesner-Magnussen soot model

This model represents the sooting process using a more detailed mechanism. It is also a popular combination which has been studied by various researchers[198,57,226]. The soot expressions are implemented within the framework of a unique partitioned thermodynamic structure, as described in Appendix B. The yields, particle number density and rates derived from the Tesner-Magnussen soot model are illustrated in Figs. 5.33 - 5.35 for the standard case of the experimental data-set.

Initially, the formation and oxidation rates are very similar in magnitude to those obtained using the Hiroyasu expressions (Fig. 5.31). Therefore, the soot concentration rises to a similar peak level, which is a good match with the experimental data. During this period, the model calculations indicate a rapid increase in the soot-particle concentration, as shown in Fig. 5.34. The calculated rate in this region is given in Table 5.8, together with several experimentally observed rates. Except for the Tesner and Xu data, these values refer to cylinder pressure and temperature conditions. Thus, the calculated rate is of the right order of magnitude.

Researcher	Combustion system	Peak concentration (10^{18} particles m^{-3})	Peak rate (10^{21} particles m^{-3} s^{-1})
Tesner[345]	Diffusion flame	1.1	1.0
Kontani[186]	DI diesel	0.40	0.24
Du[60]	IDI diesel	0.021	0.042
Xu[379]	DI diesel	0.0036	0.0021
Current work	DI diesel	0.10	0.076

Table 5.8 - Peak concentrations and formation rates of soot particles

After the early diffusion-burning period, the Tesner rate falls rapidly. Fig. 5.35 indicates that the Magnussen EDC rate also falls, but this is due entirely to the reduced soot concentration which is input to the rate calculation. Fig. 5.37 in section 5.2.1.3 shows that the Magnussen EDC rate remains relatively high when the Hiroyasu soot yield is used instead. Thus, the Tesner formation rate is overwhelmed by oxidation and the calculated yields and particle number densities drop to negligible levels by 40° aTDC.

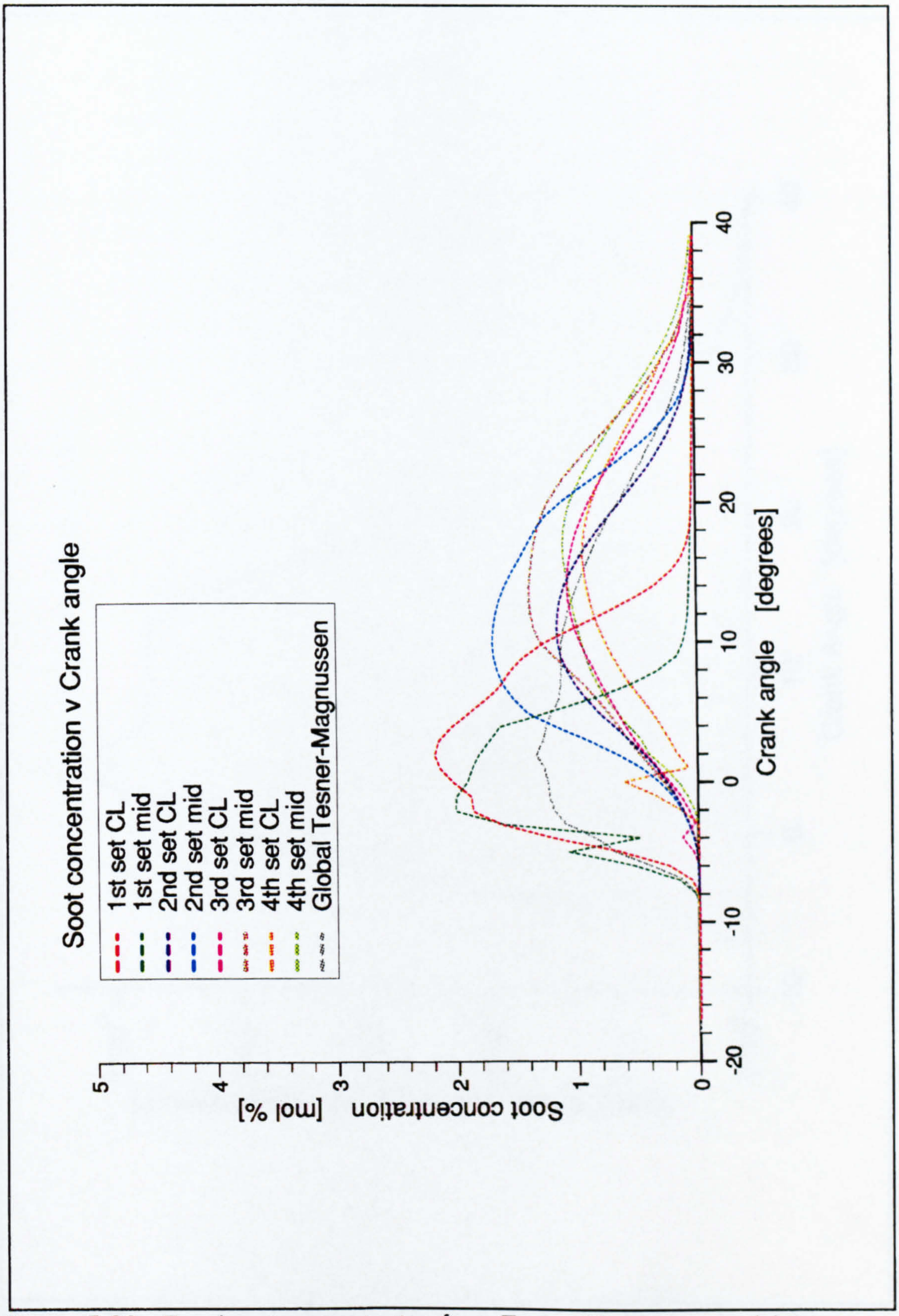

Figure 5.33 - Zonal soot concentration from Tesner-Magnussen model

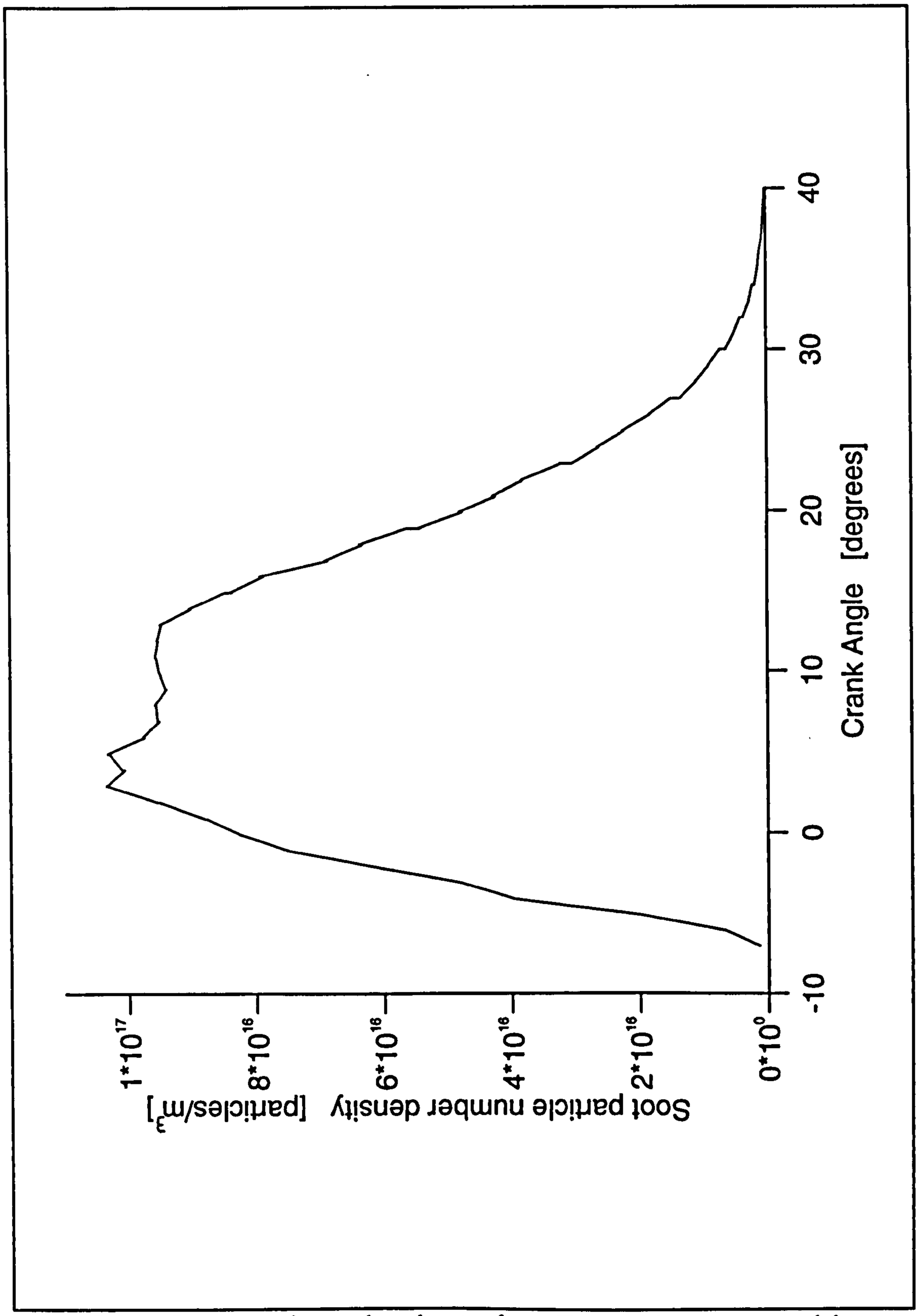

Figure 5.34 - Soot particle number density from Tesner-Magnussen model

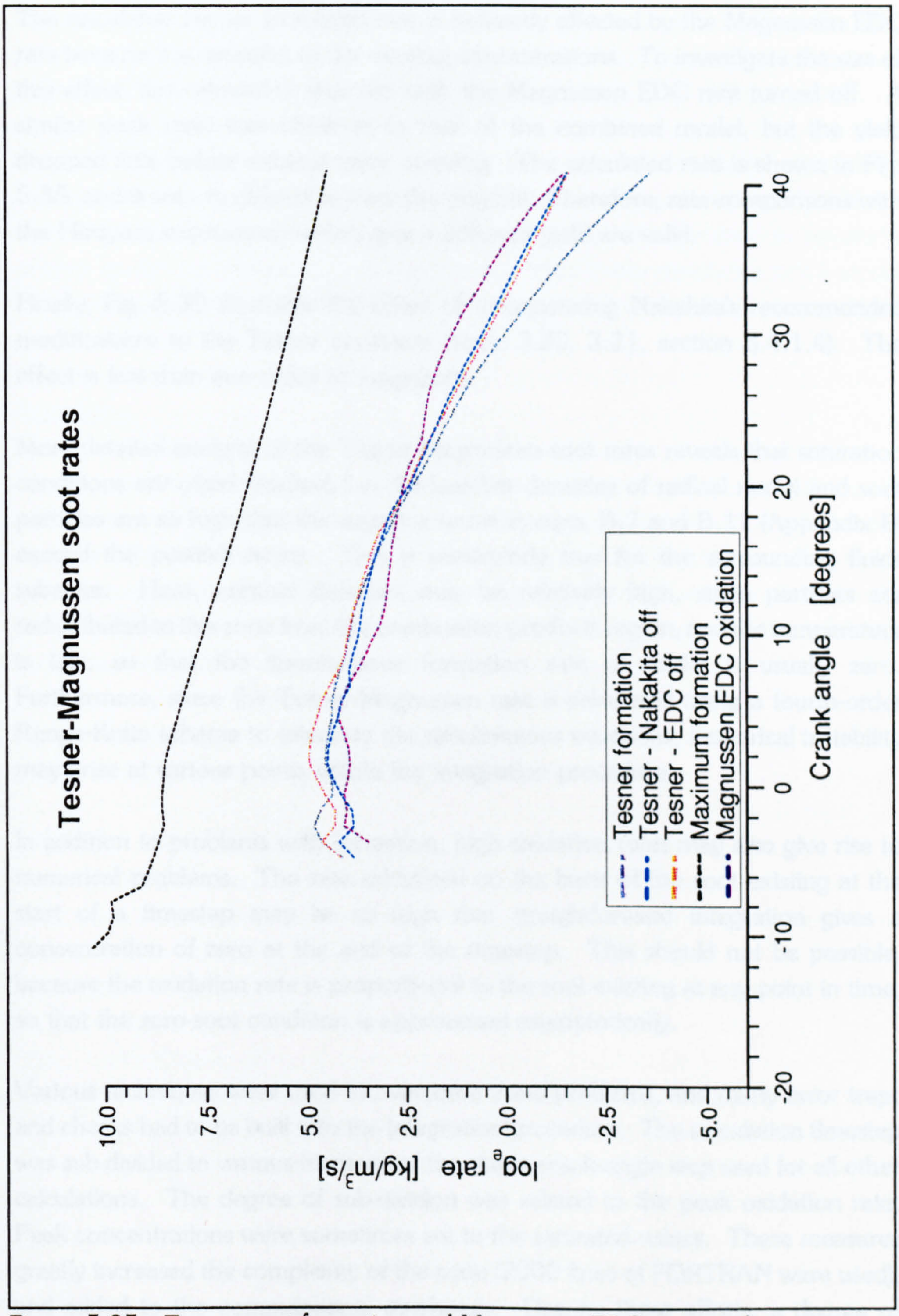

Figure 5.35 - Tesner soot formation and Magnussen EDC soot oxidation rates

The calculated Tesner formation rate is indirectly affected by the Magnussen EDC rate because it is sensitive to the existing concentrations. To investigate the size of this effect, the calculation was run with the Magnussen EDC rate turned off. A similar peak yield was obtained to that of the combined model, but the yield dropped little before exhaust valve opening. The calculated rate is shown in Fig. 5.35, and is seen to differ little from the original. Therefore, rate comparisons with the Hiroyasu expressions which give a different yield are valid.

Finally, Fig. 5.35 illustrates the effect of incorporating Nakakita's recommended modifications to the Tesner constants (equs. 3.20, 3.21, section 3.4.1.4). The effect is less than one order of magnitude.

More detailed analysis of the Tesner-Magnussen soot rates reveals that saturation conditions are often reached, i.e. the number densities of radical nuclei and soot particles are so high that the negative terms in equs. B.7 and B.11 (Appendix B) exceed the positive terms. This is particularly true for the surrounding fluids subzone. Here, number densities may be relatively high, since particles are redistributed to this zone from the combustion-products region, and the temperature is low, so that the spontaneous formation rate of nuclei is usually zero. Furthermore, since the Tesner-Magnussen rate is calculated using a fourth-order Runge-Kutta scheme to integrate the simultaneous equations, numerical instability may arise at various points within the integration procedure.

In addition to problems with formation, high oxidation rates may also give rise to numerical problems. The rate calculated on the basis of the soot existing at the start of a timestep may be so high that straightforward integration gives a concentration of zero at the end of the timestep. This should not be possible, because the oxidation rate is proportional to the soot existing at any point in time, so that the zero-soot condition is approached asymptotically.

Various techniques were used to overcome these problems, and many error traps and checks had to be built into the integration procedure. The calculation timestep was sub-divided to various fractions of the single crank-angle step used for all other calculations. The degree of sub-division was related to the peak oxidation rate. Peak concentrations were sometimes set to the saturated values. These measures greatly increased the complexity of the code (2000 lines of FORTRAN were used), and added to the computational overheads. Despite these efforts, a degree of

instability remains, as can be seen in Fig 5.33. However, it is unlikely that this instability would seriously affect the total yields calculated or the conclusions reached on use of the model.

In passing it is noted that an attempt was made to implement the Moss model[242] developed from the work of Gilyazetdinov[88]. However, even more severe problems were encountered regarding numerical stability, since terms raised to fractional powers cannot be allowed to drop below zero. Thus it was concluded that a model of this complexity is unsuitable for use when integration of simultaneous equations is involved.

Conclusion

The Tesner-Magnussen model gives realistic estimates of yield during the main diffusion-burning phase. However, the oxidation rate overwhelms the formation towards exhaust valve opening, such that the calculated yield tends to zero. Great difficulty was encountered in integration of the simultaneous rate equations in the model subzones due to numerical instabilities. The resulting model is relatively complex and computationally expensive.

5.2.1.3 Rates comparisons

This section extends the analysis of the results to include all of the soot models implemented. Comparisons are first made on the basis of the calculated overall rates plotted against crank angle. Then basic rate dependencies are investigated by plotting the rates against temperature and composition variables which were extracted from the simulation predictions.

Formation rates

Fig 5.36 shows the variation of the formation rates with crank angle up to 40° aTDC. The quantitative accuracy of the rates may be gauged by comparison with the empirically-calibrated Hiroyasu rate. It is seen that the Harmadi and Tesner rates compare well with this standard, though slightly different trends with crank angle are shown. In fact, the Tesner rate is not strictly comparable with the others, because it is associated with a different soot yield. However, Fig. 5.35 in the previous section shows that this effect is fairly small.

The Khan rate, however, rises to much higher values before about 30° aTDC and then drops more rapidly. This behaviour is a consequence of the explicit dependence on equivalence ratio in the correlation (see Appendix B, equs. B.1 - B.3 for details), and the high sensitivity to the value of the equivalence ratio (an exponent of 3 is used). Before 30° aTDC, the overall equivalence ratio in the spray and in each individual zone is rich (see Figs. 5.3 & 5.1). However, the input to the Khan expression is not the overall equivalence ratio, but that derived from the unburnt species concentrations. This is set by the balance between entrainment and combustion and its value is typically double the overall value, as can be deduced from Fig. 5.2 (see also Fig. 5.38). Thus, the formation rate is even higher than would be expected on the basis of the overall equivalence ratio. After about 30° aTDC, fuel begins to run out in the zones, and a large proportion of that which has not been completely burnt is existing as soot. However, air entrainment continues, so that the equivalence ratio drops sharply. This gives rise to a very steep drop in the Khan formation rate. Thus the equivalence-ratio term in the Khan correlation acts almost as a switch.

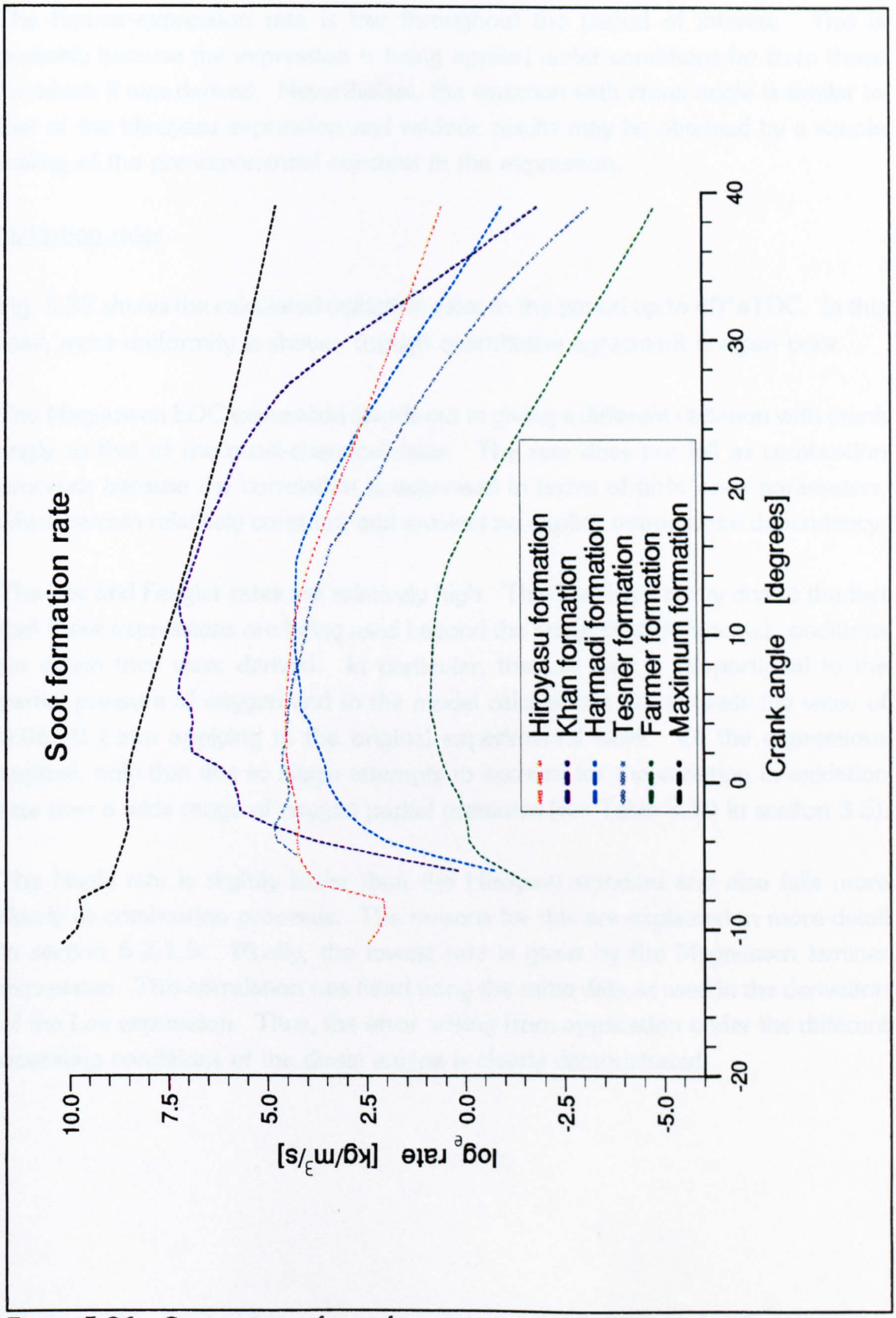

Figure 5.36 - Comparison of soot formation rates

The Farmer-expression rate is low throughout the period of interest. This is probably because the expression is being applied under conditions far from those for which it was derived. Nevertheless, the variation with crank angle is similar to that of the Hiroyasu expression and realistic results may be obtained by a simple scaling of the pre-exponential constant in the expression.

Oxidation rates

Fig. 5.37 shows the calculated oxidation rates in the period up to 40° aTDC. In this case, more uniformity is shown, though quantitative agreement is again poor.

The Magnussen EDC expression stands out in giving a different variation with crank angle to that of the quasi-chemical rates. The rate does not fall as combustion proceeds because the correlation is expressed in terms of turbulence parameters, which remain relatively constant, and involves no explicit temperature dependency.

The Lee and Feugier rates are relatively high. This is at least partly due to the fact that these expressions are being used beyond the range of experimental conditions for which they were derived. In particular, the Lee rate is proportional to the partial pressure of oxygen and in the model calculations this exceeds the value of 0.05 - 0.1 atm applying in the original experimental work. Of the expressions applied, only that due to Nagle attempts to account for the variation in oxidation rate over a wide range of oxygen partial pressures (see Table 3.10 in section 3.5).

The Nagle rate is slightly lower than the Hiroyasu standard and also falls more slowly as combustion proceeds. The reasons for this are explained in more detail in section 5.2.1.5. Finally, the lowest rate is given by the Magnussen laminar expression. This correlation was fitted using the same data as used in the derivation of the Lee expression. Thus, the error arising from application under the different operating conditions of the diesel engine is clearly demonstrated.

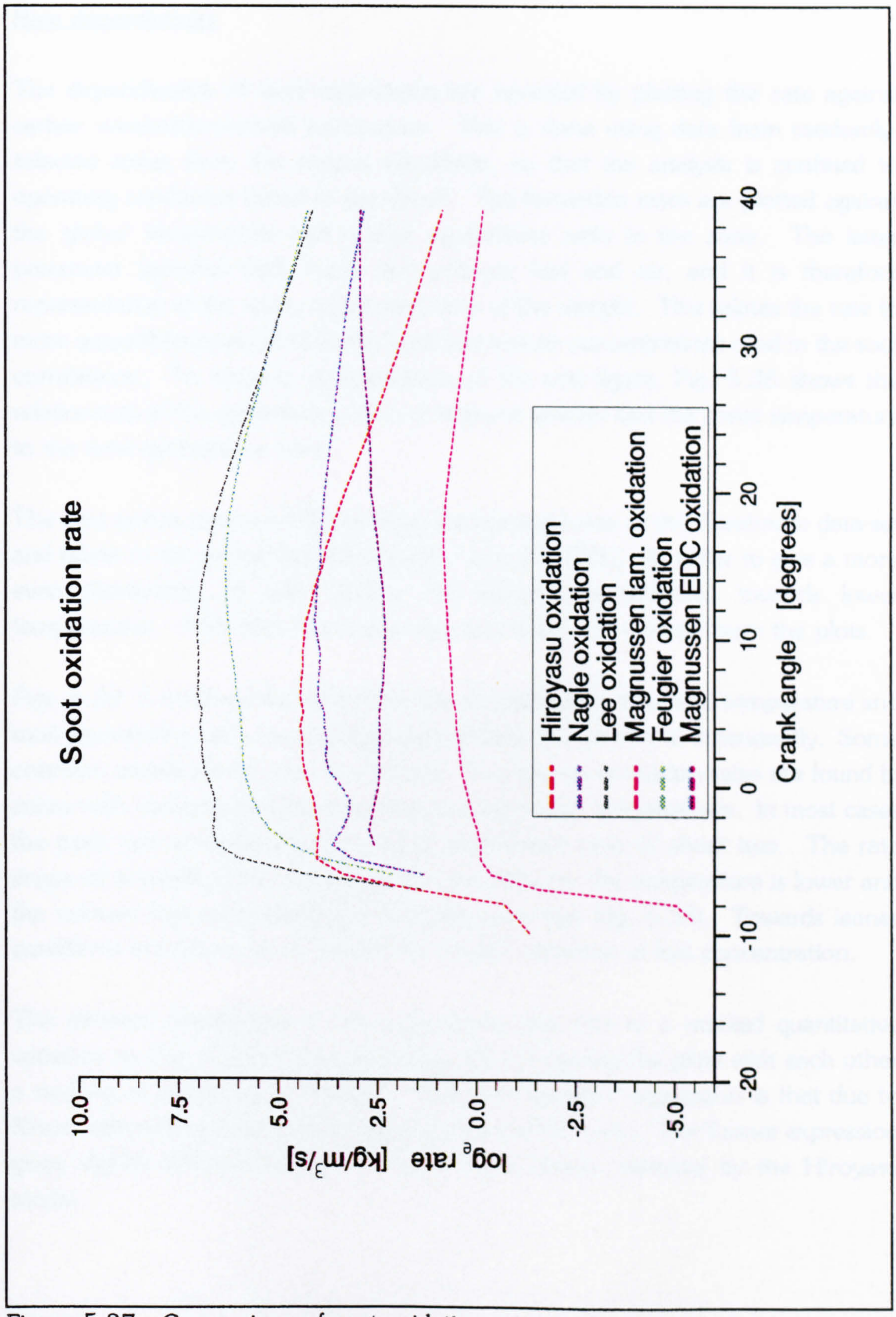

Figure 5.37 - Comparison of soot oxidation rates

Rate dependencies

The dependencies of each expression are revealed by plotting the rate against certain combustion-model parameters. This is done using data from randomly-selected zones from the engine simulation, so that the analysis is confined to operating conditions found in the diesel. The formation rates are plotted against the 'global' temperature and overall equivalence ratio in the zone. The latter parameter includes both burnt and unburnt fuel and air, and it is therefore representative of the spray region and time of the sample. This relates the rate to more general parameters than the local fuel and air concentrations used in the soot correlations. To assist in interpretation of the rate figure, Fig. 5.38 shows the relationship of the equivalence ratio of unburnt species and the zonal temperature to the total equivalence ratio.

The data points used were taken from the standard case of the Kamimoto data-set and relate to the period between ignition and 40° aTDC. In order to give a more even distribution of data points, the selection is weighted towards lower temperatures. Note also that some very rich zones are omitted from the plots.

Figs. 5.39-5.43 show the formation rate plotted against the zonal temperature and total equivalence ratio, and against each of these parameters independently. Some common trends can be seen in all cases. The highest formation rates are found in zones with medium equivalence ratios and fairly high temperatures. In most cases the peak rate corresponds to a global equivalence ratio of about two. The rate drops off towards 'richer' conditions for two reasons: the temperature is lower and the unburnt fuel concentration is actually lower (see Fig. 5.38). Towards leaner conditions the fall in rate is mainly due to the reduction in fuel concentration.

The different sensitivities of the expressions give rise to a marked quantitative variation on top of these general trends. By comparing the plots with each other a ranking of sensitivity is revealed. The most sensitive expression is that due to Khan, followed by those of Harmadi, Farmer and Hiroyasu. The Tesner expression gives slightly different behaviour, but is most closely matched by the Hiroyasu model.

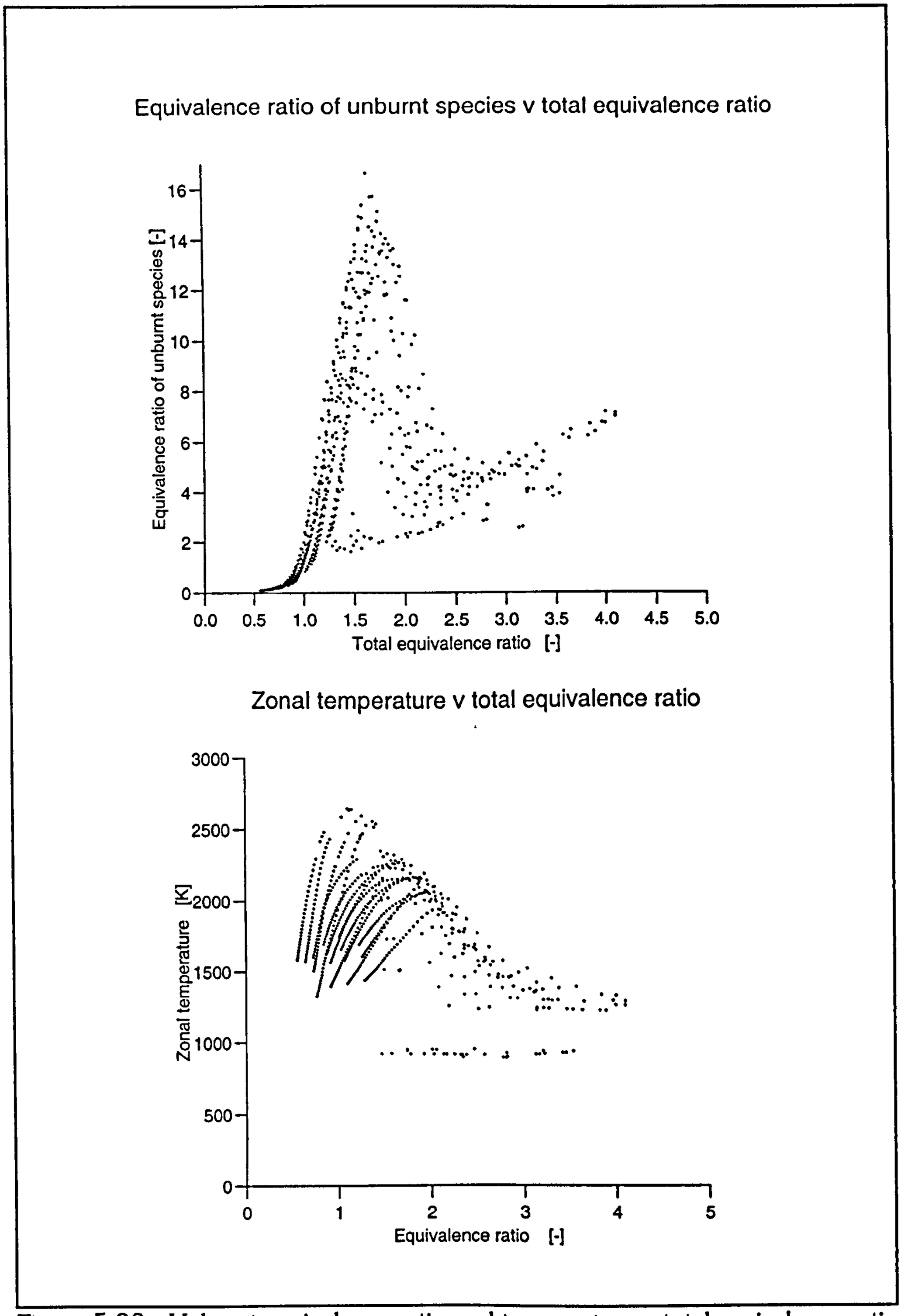

Figure 5.38 - Unburnt equivalence ratio and temperature v total equivalence ratio

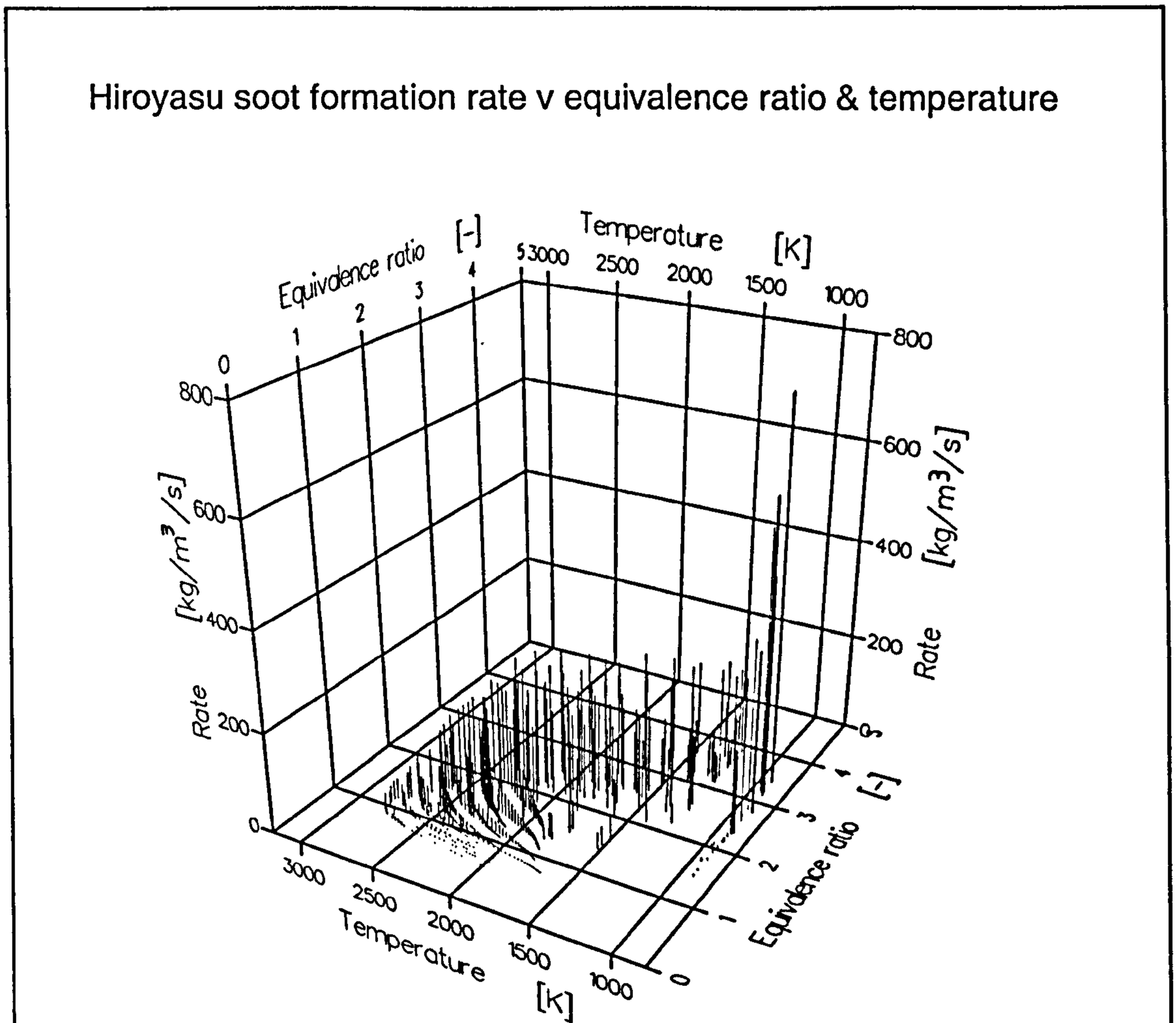

Figure 5.39 - Hiroyasu expression rate dependencies

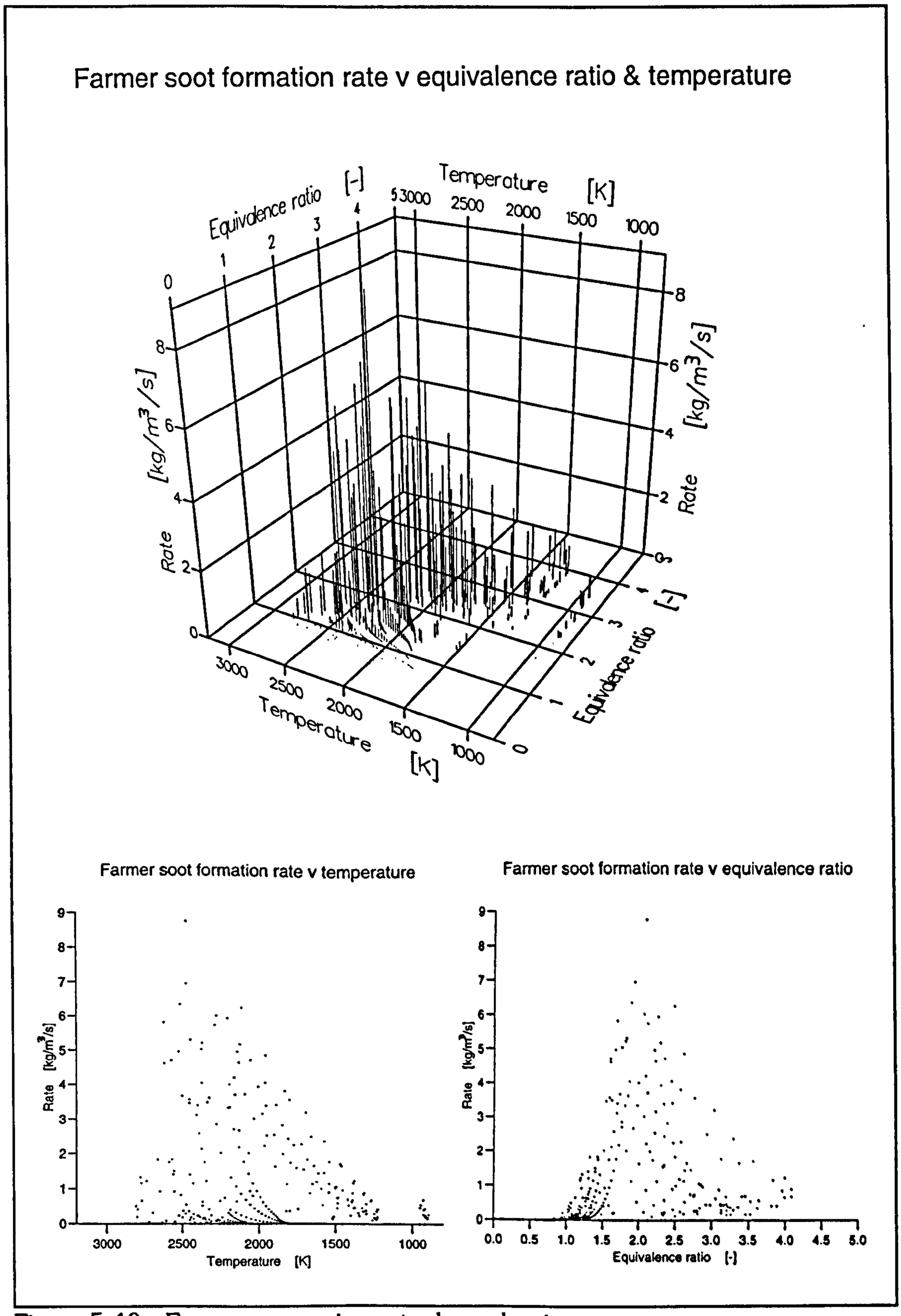

Figure 5.40 - Farmer expression rate dependencies

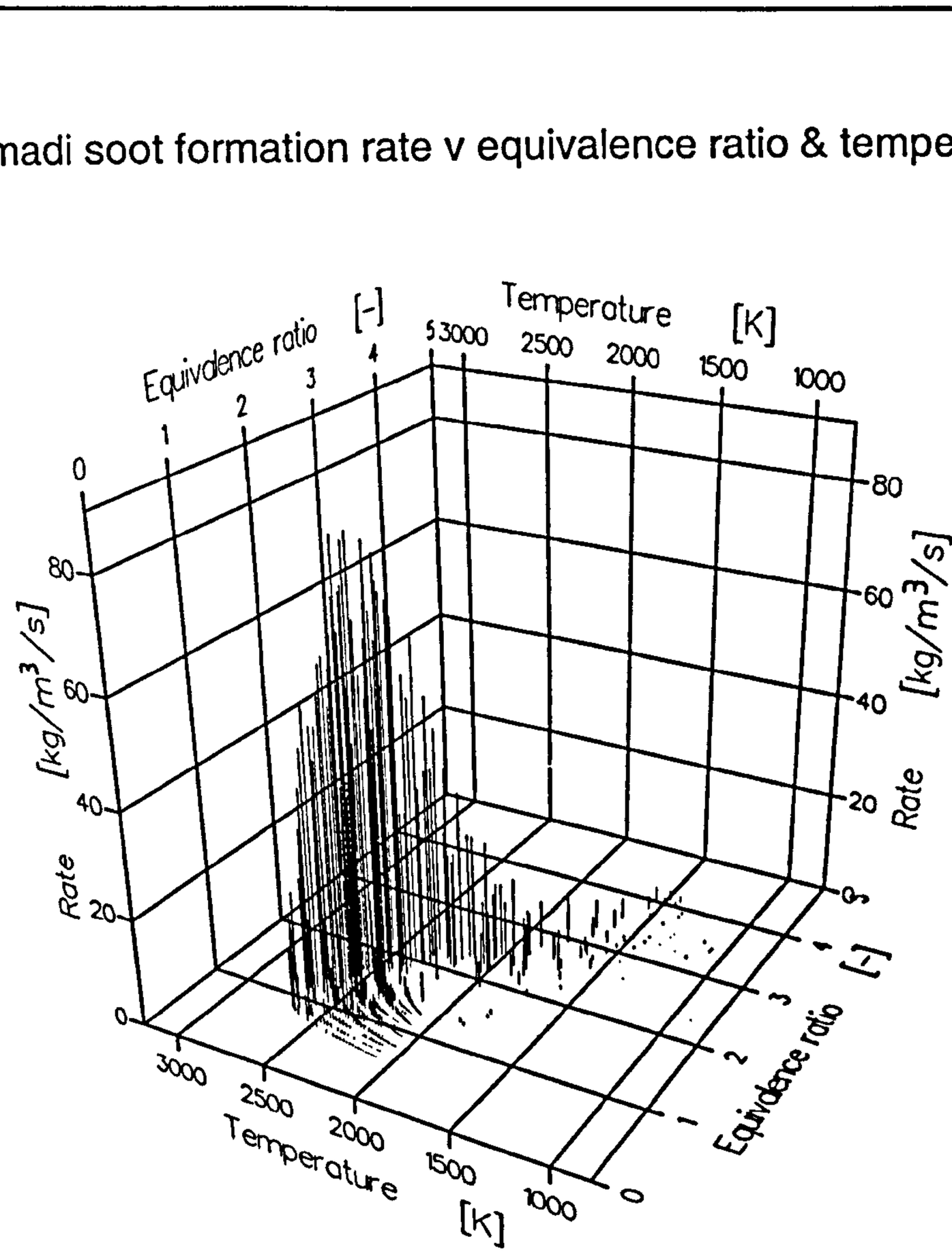

Figure 5.41 - Harmadi expression rate dependencies

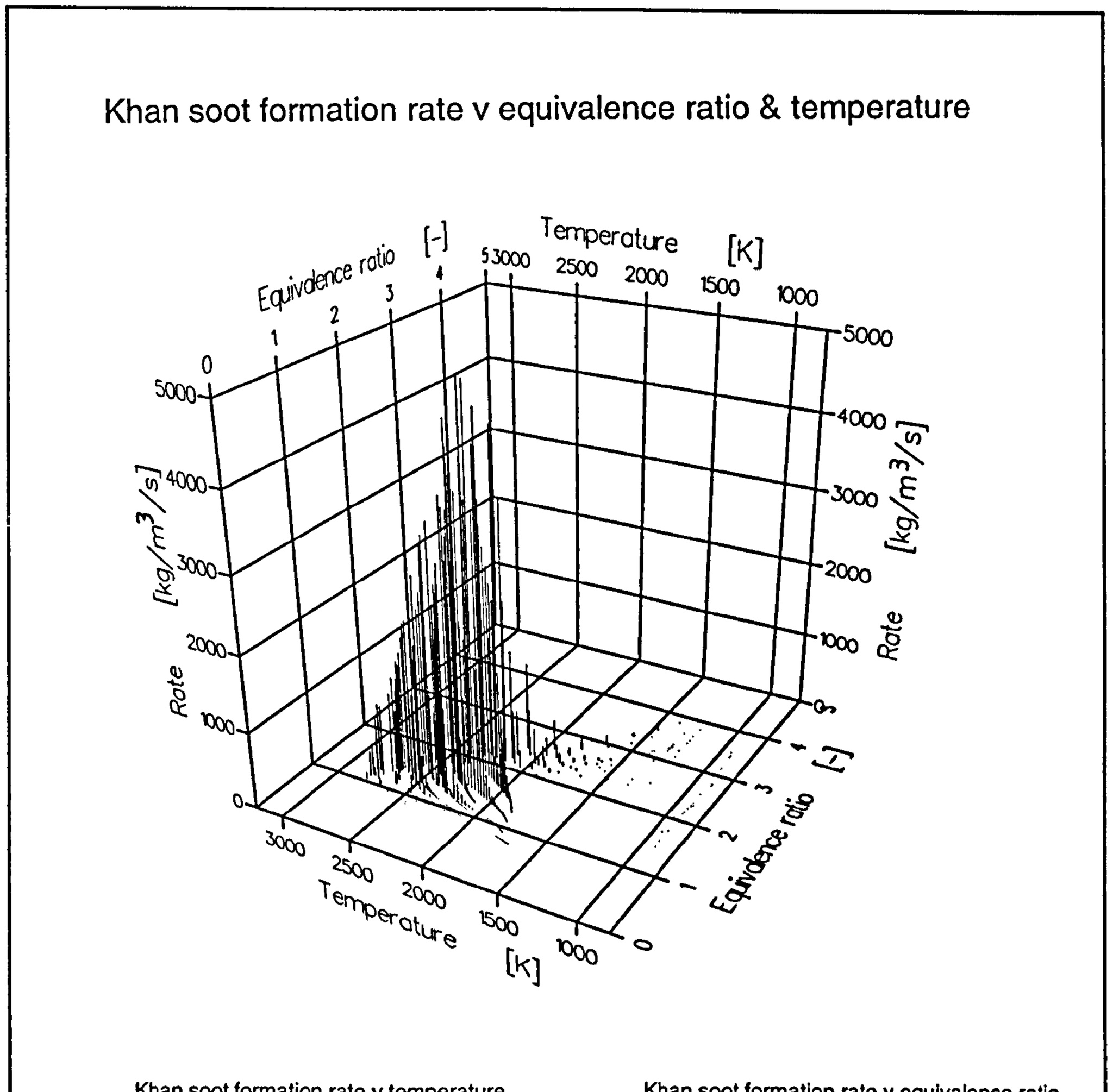

Figure 5.42 - Khan expression rate dependencies

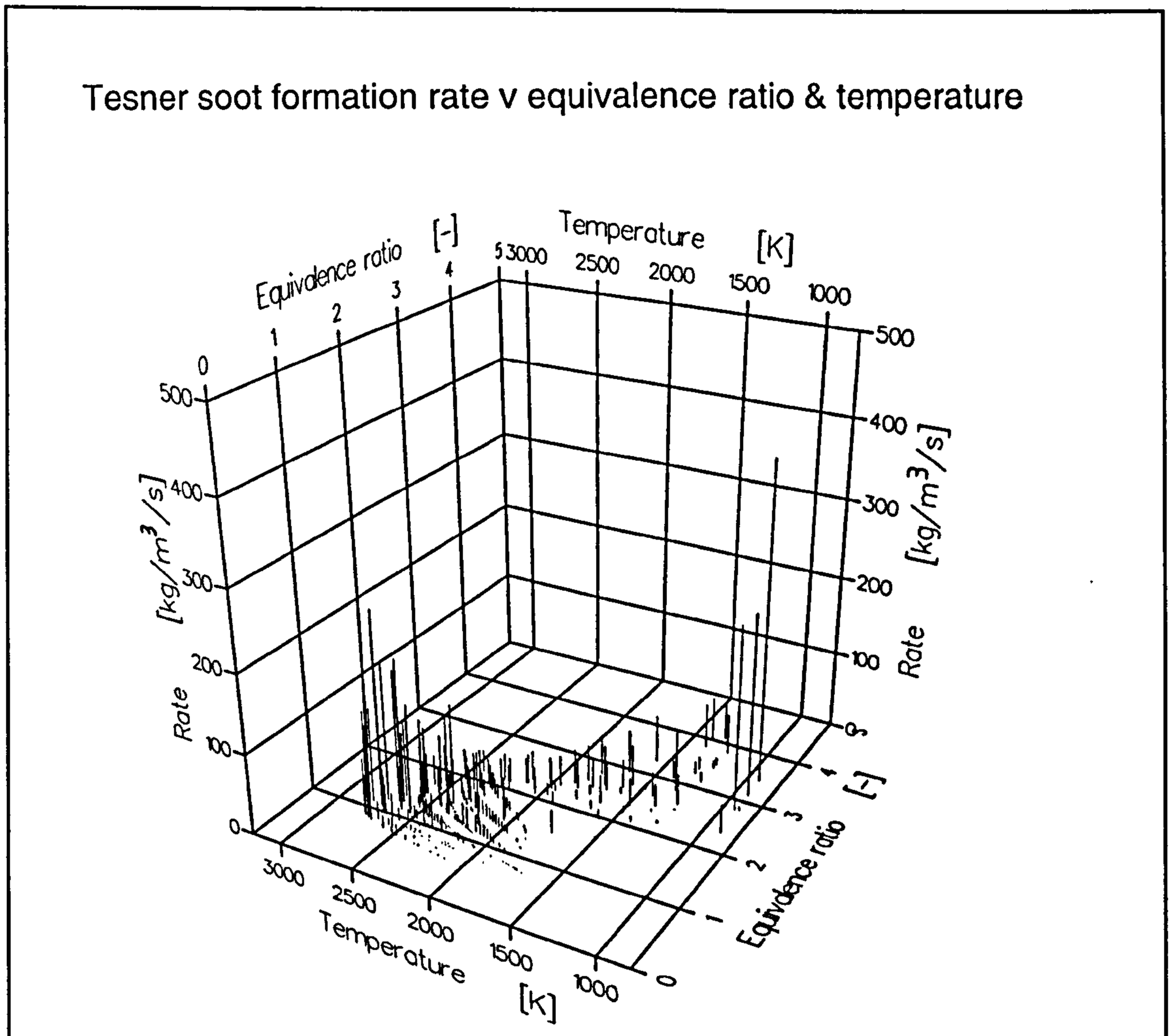

Figure 5.43 - Tesner expression rate dependencies

The Khan expression is the most sensitive and shows a very sharp peak in the rate for equivalence ratios ranging from 1 to 2.5. These zones have temperatures above 2000 K. This behaviour is to be expected, since the rate is proportional to the equivalence ratio to the third power. Lack of oxygen and high unburnt fuel concentrations give peak equivalence ratios in this region (see Fig. 5.38). Towards richer mixture the rate drops to negligible levels, due mainly to the reduced temperatures. Harmadi's expression also involves equivalence ratio and shows similar behaviour, though the rates at each end of the equivalence-ratio range are much higher in relative terms. The Farmer expression involves oxygen concentration, but the exponent is smaller again, so more moderate behaviour is observed. The medium temperature zones now give rates which are comparable with the highest. Finally the Hiroyasu correlation does not involve oxygen concentration and the fuel-concentration exponent is relatively low at a value of unity. Together with the fact that very low activation energies are used, this gives a rate which is fairly insensitive to the conditions. An anomaly is revealed on these plots since very high rates are found in certain rich zones before the start of combustion. This occurs at temperatures of less than 1000 K and this behaviour is clearly unphysical.

The Tesner rate is also fairly insensitive to temperature. This is to be expected as temperature is involved only in the nucleation term for active particles, and the concentration of active particles rapidly reaches the saturation limit (see section 5.2.1.2). Nevertheless, there is an upward trend at the highest temperatures which is not shown by the Hiroyasu expression. A different dependency on equivalence ratio is shown, with generally low sensitivity and a modest peak around an equivalence ratio of 1.5. Also, very high rates are found in certain low-temperature zones. These are zones at the rear of the jet which have not ignited, but which contain a small concentration of soot particles and nuclei (< 2% of the spray average) due to mixing (see Appendix F). Though nucleation is zero here, so is the oxidation rate, and this allows unchecked soot production. The model could be modified to correct for this.

Oxidation expressions

The sensitivities of the oxidation expressions are best seen by normalising the rate by the soot mass, since all expressions are directly proportional to the mass. Park published a comparative plot of surface-oxidation rate against reciprocal temperature which has been widely cited[269] (see Fig. 3.1, section 3.4.3.1). The form of this plot is followed in Fig. 5.44 to allow a comparison. Rates are shown for the Hiroyasu, Nagle, Lee and Magnussen (laminar) expressions; the Feugier correlation shows very similar trends to that of Lee, whilst the Magnussen EDC rate shows a very poor correlation with temperature.

The data points shown were selected at random and relate to the whole of the combustion process and the whole of the spray. The intention is to show trends, and the number of points has been artificially reduced in places for clarity. The individual rates are now considered.

The Magnussen laminar expression is very insensitive to variation in the conditions. The rate falls only when the temperature is reduced below 1400 K, very late in the process. This expression was fitted to Lee's experimental data for a temperature range from 1300 to 1680 K, and for this range, it was demonstrated to give a better fit than Lee's expression. Magnussen considers that this improvement will give a better description beyond the range of the Lee data, but this assumption is incorrect. The expression is of very limited use in the range of interest in a diesel engine.

The Hiroyasu and Lee rates each fall on a curve having two arms. Data points along the length of the upper arm and at the elbow correspond to any time before peak temperatures are reached (before 20° aTDC). As the temperature drops towards exhaust valve opening the rate steadily falls, giving the lower arm. The reason that rates are lower for the same temperature later in the process is the reduction in oxygen partial pressure. Both rates are proportional to oxygen concentration. Also, in each individual arm, the rates show an increase with temperature. The slope is greater for the Lee expression because the activation energy is much higher.

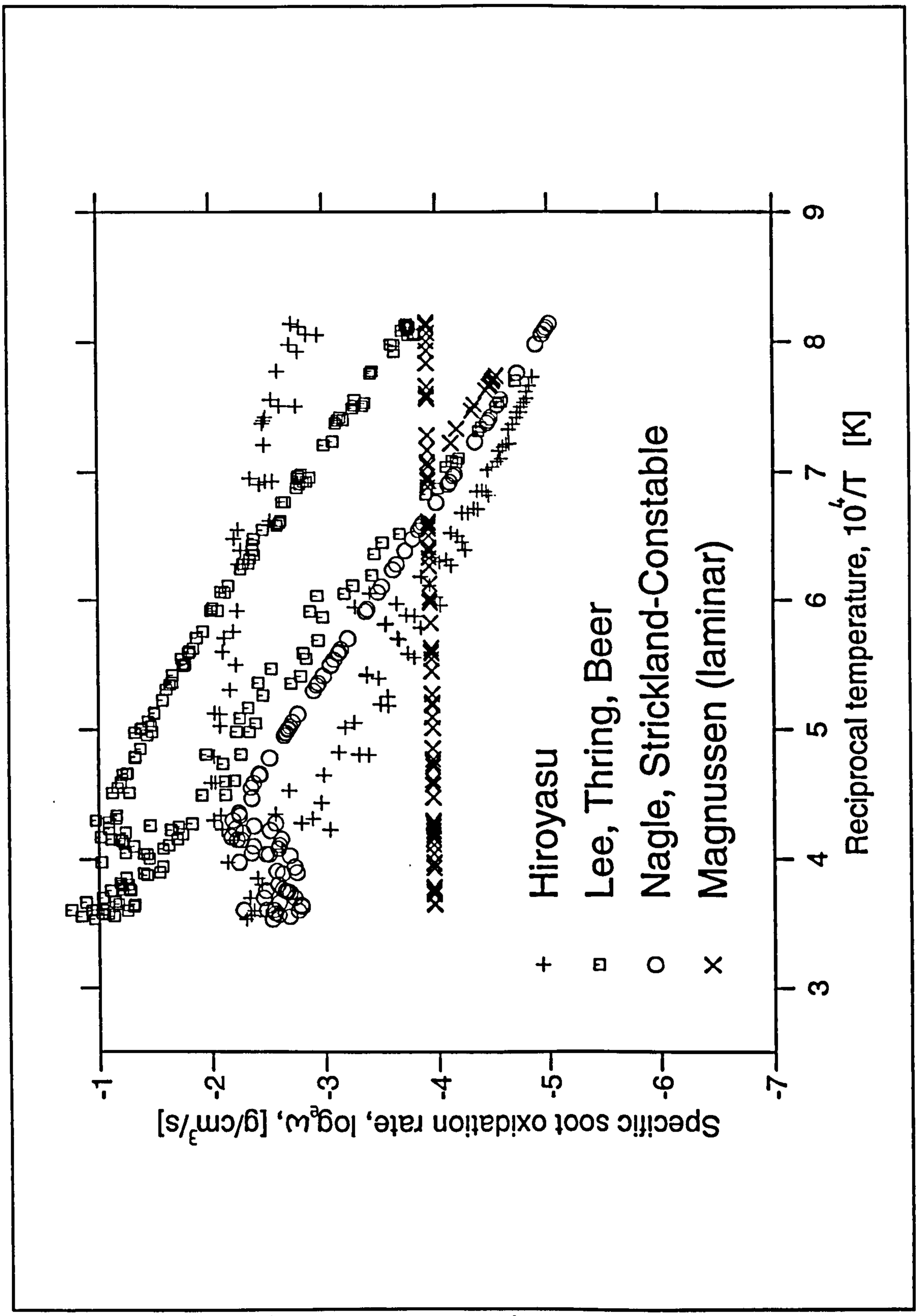

Figure 5.44 - Soot oxidation rate v reciprocal temperature

All calculated Nagle rates fall on a single curve at reciprocal temperatures greater than 5 ($T < 2000$ K). This is because the form of the expression gives independence from the chemical composition at lower temperatures. Physically, this behaviour can be interpreted as follows. All oxidation is occurring at active sites, since the value of X in equ. B.16 is approximately unity and the first term dominates. Furthermore, desorption of oxygen is the overall rate-controlling process, since the second term in the denominator is large (see also equ. 3.32 in section 3.4.3.1), and this results in the independence from oxygen partial pressure. Also, unlike the other expressions, the Nagle rate shows a plateau at temperatures above 2000 K.

Thus, the oxidation expressions show more distinct variation in behaviour than the formation expressions. They can be classified into four groups as shown in Table 5.9. For the first group of expressions, the rate is always directly proportional to the oxygen concentration and therefore similar trends with crank angle are shown (see Fig. 5.37). Though Magnussen's laminar rate expression was fitted to the same data as that of the Lee expression, a much different relationship is observed. Because the oxygen partial pressure is relatively high, the denominator of equ. 3.32 (section 3.4.3.1) is dominated by the second term. In the simulation, the rate only begins to drop after the temperature has fallen below 1400 K when the oxygen partial pressure is 28 kPa. Nagle's expression shows opposite behaviour, with oxygen concentration effects only becoming apparent when the temperatures exceed 2000 K. Finally, Magnussen's EDC rate is only proportional to the oxygen concentration when the zone (or subzone) is overall rich.

Expression	Dependency on mass fraction of oxygen in simulation*
Hiroyasu, Lee, Feugier	proportional
Magnussen laminar	proportional for $T < 1400$ K, no dependency for $T > 1400$ K
Nagle	proportional for $T > 2000$ K
Magnussen EDC	proportional when rich

Table 5.9 - Soot oxidation expression dependency on oxygen mass fraction

---

* In fact, all but the Feugier expression are given in terms of oxygen partial pressure, rather than simply the mass fraction.

Other rate comparisons

Several comparisons of soot oxidation rates are available in the literature, including the work of Park[269], Najjar[252] and Linden[210].

Park's plot is shown in Fig. 3.1 (section 3.4.3.3). Lee's data is included, but the rate is below that given by Nagle since the partial pressure of oxygen is lower. The reverse is observed in the studies of Linden[210] and Najjar[252] and in the current work. The former studies were done in the context of gas-turbine combustion at pressures of up to 30 atm. In all of these cases, oxygen partial pressures are higher than those of Lee's experiment, leading to the discrepancy. Because Nagle's expression is fairly insensitive to oxygen partial pressure, it is likely to give a more accurate measure of the oxidation rate in different combustion systems, and is more generally useful.

5.2.1.4 Expression sensitivities

The expressions proposed for soot formation and oxidation have various different dependencies, and the values of the parameters used vary widely, even amongst similar expressions. For example, a range of activation energies have been used both for formation and oxidation. The sensitivity of the calculated rates to the values of dependent-parameter exponents and the values of the constants is of great interest. There is not room in this thesis to report an extensive investigation of sensitivities, but two interesting cases are described.

The popular Hiroyasu expressions use abnormally low activation energies, derived from turbulent diffusion flame data[260]. The effect of increasing these values to more typical levels has been investigated. E_f and E_o were increased from 12.5 and 14 kcal/mol to 40 and 44 kcal/mol respectively (see equs. B.5, B.13 in Appendix B). It was found that identical peak soot levels could be obtained for only a small rise in exhaust concentration by adjusting the pre-exponential factors, A_{for} and A_{ox}, from 2 and 6×10^{-6} to 400 and 3×10^{-3} respectively. Thus sensitivity to activation energy is low.

The Khan expression contains an equivalence-ratio factor with exponent three (equ. B.1, Appendix B). This is exceptionally high and one comparative study suggests a reduction would give better results[47]. The effect of using different exponents was investigated. It was found that very similar trends could be obtained using reduced values of the exponent, though the overall rate magnitude was reduced. This is illustrated in Fig 5.44, which shows the variation in rate with overall equivalence ratio for exponent values of zero and three. In the case of the former, a dependence on equivalence ratio is still shown because the expression also includes a fuel partial-pressure term. The reason for the peak in the rate is described in the previous section (5.2.1.3). The only noticeable difference in the case of the reduced exponent is the relatively high rates given for overall equivalence ratios of less than unity. Therefore, virtually identical behaviour can be obtained using the reduced exponent by simply increasing the pre-exponential factor in the correlation.

Thus, the cases examined show that rates are not highly sensitive to either activation energies or simple exponent values. This contrasts the marked differences between expressions of different form described in the previous section.

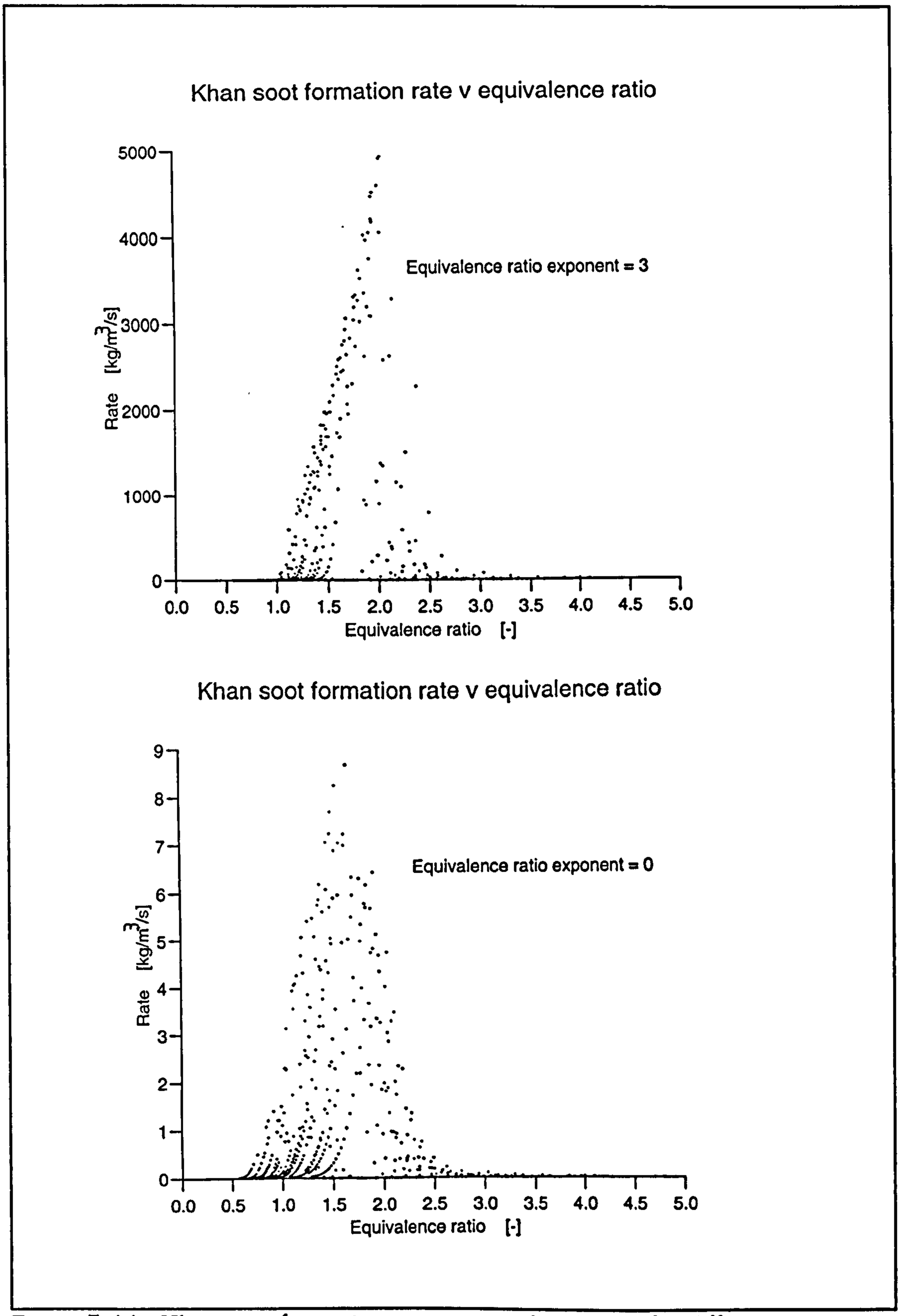

Figure 5.44 - Khan soot formation rate v equivalence ratio for different exponents

5.2.1.5 Combined rates

Given the variety of expressions proposed for soot modelling, and their different sensitivities, it is of interest whether better yield predictions could be obtained by choosing different combinations. In particular, it has been shown that exhaust smoke may be correlated in terms of chemical and turbulence parameters, and a hybrid model accounting for both effects could be used. Nakakita has reported improvements in predictions by use of this technique in a multi-dimensional simulation for an IDI diesel engine. However, Figs. 5.36 and 5.37 show that the basic rate predictions vary widely and in using different combinations of expressions some calibration is of course necessary.

The oxidation expression due to Nagle takes into account the effect of varying partial pressures of oxygen over a wide range of conditions and may be assumed to provide a better description than those expressions which were obtained under narrowly defined conditions. Magnussen's EDC oxidation rate is the only expression linking soot oxidation directly to turbulence parameters. Therefore, the effect of using a combined Nagle-Magnussen EDC oxidation rate, together with the original Hiroyasu formation rate was investigated. The oxidation expressions were calibrated by use of different multiplicative constants.

The results were not encouraging, giving much poorer performance than the Hiroyasu pair of expressions, irrespective of the magnitude of the calibration constants used. The reason for this can be seen in Fig 5.45, which shows the relationship between the Hiroyasu formation rate and the *uncalibrated* oxidation rates in the period up to 80° aTDC. The Hiroyasu oxidation rate varies in a very similar way to the formation rate during the main combustion period, whilst the Nagle and Magnussen EDC expressions remain much more stable (the reasons for this behaviour were described in section 5.2.1.3). Therefore, the calculated peak yields are higher and the exhaust levels are lower, as shown in Table 5.10. The difficulties of rate matching are discussed further in the next section (5.2.2).

Oxidation expression	Exhaust soot ($g\,m^{-3}$)	Peak soot ($g\,m^{-3}$)	Pk/exh ratio
Hiroyasu	0.363	1.58	4.35
Nagle	0.093	2.50	26.9
Magnussen EDC	0.014	6.31	441

Table 5.10 - Calculated soot yields using different expression combinations

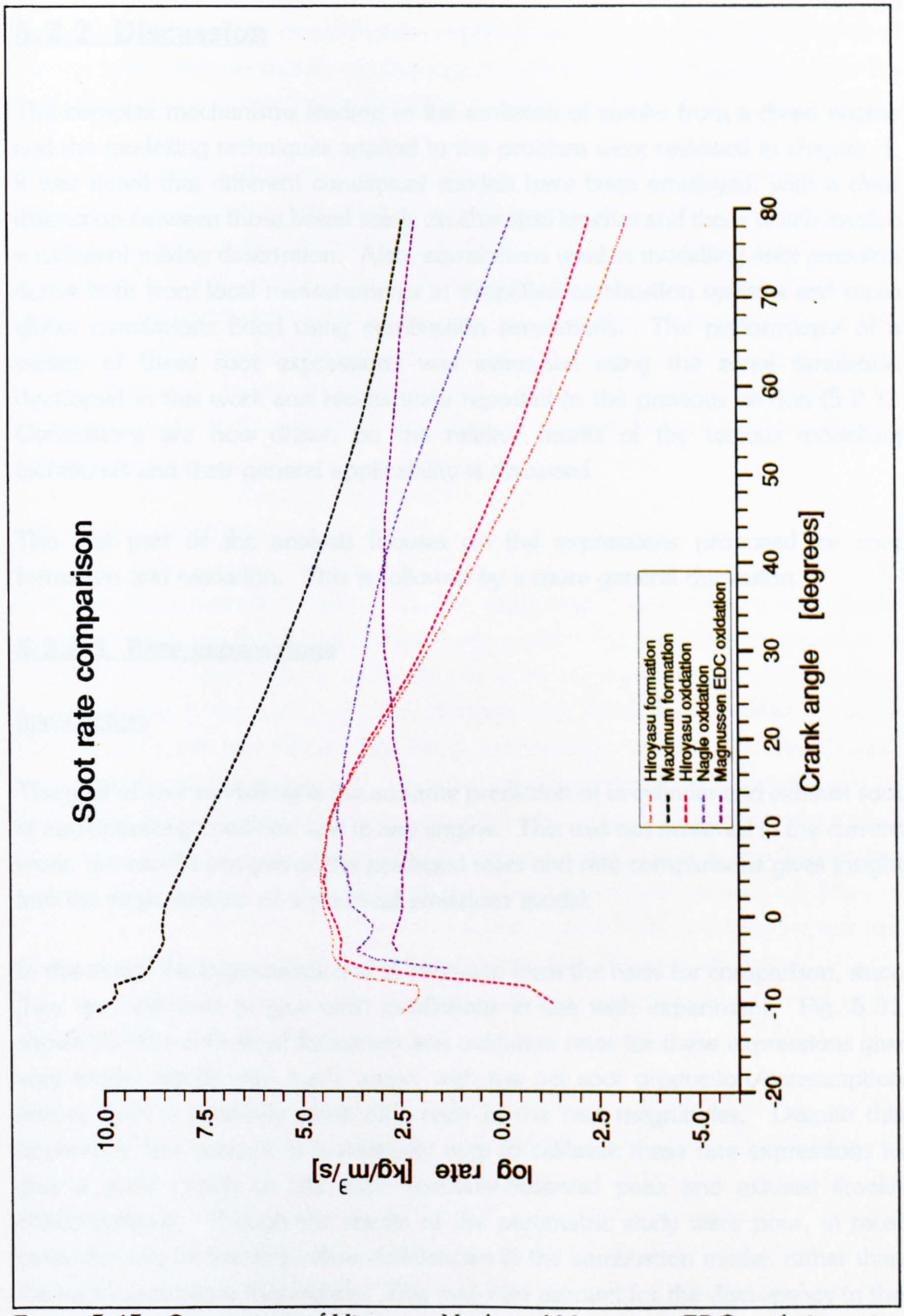

Figure 5.45 - Comparison of Hiroyasu, Nagle and Magnussen EDC oxidation rates

5.2.2 Discussion

The complex mechanisms leading to the emission of smoke from a diesel engine and the modelling techniques applied to the problem were reviewed in chapter 3. It was noted that different conceptual models have been employed, with a clear distinction between those based solely on chemical kinetics and those which involve a turbulent mixing description. Also, correlations used in modelling soot emission derive both from local measurements in simplified combustion systems and more global correlations fitted using combustion simulations. The performance of a variety of these soot expressions was examined using the zonal simulation developed in this work and results were reported in the previous section (5.2.1). Conclusions are now drawn on the relative merits of the various modelling techniques and their general applicability is discussed.

The first part of the analysis focuses on the expressions proposed for soot formation and oxidation. This is followed by a more general discussion.

5.2.2.1 Rate expressions

Introduction

The goal of soot modelling is the accurate prediction of in-cylinder and exhaust soot at any operating condition and in any engine. This was not achieved in the current work, but careful analysis of the predicted rates and rate comparisons gives insight into the requirements of a practical emissions model.

In this study, the expressions due to Hiroyasu form the basis for comparison, since they are calibrated to give yield predictions in line with experiment. Fig. 5.31 shows that the calculated formation and oxidation rates for these expressions give very similar trends with crank angle, with the net soot production/consumption arising from a relatively small difference in the rate magnitudes. Despite this apparently fine balance, it is relatively easy to calibrate these rate expressions to give a good match to the experimentally-observed peak and exhaust smoke concentrations. Though the results of the parametric study were poor, in most cases this can be traced to clear deficiencies in the combustion model, rather than the soot expressions themselves. This may also account for the discrepancy in the timing of the peak in yield. It was shown that sensitivity to the values of activation

energy used is fairly low. Nevertheless, applicability in different engines and models has not been well-established. All that can be said is that the expressions serve the purpose of smoke prediction in this type of model.

From these results, it seems that in this type of combustion model, the soot formation and oxidation rates must be well-matched, that is, they must show similar trends with crank angle. A brief look at the comparative plots of Figs. 5.36 and 5.37 reveals a wide variation in rate magnitudes and considerable variation in trends. If different expressions are to be used in conjunction with each other, calibration will generally be necessary, but even so there will usually be difficulties in combining rates, as demonstrated in section 5.2.1.5. This matching requirement is borne in mind in the following discussion of the performance of the individual expressions.

Individual expressions

The calculated formation rates from the single-step expressions reveal broadly similar behaviour to that of the Hiroyasu expressions, but with different sensitivities to the chemical composition. A ranking in terms of sensitivity to fuel and oxygen concentrations is observed, with the Hiroyasu rate being least sensitive, and the Farmer, Harmadi and Khan rates being progressively more so. The absolute magnitude of the calculated rates is generally poorly matched to the Hiroyasu rate, and calibration would probably be necessary in all cases. Yield predictions obtained using alternative (calibrated) formation expressions would be worse than those of the original combination, particularly for those expressions which are more sensitive to the chemical composition. This may not mean that these expressions are less useful for prediction of diesel smoke, but simply that they are less suited to use in the current model. Use of the Tesner formation expression is discussed under "More detailed expressions" below.

The oxidation expressions show more distinct variations in behaviour, and can be categorised into four groups as shown in Table 5.9. Consequently, the rates are not generally well-matched, even when calibration factors are used. It is likely that Nagle's expression is the most generally useful, since that study measured rates over a wide range of oxygen partial pressures, including the calculated levels of the simulation. The inadequacy of expressions derived under more limited conditions is clearly demonstrated by the Lee and Magnussen laminar results. In this case,

there is a large quantitative difference in the rates and different trends with oxygen partial pressure are shown, even though both expressions were fitted to the same experimental data.

The Hiroyasu expression is of similar form to that of Lee. Despite the lack of generality in the form of this expression, it is found to be preferable to the Nagle correlation for use in conjunction with the Hiroyasu-formation expression (see section 5.2.1.5). This is a rather unsatisfactory result, since it suggests that a combination of errors is to some degree responsible for the satisfactory predictions of the Hiroyasu expressions pair. However, it may be that deficiencies in the combustion model representation lead to a poorer matching of the Nagle rate. One obvious model deficiency is the slight overestimation of zonal temperatures. Kamimoto has shown that soot oxidation virtually ceases when the local temperature drops below about 1800 K[160]. This occurs at about 40° aTDC, but in the simulation this temperature is not reached until late in the combustion process. Thus, the problem of excessive oxidation may not occur if the calculated zonal temperature were a better match to the experimental values. Other sources of error are discussed in section 5.2.2.2 below.

More detailed expressions

In an attempt to provide a more generally useful description of the complex soot formation processes, a number of more detailed formation mechanisms have been proposed (see section 3.4.1.4). The Tesner formation mechanism is a popular example, describing the process in terms of radical nuclei and soot particles. A constant soot-particle size is assumed, though in other models the size is included as an additional variable. It may be supposed that these multistep models will provide a more accurate description of the formation process, since they represent a more complete description of the complex mechanisms involved. However, the particular case examined in this study met with limited success.

The Tesner expressions (equs. B.7 & B.11, Appendix B) were derived at atmospheric conditions in a laminar acetylene flame. Both the radical nuclei and soot particle formation rates may saturate, that is, they contain negative terms which depend on particle concentrations. This is slightly problematic in the non-constant pressure environment of the diesel engine. If a constant saturation value is used, soot may be formed or 'consumed' as the piston expands or compresses the

mixture respectively (even once nucleation has ceased). To avoid this, Nakakita introduced modifying factors, which have the effect of increasing the saturation concentrations in the diesel environment; these expressions were used in this study. Despite use of Nakakita's modifications, it was found that the soot expressions were often saturated. This led to many problems with numerical stability, and in order to cater for these conditions, many checks had to be built into the integration procedure, greatly increasing the complexity of the code.

In using some of the other multi-step models, the numerical difficulties would be even more severe. This is because fractional powers are used, so that no parameter can be allowed to fall below zero at any point of the integration procedure. However, these difficulties would not be encountered in a multidimensional model, where simultaneous integration is not necessary and the rates are merely used as source terms. Thus it seems that the more detailed models are better suited to use in CFD-type simulations.

Turbulence

Turbulent effects have been shown to be important in the diesel engine. It is well known that turbulence reduces rates of chemical reaction relative to the levels obtained under laminar conditions. Magnussen has shown that this effect is of importance in soot oxidation, since use of a laminar expression with average composition values leads to a serious overestimate of the rate[221]. Also, Dent has shown that exhaust smoke levels may be well-correlated in terms of the timescale of turbulence[55]. Other studies have shown a correlation with the flame temperature, so it seems that both effects are important. Consideration is now given to the problem of accounting for these effects in practical emissions models.

The rate comparisons of section 5.2.1.3 show that calibration is necessary in most cases. The required adjustment may be in either direction and the models affected include those fitted in combustion simulations as well as those derived from simple laminar studies. Thus, the calibration is required for a variety of reasons, and not only to account for the reduction of chemical rates due to the effects of turbulence. Consequently any attempt to explicitly describe this rate reduction will not remove the necessity for calibration, though it may increase the general applicability of the expression. It is apparent that other model deficiencies are much more significant than neglect of turbulence effects, as discussed above.

The effect of turbulence may be taken into account using an additional factor in the rate expressions which links the overall reaction rate to turbulence-related parameters. For example, the oxidation rate may be factored by the proportion of mixture in the heated fine structure, following Dent, or the minimum species concentrations at a point in the jet may be substituted for the averaged values following Magnussen[221]. Alternatively, the soot oxidation rate may be expressed directly in terms of turbulence parameters, as in Magnussen's EDC oxidation rate (see equ. B.19, Appendix B). Unfortunately, the results obtained from this model were not entirely satisfactory, apparently due to the lack of a direct dependency on temperature. The turbulence parameters in the expression are relatively constant, and the rate is also proportional to the mass fraction burnt. Thus the calculated rate remains relatively high even late in the process. Nakakita observed a similar effect and introduced a hybrid model, using Nagle's soot-oxidation expression to supplement the Magnussen rate in terms of its temperature deficiency. This seems to be a reasonable solution, but it could not be tested in this study due to the more serious problem of matching these expressions to the Hiroyasu formation rate.

Sources

The expressions examined in this study derive from widely different sources, ranging from simple laminar flow experiments to models fitted to experimental data using engine simulations. A wide range of operating conditions are covered (see Tables 3.9 & 3.10 in section 3.5). The only correlation which was derived using diesel engine data is that due to Khan, but very simplistic methods were used. Hiroyasu's correlations use some information from high-pressure and turbulent-flow situations, whilst Nagle's expression also covers the range of oxygen partial pressures found in the diesel. The model results were analysed to see whether any aspect of the behaviour could be attributed to the expression source.

In some cases, use of a soot correlation far beyond the experimental conditions of its derivation led to quantitative errors. A good example is the Lee expression which over-predicts the oxidation rate due to the high values of oxygen partial pressure in the diesel. Apart from this, there are no distinct differences in the behaviour of expressions from different sources; on the contrary remarkable similarities are shown. For example, the Hiroyasu expressions are of similar form to the formation expression of Farmer and the oxidation expressions of Lee and Feugier, which were all obtained in simple combustion systems. On the other hand, some quite distinct differences are apparent between expressions derived in similar

experimental conditions, for example the Lee and Magnussen laminar expressions. Thus, there are more important factors than the expression sources.

Conclusions

Results have been reported from a wide variety of soot correlations. Despite their simplicity, the Hiroyasu expressions are found to be relatively well-suited to use in zonal combustion models. Though Nagle's correlation seems to represent a more general description of the oxidation process, it is not so well-suited to use in this simulation since no formation mechanism gives similar trends with crank angle. Also, multi-step models are available which represent the phenomena leading to emission more precisely, but numerical difficulties mitigate against their use in zonal models. Turbulence is known to reduce the rates of reaction, but because calibration is generally necessary for models applied in the diesel environment, this factor is obscured. Finally, the source of a correlation seems to be of little importance.

More important than all of these factors is the sensitivity of an expression to certain key combustion parameters, which is related to the 'form' of an expression. The oxidation expressions show the most distinct differences in this respect, as shown in Table 5.10; the formation expressions show a ranking of sensitivities to chemical composition, but no clear qualitative differences in behaviour. These differences in sensitivity give rise to markedly different trends when rates are plotted against crank angle. This has a serious impact on the emissions prediction, because the calculated yields are very sensitive to the matching of formation and oxidation rates throughout the combustion period. For example, the Khan expression is extremely sensitive to the small air concentration existing under rich combustion conditions, giving a very high formation rate during the main combustion period (in relative terms). On the other hand, the Magnussen laminar rate shows virtually no sensitivity to any of the combustion parameters. In both of these cases, poor matching to oxidation and formation expressions respectively means that yield predictions will be poor.

Some of these effects are related to the particular combustion-model representation employed in this study, which uses zonally-averaged compositions and temperatures. The relationship to some of the combustion parameters is discussed further in the next section.

5.2.2.2 General modelling considerations

This study has demonstrated that the Hiroyasu expressions are fairly well-suited to the prediction of exhaust smoke in zonal models using averaged compositions. However, these expressions are fairly simplistic and it is known that they do not properly represent all of the phenomena leading to soot emission. For example, Nagle's oxidation correlation has been shown to give a better description of the effects of oxygen partial pressure variation. It is possible that this apparent contradiction arises due to deficiencies in the combustion model, and certainly, different results would be obtained using different types of combustion model. This section extends the discussion, considering the relationship between the soot models and the underlying combustion models.

The current model represents the combustion process using zonally-averaged compositions and temperatures, divided between reactants and combustion products regions. However, with the exception of the Tesner-Magnussen model, the soot expression inputs are zonal averages. Use of subzone values is feasible, but was beyond the scope of this work. In reality, sooting processes are highly intermittent, since the unburnt fuel, air and combustion products are contained, to some degree, in separate eddies. This segregation will affect the rates of soot formation and oxidation, possibly in different ways. In particular, use of averaged soot expression inputs tends to overestimate the initial oxidation rate, though the error reduces as the uniformity of the mixture increases. Thus, neglect of the intermittency also changes the response to parametric variations, because the calculated formation and oxidation rates would show much different trends if a more detailed description were used. As observed in the previous section, this is of great significance for the prediction of soot yields.

The only practical way of describing the complexity of the heterogeneous mixture composition is by use of stochastic models employing Monte-Carlo methods (see section 2.2). Rather mixed results have been reported from soot studies which use these techniques. For example, Brown obtained very poor parametric predictions using a sophisticated stochastic model built on top of a multidimensional simulation. The same model gave excellent results for NO_x, providing indirect validation of the thermodynamic description and indicating the model's utility in describing non-linear emission behaviour. The study of Mansouri[227,228] found that the initial soot loading was extremely sensitive to the value of the rich flammability limit; increasing this limit from $\phi = 3$ to $\phi = 4$ led to an order of magnitude increase in smoke. In Kittelson's study[174], poor results were attributed to the fact that the model used a chamber-average description. Xiao[378] is the only researcher to have used a zonal stochastic

model, and no exhaust results are given for this study.

Mansouri's findings raise some important questions. Though an equilibrium assumption was used to describe soot formation, this may not have been the primary cause of the extreme sensitivity to flammability limits. Rather, the fact that the rich zones of equivalence ratio between 3 and 4 are allowed to burn provides a region of very rich mixture which is also hot, giving rapid soot formation. This highlights the general problem of describing the interaction between the sooting processes and combustion, which is also of relevance in simple zonal models*. In the current study, the extremely small concentrations of unburnt air under rich combustion conditions had a big influence on the sooting processes. In fact, most of the simulations applied to the study of diesel smoke involve a very simplistic description of combustion chemistry, using a single-step representation. Particularly in these regions of high unburnt fuel concentration, other chemical mechanisms will be of relevance. Generally, very little attention has been paid to the balancing of soot and other chemical processes, but it is likely that these issues are of great significance for emissions modelling[61].

Thus, no improvement in soot emission prediction has been achieved by use of models which include a more detailed thermodynamic description. This is to some extent due to weaknesses in the soot models, since excellent NO_x results were given by one of these models. However, in most cases, the failure may also be partly attributed to remaining weaknesses in the thermodynamic description. A further factor may also be significant: in using a more detailed thermodynamic description, the soot rates become more sensitive to the variation in conditions as combustion proceeds. This makes matching of the formation and oxidation rates more difficult and results in less stable overall behaviour. The increased sensitivity also means that prediction of the effects of parametric change is less straightforward. Thus it seems that quasi-chemical soot correlations are not well-suited for use with more detailed combustion models.

Finally, it has been shown that phenomenological models have some intrinsic advantages over multidimensional descriptions. Though the latter provide more detailed information on the sooting processes, in practical terms they are confined to using local averages. No success in predicting exhaust levels has been reported in the literature. However, somewhat paradoxically, these models are better suited for incorporating multi-step soot models.

---

* Appendix G describes the methods used in the current simulation program.

CHAPTER 6 - CONCLUSIONS

This thesis addresses the problem of the modelling of smoke emission from a diesel engine. As a basis for the soot modelling study, a combustion simulation was developed and validated. This chapter describes some of the main findings related to the combustion model and summarises the conclusions of the soot modelling study. Finally, a set of recommendations is presented.

From the outset, it was proposed that a zonal phenomenological model would be used for the simulation. This model type gives a number of advantages. Since sooting processes are very sensitive to the local conditions, any effective model must provide some representation of the variation in conditions existing within the mixture. Zonal models use quasi-dimensional zones to characterize the different combustion regimes, and these can be supplemented using thermodynamic subzones, as in the current work, or more complex representations of mixture composition. Thus, these models provide a high degree of flexibility, placing no restriction on the complexity of the information which is fed into the emissions-model mechanisms. Though CFD models provide a detailed description of the spatial variation in conditions, in practice, the local statistical information provided cannot be used due to a lack of knowledge of the correlation between soot concentration and mixture fraction. Zonal models have the further advantage of being relatively undemanding computationally.

The zonal model developed in this work uses a flexible and controllable spray model based on that of Hiroyasu[126]. Thermodynamic partitioning was achieved by use of the Magnussen EDC model, dividing each zone between regions of pure reactants and mixture which has passed through the heated fine structures. The latter region will contain excess fuel or air when combustion is rich or lean respectively, and this is potentially of great significance for soot modelling.

The performance of the model was assessed by comparison with the large empirical data-set of Kamimoto[159]. Some parameter tuning was required to obtain good agreement with experimental heat-release curves from the parametric study. In particular, it was found necessary to adopt the air-entrainment factors given by Kuo[197] for light-duty diesel engines, and the amount of vaporised fuel burning in premixed mode at ignition was set to 27%, by fitting to the experimental data. Performance predictions are very reasonable, though the calculated temperatures

are slightly high, leading to a slight overestimation of pressure.

The main weakness which came to light was in the method used to represent the effect of swirl. Adoption of Hiroyasu's correlation for the reduction of penetration due to swirl leads to a serious overprediction of entrainment at high-swirl conditions. Moreover, the calculated air-entrainment rate rises progressively as the swirl level increases. In reality, under high-swirl conditions the jet deflects and begins to move in the direction of the swirling airflow, so that following large deflection, the air entrainment rate drops below the zero-swirl rate. Therefore, even when a reduced swirl factor is used, the predicted air-entrainment rates are a poor match to experimental trends. Otherwise, the trends shown by the pressure curves are correct, and with the exception of the swirl case, the combustion-model predictions were deemed sufficiently accurate for the purposes of emissions modelling.

Soot modelling techniques have been analysed in order to identify the key controlling features and critical model parameters. For the first time, a detailed comparative study was made of various soot model mechanisms. Previous work has reported some success in prediction of emissions by use of simple correlations, mainly quasi-chemical rate expressions. This is perhaps surprising, in view of the enormous complexity of the sooting processes and the different mechanistic steps involved.

In this work, the predictions of the popular quasi-chemical expressions due to Hiroyasu were first compared with the experimental results from the parametric study. The results matched the experimental trends in only about half of the parametric cases examined, with poor estimates of the effects of swirl, injection timing and load. In each case, though, the errors could be traced to combustion-model deficiencies. The poor representation of the effect of swirl has been mentioned above. Air entrainment was substantially under-predicted in the case of advanced injection, perhaps due to under-estimation of turbulence levels at this point. Most seriously, under high-load conditions, the reduced availability of fresh air charge to mixture at the back of the spray is not represented in the model and it is assumed that air is taken up by the spray at a fairly continuous rate until it is exhausted. In practice, the fuel which is injected late will tend to entrain combustion products from earlier combustion; since there is no simple way of representing interzone species transfers, this is a significant shortcoming.

The joint-model of Tesner-Magnussen has been selected for particular study. This model attempts to build in more understanding of the sooting phenomena by employing a more detailed formation mechanism and the sooting processes are followed in heated fine structure and surrounding fluids regions. The analysis showed that the soot formation rates are saturated for much of the main combustion period, so that radical and soot concentrations merely follow the saturation values, rendering the model ineffective for parametric predictions. Also, integration of the simultaneous formation equations is highly complex, and near to the saturation limit, numerical instabilities arise. In solving this problem, the model developed in this study became relatively complex and more computationally demanding. Similar difficulties would be faced by all detailed models of similar form and it seems that these expressions are much better suited to use in CFD-type models, where more advanced numerical integration techniques are used as standard.

Examination of the other soot rates revealed a significant variation of sensitivities to combustion-model parameters. The formation expressions show a ranking of sensitivity to composition and temperature, with the Khan rate being most sensitive followed by those of Harmadi, Farmer and Hiroyasu. The oxidation expressions examined show more distinct qualitative differences in behaviour. The Magnussen laminar rate is extremely insensitive to combustion parameters and of very limited value for diesel smoke prediction. Those expressions which are proportional to oxygen mass fraction (Hiroyasu, Lee, Feugier) show a drop in rate as the overall oxygen concentration falls during the combustion process. The Nagle expression shows very different behaviour, with very little sensitivity to oxygen mass fraction once the temperature has dropped below 2000 K. Thus the rate remains much higher later in the cycle. Finally the Magnussen EDC rate is only proportional to oxygen mass fraction under rich conditions. Since the rate is expressed in terms of turbulence parameters, which are relatively constant, it also remains much higher later in the cycle. These differences have a big impact on the predictions of exhaust soot.

In most cases, the overall rate predictions are quantitatively poor. This is often due to the use of expressions beyond the range of conditions for which they were derived. For example, the different sensitivities of the Magnussen laminar and Lee expressions lead to a difference in rate of several orders of magnitude under diesel engine conditions, though the expressions were fitted using the same experimental

data. These effects also tend to obscure the reduction of rates due to turbulence.

The source of the various soot correlations was found to have no influence on the form and sensitivities of the expressions. For instance, the Hiroyasu and Farmer formation rates are very similar in form, though the first was proposed for use in diesel engine simulation, whilst the latter derives from measurements in a simplified continuous combustion system. The same can be said of the Hiroyasu and Lee oxidation expressions. On the other hand, the Magnussen laminar and Lee correlations give very different behaviour though they both derive from the same source.

It has been observed that soot predictions are insensitive to variation of soot-model parameters such as activation energies and equivalence-ratio exponents. The predominant influence on sooting behaviour comes rather from the overall dependency or 'form' of the expressions. The qualitative differences between the oxidation expressions are of particular importance, giving different trends of rate against crank angle. This has a big impact on the sooting behaviour, because the calculated soot yield is very sensitive to the 'matching' of the formation and oxidation rates. Consequently, the Hiroyasu expressions give relatively satisfactory performance, for in this case the formation and oxidation rates follow closely similar trends. However, the success of this model may arise simply from the relative insensitivity shown to combustion parameters, rather than accuracy in representing the real dependencies of the sooting process. In fact, the oxidation expression is expected to be less generally useful than the Nagle expression. This is unsatisfactory and suggests a weakness in the combustion model. Overestimated zonal temperature may be part of the cause.

The applicability of the soot modelling techniques in different types of combustion model has been considered. It was concluded that when a more detailed thermodynamic description is used, for example in stochastic models, the problems of matching formation and oxidation rates are increased. This finding also applies to CFD models, though to a lesser degree. Thus, there is no improvement in the results obtained from detailed models, and this has been confirmed by the findings of other workers[37,227].

In conclusion, the most successful models are those which use simple quasi-chemical soot mechanisms in conjunction with simple zonal combustion models. In this type

of model, it is crucial that the overall predictions of the combustion model, particularly the air entrainment rates, are accurate. Accurate prediction of the thermodynamic state, especially the temperature, is also very important. As far as the soot models are concerned, the key issue is the matching of the formation and oxidation rates and this is highly sensitive to certain dependencies of the oxidation expressions. Paradoxically, use of more detailed thermodynamic descriptions, or more detailed soot models, leads to more unpredictable behaviour by making matching less controllable. Finally, the interaction of the soot and combustion chemistry is of great significance.

Specific conclusions are presented below in the form of a series of recommendations for diesel combustion and emissions simulation.

Model recommendations

Zonal phenomenological models should be used as a basis for soot modelling, due to their general flexibility. Stochastic models give less stable soot model performance due to enhanced sensitivity to the combustion conditions. CFD models are practically confined to using local averages and are computationally-restricted.

In order to correctly represent the effect of swirl on combustion and emissions, it is essential to use a spray model which describes the reduction in entrainment following significant deflection of the jet.

In conjunction with zonal models, single-step quasi-chemical expressions should be used for best results. Use of more detailed soot models gives no advantages and incurs substantial computational complexity.

In order to exploit the full potential of the simple quasi-chemical expressions, accurate representation of the overall behaviour is essential. In this respect, the most important parameter is the overall air-to-fuel ratio of the jet, though the zonal temperatures are also significant.

When expressions from different sources are applied in the diesel, calibration is usually necessary.

Explicit description of the reduction of chemical rates due to turbulence is not important, because the effect on soot rates is usually obscured by calibration.

In achieving a good balance between in-cylinder and exhaust soot yields, attention should be focused on the relative magnitudes of the formation and oxidation rates over the whole of the combustion period. If the calculated rates vary in markedly different ways as combustion progresses, i.e. if they are 'poorly matched', then extreme sensitivity to calibration constants will be shown.

In seeking to match soot formation and oxidation expressions, attention should be paid to certain key dependencies of the expressions. This is particularly important for the oxidation expressions, which show different sensitivities to temperature and oxygen partial pressure according to the absolute magnitude of these parameters. In this respect, the Nagle expression is found to be particularly problematic, since the rate is scarcely affected by the oxygen concentration below a certain temperature. It is therefore a poor match to all of the formation mechanisms studied.

Amongst the quasi-chemical models, those of Hiroyasu seem to be best for emissions prediction. This is because the formation and oxidation expressions are well-matched, and relatively insensitive to conditions.

Improved soot models could be developed by use of simulation programs like the one developed in this work. One of the most popular expressions in current use, Khan, was derived by fitting to exhaust data using a very crude model. Now that more advanced models are available, they could be used as tools for the development of more extensively validated and more generally useful expressions.

In soot modelling work, particular attention should also be paid to the interaction of sooting processes and combustion.

APPENDIX A - Soot yield prediction

The effects of temperature and activation energies on the overall yield of soot may be investigated by applying some basic knowledge about the soot formation and oxidation processes. This appendix sets out the derivation of a yield equation which can be used to test sensitivities.

The basic assumption of this analysis is that soot emission occurs in two discrete stages - formation and oxidation. A case can be made that this is a reasonable approximation to the processes occurring in a diesel, because soot formed in fuel-rich eddies is oxidised only when these eddies break-up. Even if it is not a strictly accurate description, the analysis allows a bound to be set on the expected behaviour.

Crudely, the soot formation rate may be defined by the following equation (this assumes the dominance of chemical processes):

$$\frac{dm_{soot}}{dt} = A e^{-\frac{E_f}{RT}} \qquad (A.1)$$

Integration gives simply:

$$m_{soot}(t,T) = A\,t\,e^{-\frac{E_f}{RT}} \qquad (A.2)$$

Thus, the yield at time 't_*' will scale with temperature according to:

$$\frac{m_{soot}(t_*,T)}{m_{soot}(t_*,T_o)} = e^{\frac{E_f}{R}\left(\frac{1}{T}-\frac{1}{T_*}\right)} \qquad (A.3)$$

The oxidation rate, however, is proportional to the mass of soot already existing:

$$\frac{dm_{soot}}{dt} = -A m_{soot} e^{-\frac{E_f}{RT}} \qquad (A.4)$$

In this case, integration gives an exponential term:

$$m_{soot}(t',T) = m_{soot}(t_*,T)\, e^{Bt' e^{-\frac{E_o}{RT}}} \qquad (A.5)$$

The time, t', is measured relative to t_*. The term Bt' is set by the boundary condition, $T=T_o$. Thus, the yield at time 't' will scale with temperature according to:

$$\frac{m_{soot}(t',T)}{m_{soot}(t_*,T)} = e^{\log_e\left(\frac{m_{soot}(t',T_o)}{m_{soot}(t_*,T_o)}\right) e^{\frac{E_o}{RT_*}} e^{-\frac{E_o}{RT}}} \qquad (A.6)$$

The yield at $T=T_o$ is defined as X:

$$\frac{m_{soot}(t',T_o)}{m_{soot}(t_*,T_o)} = X \qquad (A.7)$$

To determine how the final yield scales with temperature, it is necessary to substitute into equ. A.6 from equ. A.3. Using equ. A.7 and simplifying gives:

$$\frac{m_{soot}(t',T)}{m_{soot}(t',T_o)} = \frac{1}{X} e^{-E_f R\left(\frac{1}{T}-\frac{1}{T_*}\right)} e^{\log_e X\, e^{\frac{E_o}{R}\left(\frac{1}{T}-\frac{1}{T_*}\right)}} \qquad (A.8)$$

This equation can be used to investigate the variation in yield with temperature and the activation energies. Fig. A.1 shows the ratio of yields obtained in the temperature range 2000 - 3000 K plotted on a $\log_e$ scale. The following activation energy combinations were used:

$E_f = 40$ kcal/mol, $E_o = 40$ kcal/mol
$E_f = 40$ kcal/mol, $E_o = 50$ kcal/mol
$E_f = 30$ kcal/mol, $E_o = 40$ kcal/mol

A yield of 0.1 is assumed for a temperature of 2500 K.

It is seen that the yield falls with temperature over most of the range, whatever the activation energy. This is a consequence of the fact that the formation process gives a linear increase of soot at a rate set by the Arrhenius term, whilst the oxidation is an exponential decay in which the exponent is a function of a similar Arrhenius term. Thus it is not necessary to conclude that the oxidation process is more temperature sensitive.

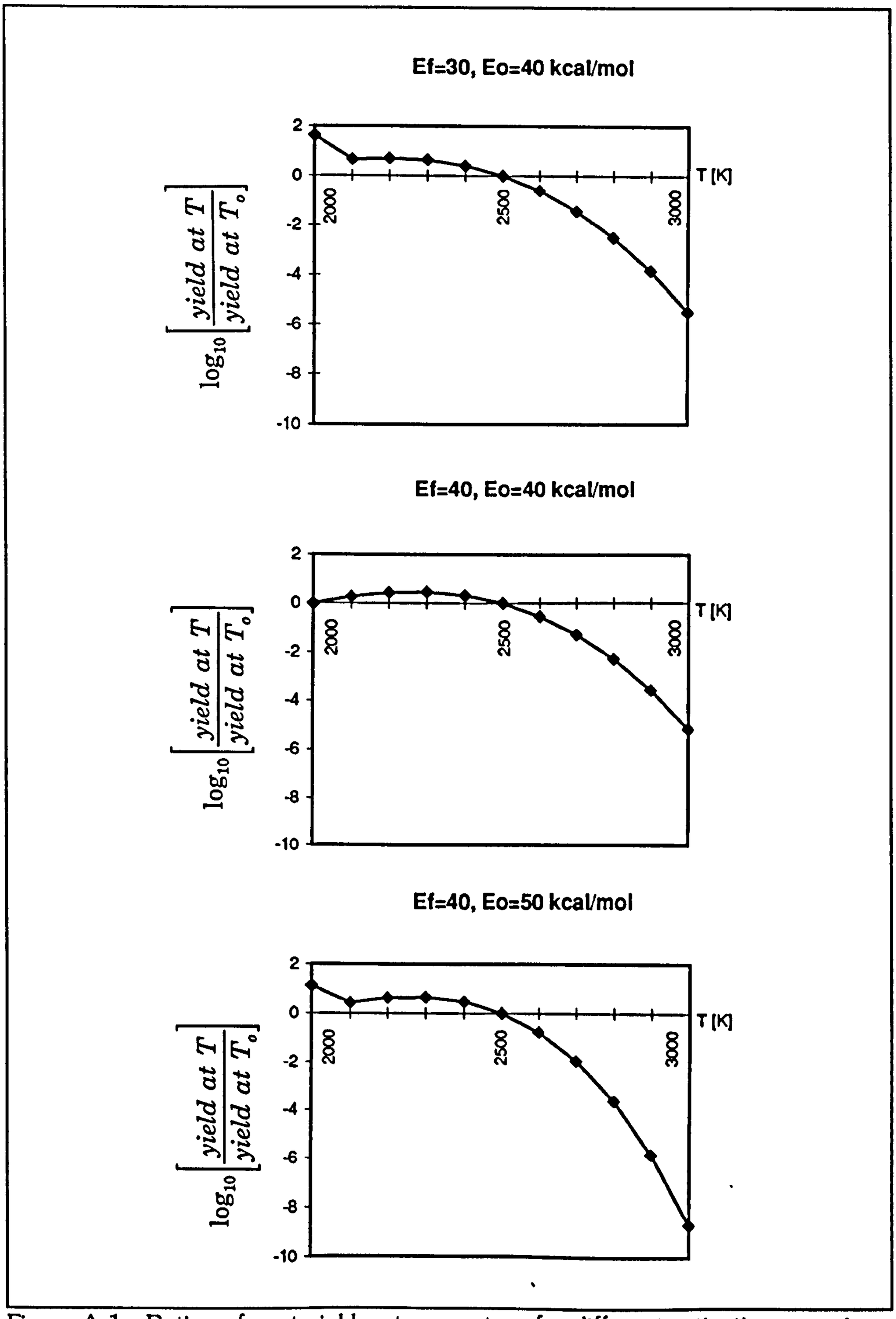

Figure A.1 - Ratios of soot yields v temperature for different activation energies

APPENDIX B - Soot model expressions

This Appendix gives details of the implementation of the soot model expressions. In each case, the equation is shown together with the constant values used. The expressions are presented in the order that they appear in the review of chapter 3 (section 3.4).

Formation expressions

Khan; 1971[170]

$$\frac{dm_{soot}}{dt} = A\,\phi^3\,p_{evap}\,e^{-\frac{E_f}{RT}} \qquad \text{(B.1)}$$

$A = 0.468$
$E_f = 40.0$ kcal/mol

Khan defines ϕ as the equivalence ratio of unburnt fuel in the soot-formation zone. This is expressed in terms of parameters used in the combustion model, i.e. the total fuel and air in the spray and the fraction of each which is said to be mixed, as follows:

$$\phi = \frac{m_{f\,total}}{m_{f\,mixed}}\,\phi_{mean} \qquad \text{(B.2)}$$

where ϕ_{mean} is the mean value of the equivalence ratio of unburnt fuel in the spray, i.e.:

$$\phi_{mean} = \frac{m_{eva}}{m_{air}} \qquad \text{(B.3)}$$

In the current work, a separate soot-formation region is not defined. The ϕ term input is simply taken as the equivalence ratio of unburnt fuel in the zone. This will generally be lower than the ϕ values calculated by Khan.

Harmadi; 1982[110]

$$\frac{dm_{soot}}{dt} = A\,\phi^{1.25}\,T^{-1}\,e^{-\frac{E_f}{RT}} \qquad \text{(B.4)}$$

$A = 2.0\text{x}10^{12}$
$E_f = 40.0$ kcal/mol

Hiroyasu; 1982[124]

$$\frac{dm_{soot}}{dt} = A\,m_{eva}\,p^{\frac{1}{2}}\,e^{-\frac{E_f}{RT}} \qquad \text{(B.5)}$$

The value of A is variable. For the standard case illustrated in this thesis, the following value was used:

$A = 0.2$
$E_f = 12.5$ kcal/mol

The values of these constants used by some other authors are summarised below (following equ. B.13).

Farmer; 1981[69]

$$\frac{dm_{soot}}{dt} = A\,m_f^{l}\,m_{O_2}^{m}\,T^{n}\,e^{-\frac{E_f}{RT}} \qquad \text{(B.6)}$$

$A = 4.66\text{x}10^{14}$
$l = 1.81$
$m = -0.5$
$n = 1.94$
$E_f = 32.0$ kcal/mol

Tesner; 1971[345]

Radical nuclei formation rate:

$$\frac{dn_{nuc}}{dt} = n_o + (f - g)\, n_{nuc} - g_o N_{soot}\, n_{nuc} \qquad \text{(B.7)}$$

where

$$n_o = a_o\, m_{evap}\, e^{-\frac{E_f}{RT}} \qquad \text{(B.8)}$$

$$g_o = g_{o,ref} \frac{T_{local}}{T_{ref}} \frac{p_{ref}}{p_{local}} \qquad \text{(B.9)}$$

$$b = b_{ref} \frac{T_{local}}{T_{ref}} \frac{p_{ref}}{p_{local}} \qquad \text{(B.10)}$$

Soot particle formation rate:

$$\frac{dN_{soot}}{dt} = A(a - bN_{soot})\, n_{nuc} \qquad \text{(B.11)}$$

$f - g = 100\ s^{-1}$
$g_{o,ref} = 1x10^{-6}\ m^3\ particle^{-1}\ s^{-1}$
$a_o = 1x10^{13}\ particles\ kg^{-1}\ s^{-1}$
$b_{ref} = 8x10^{-5}\ m^3\ particle^{-1}\ s^{-1}$
$a = 1.6x10^{5}\ particles\ m^{-3}\ s^{-1}$

The method used for implementation of the joint Tesner-Magnussen soot model in a partitioned thermodynamic structure is briefly described at the end of this appendix.

Oxidation

Feugier; 1972[73,74]

$$\frac{dm_{soot}}{dt} = A\, m_{soot} X_{O_2} e^{-\frac{E_o}{RT}} \qquad \text{(B.12)}$$

$A = 1.3\text{x}10^{6}$
$E_o = 32.0$ kcal/mol

Hiroyasu; 1982[126]

$$\frac{dm_{soot}}{dt} = A\, m_{soot} X_{O_2} p^{1.8} e^{-\frac{E_o}{RT}} \qquad \text{(B.13)}$$

The value of A is variable. For the standard case illustrated in this thesis, the following value was used:

$A = 6\text{x}10^{-6}$
$E_o = 14.0$ kcal/mol

Other authors have used different values for the constants in the Hiroyasu formation and oxidation expressions. Some of these values are summarised in Table B.1 (possibly the other authors have used different units in the oxidation expression):

Author	Condition	A_{for}	A_{ox}	E_f (kcal/mol)	E_o (kcal/mol)
Kittelson[174]	-	15.5	-	-	-
Kuo[197]	0.5 l engine	2.80	500	12.5	14.0
Kuo[197]	2.0 l engine	4.66	500	12.5	14.0
Kouremenos[190]	1 zone model	17	1	20.0	30.0
Kouremenos[192]	2 zone model	70	5	19.1	28.7
This study	0.78 l engine	0.2	$6\text{x}10^{-6}$	12.5	14.0

Table B.1 - Constant values used in Hiroyasu expressions

Lee, Thring, Beer; 1962[207]

$$\frac{dm_{soot}}{dt} = A\, m_{soot} X_{O_2} p\, T^{-\frac{1}{2}} e^{-\frac{E_o}{RT}} \qquad \text{(B.14)}$$

$A = 1.085\text{x}10^4$
$E_o = 39.3\,\text{kcal/mol}$

Magnussen; 1971[221]

$$\frac{dm_{soot}}{dt} = \frac{A\, m_{soot}\, e^{-\frac{E_{o1}}{RT}}\, p_{O_2}^{\,2}}{1 + B\, e^{-\frac{E_{o2}}{RT}}\, p_{O_2}^{\,2}} \qquad \text{(B.15)}$$

$A = 3.05\text{x}10^6$
$B = 3.10\text{x}10^{10}$
$E_{o1} = 57.6\,\text{kcal/mol}$
$E_{o2} = 58.2\,\text{kcal/mol}$

Nagle; 1962[249]

$$\frac{dm_{soot}}{dt} = A\, m_{soot}\left[\left(\frac{k_A p_{O_2}}{(1 + \frac{p_{O_2}}{k_Z})}\right) X + k_B p_{O_2}(1 - X)\right] \qquad \text{(B.16)}$$

where X, the fraction of the surface covered by active sites, is:

$$X = \frac{1}{1 + \frac{k_T}{p_{O_2} k_B}} \qquad \text{(B.17)}$$

and k is a simple Arrhenius term:

$$k = K e^{-\frac{E_o}{RT}} \qquad \text{(B.18)}$$

$K_A = 20.$
$K_B = 4.46\text{x}10^{-3}$
$K_T = 1.51\text{x}10^{5}$
$K_Z = 1./21.3$
$E_{o,A} = 30.0$ kcal/mol
$E_{o,B} = 15.2$ kcal/mol
$E_{o,T} = 97.0$ kcal/mol
$E_{o,Z} = 4.1$ kcal/mol

Magnussen; 1976[223,225]

The rate of soot oxidation is related directly to the rate of combustion:

$$\frac{dm_{soot}}{dt} = \frac{dm_f}{dt}\frac{m_{soot}}{m_f} \qquad \text{(B.19)}$$

The combustion rate is expressed in terms of turbulence parameters as follows:

$$\frac{dm_f}{dt} = 23.6\left(\frac{\nu\varepsilon}{k^2}\right)^{\frac{1}{4}}\frac{\varepsilon}{k}m_{\min}\chi \qquad \text{(B.20)}$$

The method used for implementation of the Tesner-Magnussen model is now briefly described.

Tesner-Magnussen model implementation

The implementation of a joint model using the Tesner formation mechanism and the Magnussen EDC oxidation expression is described in various publications by Magnussen[223,224,225,226] and also by Ahmad[3]. The basic principle of the model is to compute the rates of soot formation and oxidation within the framework of a thermodynamic structure which has been partitioned between regions of 'surrounding fluids' and 'heated fine structure'. The partitioning also permits simultaneous computation of the fast combustion chemistry by using the modelled rate of mixture transfer through the heated fine structure region, where fuel is allowed to burn (see section 4.4.3.4 for more details). Turbulence parameters are used to define the region sizes and the transfer rate, using a model known as the eddy dissipation concept (EDC).

In implementing this model, it is important to define the method used to obtain the temperatures and compositions in each of the thermodynamic regions. In fact, in the current work a separate thermodynamic partitioning has also been defined between reactant and combustion products regions, as described in section 4.4.4. These regions are consistent with the Magnussen concept, since the evolution of the combustion products region is defined according to the rate of transfer through the heated fine structure region. The temperature of the surrounding fluids region is simply taken as that of the reactants in the current model, whilst the temperature of the heated fine structure corresponds to that of the combustion products region. The error introduced by this approximation will be small.

Definition of the mixture and soot compositions to be used for each region is not so straightforward. In the earliest paper of the series, it is stated that the variables used in the soot model expressions are related to the mean values[223]. However, in that study, soot formation was limited to the regions of unburnt fuel, i.e. it was not allowed in the heated fine structure region. In the later studies, soot formation was permitted in both surrounding fluid and heated fine structure regions[224,225,226]. The fuel concentration input is apparently still taken to be the mean concentration. However, the computation of the soot formation rates is now greatly complicated by the fact that mixing processes occur in parallel with the formation process transferring soot particles to and from the heated fine structure region. If these transfers are to be fully accounted for, then it would be necessary to simultaneously integrate both pairs of soot model expressions for each of the thermodynamic regions. This is not practical.

This difficulty is bypassed by assuming local equilibrium between the surrounding fluid and heated fine structure regions following Magnussen's recommendation. The equations given by Magnussen are unclear, and in the current work, the soot nuclei and soot particle concentrations input to the soot model expressions were simply taken as the zonal average values from the previous timestep. This will have an impact on the behaviour of the expressions, since a timestep dependency has been introduced, but it is the only practical way of implementing the model. The timestep dependency was investigated by introducing a fractional timestep for computation of the Tesner-Magnussen soot model alone. It was found that the calculated rates were fairly insensitive to the length of the calculation timestep and the conclusions which were reached regarding use of the model are not affected.

APPENDIX C - Expression derivations

This Appendix lists various expressions which were derived by the author for use in the computer model. They are set out in the order in which they appear in the thesis.

Cross-jet velocity profile

Hiroyasu gives a cross-jet penetration correlation[126]:

$$S_l = S\,e^{-8.557\times10^{-3}(l-1)^2} \qquad \text{(C.1)}$$

where l is the zone number in the radial direction.

Since the spray model used is simple, the velocity distribution coefficient, C_f, can be obtained directly:

$$C_f = e^{-8.557\times10^{-3}(l-1)^2} \qquad \text{(C.2)}$$

Hiroyasu uses 10 cross-jet zones. Generalising to the case of n cross-jet zones, C_f may be written as:

$$C_f = e^{-0.693\left(\frac{l-1}{n-1}\right)^2} \qquad \text{(C.3)}$$

This can be simplified to give (equ 4.8):

$$C_f = 2.0^{-\left(\frac{l-1}{n-1}\right)} \qquad \text{(C.4)}$$

Break-up region penetration expression

A diagram showing the break-up region is given in Fig 4.3. In order to define the velocity of an arbitrary cross-jet zone, a linear variation of velocity is assumed between the position of break-up for the zone in question and the end of the break-up region, where the centre-line zone breaks up. The boundary conditions are as follows:

At the break-up position of a zone:

$$\begin{aligned} S &= L_{zone} \\ \frac{dS}{dt} &= U_{zone} \\ t &= t_{brk,zone} \end{aligned} \tag{C.5}$$

At the end of the break-up region:

$$\begin{aligned} S &= L_{cl} \\ \frac{dS}{dt} &= C_f U_{cl} \\ t &= t_{brk} \end{aligned} \tag{C.6}$$

Therefore, an the expression for zonal velocity in the break-up region can be written:

$$\frac{dS}{dt} = U_{zone}\left(\frac{L_{cl} - S}{L_{cl} - L_{zone}}\right) + C_f U_{cl}\left(\frac{S - L_{cl}}{L_{cl} - L_{zone}}\right) \tag{C.7}$$

An expression for the penetration, S, in terms of the general time, t, can then be derived by integrating this expression over the length of the break-up region, and applying the boundary conditions:

$$S = \left(\frac{U_{cl}C_f L_{zone} - U_{zone}L_{cl}}{U_{cl}C_f - U_{zone}}\right)\left[1 - \left(\frac{U_{cl}C_f(L_{cl} - L_{zone})}{U_{zone}L_{cl} - U_{cl}C_f L_{zone}}\right) e^{\frac{(t - t_{brk})(U_{cl}C_f - U_{zone})}{L_{cl} - L_{zone}}}\right] \tag{C.8}$$

Finally, a general expression for the zone velocity can be obtained:

$$\frac{dS}{dt} = U_{cl}C_f \; e^{\frac{(t - t_{brk})(U_{cl}C_f - U_{zone})}{L_{cl} - L_{zone}}} \tag{C.9}$$

Squish effect on penetration

If air which is taken up by the fuel spray is moving in the opposite direction with a squish velocity, v_{sq}, then by applying the principle of conservation of momentum, the following equation may be written:

$$U m_{tot} = U_o m_f - \Sigma \delta m_a v_{sq} \qquad \text{(C.10)}$$

where δm_a is the mass of air entrained during each calculation timestep

Thus, the general zonal velocity, U, is:

$$U = \frac{U_o m_f}{m_{tot}} - \frac{\Sigma \delta m_a v_{sq}}{m_{tot}} \qquad \text{(C.11)}$$

In the case where the squish velocity is zero,

$$U = \frac{U_o m_f}{m_{tot}} \qquad \text{(C.12)}$$

However, for this case,

$$U = \frac{dS}{dt}_s \qquad \text{(C.13)}$$

Thus, the first term represents the zone velocity relative to the air. This is already known for the case of zero squish, being obtained from equs. 4.4 - 4.12. Simple consideration of the velocity reduction in the squish case allows us to write:

$$U = \frac{U_o + v_{sq}}{U_o} \frac{dS}{dt}_s - \frac{\Sigma \delta m_a v_{sq}}{m_{tot}} \qquad \text{(C.14)}$$

This is equ. 4.16. The second term on the right hand side accounts for the effect on the absolute velocity of the entrainment of air moving in a direction counter to that of the jet. A simple check is to consider the case where the relative velocity, dS/dt_s, tends to zero. As it does so, $\Sigma \delta m_a$ tends to m_{tot} so that the absolute zonal velocity tends to $- v_{sq}$ as expected.

Combustion rate limit

In chapter 4, an expression for the limit on the combustion rate due to the change in the mass components of the subzones in the evaporation, air entrainment, sooting and combustion processes was derived. Similar expressions can be obtained considering the change in the air masses and fuel masses independently.

For the air limit, consider an air mass in the reactants subzone, m_a^-, to which is entrained a mass of air given by $(dm_a/dt)_{ent}\,\delta t$, and which looses a mass of air $(dm_f/dt)_{soot}\,\delta t\,AFR_{sto}$ in oxidation of soot during a small time interval δt; at the end of the timestep Δt, mass m_a^+ of mixture remains.

By balancing the mass consumed in burning during the timestep with the change in air mass in the reactants subzone, a limit on the average rate of consumption of fuel can be set:

$$\frac{dm_f}{dt}_{\lim} \delta t\, AFR_{sto} < -\left[m_a^+ - \left(m_a^- + \frac{dm_a}{dt}_{ent} \delta t - \frac{dm_f}{dt}_{soot} \delta t\, AFR_{sto}\right)\right]$$

$$\Rightarrow \frac{dm_f}{dt}_{\lim} < \frac{-\sum\left(\frac{\frac{dm_a}{dt}_{ent}}{AFR_{sto}} - \frac{dm_f}{dt}_{soot} - \frac{R_{xfer} m_a}{AFR_{sto}}\right)\delta t}{\Delta t} + \frac{\frac{dm_a}{dt}_{ent}}{AFR_{sto}} - \frac{dm_f}{dt}_{soot} \qquad (C.15)$$

where m_a is the instantaneous mass of air in the reactants subzone which is followed during the evaluation of the numerical integral

For the evaporated fuel limit, consider an evaporated fuel mass in the reactants subzone, m_e^-, which gains a mass of fuel $(dm_{eva}/dt)_{evap}\,\delta t$ due to evaporation, and which looses a mass of evaporated fuel $(dm_f/dt)_{soot}\,\delta t$ in oxidation of soot during a small time interval δt; at the end of the timestep Δt, evaporated fuel mass m_e^+ remains.

By balancing the mass consumed in burning during the timestep with the change in evaporated fuel mass in the reactants subzone, a limit on the average rate of

consumption of fuel can be set:

$$\frac{dm_f}{dt}_{\lim} \delta t \quad < \quad -\left[m^{+}_{eva} - \left(m^{-}_{eva} + \frac{dm_{eva}}{dt}_{evap} \delta t - \frac{dm_f}{dt}_{soot} \delta t\right)\right] \tag{C.16}$$

$$\Rightarrow \frac{dm_f}{dt}_{\lim} < \frac{-\sum\left(\frac{dm_{eva}}{dt}_{evap} - \frac{dm_f}{dt}_{soot} - R_{xfer} m_{eva}\right)\delta t}{\Delta t} + \frac{dm_{eva}}{dt}_{evap} - \frac{dm_f}{dt}_{soot}$$

where m_e is the instantaneous mass of evaporated fuel in the reactants subzone which is followed during the evaluation of the numerical integral

Temperature change when composition is changing rapidly

In most cases, c_p is not constant during the calculation timestep. By assuming a linear increase in the value of c_p (= dU/dT) during the timestep, a more accurate expression can be derived. Thus, we write:

$$\frac{dU}{dT} = \left(\frac{dU}{dT_2} - \frac{dU}{dT_1}\right)\frac{\Delta U}{U_2 - U_1} + \frac{dU}{dT_1} \tag{C.17}$$

$$= \left(\frac{dU}{dT_2} - \frac{dU}{dT_1}\right)\frac{U - U_1}{U_2 - U_1} + \frac{dU}{dT_1}$$

where *1* applies to conditions at the start of a calculation timestep
2 applies to conditions at the end of a calculation timestep

Also:

$$dT = \frac{dU}{\left(\frac{dU}{dT}\right)} \tag{C.18}$$

Substituting from equ. C.17 into C.18, integrating, and simplifying, gives the following expression:

$$\Delta T = \frac{\Delta U_{tot} \log_e \left(\frac{\frac{dU}{dT_2}}{\frac{dU}{dT_1}} \right)}{\frac{dU}{dT_2} - \frac{dU}{dT_1}} \qquad \text{(C.19)}$$

Replacing dU/dT by c_p we obtain the following, which is equ. **4.101**:

$$\Delta T = \frac{\Delta U_{tot} \log_e \left(\frac{c_{p_2}}{c_{p_1}} \right)}{c_{p_2} - c_{p_1}} \qquad \text{(C.20)}$$

APPENDIX D - Property Values

Units are SI unless otherwise stated.

Liquid fuel data

'Light' diesel, as defined by Kanury[162] and Heywood[116], is used as a standard fuel in the simulation program. The reaction chemistry is always computed on this basis, as well as other minor properties. However, for ignition delay, atomisation/ evaporation and heat-release calculations better results can be achieved by a more detailed specification of fuel properties. Thus, tridecane and gas oil are of interest in this study as these fuel were used in the experimental work of Kamimoto[159]. Property values are given below for each of these fuels in turn.

'Light' diesel

Fuel chemistry

'Light' diesel has an average molecular weight 170 and formula $C_nH_{1.8n}$ (giving $n \approx 12.3$) (Heywood[116]). Kanury gives the average boiling point as 250° C [162]. The oxygen content of the air is taken as 21.0% (Heywood[116]), so that stoichiometric air-fuel ratio is 14.47, and F (stoichiometric mass fuel/mass oxygen) is 0.316.

Latent heat

2.674×10^5 J kg^{-1} for light diesel, Kanury[162].

Heat of combustion

Heywood[116] gives a 'higher' heating value of 44.8 MJ kg^{-1} for light diesel.

Density

A value of 876 kg m^{-3} is given by Kanury[162] for light diesel.

Specific heat capacity

For the liquid fuel (light diesel), Kanury[162] gives a value of 1883 J kg^{-1} K^{-1}.

Coefficient of viscosity

The coefficient of viscosity of the liquid fuel is approximately 1.35×10^{-5} kg $m^{-2}\, s^{-1}$ at 25° C (dodecane value, Kanury[162]).

Surface tension

The following equations from Perry's Chemical Engineers Handbook[273] are used to relate the surface tension to the droplet temperature and the critical point conditions for the fuel:

$$\sigma = p_c^{\frac{2}{3}} T_c^{\frac{1}{3}} q (1 - T_r)^{\frac{11}{9}} \qquad (D.1)$$

where:

$$T_r = \frac{T_f}{T_c} \qquad (D.2)$$

and:

$$q = 0.1207 \left(1 + \frac{T_{br} \log_e p_c}{1 - T_{br}} \right) - 0.281 \qquad (D.3)$$

where:

$$T_{br} = \frac{T_B}{T_c} \qquad (D.4)$$

The Chemical Engineers' Handbook[272] gives a critical temperature of 449° C for fuel of API = 30, and a corresponding critical pressure of 23.1 atmospheres. For dodecane, Faeth[66] gives a value of 20.8 atm for the critical pressure of pure fuel, and predicts 36 - 57 atm for a droplet critical burning pressure.

Gas oil and tridecane properties

Fuel chemistry

Average molecular weight of gas oil: 208, formula $C_nH_{1.82n}$
Average molecular weight of tridecane: 184.4, formula $C_nH_{2.15n}$

Heat of combustion

'Higher' heating value of gas oil: 45.7 MJ kg^{-1}
'Higher' heating value of tridecane: 44.3 MJ kg^{-1}

Density

Gas oil: 840.3 kg m^{-3}
Tridecane: 756.8 kg m^{-3}

Cetane number

Gas oil: 57
Tridecane: 81

Gaseous species data

Air density - taken from the thermodynamic-state calculations already implemented.

Coefficient of viscosity

The following expression is given by Heywood[116] for air and combustion products:

$$\mu = \frac{3.3 \times 10^{-7} T^{0.7}}{1 + 0.027\phi} \qquad \text{(D.5)}$$

This expression fits experimental data accurately up to an equivalence ratio of at least four.

Thermal conductivity

The following general formula is given by Kanury[162]:

$$\lambda = \lambda_o \left(\frac{T}{T_o} \right)^n \qquad \text{(D.6)}$$

where n ≈ 0.94 for gases, n ≈ 1.83 for vapours.

The following base values are given[162]:

Species	Thermal conductivity ($J\,m^{-1}\,s^{-1}\,K^{-1}$) at 273.15 K
CO_2	0.0151
H_2O	0.0151
Air	0.0244

Table D.1 - Thermal conductivities of CO_2, H_2O and air

Maxwell gives a approximate chart for hydrocarbon data[231]. For an average molecular weight of 170, the following equation has been fitted to the chart line:

$$\lambda = 1.55 \times 10^{-4} T - 0.032 \qquad \text{(D.7)}$$

Internal energy

For the gaseous species, the following expression was derived[366] from the polynomial expansions for CH_2 hydrocarbons and their combustion products given by Krieger & Borman[194]:

$$u(t, m_a, m_f, m_{ab}, m_{fb}) = \frac{(A1\, m_a + A2\, m_f + A3\, m_{ab} + A4\, m_{fb})}{(m_a + m_f + m_{ab} + m_{fb})} \qquad \text{(D.8)}$$

where

$$A1 = 211.1 + 692.0t + 39.17t^2 + 52.93t^3 - 22.86t^4 + 2.776t^5$$

$$A2 = -1012. + 145.6t + 2734.5t^2 - 610.9t^3 - 132.7t^4 + 69.25t^5$$

$$A3 = 692.0t + 39.17t^2 + 52.93t^3 - 22.86t^4 + 2.776t^5$$

$$+ 2.326e^{\left[17.52 - \frac{22.14}{t} + \left(\frac{0.1035}{t} - 0.3356\right)\log_e p\right]}$$

$$A4 = -44216. + 827.0t + 1377.4t^2 - 312.1t^3 - 29.04t^4$$

in kJ/kg-mixture, where t = (T in K/1000)

The correction of an error in the combustion-products term given by Krieger & Borman[194] is described in the author's MSc thesis[366]. A check on the accuracy using an alternative polynomial expression given by Heywood[116] is also given in that work.

Specific heat capacity

An expression for the specific heat capacity can be derived from the above internal energy expression:

$$c_p(t, m_a, m_f, m_{ab}, m_{fb}) = \frac{(B1\, m_a + B2\, m_f + B3\, m_{ab} + B4\, m_{fb})}{(m_a + m_f + m_{ab} + m_{fb})} \qquad (D.9)$$

where

$$B1 = 692.0 + 78.35t + 158.8t^2 - 91.45t^3 + 13.88t^4$$

$$B2 = 145.6 + 5469.t - 1833.t^2 - 530.7t^3 + 346.3t^4$$

$$B3 = 692.0 + 78.35t + 158.8t^2 - 91.45t^3 + 13.88t^4$$

$$+ \frac{0.2408\,(213.9 - \log_e p)}{t^2} e^{\left[17.52 - \frac{22.14}{t} + \left(\frac{0.1035}{t} - 0.3356\right)\log_e p\right]}$$

$$B4 = 827.0 + 2755.t - 936.5t^2 - 116.2t^3$$

in kJ/kg-mixture, where t = (T in K/1000)

Soot data

Heat of combustion

For carbon oxidation, the heating value given by Heywood[116] is 33.8 MJ kg^{-1}. For the standard fuel (light diesel), the heat released in formation of soot from fuel can be obtained by difference: 11.0 MJ kg^{-1}. These values are modified as follows for the experimental fuels:

gas oil: 34.5 MJ kg^{-1}, 11.2 MJ kg^{-1}
tridecane: 33.6 MJ kg^{-1}, 10.7 MJ kg^{-1}

Density

The value for the soot particle density is normally taken to be slightly less than that for carbon[113], which is 2.0 kg m^{-3}. In this study, a value of 1.8 kg m^{-3} was used.

Particle size

Soot particle size varies considerably according to engine and operating conditions and in practice, a distribution of sizes will be found in any region. However, it is necessary in some cases to assume a particle size in order to calculate masses from number densities, and in this thesis a value of 27 nm has been assumed[113,116].

Other constants

Acceleration due to gravity - 9.81 m s^{-2}

Normal conditions - $p_{ntp} = 101325$ Pa, $T_{ntp} = 293.15$ K

APPENDIX E - Engine specification

Combustion system	Direct-injection diesel
Cylinders	4
Displaced volume	0.7801
Bore	95 mm
Stroke	110 mm
Compression ratio	14.6 (shallow bowl) 14.3 (deep bowl)
Standard operating speed	1250 rpm
Injection nozzle	Four-hole, 0.2 mm diameter
Injection pump	Bosch
Injection pump plunger diameter	7.5 mm, 9.0 mm

Table E.1 - Engine specification[11]

APPENDIX F - Mixing expressions

The spray and combustion models do not permit mixing between model zones. This means that the both the zonal compositions and soot yield predictions tend to constant values after the main combustion period, whilst in reality there is a steady mixing in the time before exhaust valve opening. To remedy this, the calculated zonal compositions and temperatures are post-processed according to a mixing law before being used as inputs to the soot-model equations. The calculated soot yields are corrected using the same relationship. The equations used for mixing are give below.

A factor, X_{mix}, is defined to describe the extent of mixing. The mixed values of any parameter, P, are related to the original unmixed values, P_o, and a calculated spray average value as follows:

$$P_{mix} = P_o (1 - X_{mix}) + P_{avg} X_{mix} \qquad \text{(F.1)}$$

The mixing factor is related to the fraction of time which has elapsed between ignition, t_{ign}, and a 'fully-mixed' time, t_{full}. The later value is entered as a model constant; a default value of BDC timing was used. If a linear relationship with elapsed time were used, then X_{mix} would be defined as follows:

$$X_{mix} = \left(\frac{t - t_{ign}}{t_{full} - t_{ign}} \right) \qquad \text{(F.2)}$$

However, a more realistic representation is achieved by using weighting in the form of an S-curve rather than a straight-line. Thus, a modified expression is required. Equation F.2 can be re-expressed as follows:

$$X_{mix} = \left[1 - \left(1 - \left(\frac{t - t_{ign}}{t_{full} - t_{ign}} \right) \right) \right] \qquad \text{(F.3)}$$

By including an additional term, and S-curve weighting can be achieved:

$$X_{mix} = \left[1 - \left(1 - \left(\frac{t - t_{ign}}{t_{full} - t_{ign}} \right) \right) \left(\frac{\frac{t - t_{ign}}{t_{full} - t_{ign}}}{\frac{t_{xover} - t_{ign}}{t_{full} - t_{ign}}} \right)^{n} \right] \qquad \text{(F.4)}$$

Here, t_{xover} is the time at which the expression crosses over from underweighting the scaling predicted by the linear expression (equ. F.2), to overweighting the scaling. The default value $t_{xover} - t_{ign}$ was set to 20% of the total time $t_{full} - t_{ign}$. The exponent, n, simply allows the degree of curvature of the S-curve to be adjusted. A value of zero corresponds to zero curvature; a value of 1.5 was chosen for default use.

APPENDIX G - Soot-combustion interaction

This Appendix briefly outlines the methods used to describe the interaction of sooting processes and combustion.

The main processes affecting the composition of the mixture in a zone are air entrainment, evaporation, combustion and soot formation and oxidation. At a given time and location, all of these processes will be occurring in parallel and description of the inter-relationship is complex. However, the *rates* of air entrainment and evaporation are relatively independent of the other parameters and can be taken as constants during a timestep. More problematic is the relationship between the soot and combustion processes. If the rates were integrated simultaneously, the combustion rate would generally dominate, consuming virtually all of the available unburnt fuel. This would have a serious effect on the soot production. However, the formation of soot is in fact an intrinsic part of the combustion process. Thus in modelling the process, the soot mechanism can be allowed access to all of the unburnt fuel. This does not imply that the sooting processes are more rapid than the combustion process, but simply that they form a fundamental component of the total burning. This approach was followed in the current work.

Therefore, the calculated soot formation and oxidation rates are used as constant inputs to the balance calculation for the combustion rate (equ. 4.98, and equs. C15 & C16, in Appendix C). However, in calculating the soot formation rate, it is necessary to take account of the variation in the concentration of evaporated fuel during the timestep. Similarly, the soot oxidation rate depends on the soot concentration which will also be varying. These problems were solved by means of a simple numerical integration for the soot and evaporation processes, neglecting the effect of combustion. The number of timesteps used for the integration was set according to the ratio of the initial rate and the existing soot concentration.

REFERENCES

1. ABBAS,A.S., LOCKWOOD,F.C.: "Note: Prediction of soot concentration in turbulent diffusion flames", J. Inst. Energy, pp. 112-115, Sept., 1985

2. ABRAMOVICH,G.N.: *The theory of turbulent jets*, MIT Press, Cambridge, Mass., 1963

3. AHMAD,T., PLEE,S.L., MYERS,J.P.: "Computation of nitric oxide and soot emissions from spray and gas-jet flames", ASME paper no. 82 WA/HT 1, 1982

4. AHMAD,T., PLEE,S.L., MYERS,J.P.: "Diffusion flame temperature - its influence on diesel particulate and hydrocarbon emissions", IMechE, C101/82, pp. 267-275, 1982

5. AIGAL,A.K., SINGAL.S.K., PUNDIR,B.P.: "Analysis of measured droplet size distribution of air deflected spray", Proc. IMechE, vol. 209, pp. 33-43, 1995

6. ALKIDAS,A.C.: "Relationship between smoke measurements and particulate measurements", SAE 840412, 1984

7. AMANN,C., STIVENDER,D.L., PLEE,S.L., MacDONALD,J.S.: "Some rudiments of diesel particulate emissions", SAE 800251, 1980

8. AMATO,U., BELARDINI,P., BERTOLI,C., DEL GIACOMO,N.: "The joint use of multi-dimensional modelling and field experiments in order to design diesel combustion systems", IMechE, C430/045, 1991

9. ANNAND,W.J.D.: "Heat transfer in the cylinders of reciprocating internal combustion engines", Proc. IMechE, vol. 177, no. 36, pp. 973-979, 1963

10. ANNAND,W.J.D.: "Heat transfer in the cylinder and porting", pp. 773-802, in *The thermodynamics and gas dynamics of internal combustion engines*, vol. 2, eds. HORLOCK,J.H., WINTERBONE,D.E., Clarendon Press, 1986

11. AOYAGI,Y., KAMIMOTO,T., MATSUI,Y., MATSUOKA,S.: "A gas sampling study on the formation processes of soot and NO in a DI diesel engine", SAE 800254, 1980

12. ARAI,M., TADOKORO,Y., KADOTA,T., HIROYASU,H.: "Soot formation in spray flames", Bull. of the JSME, vol. 24, no. 187, pp. 153-159, Jan., 1981

13. ARCOUMANIS,C.: *Internal combustion engines*, Academic Press, 1988

14. ARCOUMANIS,C., WHITELAW,J.H., HENTSCHEL,W., SCHINDLER,K-P.: "Flow and combustion in a transparent 1.9l direct-injection diesel engine", IMechE, 'Automobile emissions and combustion', AUTOTECH '93, pp. 125-141, 1993

15. ASSANIS,D., KARVOUNIS,E., SEKAR,R., MARR,W.: "Heat release analysis of oxygen-enriched diesel combustion", Trans. ASME, Journal of Engineering for Gas Turbines and Power, vol. 115, pp. 761-768, Oct., 1993

16. AXELBAUM,R.L., LAW,C.K.: "Soot formation and inert addition in diffusion flames", Twenty-third Symposium (Int.) on Combustion, pp. 1517-1523, The Combustion Institute, 1990

17. BALL,D.: "Black lungs and black walls", New Scientist, pp. 22-23, 12th Feb., 1987

18. BALL,D.J.: "Particulate carbon emissions and diesel vehicles", IMechE, C337/87, 1987

19. BAZARI,Z.: "A DI diesel combustion and emission predictive capability for use in cycle simulation", SAE 920462, 1992

20. BAZARI,Z., FRENCH,B.A.: "Performance and emissions trade-off for a HSDI diesel engine - an optimization study", SAE 930592, 1993

21. BECKER,H.A., YAMAZAKI,S.: "Soot concentration field of turbulent propane/air diffusion flames", Sixteenth Symposium (Int.) on Combustion, pp. 681-691, The Combustion Institute, 1977

22. BENSON,R.S., WHITEHOUSE,N.D.: *Internal combustion engines*, Pergamon Press, 1979

23. BITTNER,J.D., HOWARD,J.B.: "Pre-particulate chemistry in soot formation", pp. 109-142, in *Particulate carbon formation during combustion*, eds. SIEGLA,D.C., SMITH,G.W., Plenum Press, New York, 1981

24. BLIZARD,N.S., KECK,J.C.: "Experimental and theoretical investigation of turbulent burning model for internal combustion engines", SAE 740191, 1974

25. BOCKHORN,H.: "Soot formation during combustion, recent developments in mechanisms and models", Proc. Anglo-German Combustion Symposium, The British Section of the Combustion Institute, pp. 1-9, Cambridge, 29th Mar.-2nd Apr., 1993

26. BOCKHORN,H., (ed.): *Mechanisms and models of soot formation*, Springer, Berlin, 1994

27. BÖHM,H., HESSE,D., JANDER,H., LÜERS,B., PIETSCHER,J., WAGNER,H.G., WEISS,M.: "The influence of pressure and temperature on soot formation in premixed flames", Twenty-second Symposium (Int.) on Combustion, The Combustion Institute, pp. 403-411, 1988

28. BÖHM,H., FELDERMANN,C.H.R., HEIDERMANN,T.H., JANDER,H., LÜERS,B., WAGNER,H.G.: "Soot formation in premixed C_2H_4-air flames for pressures up to 100 bar", Twenty-fourth Symposium (Int.) on Combustion, The Combustion Institute, pp. 991-998, 1992

29. BÖHM,H., BÖNIG,M., FELDERMANN,C.H.R., JANDER,H., RUDOLPH,G., WAGNER,H.G.: "Pressure dependency of formation of soot and PAH in premixed flames", pp. 145-164, in *Mechanisms and models of soot formation*, ed. BOCKHORN,H., Springer, Heidelberg, 1994

30. BÖNIG,M., FELDERMANN,C., JANDER,H., LÜERS,B., RUDOLPH,G., WAGNER,H.G.: "Soot formation in premixed C_2H_4 flat flames at elevated pressure", Twenty-third Symposium (Int.) on Combustion, The Combustion Institute, pp. 1581-1587, 1990

31. BORMAN,G.L., JOHNSON,J.H.: "Unsteady vaporization histories and trajectories of fuel droplets injected into swirling air", in *Burning in a wide range of fuels in diesel engines*, SAE Progress in Technology, vol. 11, SAE, 1967

32. BOWN,W.: "Dying from too much dust", New Scientist, pp. 12-13, 12th Mar., 1994

33. BRACCO,F.V.: "Modelling of engine sprays", SAE 850394, 1985

34. BRANDTL,F., REVERENCIE,I., CARTELLIERI,W., DENT,J.C.: "Turbulent air flow in the combustion bowl of a D.I. diesel engine and its effect on engine performance", SAE 790040, 1979

35. BROADKEY,R.S.: *Turbulence in mixing operations*, Academic Press, London, 1975

36. BROOME,D., KHAN,I.M.: "The mechanisms of soot release from combustion of hydrocarbon fuels with particular reference to the diesel engine", Symposium on 'Air pollution control in transport engines', Solihull, Automotive Division, IMechE, C140/71, p. 185, Nov., 1971

37. BROWN,A.J., HEYWOOD,J.B.: "A fundamentally-based stochastic mixing model method for predicting NO and soot emissions from direct-injection diesel engines", Calculations of Turbulent Reactive Flows - AMD - vol.81 (Book Number H00350), The ASME, pp. 293-312, 1987

38. CALCOTE,H.F., GILL,R.J.: "Comparison of the ionic mechanism of soot formation with a free radical mechanism", pp. 471-484, in *Mechanisms and models of soot formation*, ed. BOCKHORN,H., Springer, Berlin, 1994

39. CATANIA,A.E., MITTICA,A.: "Induction system effects on small-scale turbulence in a high-speed diesel engine", Trans. ASME, Journal of Engineering for Gas Turbines and Power, vol. 109, pp. 491-502, Oct., 1987

40. CATON,J.A., HEYWOOD,J.B.: "An experimental and analytical study of heat transfer in an engine exhaust port", Int. J. Heat Mass Transfer, vol. 24, no. 4, pp. 581-595, 1981

41. CHAN,M.-L., MOODY,K.N., MULLINS,J.R., WILLIAMS,A.: "Low-temperature oxidation of soot", Fuel, vol. 66, pp. 1694-1698, Dec., 1987

42. CHEN,B.-X., WANG,R.-S., HU,G.-D.: "Computer simulation of three types of combustion systems for DI diesel engines", pp. 599-609, in *Heat and mass transfer in gasoline and diesel engines*, eds. SPALDING,D.B., AFGAN,N.H., Hemisphere, 1989

43. CHERVINSKY,A.: "Supercritical burning of liquid droplets in stagnant environment", AIAA Journal, vol. 7, pp. 1815-1817, Sept., 1969

44. CHIGIER,N.: "The atomization and burning of liquid fuel sprays", Prog. Energy Comb. Sci., vol. 2, pp. 97-114, 1976

45. CHIU,W.S., SHAHED,S.M., LYN,W.T.: "A transient spray mixing model of diesel combustion", SAE 760128, 1976

46. CHMELA,F.G., WERLBERGER,P.: "Experience with an endoscopic video system for engine combustion observation", IMechE, 'Automobile emissions and combustion', AUTOTECH '93, pp. 173-182, 1993

47. COELHO,P.J., FARIAS,T.L., PEREIRA,J.C.F., CARVALHO,M.G.: "Numerical prediction of turbulent sooting diffusion flames", AGARD meeting on 'Fuels and combustion technology for advanced aircraft engines', no. 8, May, 1993

48. CORRSIN,S.: "Simple theory of an idealized turbulent mixer", AIChEJ, vol. 3, no. 3, 1957

49. CURL,R.L.: "Dispersed phase mixing: Theory and effects in simple reactors", AIChE Journal, vol. 9, no. 2, pp. 175-181, 1963

50. D'ANNA,A., D'ALESSIO,A., MINUTOLO,P.: "Spectroscopic and chemical characterization of soot inception processes in premixed laminar flames", pp. 83-103, in *Mechanisms and models of soot formation*, ed. BOCKHORN,H., Springer, Berlin, 1994

51. DEN OUDEN,C.J.J., CLARK,R.H., COWLEY,L.T., STRADLING,R.J., LANGE,W.W., MAILLARD,C.: "Fuel quality effects on particulate matter emissions from light- and heavy-duty diesel engines", SAE 942022, 1994

52. DENT,J.C.: "A basis for the comparison of various experimental methods for studying spray penetration", SAE 710571, 1971

53. DENT,J.C., SALAMA,N.S.: "The measurement of the turbulence characteristics in an internal combustion engine cylinder", SAE 750886, 1975

54. DENT,J.C., SULIAMAN,S.J.: "Convective and radiative heat transfer in a high swirl direct injection diesel engine", SAE 770407, 1977

55. DENT,J.C.: "Turbulent mixing rate - its effect on smoke and hydrocarbon emissions from diesel engines", SAE 800092, 1980

56. DENT,J.C., MEHTA,P.S.: "Phenomenological combustion model for a quiescent chamber diesel engine", SAE 811235, 1981

57. DENT,J.C., MEHTA,P.S., SWAN,J.: "A predictive model for automotive DI diesel engine performance and smoke emissions", IMechE, C126/82, pp. 237-245, 1982

58. DENT,J.C.: "Some diagnostic methods applied to air-fuel mixing processes in internal combustion engines, and their phenomenological modelling", in Proceedings of International Symposium on Diagnostics and Modeling of Combustion in Reciprocating Engines, COMODIA 85, pp. 39-52, Tokyo, 4th-6th Sept., 1985

59. DESANTES,J.M., LAPUERTA,M., SALAVERT,J.M.: "Modelling of the wall jet in a direct injection diesel engine", Proc. IMechE, vol. 206, pp. 185-196, 1992

60. DU,C.J., KITTELSON,D.B.: "Total cylinder sampling from a diesel engine: Part III - particle measurements", SAE 830243, 1983

61. EDELMAN,R.B., TURAN,A., HARSHA,P.T., WONG,E., BLAZOWSKI,W.S.: "Fundamental characterization of alternative fuel effects in continuous combustion systems", Combustion Modeling, AGARD CP-275, paper no. 13, 1979

62. EISENKLAM,P., ARUNACHALAM,S., WESTON,J.: "Evaporation rates and drag resistance of burning drops", Eleventh Symposium (Int.) on Combustion, The Combustion Institute, pp. 715-728, 1967

63. ELKOTB,M.M.: "Fuel atomization for spray modeling", Prog. Energy Comb. Sci., vol. 8, pp. 61-90, 1982

64. ESCUDIER,M.P.: "Aerodynamics of a burning turbulent gas jet in a cross flow", Comb. Sci. & Tech., vol. 4, pp. 293-301, 1972

65. FAETH,G.M., DOMINICIS,D.P., TULPINSKY,J.F., OLSON,D.R.: "Supercritical bipropellant droplet combustion", Twelfth Symposium (Int.) on Combustion, The Combustion Institute, pp. 9-18, 1969

66. FAETH,G.M.: "Current status of droplet and liquid combustion", Prog. Energy Comb. Sci., vol. 3, pp. 191-224, 1977

67. FAIRWEATHER,M., JONES,W.P., LEDIN,H.S., LINDSTEDT,R.P.: "Predictions of soot formation in turbulent non-premixed propane flames", Twenty-fourth Symposium (Int.) on Combustion, The Combustion Institute, pp. 1067-1074, 1992

68. FAIRWEATHER,M., JONES,W.P., LINDSTEDT,R.P.: "Predictions of radiative transfer from a turbulent reacting jet in a cross-wind", Comb. & Flame, vol. 89, pp. 45-63, 1992

69. FARMER,R., EDELMAN,R., WONG,E.: "Modeling soot emissions in combustion systems", pp. 299-320, in *Particulate carbon formation during combustion*, eds. SIEGLA,D.C., SMITH,G.W., Plenum Press, New York, 1981

70. FENIMORE,C.P., JONES,G.W.: "Oxidation of soot by hydroxyl radicals", J. Phys. Chem., vol. 71, pp. 593-597, 1967

71. FENIMORE,C.P., JONES,G.W.: "Coagulation of soot to smoke in hydrocarbon flames", Comb. & Flame, vol. 13, pp. 303-310, Jun., 1969

72. FEOLA,M., ROCCO,V.: "Strategies toward clean and fuel-efficient diesel engines", International Conference "Toward clean and fuel efficient automobiles", OECD, Berlin, 25-27th Mar. 1991, pp. 345-353, 1993

73. FEUGIER,A.: "Soot oxidation in laminar hydrocarbon flames", Comb. & Flame, vol. 19, pp. 249-256, 1972

74. FEUGIER,A.: "Soot oxidation in laminar hydrocarbon flames", pp. 487-494, in *Heat transfer in flames*, eds. AFGAN,N.H., BEER,J.M., Scripta, Washington, 1974

75. FIELD,M.A., GILL,D.W., MORGAN,B.B., HAWKSLEY,P.G.W.: *Combustion of Pulverised Coal*, BCURA, Leatherhead, 1967

76. FITZGEORGE,D., ALLISON,J.L.: "Air swirl in a road-vehicle diesel engine", Proc. IMechE (A.D.), no. 4, pp. 151-168, 1962-1963

77. FLOWER,W.L.: "The effect of elevated pressure on the rate of soot production in laminar diffusion flames", Comb. Sci. & Tech., vol. 48, pp. 31-43, 1986

78. FRENKLACH,M., WANG,H.: "Detailed mechanism and modeling of soot particle formation", pp. 162-192, in *Mechanisms and models of soot formation*, ed. BOCKHORN,H., Springer, Berlin, 1994

79. FRISWELL,N.J.: "The influence of fuel composition on smoke emission from gas-turbine-type combustors: effect of combustor design and operating conditions", Comb. Sci. & Tech., vol. 19, pp. 119-127, 1979

80. FRÖSSLING,N.: Gerlands Beitr. Geophys., vol. 52, p. 170, 1938

81. FUJIWARA,Y., FUKAZAWA,S., TOSAKA,S., MURAYAMA,T.: "Formation of soot particulates in the combustion chamber of a precombustion chamber type diesel engine", SAE 840417, 1984

82. FUJIWARA,Y., TOSAKA,S., MURAYAMA,T.: "Microcrystal structure of soot in the combustion chamber of prechamber type diesel engines", SAE 901579, 1990

83. FUKUDA,M., NAKAO,M., YOSHIHARA,Y., IKEGAMI,M.: "Local gas composition in the combustion chamber of a direct-injection diesel engine", JSAE Review, vol. 9, no. 4, pp. 24-30, Oct., 1988

84. FURUTANI,H., TSUGE,S., GOTO,S.: "The dependence of carbon/hydrogen ratio on soot particle size", SAE 920689, 1992

85. GARO,A., LAHAYE,J., PRADO,G.: "Mechanisms of formation and destruction of soot particles in a laminar methane-air diffusion flame", Twenty-first Symposium (Int.) on Combustion, The Combustion Institute, pp. 1023-1031, 1986

86. GARO,A., SAID,R., BORGHI,R.: "Model of soot formation: coupling of turbulence and soot chemistry", pp. 527-560, in *Mechanisms and models of soot formation*, ed. BOCKHORN,H., Springer, Berlin, 1994

87. GIBBS,R., WHITBY,R., JOHNSON,R.: "Observation of particle oxidation in diesels: prospect for combustion research and particulate control", SAE 860291, SAE P-172, 1986

88. GILYAZETDINOV,L.P.: "The kinetics and formation mechanism of carbon black during the thermal decomposition of hydrocarbons in the gas phase", Khimiya Tverdogo Topl, vol. 3, pp. 103-111, 1972

89. GLASSMAN,I., YACCARINO,P.: "The temperature effect in sooting diffusion flames", Eighteenth Symposium (Int.) on Combustion, The Combustion Institute, pp. 1175-1183, 1981

90. GLASSMAN,I.: *Combustion*, 2nd ed., Academic Press, 1987

91. GODSAVE,G.E.: "Studies of the combustion of drops in a fuel spray - the burning of single drops of fuel", Fourth Symposium (Int.) on Combustion, The Combustion Institute, pp. 818-830, 1953

92. GOKALP,I., CHAUVEAU,C., RICHARD,J.R., KRAMER,M., LEUCKEL,W.: "Observations on the low temperature vaporization and envelope or wake flame burning of n-heptane droplets at reduced gravity during parabolic flights", Twenty-second Symposium (Int.) on Combustion, The Combustion Institute, pp. 2027-2035, 1988

93. GOLOVINA,E.S., KHAUSTOVICH,G.P.: "The interaction of carbon with carbon dioxide and oxygen at temperatures up to 3000°K", Eight Symposium (Int.) on Combustion, Williams and Wilkins, pp. 784-792, 1962

94. GOSMAN,D., HARVEY,P.S.: "Computer analysis of fuel-air mixing and combustion in an axi-symmetric D.I. diesel", SAE 820036, 1982

95. GRAHAM,S.C., HOMER,J.B., ROSENFELD,J.L.J.: "The formation and coagulation of soot aerosols generated by the pyrolysis of aromatic hydrocarbons", Proc. Roy. Soc. London A., vol. 344, pp. 259-285, 1978

96. GRASSO,B.F., BRACCO,F.V.: "Evaluation of a mixing-controlled model for engine combustion", Comb. Sci. & Tech., vol. 28, pp. 185-210, 1982

97. GREEN,H.L., LANE,W.R.: *Particulate clouds, dusts, smokes and mists*, 2nd ed., E.&F.N. Spon, London, 1964

98. GREEVES,G., MEEHAN,J.O.: "Measurement of instantaneous soot concentration in a diesel combustion chamber", IMechE, C88/75, 1975

99. GREEVES,G., PARTRIDGE,I.M.: "Experiments and calculations on optimising fuel economy and emissions in passenger car diesel engines", IMechE, C228/79, 1979

100. GRIFFITHS,J.F., PAPPIN,J., AL-RUBAIE,M.R.: "Fundamental studies related to combustion in diesel engines", IMechE, C433/018, pp. 151-158, 1991

101. GRIGG,H.C., SYED,M.H.: "The problem of predicting rate of heat release in diesel engines", Symp. Diesel Engine Combustion, Proc. IMechE, vol. 184 (pt. 3J), pp. 192-, 1969-1970

102. GRIMSMO,B., MAGNUSSEN,B.F.: "Numerical calculation of combustion in Otto and Diesel engines", Proc. Anglo-German Combustion Symposium, The British Section of the Combustion Institute, pp. 400-403, Cambridge, 29th Mar.-2nd Apr., 1993

103. GÜLDER,Ö.L., SNELLING,D.R.: "Formation and temperature of soot particles in laminar diffusion flames with elevated temperatures", Twenty-third Symposium (Int.) on Combustion, pp. 1509-1515, The Combustion Institute, 1990

104. GUPTA,A.K.: *Soot modeling for direct injection diesel engine*, PhD thesis, University of Roorkee, 1986

105. GUPTA,A.K., MEHTA,P.S., GUPTA,C.P.: "Model for predicting air-fuel mixing and combustion for direct injection diesel engine", SAE 860331, 1986

106. HA,J-Y., IIDA,N., SATO,G.T., HAYASHI,A., TANABE,H.: "Experimental investigation of the entrainment into diesel spray", SAE 841078, 1984

107. HAMAMOTO,Y., TOMITA,E.: "Turbulence characteristics of swirl in an I.C. engine cylinder", JSAE Review, vol. 9, no. 4, pp. 4-9, Oct., 1988

108. HARDENBERG,H.O., HASE,F.W.: "An empirical formula for computing the pressure rise delay of a fuel from its cetane number and from the relevant parameters of direct-injection diesel engines", SAE 790493, 1979

109. HARGREAVE,G., POURKASHANIAN,M., WILLIAMS,A.: "The combustion and gasification of coke and coal chars", Twenty-first Symposium (Int.) on Combustion, The Combustion Institute, pp. 221-230, 1986

110. HARMADI,E.: *Study on soot formation and oxidation*, MSc thesis, Dept. of Heat Power Engineering, University of Hiroshima, 1982

111. HARRISON,R.M. (chairman): "Diesel vehicle emissions and urban air quality", 2nd report of the Quality of Urban Air Review Group, Department of the Environment, Dec., 1993

112.HARVEY,P.S., GOSMAN,D.: "An analysis of the influence of swirl on combustion in DI diesel engines by computer simulation", IMechE, C130/82, pp. 247-258, 1982

113.HAYNES,B.S., WAGNER,H.G.: "Soot formation", Prog. Energy Combust. Sci., vol. 7, pp. 229-273, 1981

114.HEIN,K.: "Recent results on the formation and combustion of soot in turbulent fuel oil and gas flames", Comb. Sci. & Tech., vol. 5, pp. 195-206, 1972

115.HENEIN,N.A.: "Analysis of pollutant formation and control and fuel economy in diesel engines", Prog. Energy Combust. Sci., vol. 1, pp. 165-207, 1976

116.HEYWOOD,J.B.: *Internal combustion engines*, McGraw-Hill, 1989

117.HIGHFIELD.R.: "Airborne killer that targets the heart", The Daily Telegraph, p. 14, 27th Jul., 1994

118.HIRAKI,H., RIFE,J.: "Performance and NO_x model of a direct injection stratified charge engine", SAE 800050, 1980

119.HIROYASU,H.: "Mathematical expression for drop size distribution in sprays", NASA CR-72272, 1967

120.HIROYASU,H., KADOTA,T.: "Droplet size distributions in diesel engines", SAE 740715, 1974

121.HIROYASU,H., KADOTA,T.: "Models for combustion and formation of nitric oxide and soot in direct injection diesel engines", SAE 760129, 1976

122.HIROYASU,H., KADOTA,T., ARAI,M.: "Fuel spray characterization in diesel engines", pp. 369-408, in *Combustion Modeling in Reciprocating Engines*, eds. MATTAVI,J.N., AMANN,C.A., Plenum Press, New York, 1980

123.HIROYASU,H., ARAI,M., NAKANISHI,K.: "Soot formation and oxidation in diesel engines", SAE 800252, SAE P-86, 1980

124.HIROYASU,H., YOSHIMATSU,A., ARAI,M.: "Mathematical model for predicting the rate of heat release and exhaust emissions in IDI diesel engines", IMechE, C102/82, 1982

125.HIROYASU,H., KADOTA,T., ARAI,M.: "Development and use of a spray combustion modeling to predict diesel engine efficiency and pollutant emissions (Part 1: Combustion Modeling)", Trans. JSME, 42-432 B, p. 1606, 1982

126.HIROYASU,H., KADOTA,T.: "Development and use of a spray combustion modeling to predict diesel engine efficiency and pollutant emissions (Part 1: Combustion Modeling)", Bulletin JSME, vol. 26, no. 214, paper no. 214-12, pp. 569-575, Apr., 1983

127.HIROYASU,H., KADOTA,T., ARAI,M.: "Development and use of a spray combustion modeling to predict diesel engine efficiency and pollutant emissions (Part 2: Computational Procedure and Parametric Study)", Bull. of the JSME, vol. 26, no. 214, paper no. 214-13, pp. 576-583, Apr., 1983

128.HIROYASU,H.: "Diesel engine combustion and its modeling", in Proceedings of International Symposium on Diagnostics and Modeling of Combustion in Reciprocating Engines, COMODIA 85, pp. 53-75, Tokyo, 4th-6th Sept., 1985

129.HIROYASU,H., ARAI,M., TABATA,M.: "Empirical equations for the Sauter Mean Diameter of a diesel spray", SAE 890464, 1989

130.HIROYASU,H., ARAI,M.: "Structures of fuel sprays in diesel engines", SAE 900475, 1990

131.HIROYASU,H., NISHIDA,K., SUZUKI,M., ODA,H., YOSHIKAWA,S., ARAI,M.: "Total in-cylinder sampling experiment on emission formation processes in a DI diesel engine", SAE 902062, 1990

132.HODGETTS,D., SHROFF,H.D.: "More on the formation of nitric oxide in a diesel engine", IMechE, C95/75, 1975

133.HOHENBERG,G.F.: "Advanced approaches for heat transfer calculation", SAE 790825, 1979

134.HORROCKS,R.W.: "Particulate control systems for diesel engines", IMechE, C349/87, 1987

135.HOTTEL,H.C., WILLIAMS,G.C., SIMPSON,H.C.: "Combustion of droplets of heavy liquid fuels", Fifth Symposium (Int.) on Combustion, pp. 101-129, 1955

136.HOULT,D.P., FAY,J.A., FORNEY,L.J.: "A theory of plume rise compared with field observations", J. Air Pollut. Control Ass., vol. 19, pp. 585-590, 1969

137.HOULT,D.P., WEIL,W.C.: "Turbulent plume in a laminar cross flow", Atmospheric Environment, vol. 6, pp. 514-531, 1972

138.HOWARD,G.P.: "World powertrains for passenger cars, A review of future trends in engine design and manufacture", The Economist Intelligence Unit, Special Report No. 2094, Sept., 1991

139.HUCKNALL,D.J.: *Chemistry of hydrocarbon combustion*, Chapman & Hall, 1985

140.HUTH,M., LEUCKEL,W.: "Experiments on soot formation from propane under partial oxidation conditions in a turbulent plug-flow reactor", Twenty-third Symposium (Int.) on Combustion, pp. 1493-1499, The Combustion Institute, 1990

141.IGARASHI,T., NAGAKURA,H., SHIMODA,M., OTANI,T.: "Current situation and problems of diesel particulate trap", JSAE Review, vol. 11, no. 1, pp. 13-17, 1989

142.IIDA,N. "Surrounding gas effects on soot formation and extinction - observation of diesel spray combustion using a rapid compression machine", SAE 930603, 1993

143.IIYAMA,A., MATSUMOTO,Y., KAWAMOTO,K., OHISHI,T.: "Spray formation improvement of VCO nozzle for DI diesel smoke reduction", Diesel Fuel Injection Systems, IMechE, pp. 131-136, 1992

144.IKEGAMI,M., SHIOJI,M.: "A stochastic model of an unsteady turbulent diffusion flame in a confined space", Bull. of the JSME, vol. 23, no. 186, pp. 2076-2087, Dec., 1980

145. IKEGAMI,M., SHIOJI,M., KOIKE,M.: "A stochastic approach to model the combustion process in direct-injection diesel engines", Twentieth Symposium (Int.) on Combustion, pp. 217-224, The Combustion Institute, 1984

146. IKEGAMI,M., SHIOJI,M., NISHIMOTO,K.: "Turbulence intensity and spatial integral scale during compression and expansion strokes in a four-cycle reciprocating engine", SAE 870372, 1987

147. IKEGAMI,M., SHIOJI,M., KIMOTO,T.: "Diesel combustion and pollutant formation as viewed from turbulent mixing concept", SAE 880425, 1988

148. JANDER,H., WAGNER,H.G.: "Soot formation in combustion - An International Round Table discussion", Nachrichten der Akademie der Wissesnschaften in Göttingen, II Mathematisch-Physikalische Klasse, Jahrgang 1989, Nr. 3, Vandenhoeck und Ruprecht, Göttingen, 1990

149. JANSSEN,R.D., LUDFORD,G.S.S.: "Burning rate response of a methanol drop to ambient air pressure", Nineteenth Symposium (Int.) on Combustion, The Combustion Institute, pp. 999-1006, 1982

150. JENSEN,D.E.: "Prediction of soot formation rates: a new approach", Proc. Roy. Soc. London A., vol. 338, pp. 375-396, 1974

151. JIANG,Q., VAN GERPEN,J.H.: "Prediction of diesel engine particulate emission during transient cycles", SAE 920466, 1992

152. JIN,J.D., BORMAN,G.L.: "A model for multi-component droplet vaporization at high ambient pressures", SAE 850264, 1985

153. KADOTA,T. et al.: "Spontaneous ignition delay of a fuel droplet in high pressure and high temperature gaseous environments", Bull. of the JSME, vol. 19, no. 130, pp. 437-445, Apr., 1976

154. KADOTA,T., HIROYASU,H.: "Evaporation of a single droplet at elevated pressures and temperatures (2nd report, Theoretical Study)", Bull. of the JSME, vol. 19, no. 138, pp. 1515-1521, Dec., 1976

155. KADOTA,T., HIROYASU,H., FARAZANDEHMEHR,A.: "Soot formation by combustion of a fuel droplet in high pressure gaseous environments", Comb. & Flame, vol. 29, pp. 67-75, 1977

156. KADOTA,T., HENEIN,N.: "Time-resolved soot particulates in diesel spray combustion", pp. 391-421, in *Particulate carbon formation during combustion*, eds. SIEGLA,D.C., SMITH,G.W., Plenum Press, New York, 1981

157. KAKEGAWA,T., SAKAI,T., SHIOJI,M., TSUJIMURA,K.: "Stochastic model for diesel combustion considering some turbulent mixing zones", SAE 920693, 1992

158. KAMIMOTO,T., MATSUOKA,S., MATSUI,Y., AOYAGI,Y.: "The measurement of flame temperature and the thermodynamic analysis of combustion processes in a direct injection diesel engine", IMechE, C96/75, 1975

159.KAMIMOTO,T., AOYAGI,Y., MATSUI,Y., MATSUOKA,S.: "Some effects of engine variables on measured rate of air entrainment and heat release in a DI diesel engine", SAE 800253, 1980

160.KAMIMOTO,K., MATSUOKA,S., MIYAIRI,M.: "Soot oxidation in the flame in a DI diesel engine", IMechE, C103/82, 1982

161.KAMIMOTO,T., KOBAYASHI,H.: "Combustion processes in diesel engines", Prog. Energy Comb. Sci., vol. 17, pp. 163-189, 1991

162.KANURY,M.: *Introduction to combustion phenomena*, Gordon & Breach, New York, 1975

163.KARIMI,E.R., JANE,P.A.H.: "A combustion system investigation to achieve low emissions on a heavy duty diesel engine", IMechE, 'Automobile emissions and combustion', AUTOTECH '93, pp. 143-160, 1993

164.KAU,C.J., TYSON.T.J., HEAP,M.P.: "Study of the oxides of nitrogen and carbon formation in diesel engines", U.S. Dept of Commerce, N.T.I.S., PB-262204, 1976

165.KAU,C.J., HEAP,M.P., TYSON,T.J., WILSON,R.P.: "The prediction of nitric oxide formation in a direct injection diesel engine", Sixteenth Symposium (Int.) on Combustion, The Combustion Institute, pp. 337-350, 1977

166.KAWAZOE,H., NAGANO,S., OHSAWA,K.: "Reduction of soot emission by air-turbulence generator with cam in diesel engine", JSAE Review, vol. 12, no. 3, pp. 10-15, Jul., 1991

167.KENNEDY,I.M., KOLLMANN,W., CHEN,J.-Y.: "A model for soot formation in a laminar diffusion flame", Comb. & Flame, vol. 81, pp. 73-85, 1990

168.KENT,J.H., HONNERY,D.R.: "Soot formation rates in diffusion flames - a unifying trend", Comb. Sci. & Tech., vol. 75, pp. 167-177, 1990

169.KHAN,I.M.: "Formation and combustion of carbon in a diesel engine", Symp. Diesel Engine Combustion, Proc. IMechE, vol. 184, pt. 3J, pp. 36-43, 1969

170.KHAN,I.M., GREEVES,G., PROBERT,D.M.: "Predictions of soot and nitric oxide concentrations in diesel engine exhaust", Symposium on 'Air pollution control in transport engines', Solihull, Automotive Division, IMechE, C142/71, pp. 205-217, 9-11th Nov., 1971

171.KHAN,I.M., WANG,C.H.T., LANGRIDGE,B.E.: "Coagulation and combustion of soot particle in diesel engines", Comb. & Flame, 17, pp. 409-419, 1971

172.KHAN,I.M., GREEVES,G., WANG,C.H.T.: "Factors affecting smoke and gaseous emissions from direct injection engines and a method of calculation, SAE 730169, 1973

173.KHAN,I.M., GREEVES,G.: "A method for calculating the formation and combustion of soot in diesel engines", pp. 391-404, in *Heat transfer in flames*, eds. AFGAN,N.H., BEER,J.M., Scripta, Washington, 1974

174.KITTELSON,D.B., PIPHO,M.J., AMBS,J.L., SIEGLA,D.C.: "Particle concentrations in a diesel cylinder: comparison of theory and experiment", SAE 861569, 1986

175.KITTELSON,D.B., PIPHO,M.J., AMBS,J.L., LUO,L.: "In-cylinder measurements of soot production in a direct-injection diesel engine", SAE 880344, 1988

176.KITTELSON,D.B., AMBS,J.L., HADJKACEM,H.: "Particulate emissions from diesel engines: influence of in-cylinder surface", SAE 900645, 1990

177.KLINGENBERG,H.: "Modern cars to reduce CO_2-emissions", International Conference "Toward clean and fuel efficient automobiles", OECD, Berlin, 25-27th Mar. 1991, pp. 463-469, 1993

178.KNIGHT,B.E.: "Communication on the performance of a type of swirl atomizer", Proc. IMechE, vol. 104, 1955

179.KOBAYASHI,H., KAMIMOTO,T., MATSUOKA,S.: "A photographic and thermodynamic study of diesel combustion in a rapid compression machine", SAE 810259, 1981

180.KOBAYASHI,H., YAGITA,M., KAMIMOTO,T., MATSUOKA,S.: "Prediction of transient diesel sprays in swirling flows via a modified 2-D model", SAE 860332, 1986

181.KOBAYASHI,S., SAKAI,T., NAKAHIRA,T., KOMORI,M., TSUJIMURA,K.: "Measurement of flame temperature distribution in DI diesel engine with high pressure fuel injection", SAE 920692, 1992

182.KOLMOGOROV,A.N.: C. R. Acad. Sci. USSR, vol. 30, p. 301, 1941

183.KONNO,M., CHIKAHISA,T., MURAYAMA,T.: "Reduction of smoke and NO_x by strong turbulence generated during the combustion process in DI diesel engines", SAE 920467, 1992

184.KONO,S., NAGAO,A., MOTOOKA,H.: "Prediction of in-cylinder flow and spray formation effects on combustion in direct injection diesel engines", SAE 850108, 1985

185.KONSTANDINIDIS,P.: *Diesel engine simulation programme*, MSc thesis, Cranfield Institute of Technology, 1990

186.KONTANI,K., GOTOH,S.: "Measurement of soot in a diesel combustion chamber by light extinction method and in-cylinder observation by highspeed shadowgraphy", SAE 831291, 1983

187.KONTANI,K., GOTO,S.: "Soot particle measurement in diesel engine combustion chambers", JSAE Review, vol. 7, no. 3, pp. 12-19, Oct., 1986

188.KORT,R.T., MANSOURI,S.H., HEYWOOD,J.B., EKCHIAN,A.: "Divided-chamber diesel engine, Part II: Experimental validation of a predictive cycle -simulation and heat release analysis", SAE 820274, 1982

189.KOUREMENOS,D.A., RAKOPOULOS,C.D., HOUNTALAS,D.T.: "Modeling of spray mixing in a quiescent chamber diesel allowing for jet wall impingement", Proc. Intern. AMSE-France Conf., vol. 3.3, pp. 199-206, Naples, 29th Sept. - 1st Oct., 1986

190.KOUREMENOS,D.A., RAKOPOULOS,C.D., KARVOUNIS,E.: "Thermodynamic analysis of direct injection diesel engines by multi-zone modeling", ASME Winter Annual Meeting, AES-vol. 3.3, pp. 67-77, Boston, M.A., 13-18th Dec., 1987

191. KOUREMENOS,D.A., RAKOPOULOS,C.D., HOUNTALAS,D.T.: "Predicting the nitric oxide and soot emissions from compression ignition engines by one-zone and two-zone combustion modelling", Proc. Intern. AMSE-France Conf., vol. 3.B, pp. 49-57, Karlsruhe, 20-22nd Jul., 1987

192. KOUREMENOS,D.A., RAKOPOULOS,C.D., HOUNTALAS,D.T.: "Computer simulation with experimental validation of the exhaust nitric oxide and soot emissions in divided chamber diesel engines", ASME Winter Annual Meeting, AES session, San Francisco, 10-15 Dec., 1989

193. KOUREMENOS,D.A., RAKOPOULOS,C.D., HOUNTALAS,D.T.: "Thermodynamic analysis of indirect injection diesel engines by two-zone modelling of combustion", Trans. ASME, Journal of Engineering Gas Turbines and Power, vol. 112, pp. 138-149, Jan., 1990

194. KRIEGER,R.B., BORMAN,G.L.: "The computation of apparent heat release for internal combustion engines", ASME paper 66-WA/ DGP-4, 1966

195. KUO,T.-W., BRACCO,F.V.: "On the scaling of impulsively started incompressible turbulent round jets", ASME Journal of Fluids Engineering, vol. 104, pp. 191-197, 1982

196. KUO,T.-W., YU,R.C., SHAHED,S.M.: "A numerical study of the transient evaporating spray mixing process in the diesel environment", SAE 831735, 1983

197. KUO,T-W.: "Evaluation of a phenomenological spray-combustion model for two open-chamber diesel engines", SAE 872057, 1987

198. KYRIAKIDES,S.C., DENT,J.C., MEHTA,P.S.: "Phenomenological diesel combustion model including smoke and NO emission", SAE 860330, 1986

199. LAHAYE,J., PRADO,G.: "Morphology and internal structure of soot and carbon blacks", pp. 33-55, in *Particulate carbon formation during combustion*, eds. SIEGLA,D.C., SMITH,G.W., Plenum Press, New York, 1981

200. LAHAYE,J., PRADO,G. (eds.): *Soot in combustion systems and its toxic properties*, Plenum Press, New York, 1983

201. LANCASTER,D.R.: *Effects of turbulence on spark ignition engine combustion*, PhD thesis, University of Illinois, 1975

202. LAPUERTA,A.M.: *Un modelo de combustion fenomenológico para un motor Diesel de inyección directa rápido*, PhD thesis, Universidad Politécnica de Valencia, 1988

203. LAPUERTA,A.M., PEDROCHE,S.F., CHUST,P.M.D.: "Esquemas de calculo para un modelo de combustion tridimensional simplificado aplicado a motores diesel I.D.", 1991

204. LAURENDEAU,N.M.: "Heterogeneous kinetics of coal char gasification and combustion", Prog. Energy Combust. Sci., vol. 4, pp. 221-270, 1978

205. LAW,C.K., PRAKASH,S., SIRIGNANO,W.: "Theory of convective, transient, multicomponent droplet vaporization", Sixteenth Symposium (Int.) on Combustion, The Combustion Institute, pp. 605-617, 1977

206. LAZAR,R.S., FAETH,G.M.: "Bipropellant droplet combustion in the vicinity of the critical point", Thirteenth Symposium (Int.) on Combustion, The Combustion Institute, pp. 801-811, 1971

207. LEE,K.B., THRING,M.W., BEÉR,J.M.: "On the rate of combustion of soot in a laminar soot flame", Comb. & Flame, vol. 6, pp. 137-145, 1962

208. LEPPERHOFF,G.L., HOUBEN,M.: "Particulate emission and soot formation processes by diesel engines", IMechE, C394/03, pp. 115-120, 1990

209. LEUNG,K.M., LINDSTEDT,R.P., JONES,W.P.: "A simplified reaction mechanism for soot formation in nonpremixed flames", Comb. & Flame, vol. 87, pp. 289-305, 1991

210. LINDEN,L.H., HEYWOOD,J.B.: "Smoke emission from jet engines", Comb. Sci. & Tech., vol. 2, pp. 401-411, 1971

211. LINDSTEDT,P.R.: "Simplified soot nucleation and surface growth steps for non-premixed flames", pp. 417-441, in *Mechanisms and models of soot formation*, ed. BOCKHORN,H., Springer, Berlin, 1994

212. LIOU,T.-M., HALL,M., SANTAVICCA,D., BRACCO,F.V.: "Laser Doppler velocimetry measurements in valved and ported engines", SAE 840375, 1984

213. LIPKEA,W.H., DeJOODE,A.D.: "A model of a direct injection diesel combustion system for use in cycle simulation and optimization studies", SAE 870573, 1987

214. LI,Q.: *Development of quasi-dimensional diesel engine simulation for energy and availability analysis*, PhD thesis, University of Illinois at Urbana-Champaign, 1992

215. LI,Q., ASSANIS,D.N.: "A quasi-dimensional combustion model for diesel engine simulation", ICE-Vol. 20, Alternate fuels, engine performance and emissions, ASME, pp. 109-118, 1993

216. LIU,X.J., SIEGLA,D., KITTELSON,D.B.: "In-cylinder NO_x histories in an indirect injection diesel engine: comparison between experimental data and model predictions", Twentieth Symposium (Int.) on Combustion, The Combustion Institute, pp. 45-52, 1984

217. LÖFFLER,S., LÖFFLER,Ph., WEILMÜNSTER,P., HOMANN,K.-H.: "Growth of large ionic polycyclic aromatic hydrocarbons in sooting flames", pp. 66-82, in *Mechanisms and models of soot formation*, ed. BOCKHORN,H., Springer, Berlin, 1994

218. LORELL,J., WISE,H., CARR,R.E.: "Steady-state burning of a liquid droplet, II bipropellant flame", Journal Chem. Phy., vol. 25, no. 2, pp. 325-331, Aug., 1956

219. LUNDELL,J.H., DICKEY,R.R.: AIAA 72-298, 7th Thermophysics Conference, Houston, Texas, Apr., 1972

220. MacFARLANE,J.J., HOLDERNESS,F.H., WHITCHER,F.S.E.: "Soot formation rates in premixed C_5 and C_6 hydrocarbon-air flames at pressures up to 20 atmospheres", Comb. & Flame, vol. 8, pp. 215-229, 1964

221. MAGNUSSEN,B.F.: "The rate of combustion of soot in turbulent flames", Thirteenth Symposium (Int.) on Combustion, pp. 869-877, The Combustion Institute, 1971

222. MAGNUSSEN,B.F.: "An investigation into the behaviour of soot in a turbulent free jet C_2H_2-flame", Fifteenth Symposium (Int.) on Combustion, pp. 1415-1425, The Combustion Institute, 1975

223. MAGNUSSEN,B.F., HJERTAGER,B.H.: "On mathematical modeling of turbulent combustion with special emphasis on soot formation and combustion", Sixteenth Symposium (Int.) on Combustion, pp. 719-729, The Combustion Institute, 1977

224. MAGNUSSEN,B.F., HJERTAGER,B.H., OLSEN,J.G., BHADURI,D.: "Effects of turbulent structure and local concentrations on soot formation and combustion in C_2H_2 diffusion flames", Seventeenth Symposium (Int.) on Combustion, pp. 1383-1393, The Combustion Institute, 1978

225. MAGNUSSEN,B.F.: "Modeling of reaction processes in turbulent flames with special emphasis on soot formation and combustion", pp. 321-341, in *Particulate carbon formation during combustion*, eds. SIEGLA,D.C., SMITH,G.W., Plenum Press, New York, 1981

226. MAGNUSSEN,B.F.: "Heat transfer in gas turbine combustors", AGARD, CP-390, paper no. 23, 1985

227. MANSOURI,S.H., HEYWOOD,J.B., EKCHIAN,J.: "Studies of NO_x and soot emissions from an engine cycle simulation", IMechE, C120/82, pp. 215-227, 1982

228. MANSOURI,S.H., HEYWOOD,J.B., RADHAKRISHNAN,K.: "Divided-chamber diesel engine, Part I: A cycle-simulation which predicts performance and emissions", SAE 820273, 1982

229. MARKATOS,N.C.: *Computer simulation for fluid flow, heat and mass transfer, and combustion in reciprocating engines*, Hemisphere, 1989

230. MATSUI,Y., KAMIMOTO,K., MATSUOKA,S.: "Formation and oxidation processes of soot particulates in a D.I. diesel engine - an experimental study via the two-colour method", SAE 820464, SAE P-107, 1982

231. MAXWELL,J.B.: *Databook on hydrocarbons: application to process engineering*, Van Nostrand, New York, 1950

232. McARRAGHER,J.S., TAN,K.J.: "Soot formation at high pressures: a literature review", Comb. Sci. & Tech., vol. 5, pp. 257-261, 1972

233. McCREATH,C.G., CHIGIER,N.A.: "Liquid spray burning in the wake of a stabiliser disc", Fourteenth Symposium (Int.) on Combustion, pp. 1355-1363, 1972

234. MEGUERDICHIAN,M., WATSON,N.: "Prediction of mixture formation and heat release in diesel engines", SAE 780225, 1978

235. MEHTA,P.S.: *Phenomenological combustion model for direct injection diesel engine*, PhD thesis, Loughborough University of Technology, 1981

236. MEHTA,P.S., GUPTA,A.K.: "Modelling of spray-swirl interaction in direct injection diesel engine combustion chambers", IMechE, vol. 199, no. D3, pp. 187-199, 1985

237. MEHTA,P.S., GUPTA,A.K., GUPTA,C.P.: "Model for prediction of incylinder and exhaust soot emissions from direct injection diesel engines", SAE 881251, 1988

238. MILBERG,M.E.: "Carbon formation in an acetylene-air diffusion flame", J. Phys. Chem., vol. 63, pp. 578-582, 1959

239. MOHAMMAD,I.S., BORMAN,G.L.: "Measurement of soot and flame temperature along three directions in the cylinder of a direct injection diesel", SAE 910728, 1991

240. MOREL,T., MANSOUR,N.N.: "Modeling of turbulence in internal combustion engines", SAE 820040, 1982

241. MOREL,T., KERIBAR,R.: "Heat radiation in DI diesel engines", SAE 860445, 1986

242. MOSS,J.B., STEWART,C.D., SYED,K.J.: "Flowfield modelling of soot formation at elevated pressure", Twenty-second Symposium (Int.) on Combustion, pp. 413-423, The Combustion Institute, 1988

243. MULLINS,J., SIMMONS,B., WILLIAMS,A.: "Rates of formation of soot from hydrocarbon flames and its destruction", AGARD CP-422, paper no. 23, 1987

244. MURAKAMI,A., SAKIMOTO,M., ARAI,M., HIROYASU,H.: "Measurement of turbulent flow in the combustion chamber of a D.I. diesel engine", SAE 900061, 1990

245. MURAYAMA,T., MIYAMOTO,N., SASAKI,S.: "A mathematical model on nitric oxide formation in diesel engines", Bull. of the JSME, vol. 22, no. 163, pp. 79-85, Jan., 1979

246. MURAYAMA,T., MIYAMOTO,N., CHIKAHISA,T., TOSAKA,S.: "Efficient and low-smoke combustion of various low-grade fuels in high-speed small diesel engines", Trans. ASME, Journal of Engineering for Gas Turbines and Power, vol. 110, pp. 385-392, Jul., 1988

247. MURAYAMA,T., FUJIWARA,Y., TOSAKA,S.: "The properties, formation, and oxidation of soot particulate in diesel engines", ICE-Vol. 17, Diesel engine processes: Turbocharging, combustion and emission, ASME, 1992

248. NAEGELI,D.W., DODGE,L.G., MOSES,C.A.: "Effects of flame temperature and fuel composition on soot formation in gas turbine combustors", Comb. Sci. & Tech., vol. 35, pp. 117-131, 1983

249. NAGLE,J., STRICKLAND-CONSTABLE,R.: "Oxidation of Carbon between 1000-2000°C", Proc. Fifth Carbon Conf., vol. 1, pp. 154-164, 1962

250. NAJJAR,Y.S.H.: *Soot formation and oxidation with heavy fuels in gas turbine combustors*, PhD thesis, Cranfield Institute of Technology, Aug., 1979

251. NAJJAR,Y.S.H., GOODGER,E.M.: "Soot formation in gas turbines using heavy fuels, 1.", Fuel, vol. 60, pp. 980-986, Oct., 1981

252. NAJJAR,Y.S.H., GOODGER,E.M.: "Soot oxidation in gas turbines using heavy fuels, 2.", Fuel, vol. 60, pp. 987-990, Oct., 1981

253. NAKAJIMA,M., SHIMODA,M., NAKAGOME,K.: "Relation between particulates and black smoke/HC in diesel engines", JSAE Review, vol. 9, no. 4, pp. 32-36, Oct., 1988

254. NAKAKITA,K., NAGAOKA,M., FUJIKAWA,T., OHSAWA,K., YAMAGUCHI,S.: "Photographic and three dimensional numerical studies of diesel soot formation process", SAE 902081, 1990

255. NARASIMHAN,K.S., FOSTER,P.J.: "The rate of growth of soot in turbulent flow with combustion products and methane", Tenth Symposium (Int.) on Combustion, The Combustion Institute, pp. 253-257, 1965

256. NATARAJAN,R., BRZUSTOWSKI,T.: "Some new observations on the combustion of hydrocarbon droplets at elevated pressures", Comb. Sci. & Tech., vol. 2, pp. 259-269, 1970

257. NEOH,K.G., HOWARD,J.B., SAROFIM,F.: "Soot oxidation in flames", pp. 261-282, in *Particulate carbon formation during combustion*, eds. SIEGLA,D.C., SMITH,G.W., Plenum Press, New York, 1981

258. NEWMAN,J.A., BRZUSTOWSKI,T.A.: "Behaviour of a liquid jet near the thermodynamic critical region", AIAA Journal, vol. 9, no. 8, 1971

259. NING,M., YUAN-XIAN,Z., ZHEN-HUAN,S., HU-GUO-DONG: "Soot formation, oxidation and its mechanism in different combustion systems and smoke emission pattern in DI diesel engines", SAE 910230, 1991

260. NISHIDA,O., MUKOHARA,S.: "Distribution of the soot concentrations in the diffusion flames", Journal of the MESJ, vol. 14, no. 3, pp. 288-295, Mar., 1979

261. NISHIDA,O., MUKOHARA,S.: "Characteristics of soot formation and decomposition in turbulent diffusion flames", Comb. & Flame, vol. 47, pp. 269-279, 1982

262. NISHIDA,K., HIROYASU,H.: "Simplified three-dimensional modeling of mixture formation and combustion in a D.I. diesel engine", SAE 890269, 1989

263. NISHIDA,M., NAKAHIRA,T., KOMORI,M., TSUJIMURA,K., YAMAGUCHI,I.; "Observation of high pressure fuel spray with laser light sheet method", SAE 920459, 1992

264. NORRIS-JONES,S.R., HOLLIS,T., WATERHOUSE,C.N.F.: "A study of the formation of particulates in the cylinder of a direct injection diesel engine", SAE 840419, 1984

265. ODAKA,M., KOIKE,N., TSUKAMOTO,Y., NARUSAWA,K.: "Optimizing control of NO_x and smoke emissions from DI engine with EGR and methanol fumigation", SAE 920468, 1992

266. OHKOSHI,M., KOKUBO,K., HOSOGAI,D., NISHIMURA,J., KOBAYASHI,T.: "Diesel smoke reduction by gasoline fumigation using an ultrasonic atomizer", SAE 920691, 1992

267. OKAJIMA,S., KUMAGI,S.: "Experimental investigation of soot and NO_x reduction by impinging spray combustion in a closed vessel", Twenty-third Symposium (Int.) on Combustion, The Combustion Institute, pp. 275-279, 1990

268. OLSON,D.B., CALCOTE,H.F.: "Ionic mechanisms of soot nucleation in pre-mixed flames", pp. 177-205, in *Particulate carbon formation during combustion*, eds. SIEGLA,D.C., SMITH,G.W., Plenum Press, New York, 1981

269. PARK,C., APPLETON,J.P.: "Shock-tube measurements of soot oxidation rates", Comb. & Flame, vol. 20, pp. 369-379, 1973

270.PARKER,A.S., HOTTEL,H.C.: Ind. Eng. Chem., vol. 28, p. 1334, 1936

271.PAYRI,F., DESANTES,J.M., LAPUERTA,M.: "A phenomenological model for calculating DI diesel engine performance and emissions", SIA 90139, 1990

272.PERRY,J.H.: *Chemical Engineers' Handbook*, 2nd ed., McGraw-Hill, New York, 1941

273.PERRY,R.H., GREEN,D.: *Perry's Chemical Engineers' Handbook*, 6th ed., McGraw-Hill, New York, 1984

274.PINCHON,P.: "Three dimensional modelling of combustion in a prechamber diesel engine", SAE 890666, 1989

275.PISCHINGER,F., LEPPERHOFF,G., HOUBEN,M.: "Soot formation and oxidation in diesel engines", pp. 382-395, in *Mechanisms and models of soot formation*, ed. BOCKHORN,H., Springer, Berlin, 1994

276.PLEE,S.L., AHMAD,T., MYERS,J.P., SIEGLA,D.C.: "Effects of flame temperature and air-fuel mixing on emission of particulate carbon from a divided chamber diesel engine", pp. 423-487, in *Particulate carbon formation during combustion*, eds. SIEGLA,D.C., SMITH,G.W., Plenum Press, New York, 1981

277.PLEE,S.L., AHMAD,T.: "Relative roles of premixed and diffusion burning in diesel combustion", SAE 831733, 1983

278.POPE,S.B.: "Computations of turbulent combustion: progress and challenges", Twenty-third Symposium (Int.) on Combustion, pp. 591-612, The Combustion Institute, 1990

279.PRADO,G., LAHAYE,J.: "Physical aspects of nucleation and growth of soot particles", pp. 143-175, in *Particulate carbon formation during combustion*, eds. SIEGLA,D.C., SMITH,G.W., Plenum Press, New York, 1981

280.PRIMUS,R.J., WONG,V.W.: "Performance and combustion modelling of heterogeneous charge engines", SAE 850343, SAE SP-156, 1985

281.QUOC,H.X., VIGNON,J-M., BRUN,M.: "A new approach of the two-colour method for determining local instantaneous soot concentration and temperature in a D.I. diesel combustion chamber", SAE 910736, 1991

282.RADCLIFFE,S.W., APPLETON,J.P.: "Soot oxidation rates in gas turbine engines", Comb. Sci. & Tech., vol. 4, pp. 171-175, 1971

283.RAGUCCI,R., CAVLIERE,A., CIAJOLO,A., D'ANNA,A., D'ALESSIO,A.: "Structures of diesel sprays in isobaric combustion conditions", Twenty-fourth Symposium (Int.) on Combustion, The Combustion Institute, pp. 1565-1571, 1992

284.RAMOS,J.I.: *Internal combustion engine modelling*, Hemisphere, 1989

285.RANZ,W.E., MARSHALL,W.R.,Jr.: "Evaporation from drops, Part 1", Chemical Engg. Prog., vol. 48, no. 3, pp. 141-146, 1952

286.RANZ,W.E., MARSHALL,W.R.,Jr.: "Evaporation from drops, Part 2", Chemical Engg. Prog., vol. 48, no. 4, pp. 173-180, 1952

287.RAO,V.K., BARDON,M.F.: "The effect of water on gas phase soot formation in laminar diffusion flames", Comb. & Flame, vol. 55, pp. 73-78, 1984

288.RASK,R.B.: "Comparison of window, smoothed-ensemble, and cycle-to-cycle data reduction techniques for laser Doppler anemometry measurements of in-cylinder velocity", pp. 11-20, in *Fluid Mechanics of Combustion Systems*, eds. MOREL,T., LOHMANN,R.P., RACKLEY,J.M., ASME, New York, 1981

289.REITZ,R.D., BRACCO,F.V.: "Ultra-high-speed filming of atomizing jets", Physics of fluids, vol. 22, no. 6, pp. 1054-1064, 1979

290.REITZ,R.D., BRACCO,F.V.: "On the dependence of spray angle and other spray parameters on nozzle design and operating conditions", SAE 790494, 1979

291.REITZ,R.D., BRACCO,F.V.: "Mechanism of atomization of a liquid jet", Physics of fluids, vol. 25, no. 10, pp. 1730-1742, 1982

292.REITZ,R.D., BRACCO,F.V.: "Mechanisms of breakup of round liquid jets", in *Encyclopedia of Fluid Mechanics*, ed. N.P. CHEREMISINOFF, vol. 3, pp. 233-249, Gulf, Houston, Texas, 1986

293.RICOU,J.P., SPALDING,D.B.: "Measurement of entrainment by axial symmetric turbulent jets", J. Fluid Mech., vol. 9, pp. 21-32, 1961

294.RIFE,J.M., HEYWOOD,J.B.: "Photographic and performance studies of diesel combustion using a rapid compression machine", SAE 740948, 1974

295.ROCCO,V.: "D.I. diesel engine in-cylinder pressure data analysis under T.D.C. setting error", SAE 930595, 1993

296.RODI,W., SPALDING,D.B.: "A two-parameter model of turbulence, and its application to free jets", *Wärme- und Stoffübertragung*, vol. 3, no. 2, pp. 85-95, Springer, 1970

297.ROSNER,D.E.: "On liquid droplet combustion at high pressures", AIAA Journal, vol. 5, pp. 163-166, Jan., 1967

298.RUSSELL JONES,R.: "The health effects of vehicle emissions", IMechE, C355/87, 1987

299.SAAD,M.A., AFIFY,E.M., KLETT,D.E.: "Multidimensional modeling of combustion and NO emission of the Ricardo Hydra direct injection diesel engine: KIVA-II versus experiment", ICE-Vol. 20, Alternate fuels, engine performance and emissions, ASME, pp. 89-98, 1993

300.SAITO,T., DAISHO,Y., UCHID,N., IKEY,N.: "Effects of combustion chamber geometry on diesel combustion", SAE 861180, 1986

301.SATO,G.T.: "Structure of diesel spray", ICLASS-85, IP/1, 1985

302.SATO,H., TREE,D.R., HODGES,J.T., FOSTER,D.E.: "A study on the effect of temperature on soot formation in a jet stirred combustor", Twenty-third Symposium (Int.) on Combustion, The Combustion Institute, pp. 1469-1475, 1990

303.SATO,H., SATO,Y., ISHIDA,S.: "The progress of IDI diesel engine for passenger car", SAE 930720, 1993

304. SCHALLA,R.L., McDONALD,G.E.: "Mechanism of soot formation in diffusion flames", Fifth Symposium (Int.) on Combustion, The Combustion Institute, pp. 316-324, 1955

305. SCHEID,E., PISCHINGER,F., KNOCHE,K.F., DAAMS,H.-J., HASSEL,E.P., REUTER,U.: "Spray combustion chamber with optical access, ignition zone visualisation and first Raman measurements of local air-fuel ratio", SAE 861121, 1986

306. SCHUG,K.P., MANHEIMER-TIMNAT,Y., YACCARINO,P., GLASSMAN,I.: "Sooting behaviour of gaseous hydrocarbon diffusion flames and the influence of additives", Comb. Sci. & Tech., vol. 22, pp. 235-250, 1980

307. SEMENOV,E.S.: "Studies of turbulent gas flow in piston engines", NASA Technical Translation F97, 1963

308. SENDA,J., OGAWA,T., FUGIMOTO,H., KUBOTA,H., KIMURA,N.: "Characteristics of combustion in an IDI diesel engine with a swirl chamber made of ceramics", SAE 920696, 1992

309. SHAHED,S.M., CHIU,W.S., LYN,W.T.: "A mathematical model of diesel combustion", IMechE, C94/75, 1975

310. SHAHED,S.M., FYLNN,P.F., LYN,W.T.: "A model for the formation of emissions in a direct-injection diesel engine", in *Combustion Modeling in Reciprocating Engines*, pp. 345-368, eds. MATTAVI,J.N., AMANN,C.A., Plenum Press, New York, 1980

311. SHIBAYAMA,S., KOIZUMI,M., AOKI,I.: "The combustion of soot in fuel-oil-firing", Trans. JSME, vol. 34, no. 260, pp. 769-775, 1968

312. SHIMIZU,I., SHIMODA,M., SUZUKI,T., EMORI,Y.: "A light scattering and holographic technique for determining droplet size and volume density distribution in diesel fuel sprays", SAE 820355, 1982

313. SHIMODA,M., SUZUKI,T., SHIGEMORI,M.: "Observation of the particulate formation process in the cylinder of a direct injection diesel engine", SAE 870268, 1987

314. SHIOZAKI,T., OTANI,T., JOKO,I.: "A study of the white smoke generation and its numerical simulation", IMechE, C427/28/136, 1991

315. SHIOZAKI,T., OTANI,T., JOKO,I.: "A study of white smoke generation and its numerical simulation", Proc. IMechE, vol. 207, pp. 101-106, 1993

316. SHIRAKAWA,S., OMSAWA,K., AYOYAMA,T.: "Simulation of spray combustion in an axisymmetric small direct injection diesel", IMechE, C01/87, pp. 191-198, 1987

317. SHROFF,H.D., HODGETTS,D.: "Simulation and optimization of thermodynamic processes of diesel engine", SAE 740194, 1974

318. SIEGLA,D.C., SMITH,G.W., (eds.): *Particulate carbon formation during combustion*, Plenum Press, New York, 1981

319. SIMMONS,B., WILLIAMS,A.: Combustion Research Conference, Harwell UKAEA, Mar., 1986

320.SIMMONS,B., WILLIAMS,A.: "A shock tube investigation of the rate of soot formation for benzene, toluene, and toluene/n-heptane mixtures", Comb. & Flame, vol. 71, pp. 219-232, 1988

321.SINGAL,S.K., PUNDIR,B.P., MEHTA,P.S.: "Modelling spray/wall interaction in swirling flows for DI diesel engines", Proc. IMechE, vol. 204, pp. 245-253, 1990

322.SINGAL,S.K., PUNDIR,B.P., MEHTA,P.S.: "Fuel spray-air motion interaction in DI diesel engines: a review", SAE 930604, 1993

323.SINNAMON,J.F., LANCASTER,D.R., STIENER,J.C.: "An experimental and analytical study of engine fuel spray trajectories", SAE 800135, 1980

324.SIRIGNANO,W.: "Fuel droplet vaporisation and spray combustion theory", Prog. Energy Comb. Sci., vol. 9, pp. 291-322, 1983

325.SMITH,G.W.: "Kinetic aspects of diesel soot coagulation", SAE 820466, 1982

326.SMITH,I.W.: "The intrinsic reactivity of carbons to oxygen", Fuel, vol. 57, pp. 409-414, Jul., 1978

327.SMITH,L., BANISOLEIMAN,K., BAZARI,Z., FRENCH,B.: "Prediction of performance and emissions for a high-speed DI diesel engine with exhaust gas recirculation", IMechE, C465/054/93, 1993-10, 1993

328.SMITH,O.I.: "Fundamentals of soot formation in flames with application to diesel engine particulate emissions", Prog. Energy Combust. Sci., vol. 7, pp. 275-291, 1981

329.SOTERIOU,C.C.E., SMITH,M., ANDREWS,R.J.: "Cavitation hydraulic flip and atomisation in direct injection diesel sprays", IMechE, C465/051/93, 1993-10, 1993

330.SPALDING,D.B.: "The combustion of liquid fuels", Fourth Symposium (Int.) on Combustion, The Combustion Institute, pp. 847-864, 1952

331.SPALDING,D.B.: "Theory of particle combustion at high pressures", Journal of the American Rocket Society, vol. 29, pp. 828-853, 1959

332.SPALDING,D.B., AFGAN,N.H.: *Heat and mass transfer in gasoline and diesel engines*, Hemisphere, 1989

333.SREZNEVSKY,B.: Zh. R. F. Kho., vol. 14, p. 420, p. 483, 1882

334.STEWART,C.D., SYED,K.J., MOSS,J.B.: "Modelling soot formation in non-premixed kerosine-air flames", Comb. Sci. & Tech., vol. 75, pp. 211-226, 1991

335.SUROVIKIN,V.F.: "Analytical description of the processes of nucleus-formation and growth of particles of carbon black in the thermal decomposition of aromatic hydrocarbons in the gas phase", Khimiya Tverdogo Topliva, vol. 10, no. 1, pp. 111-122, 1976

336.SUZUKI,T., OHTA,S.: "Controlling exhaust emissions from the high speed diesel engine with a direct injection type combustion chamber", IMechE, C87/75, pp. 59-71, 1975

337. SYED,S., BRACCO,F.V.: "Further comparisons of computed and measured divided-chamber engine combustion", SAE 790247, 1979

338. TABACZYNSKI,R.J.: "Turbulence and turbulent combustion in Spark-Ignition engines", Prog. Energy Combust. Sci., vol. 2, pp. 143-165, 1976

339. TABACZYNSKI,J.C.: "A turbulent entrainment model for spark-ignition engine combustion", SAE 770647, 1977

340. TAKEUCHI,K., SENDA,J., ITO,Y., ISHIDA,K.: "Distribution of fuel droplets, hydrocarbon and soot in diesel combustion chamber", SAE 830456, 1983

341. TANASAWA,Y., TOYODA,S.: "On the atomisation of liquid jet issuing from a cylindrical nozzle", Tech. Report of Tohoku Univ., 19-2, p. 135, 1955

342. TAYLOR,D.H., WALSHAM,B.E.: "Combustion processes in a medium speed diesel engine", Symposium on Diesel Engine Combustion, Proc. IMechE, London, pt. 3, p. 1970, 1967

343. TERBLANCHE,P.S., LER MURRAY,P.W.: "Health aspects of diesel emissions", presented at NACA Annual Conference, Nov. 1990, Journal of the Mine Ventilation society of South Africa, pp. 80-84, May, 1991

344. TESNER,P.A., TSIBULEVSKY,A.M.: *Combustion, explosion and shock waves*, vol. 3, no. 2, pp. 261-267, 1967

345. TESNER,P., SNEGIRIOVA,T.D., KNORRE,V.G.: "Kinetics of dispersed carbon formation", Comb. & Flame, vol. 17, pp. 253-260, 1971

346. TESNER,P.A., TSYGANKOVA,E.I., GUILAZETDINOV,L.P., ZUYEV,V.P., LOSHAKOVA, G.V.: "The formation of soot from aromatic hydrocarbons in diffusion flames of hydrocarbon-hydrogen mixtures", Com. & Flame, vol.17, pp. 279-285, 1971

347. THEOBALD,M., CHENG,W.K.: "A numerical study of diesel ignition", ASME, 87-FE-2, 1987

348. THOMAS,A.: "Carbon formation in flames", Comb. & Flame, vol. 6., pp. 46-62, 1962

349. TINAUT,F.V.: *Contribucion al Estudio del Proceso de Combustion en Motores de Encendido por Compresion de Inyeccion Directa*, Dr.Eng. thesis, Poly-technic University of Valencia, 1986

350. TINDAL,M.H., UYEHARA,O.A.: "Diesel engines", pp. 101-149, in *Internal combustion engines*, ed. ARCOUMANIS,C., Academic Press, London, 1988

351. TSUKUHARA,M., YOSHIMOTO,Y.: "Reduction of NO_x, smoke, BSFC, and maximum combustion pressure by low compression ratios in a diesel engine fuelled by emulsified fuel", SAE 920464, 1992

352. TU,C.M., DAVIS,H., HOTTEL,H.C.: Ind. Eng. Chem., vol. 26, p. 749, 1934

353. TUTTLE,J.H., COLKET,M.B., BILGER,R.W., MELLOR,A.M.: "Characteristic times for combustion and pollutant formation in spray combustion", Sixteenth Symposium (Int.) on Combustion, The Combustion Institute, pp. 209-219, 1977

354. UCHIDA,N., DAISHO,Y., SAITO,T., SUGANO,H.: "Combined effects of EGR and supercharging on diesel combustion and emissions", SAE 930601, 1993

355. ULRICH,G.D., MILNES,B., SUBRAMANIAN,N.S.: "Particles growth in flames. II: experimental results for silica particles", Comb. Sci. & Tech., vol. 14, pp. 243-249, 1976

356. WADE,W.R., HUNTER,C.E., TRINKER,F.H., CIKANEK,H.: "Reduction of NO_x and particulate emissions in the diesel combustion process", Trans. ASME, vol. 109, pp. 426-434, Oct., 1987

357. WAGNER,H.G.: "Soot formation", pp. 1-29, in *Particulate carbon formation during combustion*, eds. SIEGLA,D.C., SMITH,G.W., Plenum Press, New York, 1981

358. WALL,J.C., HEYWOOD,J.B., WOODS,W.A.: "Parametric studies of performance and NO_x emissions of the three-valve stratified charge engine using a cycle simulation", SAE 780320, 1978

359. WALLS,J.R., STRICKLAND-CONSTABLE,R.F.: "Oxidation of carbon between 1000-2400°C", Carbon, vol. 1, pp. 33-38, 1964

360. WALSH,M.P.: "Motor vehicle air pollution in Europe - a problem still not solved", IMechE, C339/87, 1987

361. WANG,C.-S., CHANG,S.-L.: "Spray combustion in diesel engines", SAE 882511, 1988

362. WANG,C.H., LIU,X.Q., LAW,C.K.: "Combustion and microexplosion of freely falling multicomponent droplets", Comb. & Flame, vol. 56, pp. 175-197, 1984

363. WANG,T.S., MATULA,R.A., FARMER,R.C.: "Combustion kinetics of soot formation from toluene", Eighteen Symposium (Int.) on Combustion, The Combustion Institute, pp. 1149-1158, 1981

364. WATKINS,P., WANG,D.M., KHALEGHI,H.: "Modelling spray phenomena in direct-injection diesel engines", IMechE, C433/088, pp. 131-141, 1991

365. WATSON,H.C., KUMAR,S., MILKINS,E., EDSELL,J.: "A diagnostic model for the combustion of seed oils in diesel engines", in Proceedings of International Symposium on Diagnostics and Modeling of Combustion in Reciprocating Engines, COMODIA 85, pp. 571-580, Tokyo, 4th-6th Sept., 1985

366. WELCH,S.: *The measurement and prediction of diesel exhaust smoke*, MSc thesis, Cranfield Institute of Technology, 1991

367. WERSBORG,B.L., HOWARD,J.B., WILLIAMS,G.C.: "Physical mechanisms in carbon formation in flames", Fourteenth Symposium (Int.) on Combustion, The Combustion Institute, pp. 292-940, 1973

368. WILLIAMS,A.: *Fundamentals of oil combustion*, Prog. Energy Comb. Sci., vol. 2, pp. 167-179, 1976

369. WILLIAMS,F.: *Combustion Theory, The fundamental theory of chemically reacting flow systems*, Addison-Wesley, 1965

370. WILSON,M., WALLACE,F.J.: "A comprehensive phenomenological model of the jet mixing process in D.I. diesel engines", SAE 861273, 1986

371. WILSON,R.P., WALDMAN,G.H., MUZIO,L.J.: U.S. Dept. of Commerce, N.T.I.S., Pb-231067, 1974

372. WINCKLER,J.: "Specific problems of sampling and measuring diesel exhaust emissions", IMechE, C350/87, 1987

373. WINDSOR,R.E.: *Relationship of cyclic combustion variations and mixture motion in a spark ignition engine*, PhD thesis, University of Michigan, 1972

374. WISE,H., AGOSTON,G.: "Burning of a liquid droplet", Advances in Chemistry Series, no. 20, Am. Chem. Soc., pp. 116-135, 1958

375. WÖLFLE,M., STROMBERG,S., HOUBEN,M., LEPPERHOFF,G.: "Influence of engine operating parameters on pollutant formation during diesel engine combustion", IMechE, C465/040/93, 1993-10, 1993

376. WOSCHNI,G.: "A universally applicable equation for the instantaneous heat transfer coefficient in the internal combustion engine", SAE 670931, 1967

377. WU,K.-J., REITZ,R.D., BRACCO,F.V.: "Measurement of drop size at the spray edge near the nozzle in atomizing liquid jets", Physics of Fluids, vol. 29, no. 4, pp. 941-951, 1986

378. XIAO,Y., BORGNAKKE,C.: "A stochastic combustion model of direct injection diesel engines", SAE 912354, 1991

379. XU,H., MYERS,P.S., UYEHARA,H.: "In-cylinder measurement of particulate number density and size", SAE 820462, 1982

380. YATES,D.A., GOMES,P.C.F.: "Diesel engine temperatures and soot particle densities measured by the two-colour method", IMechE, C465/029/93, 1993-10, 1993

381. YULE,J., MO,S.-L., THAM,S.Y., AVAL,S.M.: "Diesel spray structure", ICLASS-85, IIB/2, 1985

382. ZAHDEH,A.R., HENEIN,N.A., BRYZIK,W.: "Diesel engine cold starting: P-C based comprehensive heat release model: Part I - single cycle analysis", Trans. ASME, vol. 113, pp. 464-473, Jul., 1991

383. ZELEZNIK,F.J.: "Combustion modeling in internal combustion engines", Comb. Sci. & Tech., vol. 12, pp. 159-164, 1976

384. ZELLAT,M., ZELLER,H.: "Modelisation multidimensionnelle de l'autoinflammation dans un moteur diesel, Premières validations expérimentales", Rapport IFP No. 35551, Sept., 1987

385. ZELLAT,M., ZELLER,H.: "Modelisation multidimensionnelle de la combustion dans un moteur Diesel: Comparaison avec l'experience", Rapport IFP No. 35832, 1988

386. ZELLAT,M., POUILLE,J.: "Modelisation and visualisation in an indirect injection diesel engine", SIA 90138, 1990

387. ZELLAT,M., ROLLAND,T., POPLOW,F.: "Three dimensional modeling of combustion and soot formation in an indirect injection diesel engine", SAE 900254, 1990

388. ZHANG,L., MINAMI,T., TAKATSUKI,T., YOKOTA,K.: "An analysis of the combustion of a DI diesel engine by photograph processing", SAE 930594, 1993

389. ZHOU,Q.-B., WEI,X.-Y., ZHU,T.-Z., WANG,R.-S.: "The study of the heat radiation transfer process in DI diesel engines", pp. 111-120, in *Heat and mass transfer In gasoline and diesel engines*, eds. SPALDING,D.B., AFGAN,N.H., Hemisphere, 1989